



UNIVERSITY OF
BIRMINGHAM

**Particulate Emission Characteristics of a Light Duty
Diesel Engine under Transient Operation Conditions**

By

Jianyi Tian

A thesis submitted to

The University of Birmingham

for the degree of

DOCTOR OF PHILOSOPHY

The University of Birmingham

School of Mechanical Engineering

August 2015

UNIVERSITY OF
BIRMINGHAM

University of Birmingham Research Archive

e-theses repository

This unpublished thesis/dissertation is copyright of the author and/or third parties. The intellectual property rights of the author or third parties in respect of this work are as defined by The Copyright Designs and Patents Act 1988 or as modified by any successor legislation.

Any use made of information contained in this thesis/dissertation must be in accordance with that legislation and must be properly acknowledged. Further distribution or reproduction in any format is prohibited without the permission of the copyright holder.

Thesis Abstract

Engine transient operation has attracted a lot of attention from researchers due to its high frequency of occurrence during daily vehicle operation. Some researchers have reported that transient conditions will produce relatively higher instantaneous emissions compared with those of steady state conditions due to the turbo-lag issue. This research work focused on evaluations of improving the acceleration, cold start transient performances and emissions in a common rail direct injection (CRDI) turbocharged diesel engine.

Experimental work of temperature impacts on the engine emissions was conducted at ambient temperatures ranging between -7 and 20 °C. The results show that almost all of the engine emissions increase with the decreasing ambient temperature; the highest specific gaseous and particulate emissions are produced at the earlier stage of the NEDC. As the driving cycle runs consecutively, the emissions of the engine are highly dependent on the engine temperature rather than the ambient temperature. The size of the total particulate number spikes is mainly determined by the nucleation mode particulate number. The particulates emitted at extremely high AFR conditions are more dominant compared to those that are caused by the turbo-lag problem over the NEDC. In terms of the SVOC particulate 2D-GC/MS investigation, it can be concluded that both fuel and engine oil contribute as main carbon sources to produce the SVOC particulate emissions from the engine combustion, based on the analysis of the n-alkenes species. The fuel injection quantity is a dominating factor in determining the SVOC particles under a cold start condition; it is proportional to the number of chemical compounds in the low carbon length region.

A controlled intake air thermal heating system was implemented to improve the engine performances at cold ambient conditions. The experimental results showed that both the

gaseous and particulate (in number and mass) emissions can be significantly reduced by using the heating strategy, especially during the first UDC stage. However, the higher degree of intake air heating temperature has a very tiny influence on the NO_x emissions' reduction. By using the thermal heating system, the engine efficiency during the first UDC can be improved by up to 1.46% with the heating temperature of 15 °C at a -7 °C environment.

It is observed from the experimental results that transient particulate emissions' spikes are produced during acceleration transience. However, by using high blending biodiesel fuels, the spikes can be significantly eliminated; this is mainly due to the increased oxygen content availability in the fuel-rich combustion regions. The engine with higher initial/final engine load and speed operating conditions emitted lower particulate and gaseous emission spikes, compared to the low speed and load engine transient operation. The cumulative PN and THC emissions of biodiesel can be reduced by up to 75% and 50% respectively; while the NO emissions were almost doubled, compared to diesel.

An incremental transient EGR strategy was evaluated to improve the instantaneous particulate emission performance during acceleration conditions. With the improvement of the turbocharger performance and boosted intake fresh air mass flow, the novel strategy resulted in a reduced fuel injection quantity due to the higher AFR and consequently, improved combustion. The THC and PM can be reduced by up to 23.6% and 83.5% for the cases of 50 and 100% EGR reduction in the 1 second time interval respectively. The case with 50% EGR reduction in the 2 second time interval provided the best result considering both the performance and emissions' trade-off.

Acknowledgements

I would like to express the deepest sense of thanks to my supervisor Professor Hongming Xu for his guidance and encouragement during my PhD study. It would be impossible to complete this thesis without his professional advice and strategic direction. I would also like to thank my associate supervisor Dr. Karl Dearn for his helpful suggestions during the research.

I appreciate the help from the European Regional Development Fund and Advantage West Midlands for the test facilities. Special thanks are also given to Ben Neaves from Jaguar-Land Rover and David Korinec from AVL for their technical advice and facility support.

I would like to acknowledge the DECOST (Diesel Engine Cold Start and Transient Improvement) team member, Dr. Arumugam Sakunthalai Ramadhas and Dr Dai Liu for their generous help in the transient study. Thanks to Dr. Mohammed Salim Alam in the School of Environmental Science at the University of Birmingham for supporting the 2D-GC/MS test analysis.

I am also grateful to the FPS laboratory technicians Carl Hingley, Peter Thornton and Lee Gauntlett for their support on the test facility and instrumentation. Many thanks also to Janet's Proofreading Service for copy editing this thesis for conventions of language.

My appreciation goes to Dr. Yanfei Li, Dr. Xiao Ma, Dr. Fan Zhang, Dr. He Ma, Dr. Haiying Li, Dr. Chongming Wang, Dr. Changzhao Jiang, Dr. Daliang Jing, Dr. Guoxiang Lu and Dr. Ziman Wang for their generous help and technical support during my PhD study.

Special thanks should go to my friends and colleagues: Haichun Ding, Cheng Tan, Yunfan Zhang, Powen-Tu, Thomas Lattimore and Muhao Wang for their great help with my studies and living arrangements.

Finally, I would like to express my deep and sincere gratitude to my parents and family members for their unconditional support and encouragement. Last but not least, I would like to thank my girl friend Yimeng Zhang for understanding and supporting my entire PhD study.

I wish to dedicate this thesis to my family for their love and great support along the way

Table of Contents

Thesis Abstract	i
Acknowledgements	iii
Table of Contents	v
List of Abbreviations	xi
List of Symbols	xiv
List of Figures	xv
List of Tables	xx
List of Publications	xxi
CHAPTER 1 INTRODUCTION	1
1.1 RESEARCH BACKGROUND	1
1.1.1 Energy Shortage and Engine Emission Legislation	1
1.1.2 Modern Diesel Engine Development	4
1.1.3 Diesel Engine Transient and Cold Start	6
1.2 RESEARCH OBJECTIVES AND APPROACHES	7
1.3 THESIS OUTLINE	8
CHAPTER 2 LITERATURE REVIEW	11
2.1 FORMATION MECHANISMS OF DIESEL ENGINE EMISSIONS	11

2.1.1	Total Hydrocarbons.....	11
2.1.2	Carbon Monoxide	12
2.1.3	NO _x Emissions	13
2.1.4	Particulate Matter	16
2.2	ALTERNATIVE FUELS FOR DIESEL ENGINES	21
2.2.1	Characteristics of Biodiesel.....	21
2.2.2	Engine Performances and Emissions of Biodiesel.....	23
2.3	DIESEL ENGINE TRANSIENTS	30
2.3.1	Challenges of Transient Operating Conditions	30
2.3.2	Engine Transient Performances and Emissions	33
2.4	DIESEL ENGINE COLD START.....	35
2.4.1	Characteristics of Cold Start	36
2.4.2	Cold Start Emissions	38
2.4.3	Cold Start Solutions	39
2.5	EXHAUST GAS RECIRCULATION (EGR) AND DIESEL ENGINE COMBUSTION	40
2.5.1	EGR and Combustion Modes.....	40
2.5.2	EGR Transient Behaviours	42
2.6	SUMMARY	42
CHAPTER 3 EXPERIMENTAL SETUP AND APPARATUS.....		44
3.1	ENGINE SPECIFICATIONS	44

3.2	BIODIESEL TEST CELL AND FACILITIES	47
3.2.1	Dynamometer	47
3.2.2	Engine Cooling System.....	49
3.2.3	In-cylinder Pressure Measurements	50
3.2.4	Operating Control and Data Acquisition Systems	50
3.2.5	Fuel Properties	52
3.3	ENVIRONMENTAL CONTROLLED CLIMATIC CHAMBER AND FACILITIES	52
3.3.1	Dynamometer and Engine Mounting Enclosure	53
3.3.2	Dynamometer and Engine Mounting Enclosure	55
3.3.3	Engine Control Systems.....	59
3.3.4	Properties of Winter Diesel Fuel.....	59
3.4	FAST RESPONSE EMISSIONS MEASUREMENT DEVICES	60
3.4.1	Gaseous Emissions Measurements	60
3.4.2	Particulate Matter Measurements.....	64
3.5	EXPERIMENTAL DATA PROCESSING AND CALCULATIONS	69
3.5.1	Heat Release Rate Calculations	69
3.5.2	Cumulative Gaseous Emission Calculations.....	70
3.5.3	Cumulative Particulate Emission Calculations	71
3.6	SUMMARY	71
 CHAPTER 4 INVESTIGATIONS OF TEMPERATURES IMPACT ON DIESEL ENGINE EMISSIONS.....		 72

4.1	LOW AMBIENT TEMPERATURE EFFECTS ON A MODERN TURBOCHARGED DIESEL ENGINE RUNNING IN A DRIVING CYCLE.....	73
4.1.1	Test Conditions and Procedures.....	73
4.1.2	Transient Engine Performances	74
4.1.3	Transient Gaseous Emissions.....	78
4.1.4	Transient Particulate Emissions	85
4.2	INVESTIGATIONS OF SVOC COMPOUNDS IN PARTICULATES UNDER COLD AND WARM START NEDC.....	94
4.2.1	Experimental Procedure	94
4.2.2	Two-dimensional GC/MS Analysis of Cold and Warm Start Transients	95
4.3	CONCLUSIONS	105
CHAPTER 5 EVALUATIONS OF THE IMPACT OF INTAKE AIR HEATING ON DIESEL ENGINE TRANSIENT EMISSIONS IN A SUB-ZERO ENVIRONMENT....		108
5.1	AIR HEATING APPLICATION ON ENGINE COLD START.....	108
5.2	TEST CONDITIONS AND PROCEDURE.....	110
5.2.1	Calculations and Data Processing	112
5.2.2	Test Procedures	113
5.3	RESULTS AND DISCUSSION	116
5.3.1	Engine Performances	116
5.3.2	Gaseous Emissions.....	119
5.3.3	Particulate Emissions	124
5.4	CONCLUSIONS	133

CHAPTER 6 STEADY AND TRANSIENT ANALYSES RUNNING WITH BIODIESEL BLENDS	135
6.1 INTRODUCTION.....	135
6.2 TEST CONDITIONS AND PROCEDURE.....	136
6.3 COMBUSTION AND EMISSIONS UNDER STEADY STATE CONDITION...138	
6.3.1 Biodiesel Impact on Combustion Performances	138
6.3.2 Emission Profiles under Steady State Conditions.....	140
6.4 MODE SHIFTING TRANSIENT CONDITIONS	144
6.4.1 Low Initial Engine Condition Transients.....	144
6.4.2 Torque Increase Transients	151
6.4.3 Higher Initial Engine Speed and Torque Transients.....	156
6.5 ACCELERATION DURATION EFFECT ON TRANSIENT EMISSIONS	159
6.6 CONCLUSIONS	164
CHAPTER 7 NOVEL OPTIMIZED INCREMENTAL VARIATIONS OF EGR UNDER TORQUE INCREASED TRANSITION	166
7.1 EGR IMPACTS ON ENGINE TRANSIENTS.....	166
7.2 TEST CONDITIONS AND PROCEDURE.....	168
7.3 EFFECTS OF NOVEL TRANSIENT EGR STRATEGIES' EFFECTS ON ENGINE PERFORMANCES	171
7.3.1 Transient EGR Modification.....	171
7.3.2 Effects of the Varying EGR on Engine Parameters	173

7.3.3	Gaseous Emissions.....	177
7.3.4	Particulate Matter Emissions.....	181
7.4	CONCLUSIONS	188
CHAPTER 8 CONCLUSIONS AND FUTURE WORK.....		190
8.1	RESEARCH CONCLUSIONS	190
8.1.1	Temperature Impacts on Engine Transient Emissions.....	191
8.1.2	Evaluations of Intake Air Heating Influences in a Sub-zero Environment.....	192
8.1.3	Steady and Transient Performances of Biodiesel Blends	192
8.1.4	Incremental Variations of EGR under Torque Increase Transition	193
8.2	FUTURE WORK	194
Appendix A		196
Appendix B		197
References		198

List of Abbreviations

AC	Alternating Current
AFR	Air Fuel Ratio
BDC	Bottom Dead Centre
BSFC	Break Specific Fuel Consumption
CFPP	Cold Filter Plugging Point
CLD	Chemi Luminescence Detection
CN	Cetane Number
CO	Carbon Monoxide
CO ₂	Carbon Dioxide
CRDI	Common Rail Direct Injection
DCM	Dichloromethane
DMS	Differential Mobility Spectrometer
DOC	Diesel Oxidation Catalyst
DPF	Diesel Particulate Filter
ECU	Engine Control Unit
EGR	Exhaust Gas Recirculation
EMS	Engine Management System
EUDC	Extra Urban Driving Cycle
FAME	Fatty Acid Methyl Ester
FID	Flame Ionisation Detector
FTP	Federal Test Procedure
GC	Gas Chromatograph
HACA	Hydrogen Abstraction and Carbon Addition
IRD	Infrared Detector

JME	Jatropha Methyl Ester
LHV	Lower Heating Value
LTC	Low Temperature Combustion
MS	Mass Spectrometry
NEDC	New European Driving Cycle
NIST	National Institute of Standards and Technology
N ₂	Nitrogen
NO	Nitrogen Monoxide
NO _x	Nitrogen Oxide
NO ₂	Nitrogen Dioxide
N ₂ O	Nitrous Oxide
O ₂	Oxygen
PID	Proportional Integral Derivative
PCCI	Premixed Charge Compression Ignition
PCM	Phase change Material
PM	Particulate Mass
PME	Palm Methyl Ester
PMT	Photo Multiplier Tube
PN	Particulate Number
PPCI	Partially Premixed Compression Ignition
RED	Renewable Energy Directive
RME	Rapeseed Methyl Ester
RoHR	Rate of Heat Release
RoPR	Rate of Pressure Rise
SCR	Selective Catalytic Reduction
SME	Soy Methyl Ester
SOC	Start of Combustion

SOF	Soluble Organic Fraction
SOI	Start of Injection
SPC	Smart Sampler
SSD	Size Spectral Density
SVOC	Semi Volatile Organic Compounds
TDC	Top Dead Centre
THC	Total Hydrocarbon
TOF	Time of Flight
UCM	Unresolved Complex Mixtures
UDC	Urban Driving Cycle
UHC	Unburned Hydrocarbon
VGT	Variable Geometry Turbocharger
VOF	Volatile Organic Fraction
WLTP	Worldwide Harmonized Light Vehicles Test Procedures

List of Symbols

dQ	Heat released from combustion
dU	value affected by the temperature and specific heat capacities
dW	Engine work
$d\theta$	crank angle degree
MW_{gas}	molar mass of gaseous emissions
MW_{exhaust}	molar mass of exhaust gas
C_{gas}	concentration of the gaseous emission
m_{air}	intake air mass flow
m_{fuel}	mass fuel injection
v	engine speed
C_p	specific heat capacity of the intake air
P	engine power output
dT	temperature differential
Q_{HV}	lower heating value of fuel
Q_h	total heating energy
Q_f	the total energy released by the diesel fuel
γ	specific heat ratio
η	engine brake efficiency
η_c	overall thermal efficiency

List of Figures

Figure 1.1 Global CO ₂ emissions caused by fossil fuels.....	2
Figure 1.2 Characteristics of New European Driving Cycle.....	3
Figure 1.3 Share of renewable energy in fuel consumption of transport in EU countries	6
Figure 2.1 Particulate size distributions of exhaust gas particles.....	18
Figure 2.2 Typical particle structure emitted by internal combustion engines	19
Figure 2.3 Conceptual model of particulate composition	20
Figure 2.4 The transesterification process of biodiesel production	22
Figure 2.5 Comparison of the biodiesel blending ratio's effects on the NO _x emissions with petroleum diesel	26
Figure 2.6 Priority list for polyaromatic hydrocarbons (PAHs)	29
Figure 2.7 Schematic diagram of diesel engine transient turbo-lag phenomena	32
Figure 2.8 Schematic diagrams of series events during transient and cold start processes	32
Figure 2.9 Typical engine performances and emissions during load increase discrete transient.....	34
Figure 2.10 Typical cold start phenomena of engine speed.....	36
Figure 2.11 Trade-off of NO and soot as a function of local equivalence ratio and temperatures	41
Figure 3.1 Turbocharger mode map.....	45
Figure 3.2 Engine configuration lay-out	46
Figure 3.3 Engine characteristics curve	47
Figure 3.4 Test bench for biodiesel transient experiments	48
Figure 3.5 The cooling circuit of the engine coolant system	49
Figure 3.6 Schematic diagram of the engine arrangement.....	51

Figure 3.7 Test bench and facilities for climate change transient experiments	53
Figure 3.8 Schematic diagram of the cold cell arrangement.....	55
Figure 3.9 Schematic diagram of the cold cell coolant cooling system.....	57
Figure 3.10 Operating principle of Fast FID hydrocarbon emission analyzer.....	61
Figure 3.11 Operating principle of Fast CLD NO _x emission analyzer.....	62
Figure 3.12 Operating principle of DMS500 emission analyzer	64
Figure 3.13 Dilution system of DMS500 emission analyzer	65
Figure 3.14 Front panel and schematic diagram of the SPC emission analyzer	66
Figure 3.15 Structures of conventional and two-dimensional GC/MS	68
Figure 4.1 Profiles of engine torque, speed, and vehicle speed	75
Figure 4.2 (A) Air-Fuel Ratio and (B) EGR	76
Figure 4.3 (A) Boost pressure and (B) Injected fuel mass	77
Figure 4.4 Profiles of THC emissions.....	80
Figure 4.5 Profiles of CO emissions,	82
Figure 4.6 Profiles of engine coolant temperature	82
Figure 4.7 Profiles of NO _x emissions	85
Figure 4.8 Profiles of total particulate number	87
Figure 4.9 (A) AFR and (B) particulate number in the first 195 seconds.....	88
Figure 4.10 Profiles of accumulation particles	90
Figure 4.11 Profiles of nucleation particles	92
Figure 4.12 Profiles of particulate mass.....	93
Figure 4.13 3D Surface plot and contour plot of 20 °C cold NEDC sequence	96
Figure 4.14 3D Surface plot and contour plot of 85 °C warm NEDC sequence.....	97
Figure 4.15 2D-GC contour plots of diesel fuel and engine oil	98
Figure 4.16 Concentrations of n-Alkane series particulates of cold and warm NEDC	103

Figure 4.17 Concentrations of Alkyl-cyclohexane series particulates of cold and warm NEDC	104
Figure 4.18 Concentrations of PAHs of cold and warm NEDC	105
Figure 5.1 Schematic diagram of the air thermal heating system	111
Figure 5.2 Temperature profiles (A) intake air, (B) engine coolant and (C) engine oil	115
Figure 5.3 Engine speed and torque profiles at different intake air temperatures	117
Figure 5.4 Profiles of fuel injection quantity (A) instantaneous; (B) percentage of reduction using heating strategie.....	118
Figure 5.5 Total hydrocarbon emissisons at different intake air tempepratures	121
Figure 5.6 Nitrogen oxides emissisons at different intake air temepratures,	123
Figure 5.7 Particulate emissions at different intake air temperatures,	126
Figure 5.8 Particle size spectral density	128
Figure 5.9 Particle surface area at different intake air temperatures.....	129
Figure 5.10 Particulate mass characteristics with different intake air temperatures.....	131
Figure 5.11 Engine efficiency characteristics at different intake air temperatures.....	132
Figure 5.12 Overall engine efficiencies and emission characteristics at different intake air temperatures	132
Figure 6.1 Combustion profiles of diesel and biodiesel blends at (A) 1500RPM, 72Nm; (B) 1500RPM, 143Nm.....	139
Figure 6.2 Particle number concentrations of diesel and biodiesel blends under steady state	140
Figure 6.3 Particulate size distributions of steady state conditions	142
Figure 6.4 NO emissions of diesel and biodiesel blends under steady state.....	143
Figure 6.5 Total hydrocarbon emissions of diesel and biodiesel blends under steady state ..	144
Figure 6.6 Particle numbers for mode 1-3	145

Figure 6.7 (A) Diesel AFR and (B) Intake air with fuel injection for mode 1-3	146
Figure 6.8 EGR profiles for mode 1-3	147
Figure 6.9 NO emissions for mode 1-3	149
Figure 6.10 Fuel mass injected for mode 1-3.....	149
Figure 6.11 THC emissions for mode 1-3.....	150
Figure 6.12 Cumulative emissions for mode 1-3	151
Figure 6.13 Particle numbers for mode 2-3	152
Figure 6.14 Fuel mass injected for mode 2-3.....	153
Figure 6.15 NO emissions for mode 2-3	154
Figure 6.16 THC emissions for mode 2-3.....	155
Figure 6.17 Cumulative emissions for mode 2-3	155
Figure 6.18 Particle numbers for mode 2-4	156
Figure 6.19 NO emissions for mode 2-4.....	158
Figure 6.20 THC emissions for mode 2-4.....	158
Figure 6.21 Cumulative emissions for mode 2-4.....	159
Figure 6.22 Particle number of various acceleration timing transients.....	160
Figure 6.23 Mass of fuel injection of various acceleration timing transients	161
Figure 6.24 Intake air mass flow of various acceleration timing transients.....	161
Figure 6.25 EGR of various acceleration timing transients	162
Figure 6.26 NO emissions of various acceleration timing transients.....	163
Figure 6.27 THC emissions of various acceleration timing transients	163
Figure 7.1 Instantaneous EGR profiles	172
Figure 7.2 Intake air mass flow profiles	174
Figure 7.3 Fuel injection quantity profiles.....	175
Figure 7.4 Air-fuel ratio profiles.....	177

Figure 7.5 Total hydrocarbon (THC) emissions profiles	178
Figure 7.6 NOx emissions profiles.....	180
Figure 7.7 Total particle number profiles	182
Figure 7.8 Cumulative results for the particulate, NOx trade-off.....	183
Figure 7.9 Cumulative emission variations between optimized and reference sequences	185
Figure 7.10 Dynamic particle distribution behaviours of reference and optimized sequences	187

List of Tables

Table 1.1 European Union emission standards for diesel passenger cars.....	3
Table 3.1 Diesel engine specifications.....	45
Table 3.2 Specifications of the dynamometer for biodiesel experiments.....	48
Table 3.3 Pressure transducer specifications	50
Table 3.4 Properties of the tested biodiesel fuels.....	52
Table 3.5 Specifications of the cold cell dynamometer	54
Table 3.6 Specifications of the AVL air combustion system.....	56
Table 3.7 Properties of winter diesel fuel used in the cold cell facility	60
Table 3.8 Specifications of fast diagnostic equipments	63
Table 4.1 Alkanes compositions of SVOCs in particulate emissions.....	99
Table 4.2 Alkyl-cyclohexane compositions of SVOCs in particulate emissions.....	100
Table 4.3 PAH compositions of SVOCs in particulate emissions	101
Table 6.1 Engine test conditions	137
Table 7.1 Optimized two steps incremental transient EGR test sequences	170

List of Publications

Published Journals:

1. **Tian, J.**, Xu, H., Ghafourian, A., Liu, D. et al., "Transient Emissions Characteristics of a Turbocharged Engine Fuelled by Biodiesel Blends," *SAE Int. J. Fuels Lubr.* 6(2):457-465, 2013.
2. **Tian, J.**, Xu, H., A.S. Ramadhas, Liu, D., Low Temperature Effects on a Modern Turbocharged Diesel Engine Running on emission driving cycle, *SAE Int. J. Fuels Lubricants*, 7:726-736, 2014; doi:10.4271/2014-01-2713
3. **Tian, J.** Lu, G., and Xu, H., Incremental variable EGR strategy for optimizing transient emissions of turbo-charged diesel engines, Transactions of CSICE. (Submitted in May 2015)
4. Liu, D., Xu, H., **Tian, J.**, Tan, C. et al., "Cold and Warm Start Characteristics using HVO and RME Blends in a V6 Diesel Engine," *SAE Int. J. Fuels Lubr.* 6(2):478-485, 2013.
5. Sakunthalai, R.A., Xu, H., Liu, D. and **Tian, J.**, "Cold Start of Diesel Engines and its Control Strategies" International Journal of Green Energy, accepted at Feb, 2014.
6. Tan, C., Xu, H., Shuai, S., Ghafourian, A., Liu D. and **Tian, J.**, "Investigation on Transient Emissions of a Turbocharged Diesel Engine Fuelled by HVO Blends," *SAE Int. J. Engines* 6(2):1046-1058, 2013.
7. Wang, Z., Ding, H., Wyszynski, M., **Tian, J.**, Xu, H., "Experimental study on diesel fuel injection characteristics under cold start conditions with single and split injection strategies" *Fuel Processing Technology* Volume 131, 2015, Pages 213–222

SAE Technical Papers:

1. Liu, D., Xu, H. Sakunthalai, R.A. and **Tian, J.**, "Investigation on the performance of a diesel oxidation catalyst during cold start and warm start at low temperature conditions," SAE 2014 International Powertrain, Fuels & Lubricants Meeting, 2014-01-2712
2. Sakunthalai, R.A., Xu, H., Liu, D. and **Tian, J.**, "Impact of cold ambient conditions on cold start and idle emissions from diesel engines," SAE 2014 International Powertrain, Fuels & Lubricants Meeting, 2014-01-2715.
3. Tan, C., Xu, H., Ma, H., **Tian, J.** et al., "A Study of Methodology for the Investigation of Engine Transient Performance," SAE Technical Paper 2014-01-2714, 2014, doi:10.4271/2014-01-2714.

Conferences/Symposiums:

1. **J. Tian**, Hongming Xu, Y, Zhang, Z. Liang, M.S. Alam, C. Starck, R.M. Harrison. "Ambient Temperature Impacts on Diesel Engine Particulates using Fast Diagnostic and 2-dimensional GC Analyzers under Transient Operating Conditions" UnICEG 2015, JCB
2. **J. Tian**, Hongming Xu, A.S. Ramadhas, Dai Liu, C. Tan. Influences of cold ambient temperature on particulate emission under transient operating condition, SAE Outlook for Future Engines/Fuels & Future Engineers Symposium, Birmingham, UK, 23 Oct 2014

CHAPTER 1

INTRODUCTION

1.1 RESEARCH BACKGROUND

The following sections present the important background and concerns for current diesel engine developments. The latest emissions' legislation, modern technologies in diesel engines, as well as the transient and cold start issues, are introduced in the following sections.

1.1.1 Energy Shortage and Engine Emission Legislation

With the development of economy, science and technology, fossil fuels are widely used by internal combustion engines for energy conversion and have contributed to an increasing proportion of the greenhouse gas at present, as illustrated in Figure 1.1. Herzog et al. (2005) claimed that in 2004 approximately 10% of greenhouse gas was contributed by automobile transportation. In 2013, road transportation accounted for over 70% of the total transport energy consumption in the UK (Prime et al. 2014). The first concept of the diesel engine was invented by Rudolf Diesel in 1890. As there has been growing concern regarding energy shortages, diesel engines have been given increasing attention because of their high thermal efficiency, great torque performance at low engine speed and low carbon monoxide or hydrocarbon emissions (Stone 1999).

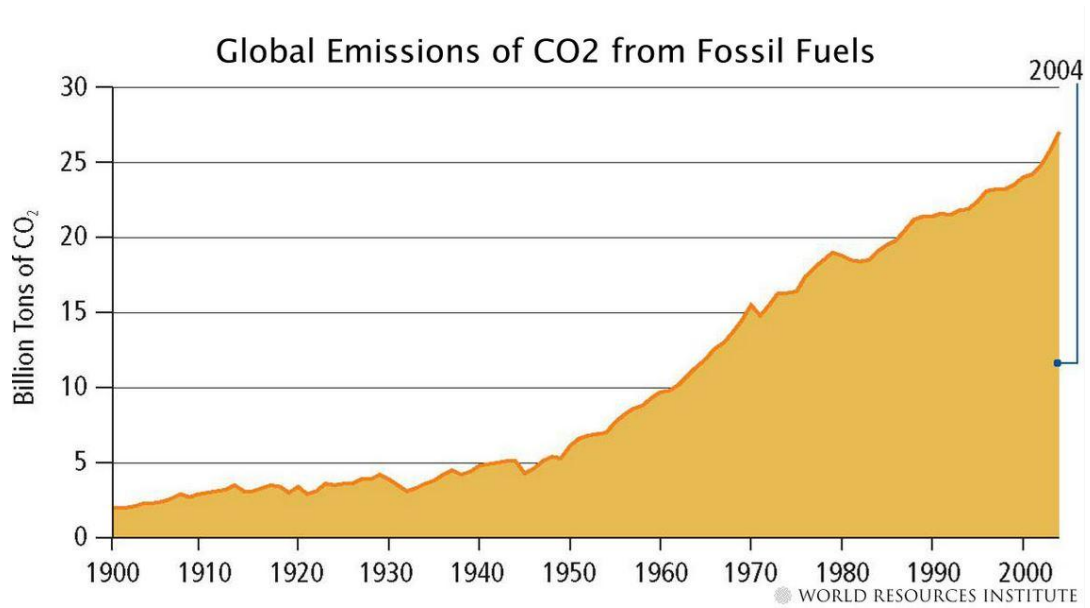


Figure 1.1 Global CO2 emissions caused by fossil fuels (Herzog, 2005)

Due to the growing environmental concerns, the first engine emission standard in Europe, EURO 1, was published in 1992 by the European Union. Since then the emission standard has become more stringent over the last two decades. Table 1.1 presents the emission standards for diesel passenger cars from EURO 1 to EURO 6. The current emission standard, EURO 6, was introduced at an obligatory level in 2014. The particulate matter emissions in mass have been severely restricted since 1996. In 2011, the particulate number was implemented in the emission standard for further particulate restrictions. The New European Driving Cycle (NEDC) (Figure 1.2) is currently used as a standard driving cycle in the emission regulation tests to represent the usage of typical vehicles' daily driving in Europe. It consists of four Urban Driving Cycles (UDC, 195 seconds each) and one Extra Urban Driving Cycle (EUDC, 400 seconds). Currently, the -7 °C cold ambient NEDC legislation is focused on gasoline vehicles. This is supposed to be applied on diesel vehicles in the near future.

Table 1.1 European Union emission standards for diesel passenger cars (Category M)

Stage	Year	Gaseous Emissions			Particulates	
		CO	HC	NO _x	PM	PN
		g/km				#/km
Euro 1	1992	2.72 (3.16)	-	-	0.14 (0.18)	-
Euro 2, IDI	1996	1.0	-	-	0.08	-
Euro 2, DI	1996	1.0	-	-	0.10	-
Euro 3	2000	0.64	-	0.50	0.05	-
Euro 4	2005	0.50	-	0.25	0.025	-
Euro 5a	2009	0.50	-	0.18	0.005	-
Euro 5b	2011	0.50	-	0.18	0.005	6.0×10^{11}
Euro 6	2014	0.50	-	0.08	0.005	6.0×10^{11}

Data adapted from: DIESELNET.com

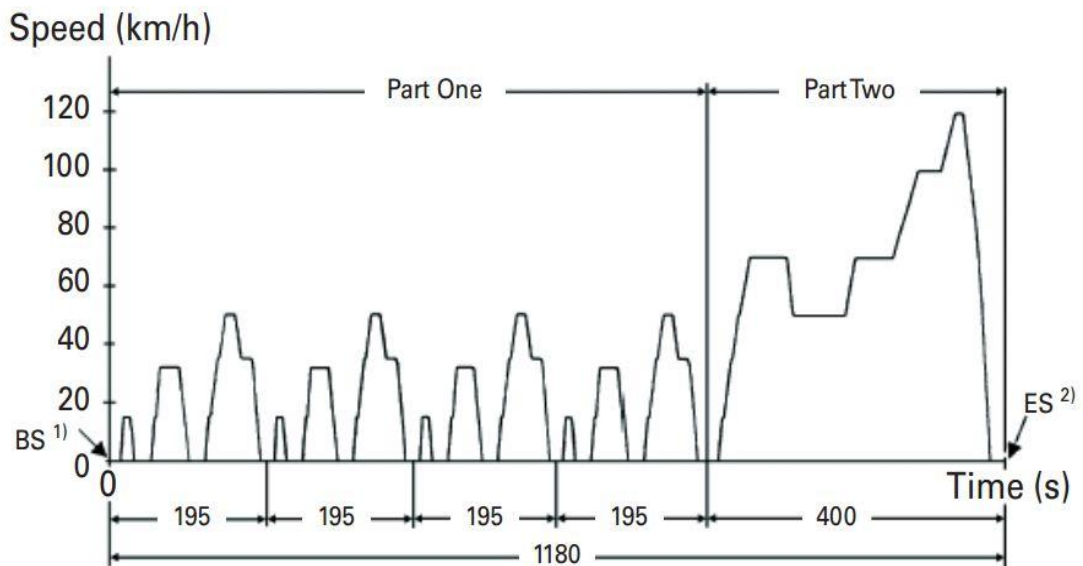


Figure 1.2 Characteristics of New European Driving Cycle

1) BS: Beginning of Sampling, engine start 2) ES: End of Sampling

Figure source: Delphi 2015

1.1.2 Modern Diesel Engine Development

Due to combustion requirements, the compression ratio of diesel engines is generally higher than that of gasoline engines. The value is set between 12 and 24 because of the restrictions of the peak in-cylinder pressure and the cold start performance (Stone 1999). Diesel engines have lower fuel consumption and are more efficient than gasoline engines. This can be contributed to their lower operating engine speeds, lower friction lose and higher compression ratio characteristics.

The basic operation of diesel engines can be summarized in the following steps. The inlet air is inducted into the engine cylinders through the intake valve during induction stoke. It is then compressed by the moving pistons to produce highly pressurized hot air for combustion. The liquid fuel is injected into the cylinder chamber by the high injection pressure around the top dead centre (TDC). Then, the injected fuel undergoes atomization, evaporation and aerodynamic interaction processes to form a combustible fuel/air mixture for self-ignition and multi-point combustion. The rapidly increased in-cylinder pressure forces the piston to move forwards to the bottom dead centre (BDC) to complete a power stoke. After that, the piston moves towards the TDC again to remove the residual gas and finish one operating cycle.

Considering the aspects of energy consumption and CO₂ emissions during a diesel engine's operating life, the down-sizing of the engine has been widely explored by researchers and automobile manufacturers (Terdich et al. 2011). The down-sizing concept is usually combined with the super- or turbo-charging boosting techniques to provide better power output and fuel economy. A diesel engine is suitable to be equipped with these boosting systems due to its absence of throttling, lean burning, less sensitivity of the air-fuel ratio and lower pumping loss characteristics (Rakopoulos, Giakoumis 2009).

To fulfil the stringent emission legislation, modern diesel engines are equipped with various techniques in terms of injection systems, engine configurations and after-treatment systems. As can be seen from Table 1.1, the NO_x and particulate matter are the most crucial emissions that need to be considered for diesel engine development and research. A common rail high pressure injection system and diesel particulate filter (DPF) after-treatment system are utilized to improve the fuel atomization and particulate emissions. The NO_x emissions can be effectively controlled by an exhaust gas recirculation (EGR) system and ammonia or urea based selective catalytic reduction (SCR) after-treatment system within a tolerance level. A diesel oxidation catalyst (DOC) is used to oxidise the unburned hydrocarbons or incomplete combustion products. A variable geometry turbocharger (VGT) system is used to improve the engine power output and fuel economy. A precise ECU control system can provide optimized control strategies for diesel engine operations. At present, more than half of the emissions of the modern diesel engine have been reduced compared to its emissions of a few years ago (Rakopoulos, Giakoumis 2009).

Biodiesel is the most commonly used alternative fuel in diesel engines. It can be produced either from traditional oil crops (such as rapeseed, palm, soybean) or from a new concept of crops (such as jatropha). It is suitable to be blended with mineral diesel at any blending ratio. The blended fuels can be used in diesel engines without any further engine modifications. Figure 1.3 shows the renewable energy share of the transportation sector in EU countries. In Europe, the low blending ratio biodiesel fuels (approximately 4-7% FAME) have already been brought onto the market. In 2009, the European Parliament and Council passed an ambitious policy of a “renewable energy directive” (RED) to raise the renewable energy share to 10% of the total energy usage in the transportation sector in 2020 (Kampman et al. 2013).

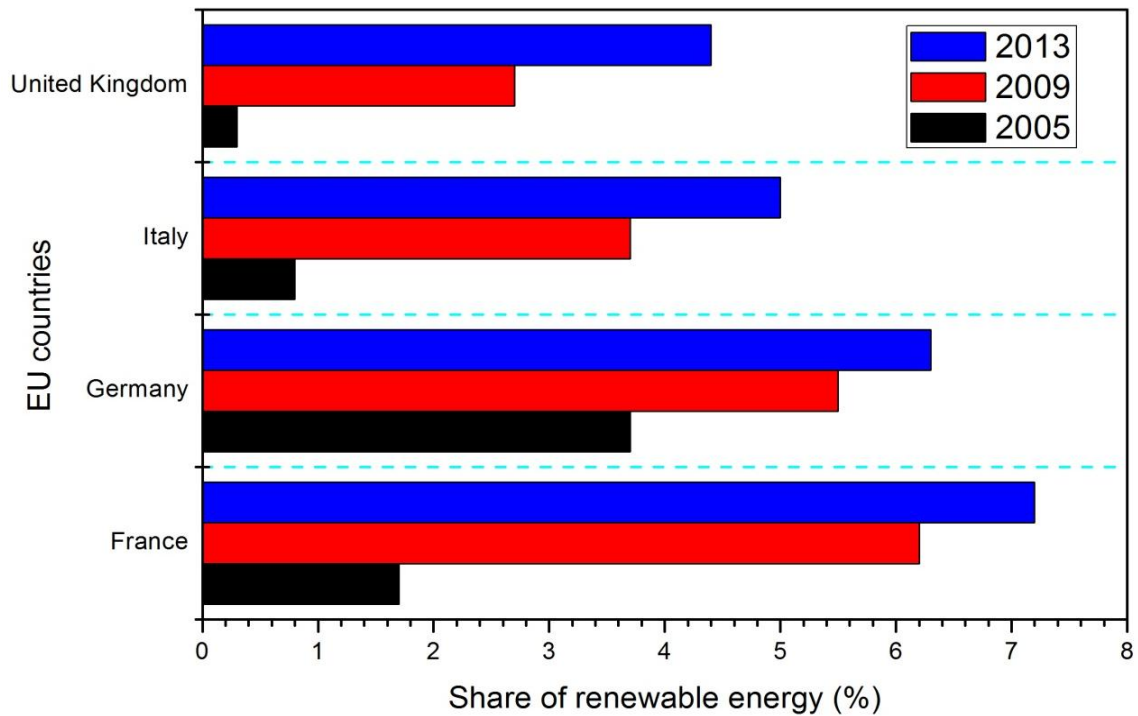


Figure 1.3 Share of renewable energy in fuel consumption of transport in EU countries

Data adapted from: EUROPA

1.1.3 Diesel Engine Transient and Cold Start

Engine transients are the most commonly used operating conditions during real driving. The emissions under transient operating conditions are the comprehensive interaction results affected by the various instantaneously changed engine parameters. The mismatch between those suddenly changed engine parameters may, to some extent, significantly deteriorate the engine's transient performances and emissions. This issue is more dominant for diesel engines due to the additional turbocharger system. Generally, the fundamental principle for engine calibrations is to ensure the necessary engine power output and reduce the fuel consumption and emissions as much as possible. However, the traditional calibration look-up

table is only focused on the steady-state conditions. It is used to combine with the basic proportional-integral-derivative (PID) control to optimize the transient performances. Currently, the automobile manufacturers are keen on researching the improvement of engine transient behaviours because of the even more stringent emission legislation for the next generation of the transition driving cycle (Worldwide harmonized Light vehicles Test Procedures, WLTP).

Cold start is a specific transition phase which accounts for a large proportion of emissions during a transient sequence. This critical transition phase ($-7\text{ }^{\circ}\text{C}$) has been amended to become part of the new emission legislation driving cycle by the European Union. Diesel engine combustion is self-ignited by the high temperature and pressurised compressed air at the end of the compression stroke. As a consequence, the success of diesel engine combustion is highly dependent upon the fuel's properties and the environment temperature (Pace & Presti 2011, Kim et al. 2012). During an engine cold start the low fuel and engine temperature adversely affect the capability of the fuel atomization and evaporation and make the engine difficult to start. On the other hand, the tendencies for engine down-sizing and the reductions of the compression ratio worsen the engine cold start performances (Nanba et al. 2013).

1.2 RESEARCH OBJECTIVES AND APPROACHES

The objective of this thesis is to experimentally investigate the different transient behaviours of a commercial diesel engine. The main purpose is to use comprehensive approaches to optimize the transient engine performances and emissions. The approaches of the research are summarized as below:

- Studying the ambient temperature's impact on the engine performances and emissions over a regulated transition cycle.
- Using a 2D-GC/MS technique to analyze the chemical components of the semi-volatile particulate emissions.
- Using thermal inlet air heating strategies to improve the transient behaviours at a sub-zero temperature environment.
- Investigating biodiesel (RME) and its blending fuels' impacts on steady state and transition conditions in terms of combustion and emission characteristics.
- Creating a novel incremental EGR transient calibration control strategy to optimize the engine emissions during discrete transient conditions.
- Commissioning the specifically designed climatic controlled transient test rig at the University of Birmingham to approach the transient research.

1.3 THESIS OUTLINE

In this thesis, the research work is focused on the investigations and solutions of diesel engine transient performances and emission issues. The main contents consist of eight chapters and the thesis structure is presented as follows.

This present Chapter 1 gives the general background information and research motivations for this thesis. It also introduces the latest advanced engine techniques, the importance of transient and cold start research, as well as the potential issues.

Chapter 2 reviews the literature studies of all the relative works presented in this thesis. The emissions' formation mechanisms, particulate chemical features, combustion and emission characteristics of biodiesel, diesel engine transient behaviours and cold start phenomena are all introduced as a basic acknowledgment for the research.

Chapter 3 describes the experimental setup and apparatus based on the two transient test rigs used in this thesis. The engine control systems, emissions' measurement devices, climatic control systems and data analysis are considered in detail in this chapter.

Chapter 4 can be divided into two sections. The first section studies the low environment temperature impact on a NEDC transient cycle. The second section uses 2D-GC/MS to analyze the particulate chemical components of NEDC cycles with cold and warm start strategies.

Chapter 5 presents the potential use of intake air heating strategies at low ambient temperature conditions over a regulated driving cycle. The evaluations are discussed in terms of reducing the engine-out emissions and improving the engine's efficiency.

Chapter 6 discusses the effects of four blended biodiesel fuels on the engine-out emissions under steady state and acceleration transient operations. Evaluations of the turbo-lag issue are

given by varying the transition timing to further investigate the elimination of the transition particulate spikes.

Chapter 7 introduces an incremental time-variable EGR reduction strategy to improve the transient performances and emissions. The novel strategy can significantly reduce the instantaneous particulates' emission spikes while maintaining the NO_x emissions within a tolerance level.

Chapter 8 summarizes the important findings of the diesel engine transient research. Potential solutions and suggestions of the transient study are given for further investigations.

CHAPTER 2

LITERATURE REVIEW

The main purpose of this chapter is to review the existing literature and to obtain better understanding for the relevant studies in this thesis. The chapter consists of the formation mechanisms of regular diesel engine emissions; biodiesel characteristics and emissions; the phenomena of a diesel engine's cold start and transient operating conditions; and introductions of exhaust gas recirculation (EGR) with the new concept of combustion modes.

2.1 FORMATION MECHANISMS OF DIESEL ENGINE EMISSIONS

At present, the EU emissions' standard regulates four kinds of typical engine-out emissions, namely: total hydrocarbon (THC), carbon monoxide (CO), oxides of nitrogen (NO_x) and particulate matter. Their formation mechanisms are introduced in the following section.

2.1.1 Total Hydrocarbons

Total hydrocarbon (THC) is also referred to as unburned hydrocarbon (UHC) in some of the articles and it can be used as an indicator of engine combustion inefficiency since it is the consequence of incomplete combustion (Raihan & Takimoto 2001, Heywood 1988). Hydrocarbon is one kind of gaseous emission. It remains at the vapour phase until partially agglomerated together and forms Soluble Organic Fraction (SOF) or is absorbed by soot to form non-volatile particles. It is worth noting that THC emissions are highly dependent on

the degree of fuel oxidization. Fuel-air mixing, combustion temperature, fuel impingement and fuel evaporation are the important factors that could affect the degree of fuel oxidization.

During the combustion process, an over-lean mixture or over-rich mixture will result in incomplete combustion, which favours hydrocarbon formations. The over-lean mixture represents the fuel-air mixture below the lean flammability limit; whereas an over-rich mixture means the fuel is not sufficiently mixed with the air and over the limitation of the combustion. The latter may convert to a combustible mixture to support the propagating flame according to the ignition delay, surrounding temperature and other combustion parameters (Heywood 1988). Additionally, the hydrocarbon emissions are very sensitive to the cold ambient temperature especially during engine cold start due to combustion misfire and poor evaporation. This will be explained in the later part of the thesis. Furthermore, the fuel injection impingement onto the cylinder wall or flame quenching is also important for hydrocarbon formation.

2.1.2 Carbon Monoxide

The formation of carbon monoxide emissions is similar to that of the hydrocarbon emissions. It is a production of incomplete combustion and favours both local fuel rich and lean regions. In the fuel rich region, the fuel is not mixed well with the air; therefore, partially mixed fuel cannot react with sufficient oxygen to complete carbon oxidation and finally results in CO emissions. On the other hand, low local temperature in the fuel lean region will result in incomplete carbon dioxide conversions. However, different sensitivities of the CO emissions' formation are founded between the above two circumstances. Compared to a fuel rich mixture, the CO concentration in a fuel lean mixture is more stable and not sensitive to the

fuel-air equivalence ratio (Heywood 1988). In diesel engine combustion, the equivalence ratio is always under a stoichiometric condition, thus the CO emissions are expected to be lower than in a spark ignition engine. Nevertheless in cold ambient temperature, poor cold temperature fluidity, evaporation and other properties of diesel fuel may influence, as expected, significant CO emissions compared with gasoline engines.

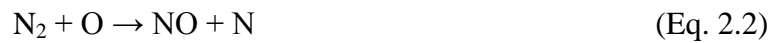
2.1.3 NOx Emissions

NOx for diesel engine emissions mainly consists of primary NO, a small amount of NO₂ and sometimes a negligible amount of N₂O, N₂O₅ and NO₃ (Hoekman & Robbins 2012). In diesel engines, the NO emissions account for nearly 70% - 90% of the total oxides of nitrogen (Jothithirumal & Jamesgunasekaran 2012). The formation mechanisms of NOx are complex and changeable. Three primary formation mechanisms of NOx were concluded by researchers, namely: thermal, prompt and fuel (Saravanan et al. 2012, Hoekman & Robbins 2012, Sun et al. 2010, Mohammadi et al. 2012). The first thermal NOx mechanism is well recognized in most of the relevant literature in terms of two key factors that can be attributed to the NOx formation, i.e. high local temperature and oxygen availability. This can be proved by Equation 2.1, in which the NO formation rate is in the unit of mol/cm³s (Schonborn 2009, Heywood 1988).

$$\frac{d[NO]}{dt} = \frac{6 \times 10^{16}}{T^{\frac{1}{2}}} \exp\left(\frac{-69060}{T}\right) [O_2]^{\frac{1}{2}} [N_2] \quad (\text{Eq. 2.1})$$

Where T is the absolute temperature; O₂ and N₂ represent the concentration of oxygen and nitrogen respectively.

It can be concluded that the availability of oxygen and nitrogen in both fuels and atmosphere will determine the rate of NO formation in the high adiabatic flame temperature. The NO_x formation processes normally take place in the cylinder chamber when the in-cylinder temperature is in excess of 1800K-2000K (Figure 2.9) (Turns 1996, Jessica 2010, Jothithirumal & Jamesgunasekaran 2012). Hoekman & Robbins (2012) stated in their paper that the rate of NO_x formation was extremely high as the local temperature increased. The thermal NO_x is achieved based on the extended Zeldovich mechanism, whose reaction processes are listed as below:



Compared with the other two NO_x formation mechanisms, thermal NO_x was considered as the dominant part of the total NO_x emissions (Sun et al. 2010, Saravanan et al. 2012, Hoekman & Robbins 2012).

The second “fast” NO_x formation mechanism, prompt NO_x, is also referred to as Fenimore NO_x. Fenimore (1971) described the transient formation mechanism as an attack of carbon or hydrocarbon radicals reacted with the nitrogen in fuel rich regions, and the yield of production was more pronounced when the fuel-air mixture is over 1.3 stoichiometric. The first step expressions of the reaction are shown as below:



Schonborn (2009) gives the rest of the prompt NO_x formation reactions as:



The prompt NO_x tends to occur in rich mixture combustion due to the abundance of hydrocarbon fragments available to react with N₂ (Hoekman & Robbins 2012).

The third NO_x formation mechanism is called fuel NO_x. Unlike the first two formation mechanisms in which the nitrogen atom mainly comes from the atmosphere, the nitrogen atom of the fuel NO_x mechanism mainly comes from fuel containing nitrogen. Therefore, the fuel NO_x proportion tends to increase when the tested fuel contains more nitrogen atoms. This can be supported by Martin (1971) in his experimental results.

As has been discussed in the above section, NO_x is formed through a series of complex processes including engine combustion and fuel-air mixing. These factors are highly dependent on the engine operating parameters. The in-cylinder temperature is closely associated with the fuel injection strategy. It is believed by many researchers that the critical period of NO_x formation is between the start of combustion and several crank angles after the peak cylinder pressure (Saravanan et al. 2012, Heywood 1988). Therefore, there is an important relationship between the fuel injection strategies and the NO_x emissions. Generally, long ignition delay can improve the fuel-air mixture during the premixed combustion phase and therefore elevate both the premixed and the diffusion combustion temperature. Many researchers (Ueki 1999, Heywood 1988) suggested that the retarded injection timing could

lead to lower NO_x emissions due to the retarded combustion and lower peak temperature. Valentino et al. (2011) successfully used dieseline (gasoline mixed with diesel) to extend the ignition delay of combustion for the purpose of reducing the NO_x and particulate matter simultaneously in the combustion mode of partial premixed combustion ignition (PPCI).

Since the thermal NO_x occupies most of the total NO_x production and it is temperature dependent, therefore, the engine load may directly affect the NO_x emissions. Tan et al. (2012) found an increased NO_x emissions' trend as the engine load increased at a constant engine speed. Similar results were found by other researchers, such as Tan et al. (2013) and Liu et al. (2013). A diesel engine normally operates at lean burn combustion, thus a higher engine load will result in a higher injected mass of fuel which burns close to stoichiometric. Therefore, this leads to higher in-cylinder pressure and temperature. As a consequence, diesel engines' NO_x emissions should be proportional to the injected mass of fuel (Heywood 1988).

2.1.4 Particulate Matter

Diesel engines' particle matters mainly include two forms of particles, namely: volatile or soluble particles and non-volatile or non-soluble particles. The former type of particles is mainly composed of sulphate or nitrate and other organic fractions. The latter consists of carbonaceous soot and ash fraction (Eastwood 2008). The schematic diagram of typical particulates from vehicles is displayed in Figure 2.1. In order to facilitate academic research on the particles' emission, the particles can be divided into three different forms, which are: nucleation mode, accumulation mode and coarse mode.

The typical patterns of engine particulates' size spectral density with their concentration and diameter are presented in Figure 2.1. Nucleation mode particles include the particles mainly

composed of soluble or volatile organic fraction (SOF/VOF); which forms mainly from exhaust dilution and cooling processes by the small amount of fuel or evaporated lubricating oil which escaped the oxidation process (D.B. Kittelson 1999). Theoretically, SOF and VOF are not the same since SOF may still remain after the processing of solvent extraction (S Chuepeng et al. 2008). The particles in the nucleation mode are expected to be dominant under low engine operating conditions, low ambient temperature environments and cold starts.

Accumulation mode particles consist of many adhered together units which contain agglomerate with some volatiles absorbed on it. Coarse mode particles mainly consist of large size agglomerate as a unit core (slightly higher densified than the other particles) and volatile materials as an outer layer of adhesion (Eastwood 2008). This particle mode, however, is not always created in the same way as the above mentioned two particles. It is largely formed by mechanical grinding (Kittelson, 1999). Despite these three modes of diesel particles not actually existing in a diesel engine exhaust, researchers have still carried out a detailed scope of division for the purpose of research and measurement. Kittelson (1998) in his review paper described the definition of the particle size range as: nucleation mode from 5 to 50 nm; accumulation mode from 50 to 1000 nm and coarse mode as larger than 1000 nm. The total mass of the nucleation mode particles is smaller than the other two. However, it accounts for a bigger amount of the total particle number than the accumulation and coarse modes in diesel engines' emissions.

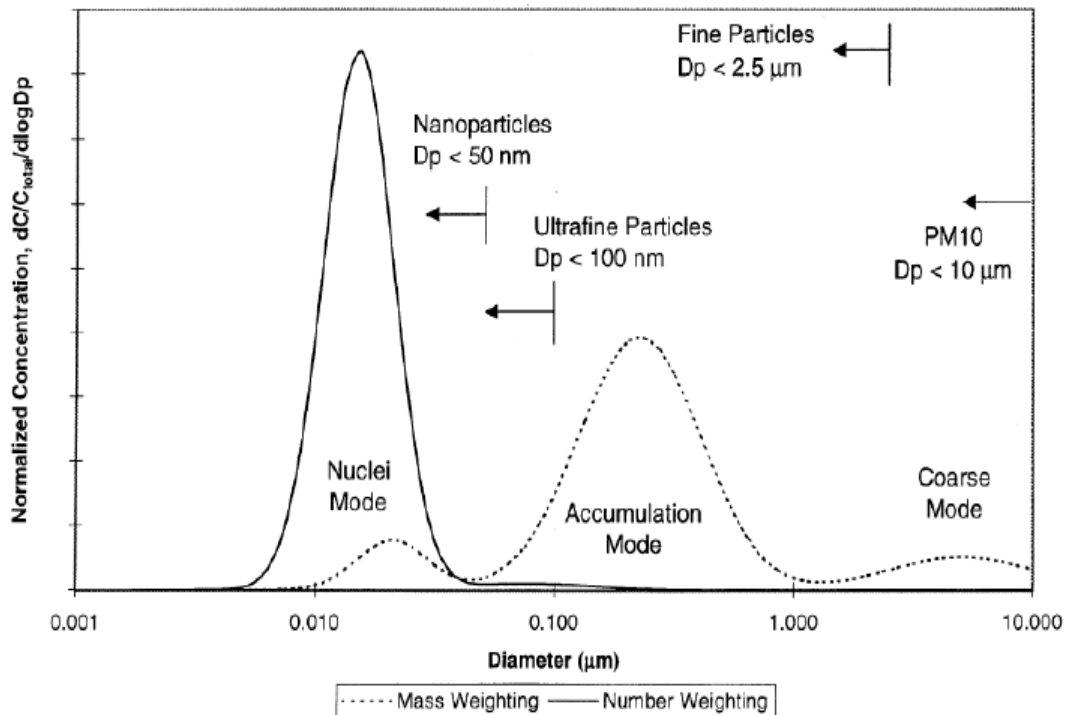


Figure 2.1 Particulate size distributions of exhaust gas particles

Figure adapted from: Kittelson et al. 1998

Diesel engine combustion is a rapid and complex process. At the beginning of the fuel injection, the outer layer of the injected fuel spray is oxidised by the inlet air; while the inner part of the injected fuel is isolated from the fresh air and will suffer pyrolysis in the high temperature environment. Generally carbon and hydrogen are the two basic elements in mineral diesel fuels. After the dehydrogenation and the ring-forming processes, the non-aromatic fuel molecules containing 12-22 carbon atoms will result in the formation of benzene with one aromatic ring (Eastwood 2008, Schonborn 2009). The benzene will grow bigger with the process of combustion to form the soot precursors often named as polynuclear aromatic hydrocarbons (PAHs). After a series of polymerisation, decomposition and nucleation, those precursors will become bigger and form particle nuclei, which are normally less than 3nm in diameter. With the combination of surface growth, coagulation, aggregation and oxidation these particles will eventually form soot during the engine combustion. Surface

growth can be described as hydrogen abstraction and carbon addition (HACA). Coagulation means the particle nuclei absorb smaller size PAHs to form the liquid layer outside nuclei. Aggregation means the formation of mature particles after the nuclei collide and merge into other particles. The particle structures from IC engines and their compositions are presented in Figures 2.2 and 2.3 respectively.

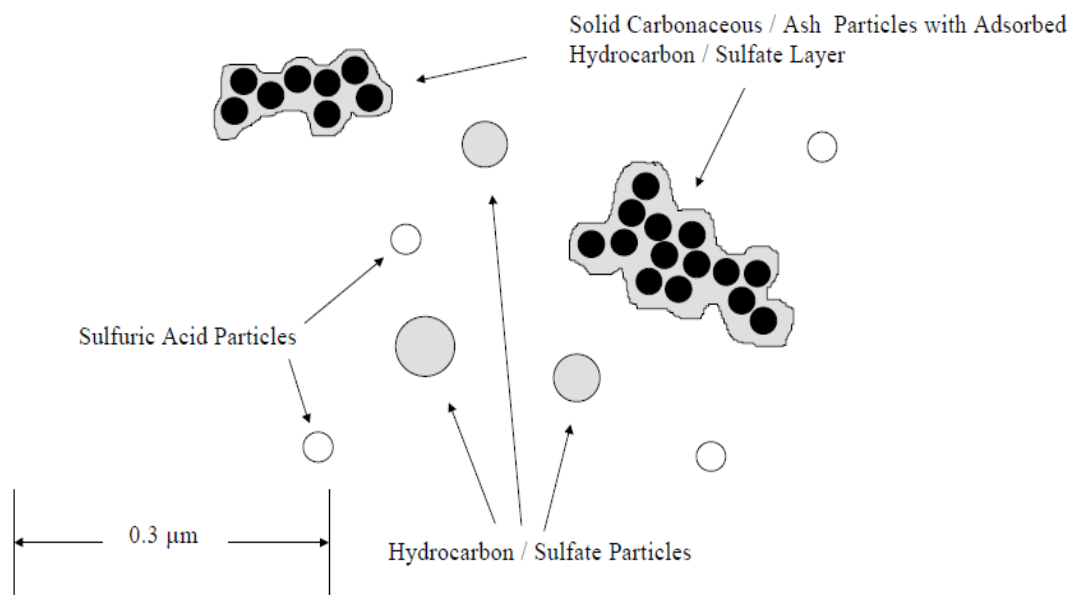


Figure 2.2 Typical particle structure emitted by internal combustion engines

Figure adapted from: Kittelson et al. 1998

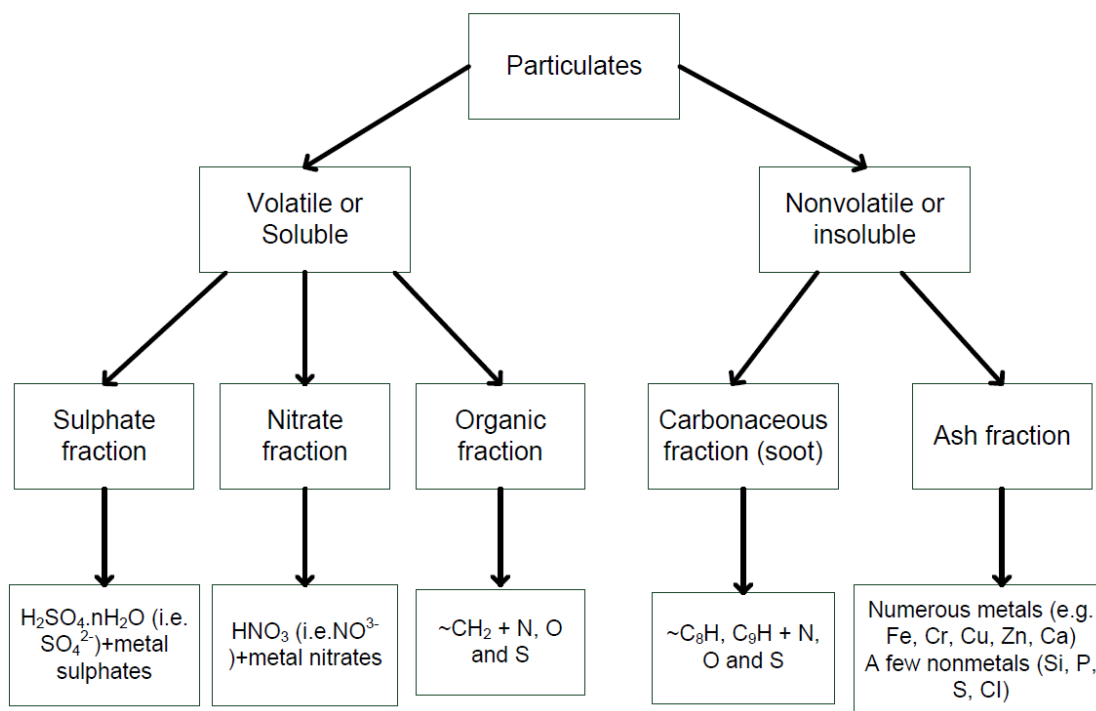


Figure 2.3 Conceptual model of particulate composition

Model adapted from: Eastwood et al. 2008

Many researchers have investigated the particulate matter emissions from diesel engines. Generally, the particulate emissions from diesel engines could be derived from both the fuel and the lubricating oil. Florio and Pellegrini (2012) researched the fuel properties' impact on the soluble organic fraction (SOF) and soot emissions from a diesel engine. The results showed that low cetane number (CN) increased the SOF emissions at low engine conditions due to the partial oxidation of fuels. Tan, Hu et al. (2013) investigated the particulate emissions from a heavy diesel engine fuelled with Jatropha Methyl Ester (JME). The results showed that biodiesel declined the total mass of PAHs by 8.57% compared to the mineral diesel fuel. The PAHs with three benzene rings like Acenaphthylene and Acenaphthene were not affected by the blended fuels. Williams (1987) studied the role of lubricating oil in diesel engine emissions from a Gas Chromatography (GC) analyzer. They concluded that the

lubricating oil contributed to about 40% of the total particulate emissions; whereas the value increased to around 70% when the engine operated at a low condition. Similar conclusions could be found from the studies of Abbass et al. (1990) and Andrews et al. (1999).

2.2 ALTERNATIVE FUELS FOR DIESEL ENGINES

Biodiesel is considered as a renewable energy source that is widely used for the substitution of mineral diesel fuel at present. The characteristics of biodiesel with its combustion and emission behaviours are introduced in the following section.

2.2.1 Characteristics of Biodiesel

Biodiesel diesel is also referred to as fatty acid methyl ester (FAME) that can be produced from the process of transesterification reactions with some base catalysts (Figure 2.4). The most commonly used reactants to produce FAME are triglycerides with long-chain fatty acids (R_1 , R_2 and R_3 in Figure 2.2) and alcohols. The former reactants can be obtained from vegetable oils or animal fats, whereas the latter can be ethanol or methanol (Al-Zaini et al. 2011). After the process of transesterification, the viscosity of the fuel can be reduced significantly; this makes the fuel have very similar properties compared to mineral diesel fuels. It needs to be mentioned that most of the commonly used FAMEs are generally defined as first generation biodiesel, where the FAMEs can be directly produced by normal feedstock, such as vegetable oils or animal fats. The second generation biodiesel is the group of FAMEs that are produced by some novel techniques or through pre-treatment procedures.

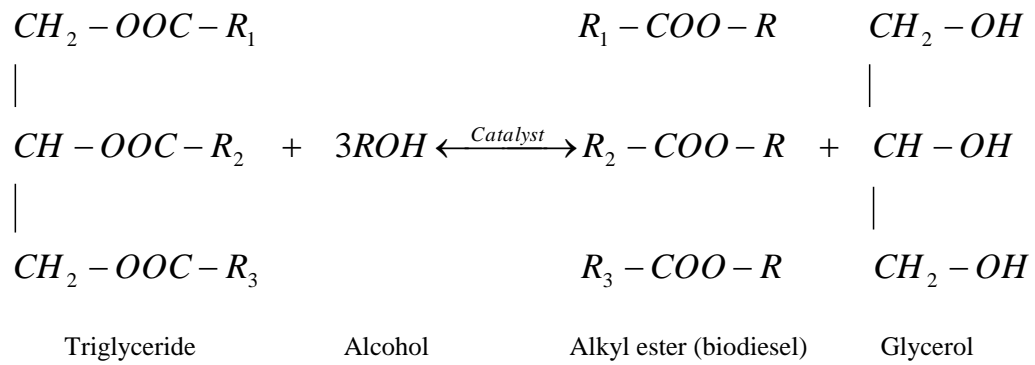


Figure 2.4 The transesterification process of biodiesel production

Figure adapted from: Demirbas et al. 2008

The cetane number (CN) of biodiesel is generally between 47 and 67 which is higher than that of mineral diesel fuels (40 to 57). The CN is an indicator to evaluate the capability of auto-ignition resistance of a fuel during the combustion process. It is determined by two chemical compounds of the fuel: hexadecane, with a CN of 100; and heptamethylnonane, with a CN of 15 (Demirbas 2008). The CN of a fuel used in diesel engines should fall in a proper range; either too high or too low will result in deteriorated combustion and emissions. A low CN will lead to ignition difficulty, which in certain cases may result in combustion misfire. Higher CN is favoured for engine cold start performances. However, when the CN is too high and over the limits, the fuel will not be allowed to have enough time to mix with the air and eventually this will lead to incomplete combustion and higher particulate emissions (Knothe et al. 2005).

2.2.2 Engine Performances and Emissions of Biodiesel

Compared to normal diesel, biodiesel properties like lower heating value, oxygen content, higher CN and viscosity can result in different engine performances and emissions. Many researchers have reported on the performances and emissions of biodiesel engines under both steady-state and transient conditions.

Bannister et al. (2010) investigated the impact of the biodiesel blending ratio on engine and vehicle performances and emissions at various ambient temperatures. The results show that increasing the biodiesel blending ratio caused a linear decrease of the engine maximum tractive force by up to 10%, due to the lower heating value. The same conclusion concerning the dropping power output of biodiesel is supported by Aydin (2010), Karabektas (2009), Ozgunay (2007) and Kaplan (2006). However, Yucesu (2006) claimed that the high viscosity biodiesel fuels' impact on fuel atomization may contribute more to the declined power output rather than the loss of heating value. The mass of the fuel injection is higher when the engine is running with biodiesel fuels compared with mineral diesel fuels. Apart from the above mentioned lower heating value of biodiesel, its high density properties can also contribute to the phenomena. At the same injection duration and pressure, higher fuel density will lead to higher mass of fuel injected in to the cylinder.

Many researchers reported that biodiesel will cause an advanced start of injection (SOI) due to the higher bulk modulus and viscosity (Szybist 2005, Monyem 2001). This combined with its high CN will subsequently result in the advanced start of combustion (SOC), which changes the combustion process close to the top dead center (TDC) and benefits by increasing power output (Altiparmak et al. 2007, Lapuerta et al. 2008). The engine parameters under biodiesel operation were also investigated by (Kawano 2006). They

researched the differences in the required injection timing between biodiesel and mineral diesel. Their results showed that injection timing was not affected by the high bulk modulus of RME in common-rail diesel engines.

Kawano et al. (2008), Savvidis et al. (2007) and Kousoulidou et al. (2009) researched the gaseous emissions of biodiesel under steady state conditions. The results indicated that biodiesel emitted lower THC and higher NO_x emissions at most engine conditions. The conclusions of the THC reduction by biodiesel were supported by Xue et al. (2011) in their reviewed paper. They summarized that nearly 90% of the academic studies came to the same conclusion. Most of the researchers found that the THC can be reduced up to 70%. Shahir et al. (2015) claimed in their reviewed paper that generally the THC emissions would reduce with the increase of the biodiesel blending ratio. However some researchers, for example, Sahoo (2009) observed a predictable THC emission trend with increasing the biodiesel blending ratio. This may due to the decreased air fuel ratio (AFR) at the local fuel rich region, which is caused by the increased fuel injection quantity.

The most commonly used explanations from the reviewed literature for increasing THC emissions of biodiesel fuel are listed as follows: the oxygen content of biodiesel provides extra available oxygen atoms at the fuel rich region to prevent incomplete combustion (Lapuerta et al. 2008, Tan et al. 2012 and Xue 2013). Furthermore, the high CN, advanced fuel injection timing and combustion phase are contributed to the THC emissions' reduction. Storey et al. (2005) and Armas et al. (2010) suggest that the THC emissions will reduce as the fuel injection timing is advanced.

The CO emissions had a similar trend to the THC as the biodiesel blending ratio increased. Kawano et al. (2008) investigated the biodiesel blending ratio's effects on the emissions of

transient and steady state conditions. The results show that the CO can be reduced significantly even only when mixed with a small amount of biodiesel. The oxygen content and lower carbon to hydrogen ratio of biodiesel can be used to explain the trend Xue et al. (2011). Moreover, the CO emissions are remarkably influenced by the corresponding engine load. The emissions of CO are increased with the increasing engine load due to the decreased AFR at a high engine condition (Agarwala et al. 2006).

The NO_x emissions of biodiesel have been investigated by many researchers and the results are varied due to the different engine configurations and parameters. McCormick (2012) reported that the NO_x emissions were almost the same as compared to the normal mineral diesel fuels. However, most of the literature reported that the NO_x emissions were elevated with the increasing of the biodiesel blending ratio in diesel engines (Figure 2.5). Many reasons are generally used to theoretically explain the increased NO_x phenomena. In the pump-line-nozzle (PLN) injection system, the injection timing is advanced which is caused by the high isentropic bulk modulus of the biodiesel fuel (Varatharajan 2012, Liu 2014). The less compressible property of biodiesel shortens the time period of the fuel delivery to the injector. However, Caresana (2011) studied the bulk modulus property of biodiesel's impact on the injection system in order to find the explanation for the NO_x emissions' tendency. The results found that the injection timing was not advanced as much as other researchers had expected.

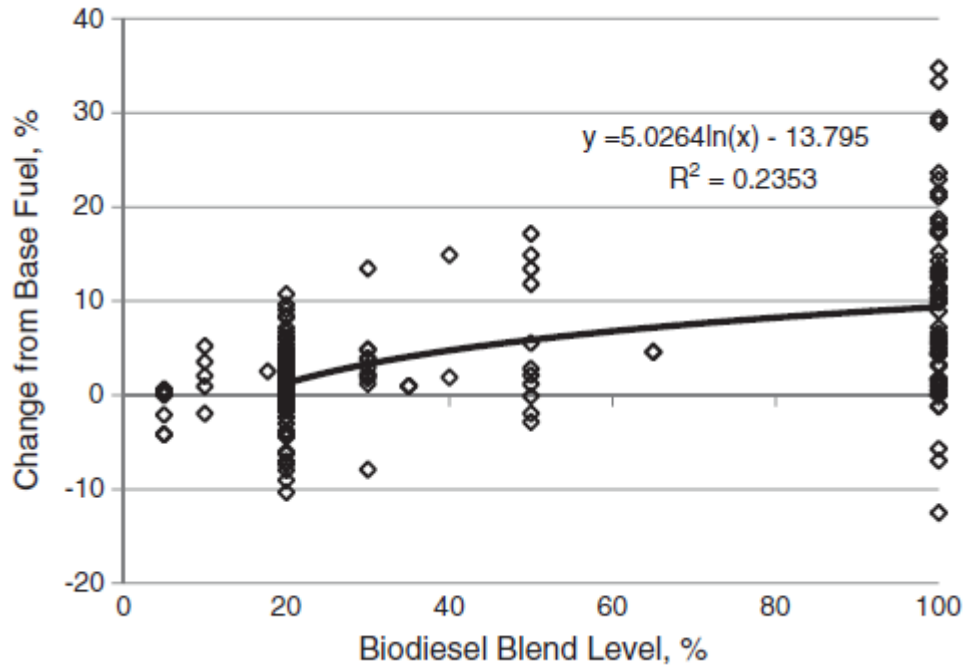


Figure 2.5 Comparison of the biodiesel blending ratio's effects on the NOx emissions with petroleum diesel

Figure adapted from: Hoekman et al. 2012

In modern common-rail diesel engines, the fuel injection strategy is dependent more upon the engine calibration than the fuel property. In this case, the reduced soot particle emissions of biodiesel fuels can be used to explain the increased NOx. Hoekman and Robbins (2012) and Cheng et al. (2006) reported that the soot particles are effective for the heat radiation; thus they could certainly reduce the flame temperature. Therefore, the decreased soot particles for biodiesel fuels can consequently lead to higher adiabatic flame temperature and NOx emissions. Furthermore, the biodiesel itself contains a higher fraction of unsaturated compounds, which has been shown as favourable for the promotion of adiabatic flame temperature and thus the NOx formation (Ban-Weiss et al. 2007). The shortened ignition delay period during combustion caused by the higher CN of biodiesel is presented by many researchers (Liu 2014, Hoekman and Robbins 2012) to explain the increased NOx emissions;

since the most crucial period of NO_x formation is between the SOC and several crank angles after the TDC (Saravanan et al. 2012).

Biodiesel and its blends have been reported by numerous researchers to produce a lower amount of particulate matter emissions compared with mineral diesel fuels (Agarwal et al. 2015, Kousoulidou et al. 2009, Wu et al. 2009, Tan et al. 2013). Kousoulidou et al. (2010) used PME (palm methyl ester) and RME (rapeseed methyl ester) blends in a light duty vehicle to detect the tailpipe particulate matter emissions. The soot emissions of PME and RME were reduced by 17 and 24% respectively, in relation to mineral diesel fuels.

On the other hand, Chuepeng et al. (2011) researched the particulate matters of RME blends (B30) under various steady-state engine conditions. They found that biodiesel produced a smaller average size of particles and higher particle number (PN) concentrations. The explanations for the elevated PN were described due to the high fraction of the SOF emissions. Similar results were claimed by Rounce et al. (2012) from their thermogravimetric analysis (TGA). They found that RME produced a lower amount of solid particles (less than half) and higher amount of liquid phase particles (SOF), compared with the ultra low sulphur diesel fuel. The decreased solid particles and increased SOF could probably be explained by the following reasons (Liu 2014, Moon et al. 2009): the oxygen contents of biodiesel improved the local fuel rich combustion to prevent the pyrolysis process for the soot formation; the reduced soot or solid particles decreased the surface area on which the low volatility unburned hydrocarbon would be absorbed.

The property of biodiesel has some significant influences on the particulate emissions. Wu et al. (2009) studied the relationship between particulate matter emissions and biodiesel properties. The results indicate that the extent of reduction of dry soot for biodiesel fuels is

greater than that of particulate matter. Viscosity has more dominant influence than oxygen when the engine operated at low engine conditions. Tan et al. (2013) studied the fuel properties effects on the engine transient particulate emissions. The results showed that the particulate matter decreased as the sulphur content decreased. Furthermore, the particulate emissions were decreased remarkably when running the engine with low aromatic content fuels; due to the higher carbon to hydrogen mass ratio of aromatic hydrocarbons compared to paraffin hydrocarbon. Nuskowski (2011) researched the cetane improver impacts on the particulate matter using heavy-duty diesel engines. The results showed that the use of cetane improving additives greatly reduced particles in terms of both the concentrations and mass.

Engine parameters also have critical effects on the particulate matter emissions of biodiesel fuels. Florio et al. (2011) investigated the engine load's impact on the particulate emissions. They found that low CN combined with low engine speed resulted in high emissions of SOF, which was detected by the presence of oxygenated species content derived from the oxidized fuel. Young et al. (2011) examined the non-volatile particulates' characteristics of a heavy-duty diesel engine between 10 and 1000nm at different engine conditions. The results showed that the total particle number could be increased from 25 to 75% as the load increased; whereas it could be reduced by up to 20% when increasing the blending ratio. In terms of fuel injection strategy, Yehliu et al. (2009) investigated the differences between single and split injection with constant SOI and EGR on biodiesel emissions. The results show that biodiesel increased the particle concentration at a low engine condition for single injection strategy due to the increasing SOF. However, the report claimed converse results for split injection strategy.

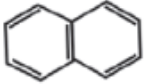
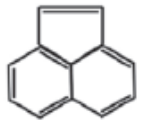
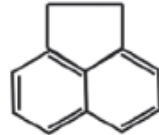
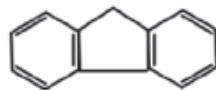
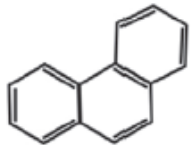
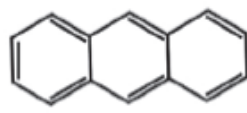
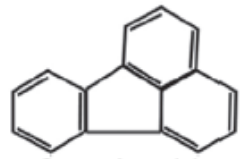
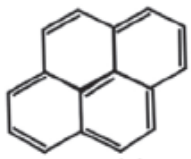
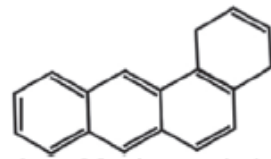
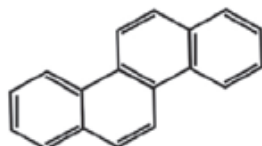
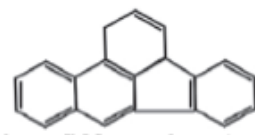
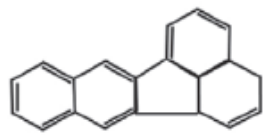
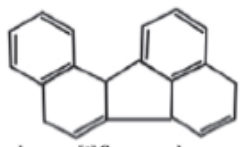
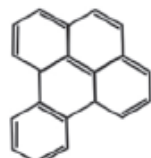
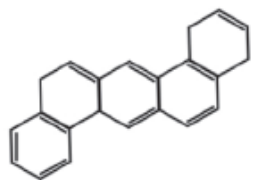
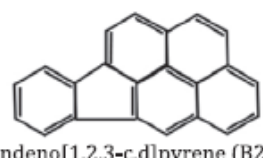
 naphthalene* $C_{10}H_8$	 acenaphthylene (D) $C_{12}H_8$	 acenaphthene $C_{12}H_{10}$
 fluorine (D) $C_{13}H_{10}$	 phenanthrene (D) $C_{14}H_{10}$	 anthracene (D) $C_{14}H_{10}$
 fluoranthene (D) $C_{16}H_{10}$	 pyrene (D) $C_{16}H_{10}$	 benzo[a]anthracene (B2) $C_{18}H_{12}$
 chrysene (B2) $C_{18}H_{12}$	 benzo[b]fluoranthene (B2) $C_{20}H_{12}$	 benzo[k]fluoranthene $C_{20}H_{12}$
 benzo[j]fluoranthene $C_{20}H_{12}$	 benzo[a]pyrene (B2) $C_{20}H_{12}$	 benzo[e]pyrene $C_{20}H_{12}$
 dibenz[a,h]anthracene (B2) $C_{22}H_{14}$	 benzo[g,h,i]perylene (D) $C_{22}H_{12}$	 indeno[1,2,3-c,d]pyrene (B2) $C_{22}H_{12}$

Figure 2.6 Priority list for polyaromatic hydrocarbons (PAHs)

Figure adapted from: Agarwal et al. 2015

The PAHs are harmful for human beings and generally considered as a soot precursor for the particulate matter research. They are also an important indicator to measure the level of the pyrolysis process for incomplete combustion (Abbass et al. 1990). Eighteen of thirty-two toxic PAHs published by the United States Environmental Protection Agency (USEPA) are

listed in Figure 2.6 (Agarwal et al. 2015). Lea-langton et al. (2008) investigated the PAH emissions of a heavy duty diesel engine with mineral diesel and biodiesels that were derived from waste cooking oil and rapeseed oil. They reported that biodiesel fuels notably reduced most of the abundant PAH species. Lower molecular weight PAHs, such as phenanthrene, fluoranthene and pyrene were the most abundant PAHs detected by the GC/MS analyzer. Since fluoranthene was absent from the fuel, thus it was considered to be produced by the pyrosynthesis process. This conclusion is also supported by (Karavalakis 2009).

2.3 DIESEL ENGINE TRANSIENTS

The emission characteristics of an engine during transient conditions have attracted attention from researchers in recent years because of stricter exhaust emissions legislation and the high frequency of occurrence of transients in daily driving. In this section, the characteristics of diesel engines' transient operation are introduced and analyzed, based on the previous literature.

2.3.1 Challenges of Transient Operating Conditions

The improved emission limits force vehicle manufacturers to put more effort into reducing the engine emissions especially for the transient research. The newly produced engines must experimentally qualify for the transition emission standards (Rakopoulos 2009, Kang et al. 2005, Hagen et al. 2006). The engine behaviours of transient operation are different from those of steady states. However, the limitations of laboratory engine control systems, fast response exhaust gas analyzers and testing equipment have left the research of engine

transients far behind the steady state engine studies. Traditionally, the majority of the engine calibrations are based on steady state conditions for the purpose of achieving the required engine output with optimized fuel consumption and emissions (Rakopoulos et al. 2009). Nevertheless, many researchers agreed that engine performances and emissions during transient conditions were even worse than their steady state performance due to sudden changes in engine parameters (Nuszkowski et al. 2008, Kang et al. 2005). This problem is more pronounced in turbocharged diesel engines, mainly because of the lag response of the turbocharger speed adjustment (Terdich et al. 2011). The schematic diagram of the turbo-lag issue caused by the acceleration process in turbocharged engines is demonstrated in Figure 2.7. During acceleration conditions, the fuel injections will adjust faster than other mechanical mechanisms according to the pedal position and calibration map. Due to the mass moment of inertia, mechanical fractions and air flow inertia of the engine components, the intake air flow is delayed compared to the suddenly increased fuel injections; this worsens the engine combustion and emissions, especially for the particulate matter and THCs (Hagena et al. 2006).

Generally, there are two typical transient patterns of experiments for research, i.e. engine cold or warm start as well as specific customized discrete or regulated driving cycle transients. Higher engine emissions and poor engine performances are expected during transient and cold start conditions. Figure 2.8 illustrates the series events of engine parameter changes and the basic processes of the emissions' generation during acceleration transients and cold start.

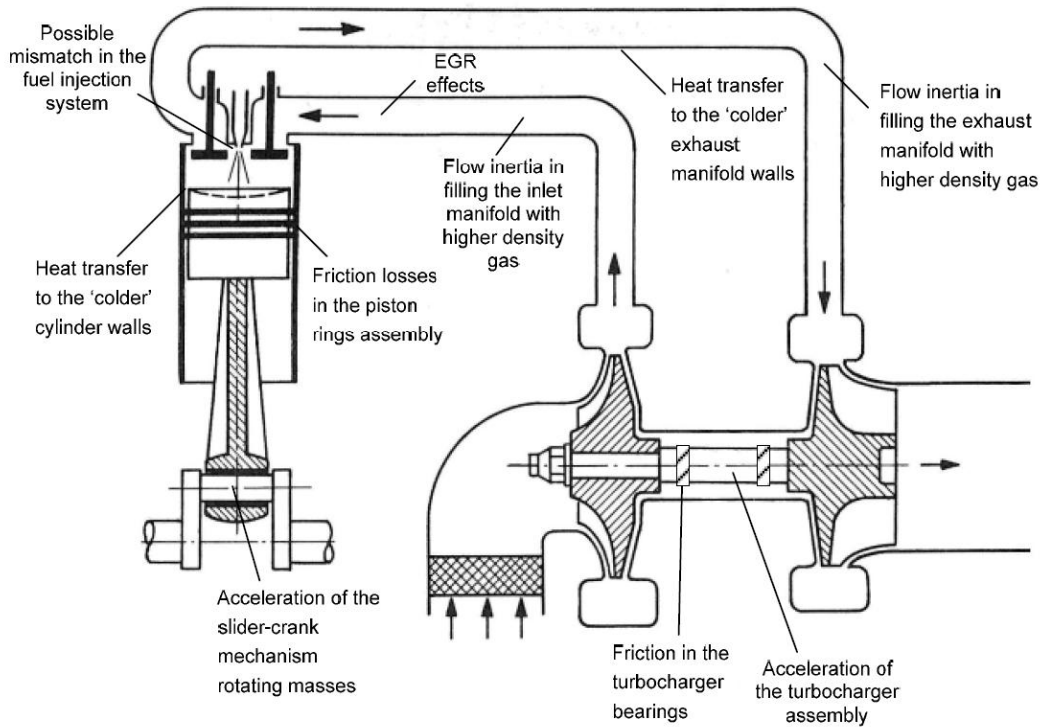


Figure 2.7 Schematic diagram of diesel engine transient turbo-lag phenomena

Figure adapted from: Rakopoulos et al. 2010

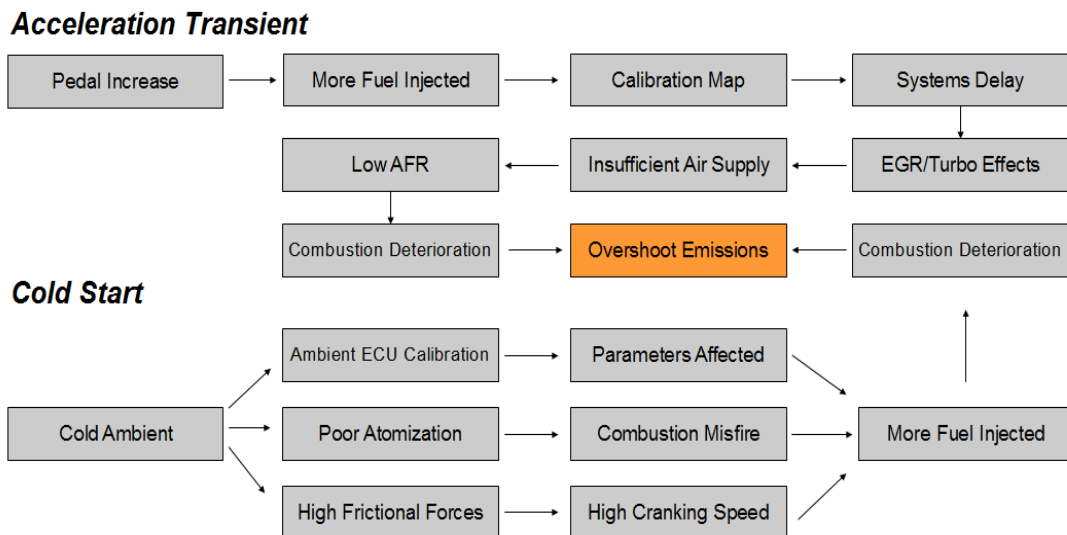


Figure 2.8 Schematic diagrams of series events during transient and cold start processes

2.3.2 Engine Transient Performances and Emissions

Many researchers have studied the instantaneous emissions during transient operating conditions. They claimed that turbo-lag is a critical issue for the emissions during transient operations (Hagena et al. 2006, Rakopoulos et al. 2010, Armas et al. 2013, Giakoumis et al. 2012). Figure 2.9 presents the most representative transient particulate matter and NO_x emissions during acceleration conditions.

Hagena et al. (2006) revealed that owing to the influence of turbocharger lag, both PM and NO_x emissions significantly increased in their V8 turbocharged engine when acceleration timing was shortened. Rakopoulos et al. (2010) investigated the gaseous and particulate emissions under different acceleration conditions. The results showed that turbo-lag was the main contributor causing the emission spikes during transient conditions. Lee and Choi (2002) optimized the transient responses of a turbocharged engine under aggressive acceleration conditions by using an extra amount of injection air into the intake manifold. The results found that the improvement is more pronounced at low engine conditions. NO, smoke and noise emissions of a diesel fuelled engine during transient conditions were also investigated by Rakopoulos et al. (2010). Their findings showed that harder acceleration could lead to a longer emissions transient period. Tian et al. (2013) investigated the size of particulate spikes during transience. The results showed that the initial engine condition determined the particulate transient size. The lower initial engine condition could result in the higher transient spikes. Moreover, the transient emission spikes are also highly dependent on the transient time interval. Tan et al. (2013) pointed out that it was increased with the decreasing transient time interval due to the delayed response of the turbocharger. Armas et al. (2013) tested their turbocharged engine under the NEDC and reported that THC, NO_x and particulates' spikes were always observed during the acceleration process.

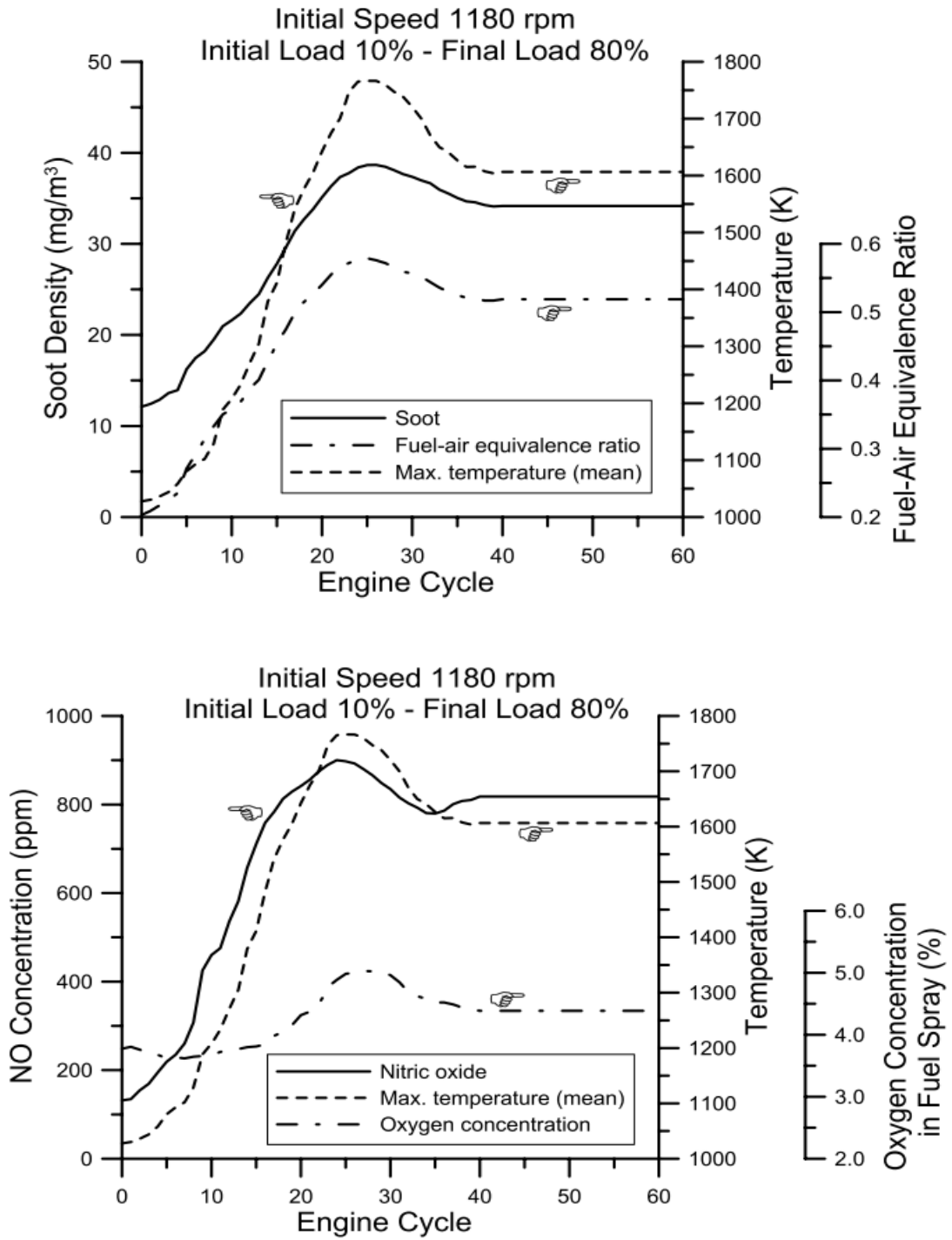


Figure 2.9 Typical engine performances and emissions during load increase discrete transient

For transient biodiesel engine studies, Jaroonjitsathian (2011) investigated the performance of a diesel engine in accelerating transient mode running with palm methyl ester (PME). Their results implied that biodiesel had poor engine driveability especially at low speed and a low load condition. Rakopoulos et al. (2010) studied the emissions of a biodiesel and n-butanol blend during transient conditions. They showed that NO peak values increased by approximately 52% and 35% and the smoke opacity decreased by around 40% and 73% respectively. Tesfa et al. (2010) have reported up to 17% higher NO_x emissions and 52% lower THC emissions for their engine running with biodiesel during transient conditions. Giakoumis et al. (2012) conducted a literature survey on biodiesel transient operations and they suggested that generally the PM and HC emissions tend to decrease; whereas NO_x emissions tend to increase as the biodiesel blending ratio increases. They also concluded that the NO_x and particulate matter emissions were significantly impacted upon by the fuel consumption or the average aggressive level of the driving cycle. Giakoumis et al. (2012) believed that the oxygen content of biodiesel blends is a key contributor for improving the soot oxidation process during turbo-lag periods.

2.4 DIESEL ENGINE COLD START

Diesel engine cold start is a vital segment for the research on transient conditions due to the remarkably elevated gaseous and particulate emissions; and also its notable accumulated emissions in the legislation emission standards (NEDC, FTP-75). This section gives an insight into the diesel engine cold start phenomena and analyzes the literature for some cold start solutions.

2.4.1 Characteristics of Cold Start

The engine cold start performances and emissions are highly dependent upon the properties of fuel, liberating oil, battery or starter conditions, fuel injection strategies and other engine parameters. The temperature and pressure also has significant impact on the cold start combustion performances. The following Arrhenius-type equation gives the relations between the ignition delay t_{id} and the temperature T and pressure P of the air (Heywood 1988):

$$t_{id} = A \cdot p^{-n} \cdot \exp\left(\frac{E_A}{RT}\right) \quad (\text{Eq. 2.11})$$

Where A and n are constant values dependent on the fuel properties; E_A is the activation energy for the fuel combustion; R is the universal constant value.

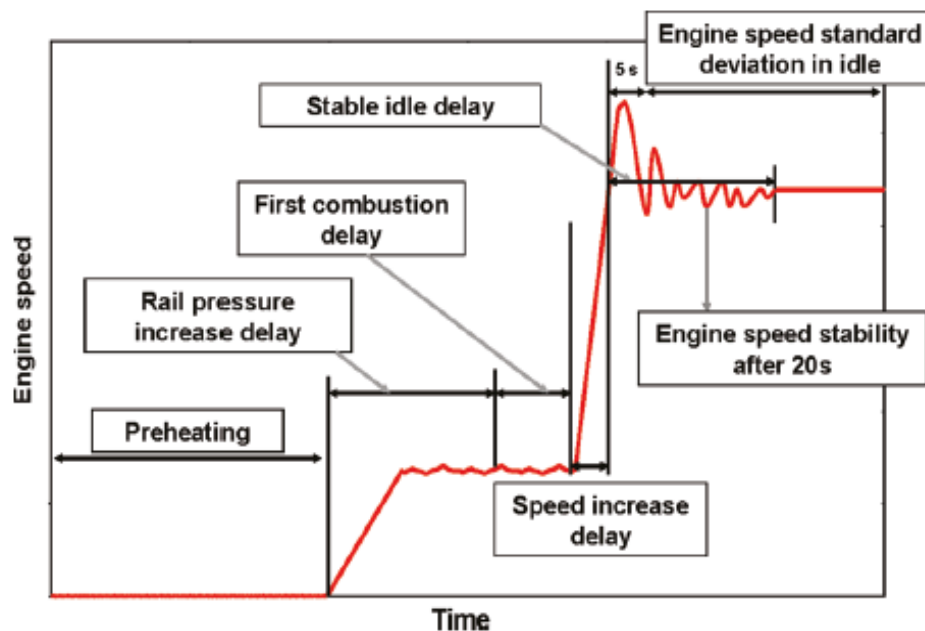


Figure 2.10 Typical cold start phenomena of engine speed

Figure adapted from: Starck et al. 2011

The typical engine speed characteristics during a cold start period are presented in Figure 2.9. Generally, an engine started at a low ambient temperature could lead to a longer cranking and starting time compared to that of a higher environment temperature (Last et al. 2008, Brown et al. 2007). In a severe cold environment, the poor battery performance will result in a lower cranking speed of the engine starter. Moreover, the increased frictions of the engine components and lubricating oil viscosity will cause a high demand of starting torque, high blow-by level as well as the excessive heat losses of the cylinders. These will lead to a low cranking speed during cold starts. However, due to the engine calibration characteristics, more fuel is injected into the cylinder during the cold start phase to ensure the start capability. Armas et al. (2013) conducted a comparison experiment between ambient cold start and warm start. The research pointed out that cold start would result in a 100 rpm higher idling speed than that at warm start, due to the calibrated injection strategy.

Furthermore, the poor fuel atomization and low combustion air temperature in certain cases may even result in combustion misfires. The fuel injection strategy may also influence the diesel engine cold startability (Osuka et al. 1994). The engine combustion could be improved significantly by injecting a small amount of pilot injection at the cold start phase to prevent the occurrence of the combustion misfire. All the above mentioned features can deteriorate the engine's cold start performances and emissions (Armas et al. 2013, Last et al. 2008, Payri et al. 2013, Will et al. 2011 and Pastor et al. 2009). On the other hand, as the engine downsizing concept becomes more attractive, the cold start issue is becoming of more concern to the researchers. The reduction of the compression ratio reduces the combustion temperature and worsens the cold start performances (Arumugam et al. 2015).

2.4.2 Cold Start Emissions

Liu et al. (2013) investigated the gaseous and particulate emissions of a commercial diesel engine under cold and warm start conditions. The result found significantly increased THC and particulate matter emissions and reduced NO emissions as the coolant temperature decreased. Similar results were also found by Lea-langton et al. (2009) and Bielaczyc (2013). Moreover, the cold start cumulative emissions are considered as decreased with the reduction in ambient temperatures (Zahedh et al. 1990).

The fuel properties' impact on the diesel engine's cold start performances were investigated by Starck et al. (2011) using RME and SME. The results demonstrated that the structure of the ester had no significant impact on the engine cold start behaviours. Moreover, the extensive usage of esters affected the fuel filter plugging capacity due to the depletion in saturated monoglycerides and saturated esters. The influence of the CN additives of a diesel engine's cold start was studied by Hara et al. (1999) using a single cylinder engine and with the environment temperatures ranging between -5 and 25 °C. The results showed that the startability was better as the CN increased. The combustion misfires and increased smoke emissions were observed when the environment temperature dropped more than 10 °C, and the misfires lasted for many cycles.

The EGR valve position performed an important role during engine starting. Armas et al. (2012) used their turbocharged diesel engine to investigate the relationship between the EGR valve and the environment temperature. They concluded that as the ambient temperature decreased the EGR valve was generally closed.

2.4.3 Cold Start Solutions

With the development of diesel engines' techniques and the stringent emission standards, the cold start issue is becoming more challenging. The improvement methods of a diesel engine's cold start could be based on both the engine calibrations and auxiliary devices.

The most frequently calibrated engine parameter for the improvement of a diesel engine's cold start is the fuel injection system. John et al. (2011) examined the cold startability of a 2.2L common rail direct injection diesel engine with various injection strategies. The results showed that a multiple injection strategy combined with starting aids with proper calibrations could significantly improve the combustion of cold start without instability. Zhong et al. (2007) claimed that with the implementation of a split-main injection strategy, a reduced in-cylinder gas temperature drop could be observed during the compression stroke, which consequently decreased the cold start cranking period.

For certain extremely cold environment cases, the engine can only be started with the combination of auxiliary heating assistants. At present, the most commonly used cold start aid in the commercial engine is the glow plug. Chartier et al. (2009) conducted a cold start at very low temperatures (-25 °C) on their optical diesel engine and reported that fuel was only likely to be ignited close to the glow plug with limited fuel evaporation ability at the cold ambient temperature. Royo et al. (2011) conducted a comparison between two different types of glow plugs. The report showed that the pollutant emissions are not highly related to the tip temperature or the uniformities of the glow plug. Higher emissions are detected for the glow plug with a bigger plug crevice.

2.5 EXHAUST GAS RECIRCULATION (EGR) AND DIESEL ENGINE COMBUSTION

The elevated NO_x and particulate matter emissions are considered as the most important critical issues for diesel engine development. Exhaust gas recirculation (EGR) is a mature approach applied in the current commercial diesel engines for the reduction of NO_x emissions. The evaluations of EGR utilization in terms of diesel engine emissions are introduced in the following section.

2.5.1 EGR and Combustion Modes

Many researchers have reported that the utilization of EGR technology was the most effective method to reduce the engine-out NO_x emissions (Reifarth et al. 2010, Kobayashi et al. 2011). Sun et al. (2013) found that the in-cylinder peak pressure and the maximum rate of pressure rise (RoPR) decreased with the increasing EGR rate. The maximum in-cylinder pressure and temperature reduced as the EGR rate increased, because of the increased heat capacity of the charging air; thus this was a advantage for NO_x formation. Furthermore, the availability of the oxygen content in the inlet air is replaced by the non-reacted CO₂ from the exhaust gas, which could also result in reductions of NO_x emissions (Rakopoulos et al. 2010). In addition, with the application of the EGR technique in the diesel engine, the combustion noise was significantly improved due to the prolonged ignition delay and reduced rapid combustion (Liu et al. 2013).

The particulate emissions of diesel engines are significantly related to the corresponding EGR rate. A primary drawback that is caused by the EGR system is the increased particulate

emissions. Figure 2.11 presents the local equivalence ratio and temperature distributions of soot and NO formations. It is clearly shown that simultaneously decreased soot and NO is achievable by the application of some appropriate new combustion modes, such as low temperature combustion (LTC) or premixed charge compression ignition (PCCI). The trade-off between the soot and NO and be explained as follows. During diesel engine combustion process, part of the injected fuel is isolated from oxidization with the inlet air to form soot. This results in a reduced carbon conversion from the fuel to CO_2 and reduce the combustion temperature thus lower the NO_x emission.

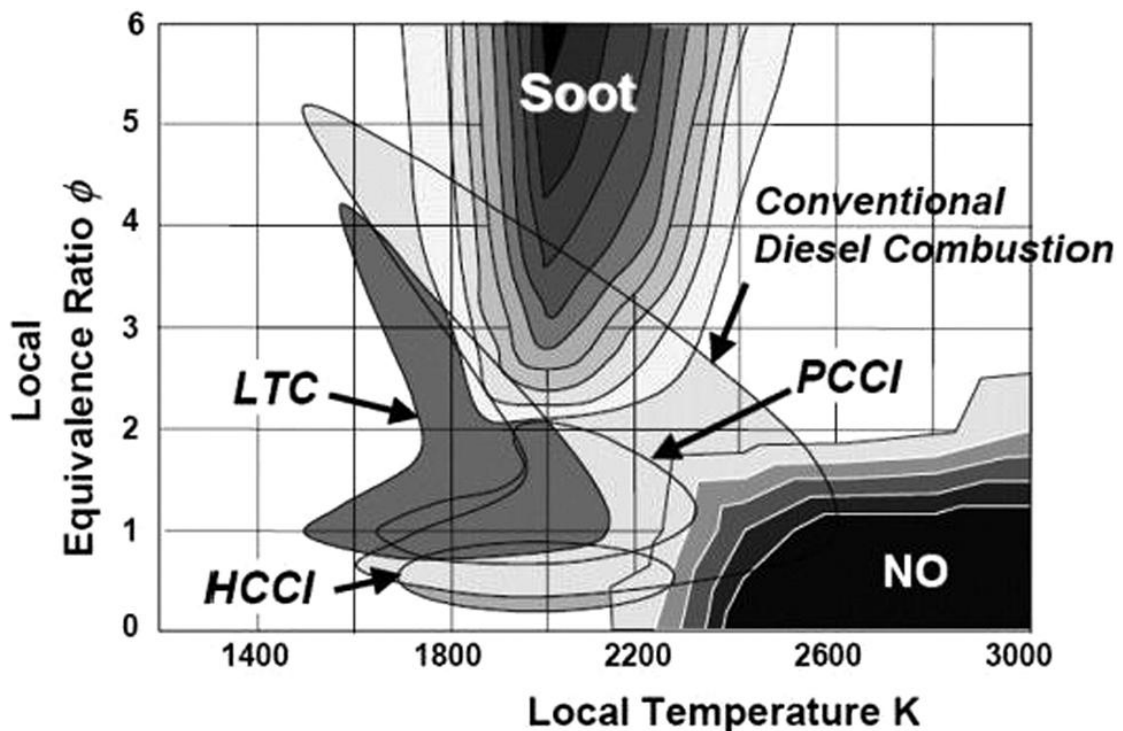


Figure 2.11 Trade-off of NO and soot as a function of local equivalence ratio and temperatures

Figure adapted from: Kim 2009, Dec 2009

Aoyagi et al. (2008) used RME in a single cylinder engine with high boost pressure and high EGR for the purpose of reducing NO_x and particulates simultaneously. For the same group, Kobayashi et al. (2011) achieved decreasing break specific fuel consumption (BSFC) and NO_x and particulate matter simultaneously, by intergraded high and low pressure EGR

systems. The low pressure EGR system reintroduced a proportion of exhaust gases, after the after-treatment system, back into the air inlet system upstream of the compressor. Zhang et al. (2011) and Valentino et al. (2011) carried out PPCI combustion with high ignition delay and volatility diesel fuel. They suggested that significant NO_x reduction and a low level of particulate emissions could be achieved by a combination of high EGR rate and an effective EGR cooler.

2.5.2 EGR Transient Behaviours

Han et al. (2008) investigated the constant speed torque increasing transition effects on the EGR system and emissions. The results observed a dramatic increase of the pressure drop across the EGR valve and an increasing EGR rate due to the turbo-lag issue. They also found a deteriorated smoke opacity which they concluded to be caused by the transient behaviours of the EGR system. Yokomura et al. (2004) demonstrated different control strategies to optimize the transient smoke spike of a heavy-duty diesel engine. The results supposed that simultaneously reduced smoke and NO_x could be achievable during transience by using a closed loop control method of the excess air ratio.

2.6 SUMMARY

In this chapter, the literature is reviewed based on the relevant research that will be presented in the following chapters. Some conclusions can be drawn from the reviewed literature. Firstly, cold start has been revealed by researchers as a critical period during transportation. Temperature effects are supposed to have significant influences on engine performances and

emissions. Investigations should be carried out based on the improvement of engine cold start performances. On the other hand, transient operating conditions are attracting increasing attention from researchers at present. However, the lag response of the turbocharger system deteriorates the engine transient combustion and emissions due to the mismatch between the fuel injection quantity and the intake air mass flow. This was the motivation for this thesis, focusing on approaches to eliminate the transient turbo-lag issue in terms of alternative fuels and engine transient calibrations.

CHAPTER 3

EXPERIMENTAL SETUP AND APPARATUS

The main purpose of this chapter is to introduce the experimental test facilities utilized in this thesis. Two specifically designed transient test cells were used for all the experimental works with the same diesel engine model. The test bench used for the biodiesel experiments was equipped with additional fuel filters and supplying systems to prevent obstruction of the fuel line filters. The rest of the experiments were conducted in the cold cell test rig in which the environmental temperatures can be varied and controlled by the operating system. The detailed information regarding the facilities and setup are presented in the following sections of this chapter.

3.1 ENGINE SPECIFICATIONS

The engine (LION AJV6-D) used for this thesis was a Jaguar V6 3.0 L diesel engine. It was equipped with 24 valves, cooled EGR, twin variable geometry turbochargers and a common rail direct injection (CRDI) system with split injection strategies. The specifications of the engine are listed in Table 3.1. An external power supply (battery) is needed with the maximum current of 35 amps at 13.5 volts for the operation of the engine management system (EMS) and related components. There are two turbocharger systems installed in the LION engine with the primary system operated at most of the engine conditions and the secondary operated under the high conditions (turbocharger map see Figure 3.1).

Table 3.1 Diesel engine specifications

Type of engine	Jaguar V6 3.0L Diesel
Bore	84.0 mm
Stroke	90.0 mm
Displacement volume	2993 cm ³
Maximum torque	600 Nm @ 2000 rpm
Maximum power	199.1 kW @ 4000 rpm
Compression ratio	16.1:1
Connecting rod length	160.0 mm

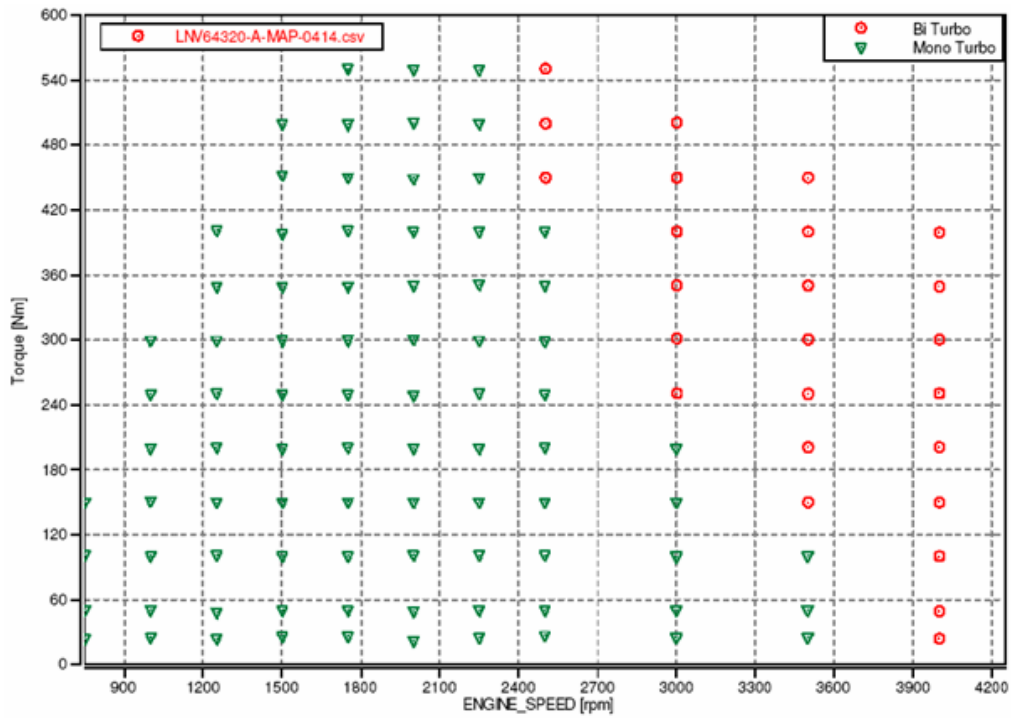


Figure 3.1 Turbocharger mode map

There are two cylinder banks located at each side of the engine with three cylinders in each bank. In order to balance the engine vibration during combustion, the engine firing order of the cylinder is set as 1-4-2-5-3-6. The engine configuration lay-out and characteristics' curve are described in Figures 3.2 and 3.3 respectively. The engine was mounted and connected to the dynamometer of the test cell via a prop shaft adaptor with an appropriate angle to simulate real in-vehicle engine conditions.

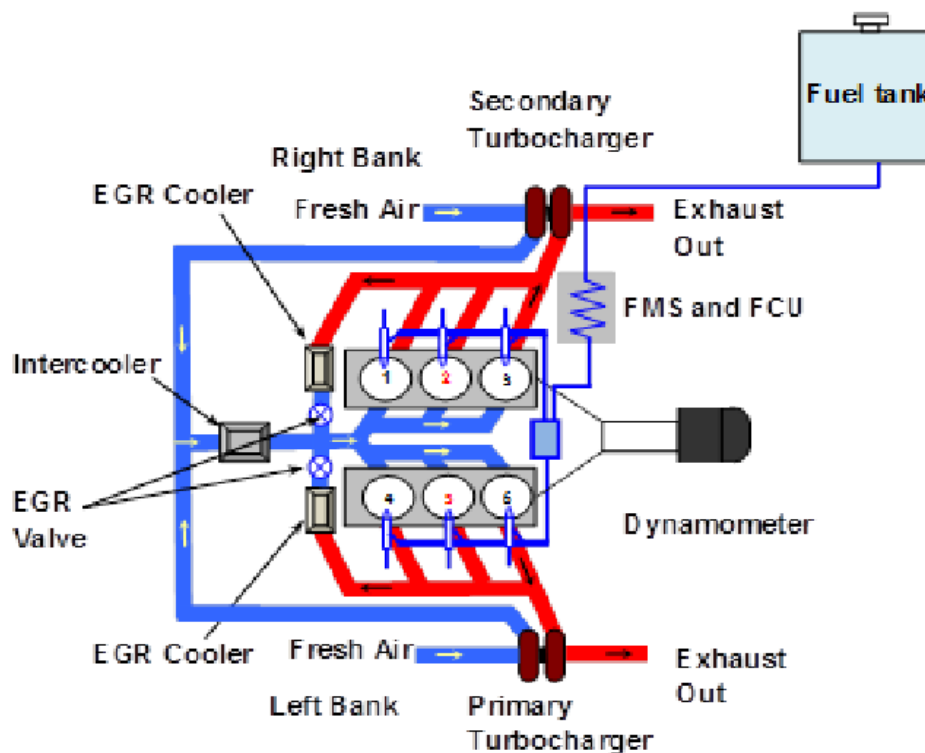


Figure 3.2 Engine configuration lay-out

Figure adapted from: Liu, 2014

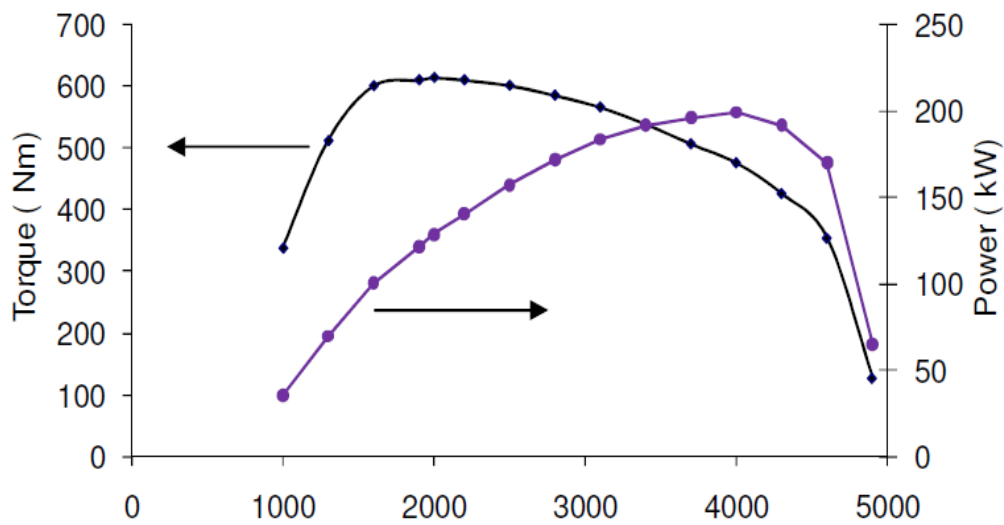


Figure 3.3 Engine characteristics curve

Figure adapted from: Abdullah 2011

3.2 BIODIESEL TEST CELL AND FACILITIES

3.2.1 Dynamometer

The test cell used for the transient biodiesel investigations is displayed in Figure 3.4. An eddy-current water-cooled 230 kW Schenck dynamometer is connected to the engine to provide sufficient transient engine loads. The detailed information of the dynamometer can be found from Table 3.2.

Table 3.2 Specifications of the dynamometer for biodiesel experiments

Type of dynamometer	Scheneck W230
Rated torque	750Nm
Maximum speed	7500rpm
Power	230kW
Moment of inertia	0.53kgm ²
Torsional stiffness	0.593 × 10 ⁶ Nm/rad
Weight	480kg

Data given by DSG Ltd.



Figure 3.4 Test bench for biodiesel transient experiments

3.2.2 Engine Cooling System

The engine coolant and air cooling systems are two specifically designed additional systems for the biodiesel test bench. Both of the cooling systems have similar operating functions and their cooling circuit lay-outs can be illustrated in the schematic diagram of Figure 3.5. A Bowman GL320 heat exchanger is installed in the system for the purpose of absorbing the heat from the engine system. The plant water is supplied from the test cell laboratory. The temperature T_1 and T_2 in the figure are used to control a 3-way valve depending on flow rate requirements. Additional compressed air is required from the laboratory to adjust the valve. The constant flow control valve is used to maintain a constant total flow rate across the system to decouple different cooling loops. The pre-set restriction is set to balance the resistance of the Bowman exchanger to help to linearise the 3-way valve's response. The pressure P_1 , P_2 and P_3 are used to determine the valve's position.

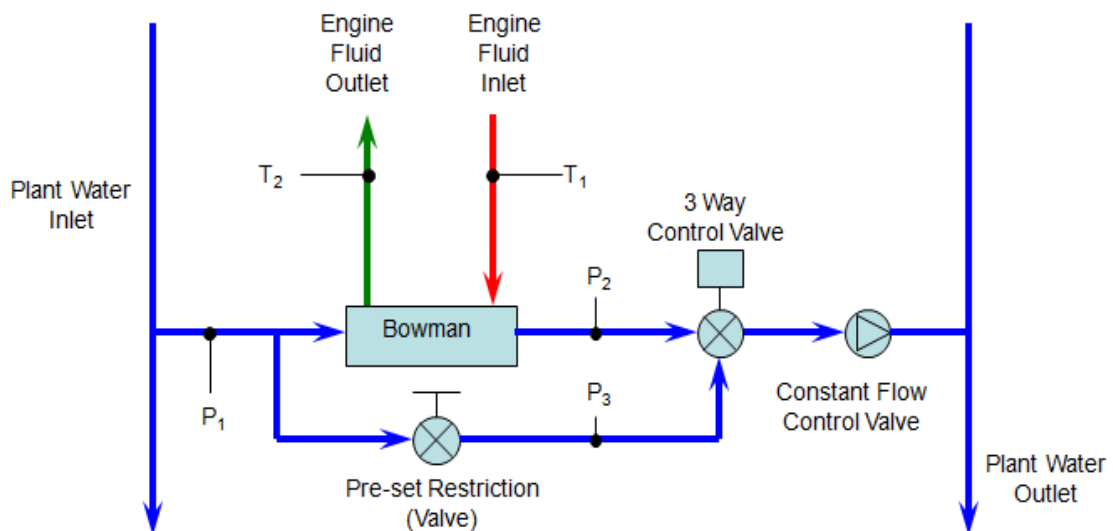


Figure 3.5 The cooling circuit of the engine coolant system

3.2.3 *In-cylinder Pressure Measurements*

The in-cylinder pressure is measured by the AVL GU13G piezo pressure transducers. The glow plugs of cylinders 2 and 5 are removed and replaced by the pressure transducers via glow plug bores. The specifications of the transducers are listed in Table 3.3. An AVL (3066A03) amplifier is utilized to convert the raw transducer's electrical signals into appropriate voltages; which eventually are recorded by IndiCom 2010 software combined with an encoder signal. The encoder creates one pulse in every 0.5 crank angles to identify the crank shaft degree for combustion analysis.

Table 3.3 Pressure transducer specifications

Measurement range	0-200bar
Sensitivity	16pC/bar
Operating temperatures	up to 400 °C
Linearity	$\leq \pm 0.3\%$ FSO
Natural frequency	130kHz

3.2.4 *Operating Control and Data Acquisition Systems*

Almost all of the test bench parameters can be monitored, controlled and recorded by a CP Engineering CADET control system. For transient operating research, the dynamometer was used to change the engine speed while the accelerator pedal was used to control the engine torque. Before each of the transition tests, the tested engine conditions are pre-programmed

into the engine control system. The intake air and coolant temperatures can be maintained at the desired value via the CADET control system. An additional ventilation system provided sufficient venting air flow to the test cell to maintain a constant engine room temperature. A CP Engineering fuel cooling system is set to control the fuel temperature constantly at ambient room temperatures.

Figure 3.6 shows the schematic diagram of the engine cell arrangement. The engine operation parameters are observed by ETAS INCA software which can be used to record the engine ECU data. In order to synchronise the transition signals between INCA, CADET and emission analyzers, the engine speed and torque signals from the CADET control system are transferred to both the DMS500 input channels and a NI card. The latter is used to record the gaseous emissions' signals.

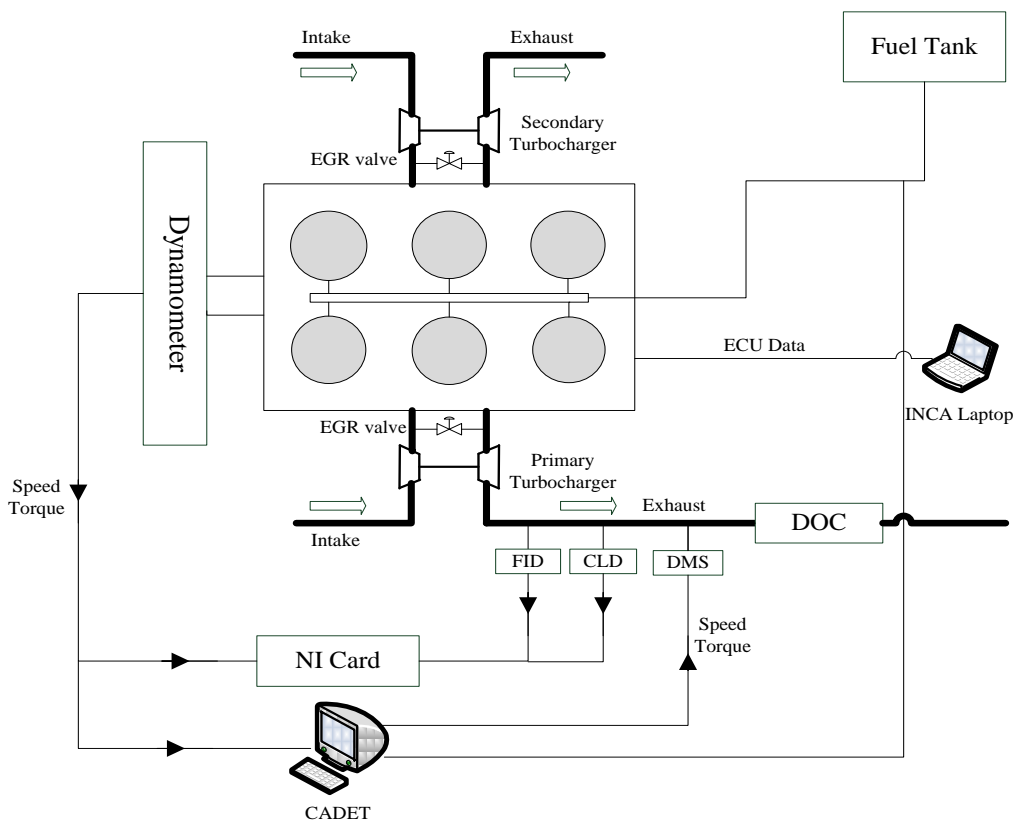


Figure 3.6 Schematic diagram of the engine arrangement

3.2.5 Fuel Properties

The test fuels used in this study were Rapeseed Methyl Ester (RME) in various blending ratios, B0, B30, B60 and B100. The Bxx means xx% neat biodiesel blend with mineral diesel by volume. The specifications of the four fuels are shown in the Table 3.4.

Table 3.4 Properties of the tested biodiesel fuels

Fuel Properties	Diesel	RME30	RME60	RME100
Cetane Number	56.7	57.8	60.3	61.2
Density at 15°C (kg/m ³)	832.7	847.9	863.3	883.3
Viscosity at 40°C (cSt)	3.6	4.3	5.27	6.77
LHV (MJ/kg)	42.72	40.76	38.98	36.41
Oxygen Content (%)	0	4.6	7.8	10.8

3.3 ENVIRONMENTAL CONTROLLED CLIMATIC CHAMBER AND FACILITIES

The climatic controllable transition test cell (also referred to as a cold cell) used in this thesis is an advanced transient engine test rig in Europe. Figure 3.7 presents the cold cell test rig with the different testing and diagnostic devices. It is specifically designed for the purpose of

cold start and transient research and has the capability of conducting a three minute cold start experiment at an environment temperature down to -20 °C.



Figure 3.7 Test bench and facilities for climate change transient experiments

3.3.1 Dynamometer and Engine Mounting Enclosure

The dynamometer (Dynodur 290) used in the cold cell is a foot mounted 290 kW AC machine associated with a squirrel cage rotor from AVL Ltd. It is equipped with drive flanges at both ends and has the capability to operate with a second dynamometer in order to conduct low-speed high-torque tests. The specifications of the dynamometer are listed in Table 3.5.

Table 3.5 Specifications of the cold cell dynamometer

Type	Dynodur 290
Rated torque	485 Nm
Maximum speed	10,000 rpm
Power	290 kW
Moment of inertia	0.31 kgm ²
Coolant	Forced air cooling, air quantity approx. 2,200m ³ /h
Weight	700 kg

As is shown in Figure 3.7, a specifically designed climatic enclosure cell was utilized in the test cell to maintain the constant sub-zero environment temperature during the experiments. The bottom of the climatic enclosure was made with a rigid insulated floor plate. The insulated panels were made from glass fibre associated with elastomeric foam. All the supporting frames inside the enclosure were made from stainless steel with thermally insulated material to prevent ice formation during the cooling soaking period (normally eight hours). For the ambient engine tests, all the insulated panels can be removed and then an external fan is used to allow sufficient air flow to surround the engine.

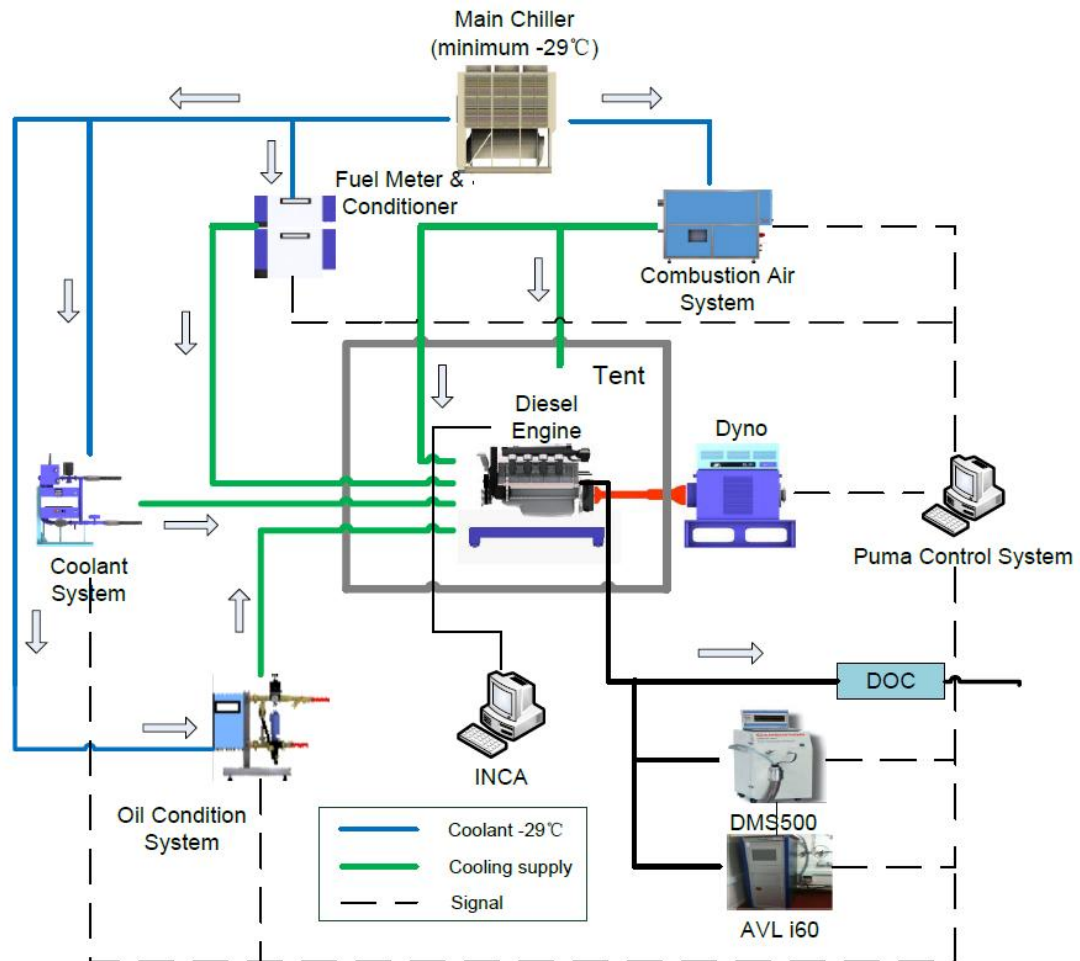


Figure 3.8 Schematic diagram of the cold cell arrangement

3.3.2 Dynamometer and Engine Mounting Enclosure

The cold cell cooling system is capable of changing the fuel, oil, coolant and combustion air temperature individually and maintains all the engine temperatures at $-7\text{ }^{\circ}\text{C}$ over a regular transition cycle, such as the New European Driving Cycle (NEDC). All the above temperatures were cooled and conditioned by a main chiller located externally on the test cell roof which could provide chilled water (normally Glycol) down to $-29\text{ }^{\circ}\text{C}$.

3.3.2.1 Combustion air conditioning systems

The combustion air system is designed to provide a conditioned air supply to the engine enclosure. For the sub-zero ambient temperature tests, an ACS 1600 combustion air system from AVL was activated with an inlet air dehumidifier to control the humidity of the incoming unconditioned air. A nominal 8 kW chiller delivered cold fluid (-29 °C) to the cooling coils in the ACS system to control the temperature of the combustion air. The humidity of the outlet air could be adjusted between 8 and 20 gH₂O/kg dry air. The maximum chilled air flow rate can be supplied up to 500m³/h at sub-zero conditions and up to 1600m³/h at normal ambient temperature conditions, through a 200 mm diameter insulated duct to the engine enclosure. The supplied combustion air temperature is kept at -7 °C from the main chiller plant throughout the whole regulatory driving cycle.

Table 3.6 Specifications of the AVL air combustion system

Type of ACS	AVL ACS 1600
Air flow outlet	40 to 1600 m ³ /h
Ambient air pressure	920 to 1020 mbar
Ambient air temperature	15 to 30 °C
Ambient air humidity	3 to 30 gH ₂ O/kg

3.3.2.2 Coolant conditioning systems

The coolant conditioning system used in the cold cell consists of two separate circuits for the operation of both conventional ambient and cold environment tests, see Figure 3.9. A three-way ball valve is controlled by the control panel to switch between the two conditioning circuits. The ambient mode cooling circuit is supplied with conventional cooling water while the low temperature circuit is supplied with chilled water (Glycol). During the low temperature soaking period, a built-in pump is utilized to circulate the engine coolant throughout the engine. The engine coolant is conditioned with the low temperature circuit via heat exchangers. A flow control valve is installed in the cooling system to control the flow rate of the coolant and the target temperature.

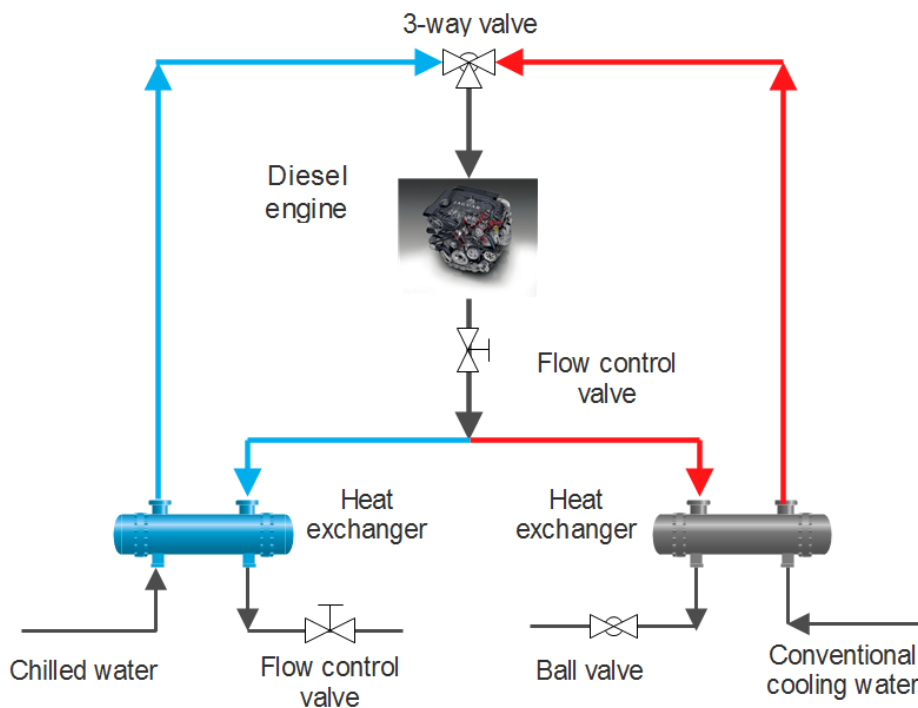


Figure 3.9 Schematic diagram of the cold cell coolant cooling system

3.3.2.3 Lubricating oil conditioning systems

The lubricating oil conditioning system is quite similar to the coolant conditioning system and it can be explained by Figure 3.7. Both of the systems are equipped with two individual cooling circuits. The viscosity variation of the lubricating oil is highly dependent upon the environment temperature. Thus, in order to minimize the viscosity impact on the cooling circuit at different temperatures, an inverter controlled pump is installed to provide a constant flow rate of the circuited lubricating oil.

3.3.2.4 Fuel measurements and conditioning systems

The instantaneous fuel injection measurement is conducted by the AVL 735S fuel meter, which is operated based on the Coriolis principle to measure mass flow rate in the fuel line. The fuel temperature is conditioned by the AVL 735C, which is capable of maintaining the temperature between -10 and 80 °C using the chilled fluid supplied from the main chiller. However, due to the limits of the low temperature tolerance (not below -15 °C) of the AVL 735C, for the -20 °C engine cold start tests an additional cold start unit was activated. To constantly control the fuel supply temperature, the fuel line flow rate was set much higher than the maximum fuel consumption rate so that a large proportion of the delivered fuel could return back to the conditioner.

3.3.3 Engine Control Systems

The engine and all the above mentioned temperature conditioning equipment are controlled by the AVL PUMA system. The schematic diagram of the cold cell arrangement is illustrated in Figure 3.8. For the transient testing, the speed and torque loading can be controlled by the dynamometer, engine and pedal respectively. The engine ECU data is recorded and monitored by ETAS INCA V5.3 software. It can then transfer via self-defined norm-names to the PUMA system for transient testing synchronizations. The in-cylinder pressure is measured by the IndiCom combustion analysis system. The combustion data can be recorded by the PUMA system in the cycle based time resolve. Furthermore, the gaseous emissions are measured by AVL i60 integrated emission analyzer which can also be individually controlled by the PUMA control system.

3.3.4 Properties of Winter Diesel Fuel

Due to the poor cold flow properties of diesel fuel, specially produced winter diesel fuel from Shell Ltd is used in the cold cell for the extremely cold ambient testing. The winter diesel fuel has a lower cold filter plugging point (CFPP) value than the normal diesel fuel (normal diesel CFPP around $-7\text{ }^{\circ}\text{C}$); making it suitable for use in low temperature. The fuel specifications are listed in Table 3.7, which are provided by Shell Ltd.

Table 3.7 Properties of winter diesel fuel used in the cold cell facility

Properties	Winter Diesel
Cetane Number	52
Cold Filter Plugging Point (CFPP)	-34°C
Viscosity at 40°C (mm ² /s)	1.86
Oxygen Content (%)	0

3.4 FAST RESPONSE EMISSIONS MEASUREMENT DEVICES

3.4.1 Gaseous Emissions Measurements

3.4.1.1 Fast FID

The instantaneous THC (C₃) emission is detected by the Flame Ionisation Detector (FID) HFR500 from Cambustion Ltd in the biodiesel test cell. The Fast FID analyzer used in the research can process the emission response time in less than 0.9ms and control the transmission time within 5ms. The operating principle of the fast response FID is demonstrated in Figure 3.10. The sample gas from the exhaust emissions is delivered into a flame chamber of the Fast FID for burning. Ions are then produced by the burning process of the hydrocarbons. The ions can subsequently be detected by a high voltage metal collector. The current of the collector indicates the strength of the ionisation that is proportional to the concentration of hydrocarbon in the sample gas. Since the ionisation process is completed in

an extremely short period, therefore the response time of the Fast FID analyzer is much shorter than the conventional FID analyzer (1-2 Seconds).

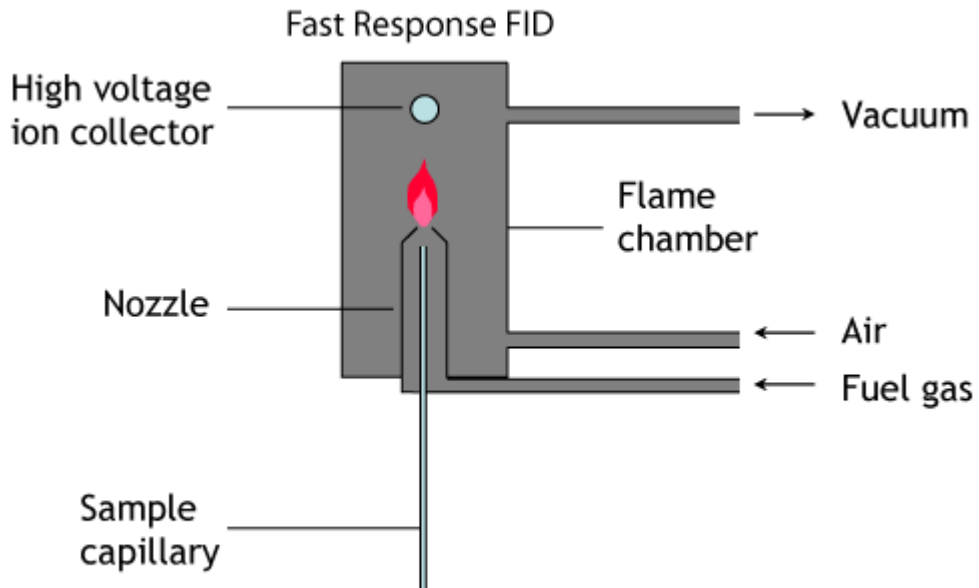


Figure 3.10 Operating principle of Fast FID hydrocarbon emission analyzer

Figure available from: Cambustion.com FID

3.4.1.2 Fast CLD

The NO emissions are detected by a Chemi Luminescence Detection (CLD) CLD500 analyzer also from Cambustion Ltd. The operating principle of the Fast CLD is based on the reaction between NO and O₃, as in Figure 3.11. Light is produced during the chemical reaction. The Fast CLD uses a photo multiplier tube (PMT) to detect the intensity of the light and transfers it into the voltage signal. It needs to be mentioned that this approach is not suitable for the detection of NO₂ since there is no light produced during the reaction. Therefore, in order to measure the NO_x emissions the NO₂ needs extra time and optional

converters to be transferred into NO for further calculations. This will reduce the response time for the transient research.

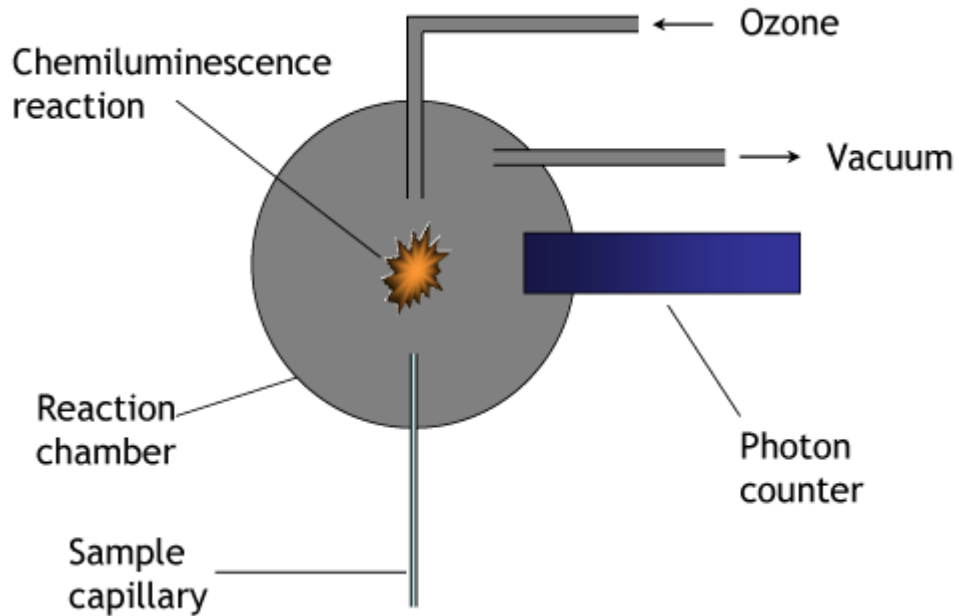


Figure 3.11 Operating principle of Fast CLD NOx emission analyzer

Figure available from: Combustion.com CLD

In the biodiesel test cell, the fast FID and fast CLD probes are placed upstream of the after-treatment and the emission analyzers were remote controlled. All the gaseous analyzers can auto-calibrate by using external calibrated span gases. The specifications of the analyzers are illustrated in Table 3.8.

Table 3.8 Specifications of fast diagnostic equipments

Test Equipment	DMS500	Fast FID	Fast NOx
Time Response	200 ms	As low as 0.9 ms	As low as 2 ms
Acquisition Frequency	10 Hz		
Measurement Range	5 nm to 1000 nm	0-1000 ppm to 0-200,000 ppm	0-100 ppm to 0-5,000 ppm

3.4.1.3 AMA i60

The AVL i60 gas analyzer is used in the cold cell test rig to detect the gaseous emissions; where various emission detectors are integrated together by using the same sample probe. It uses a CLD to measure NO and NOx; a FID for THC (C₃) and an Infrared Detector (IRD) for CO, respectively. The measurement principles of THC and NOx in the i60 are the same as that of the Combustion fast response devices. In the infrared detector, the infrared radiation is set to pass through the sample exhaust gas. During this process, the spectrum is absorbed dependent on the specific characteristic of molecules in the exhaust gas. The intensity of the absorption can be used to measure the concentration of the detected gas.

3.4.2 Particulate Matter Measurements

3.4.2.1 DMS500

The real time particle number concentrations in this thesis are measured by a Differential Mobility Spectrometer (DMS500), a fast response instrument from Cambustion Ltd. The specifications are listed in Table 3.7. The DMS 500 can achieve a maximum data record and analogue input frequency of 10Hz. The operating principle is described in Figure 3.12. The particulates are charged of positive electricity by an aerosol charger. They are then passed through the high voltage electrode classifier with the sheath flow air. With the impact of the electrode, the small particulates which contained less electric charge are easily deflected towards the electrometer detector and the larger particulates eventually land further along the classifier.

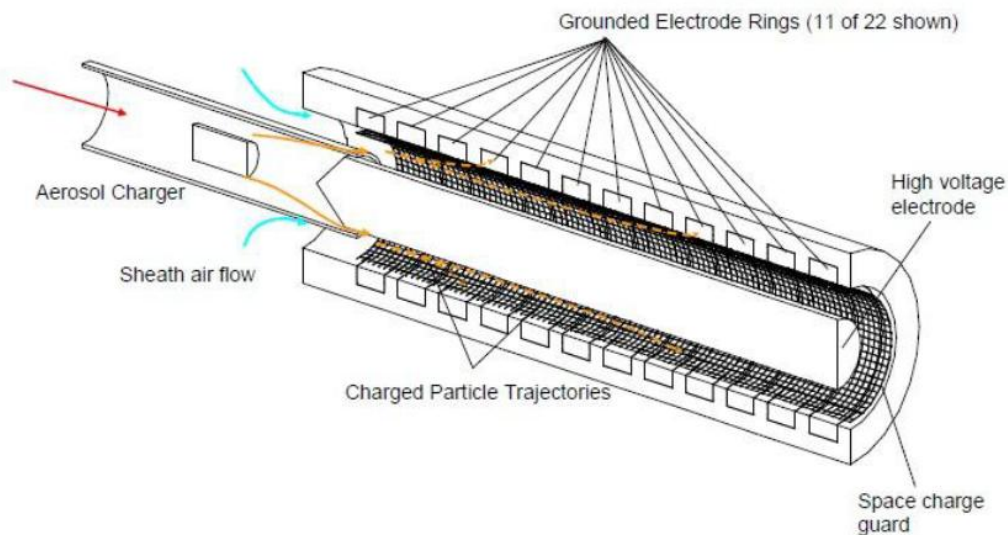


Figure 3.12 Operating principle of DMS500 emission analyzer

Figure adapted from: Rubino 2005

Two diluters are installed in the DMS500, see Figure 3.13. The first dilution is fixed at 5:1 in the heating sample line (around 150 °C) which is used to remove the water condensation. The second is a disc diluter inside the main control unit which was used to dilute the high concentration exhaust gas. This is varied with the different engine tests conditions.

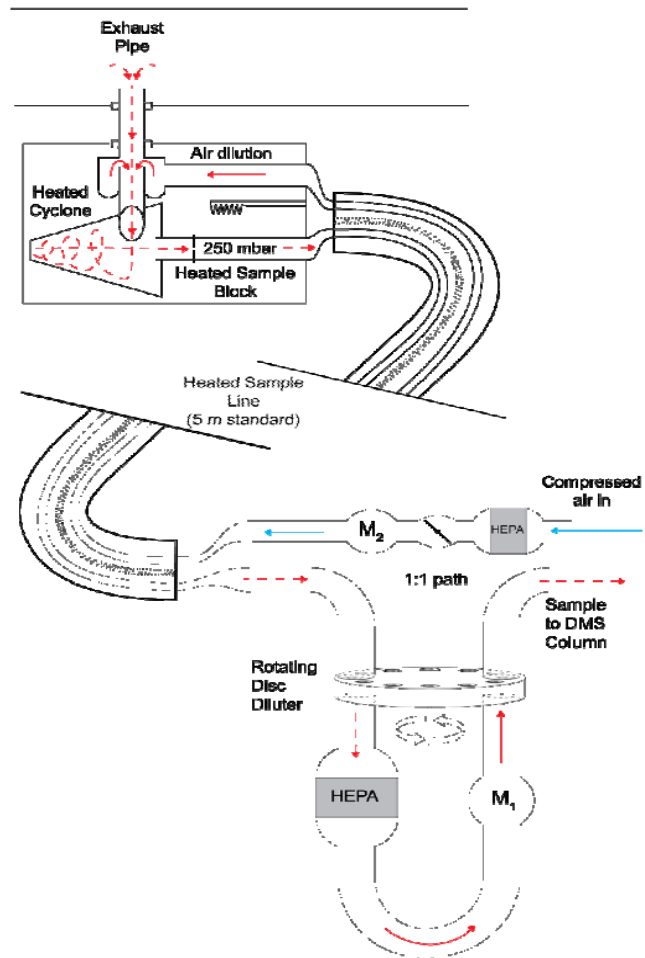


Figure 3.13 Dilution system of DMS500 emission analyzer

Figure available from: Cambustion.com

3.4.2.2 SPC and 2D-GC/MS

The AVL Smart Sampler (SPC) 472 was used in the cold cell test rig for the purpose of particulate matter collection for GC analysis. The operating panel and the schematic diagram are presented in Figure 3.13. The SPC extracts a constant proportion (sample ratio) of the exhaust gas for diluting. The system controls the total tunnel flow rate passing through the particulate filters based on the required value. With the variable dilution air, the particulate concentration in the sampling gas is proportional to the instantaneous particulate matter and suitable for emission analysis. The analyzer is equipped with a heating sample probe (around 170 °C) for the purpose of removing the volatile particles as well as preventing water condensation or freezing in the cold cell.

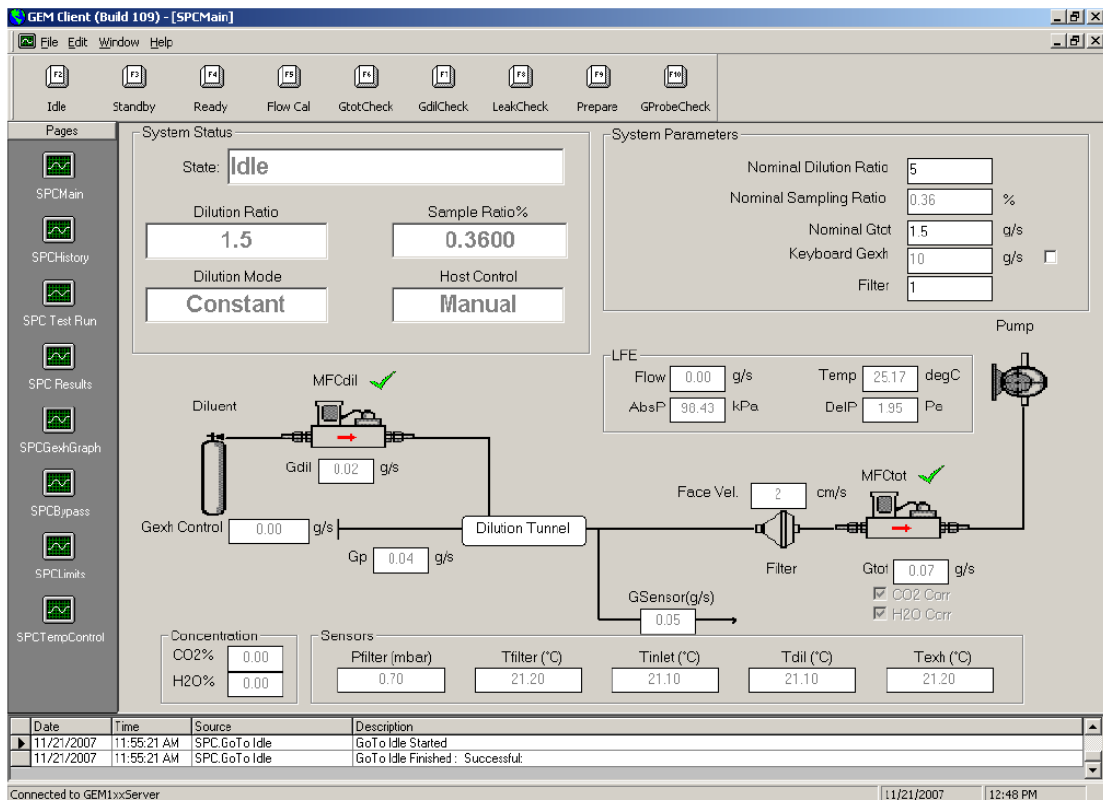
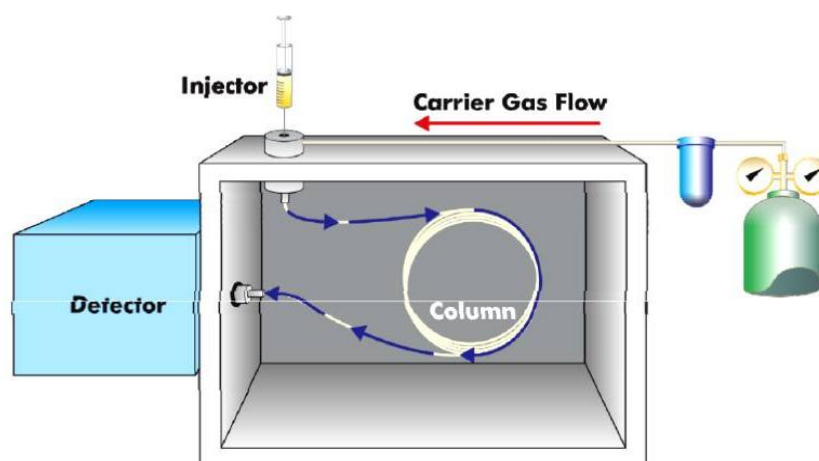


Figure 3.14 Front panel and schematic diagram of the SPC emission analyzer

The chemical components of the semi-volatile particulates were analyzed by a two-dimensional (2D) Gas Chromatograph with Mass Spectrometer (GC/MS) from Earth and Environmental Sciences Department in the University of Birmingham. Unlike the conventional GC/MS, there are two dimension columns used to separate chemical compounds of particles in the 2D-GC/MS device, see Figure 3.14. The first column is operated based on the volatility property of the measured particulates (the same as the conventional GC analyzers); whereas the second column separates the components based on their polarities.

A modulator is placed in-between the two columns in the 2D-GC/MS device to periodically deliver the exhaust from the first column to the second column to finish a detection cycle. The structure information of the effluence is then identified and quantified, by matching the detected mass spectra with reference mass spectra based on the National Institute of Standards and Technology (NIST) library from the fast response time-of-flight (TOF) mass spectrometer.



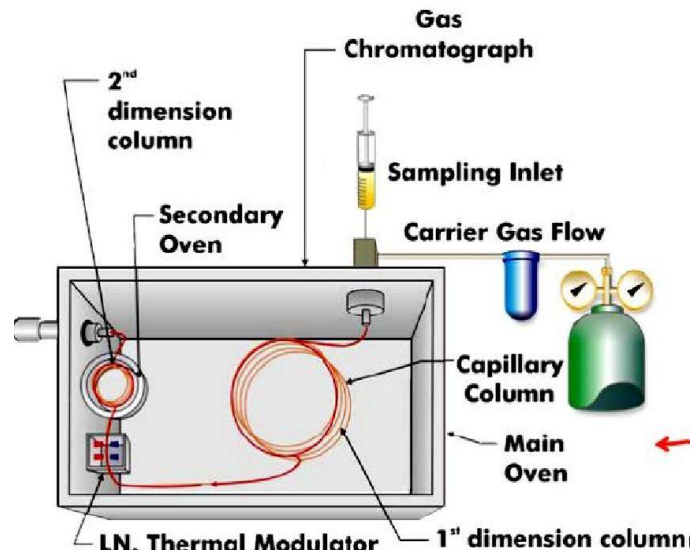


Figure 3.15 Structures of conventional and two-dimensional GC/MS

The 2D-GC/MS device has the capability of further separating the co-eluted components or identifying the Unresolved Complex Mixtures (UCMs) from the conventional GC/MS. The modulator is a crucial part of the 2D-GC/MS operation. It achieves the modulation process in an extremely short period which makes the device have higher sensitivity. The two columns are designed in special sizes with the first column longer and wider than the second. This allows the two separation processes to be finished in the same period.

3.5 EXPERIMENTAL DATA PROCESSING AND CALCULATIONS

3.5.1 Heat Release Rate Calculations

The Rate of Heat Release (RoHR) analysis discussed in Chapter 4 was calculated based on the following equations. By assuming there is no heat transfer during combustion, the first law of thermodynamics can be expressed by the following equation:

$$dQ = dU + dW \quad (\text{Eq. 3.1})$$

Where dQ is the heat released from combustion; dU is the value affected by the temperature and specific heat capacities; dW is the engine work. For the ideal gas, dU is equal to $mC_v dT$; pV is equal to mRT and $Vdp + pdV = mRT$; $R = C_p - C_v$. Therefore, the following equation can be used to compute the RoHR (Heywood 1988):

$$\frac{dQ}{d\theta} = \frac{\gamma}{\gamma - 1} P \frac{dV}{d\theta} + \frac{1}{\gamma - 1} V \frac{dp}{d\theta} \quad (\text{Eq. 3.2})$$

Where γ is the specific heat ratio; and $\gamma = C_p / C_v$ (normally around 1.3 for diesel engine); $d\theta$ is the crank angle degree; V is the cylinder volume and P is the in-cylinder pressure.

3.5.2 Cumulative Gaseous Emission Calculations

The following equations are used to calculate the cumulative emissions in this thesis. The mass flow rates of the gaseous emissions were calculated by the following equation:

$$\dot{m}_{gas} = 10^{-6} \times \frac{MW_{gas}}{MW_{exhaust}} \times C_{gas} \times (\dot{m}_{air} + \dot{m}_{fuel}) \quad (\text{Eq. 3.3})$$

Where MW_{gas} and $MW_{exhaust}$ are the molar mass of gaseous emissions and the exhaust gas; C_{gas} is the detected concentration of the gaseous emission. The $MW_{exhaust}$ is assumed at 29 g/mol; \dot{m}_{air} and \dot{m}_{fuel} represent the intake air mass flow and mass fuel injection respectively. The unit of mass fuel injected from the INCA software was mg per cycle per cylinder, which had to be converted to g per second. The following equation was used:

$$\dot{m}_{fuel} = 5 \times 10^{-5} \dot{m}_{fuel_1} \times v \quad (\text{Eq. 3.4})$$

Where v is the transient speed, rpm per min; and \dot{m}_{fuel_1} is the mass fuel injected in mg per cycle per cylinder. Therefore, the overall cumulative emissions were derived by the following relation:

$$m = \int_0^t (10^{-6} \times C \times \frac{MW_{gas}}{MW_{exhaust}} \times (\dot{m}_{air} + \dot{m}_{fuel})) dt \quad (\text{Eq. 3.5})$$

3.5.3 Cumulative Particulate Emission Calculations

The cumulative total particulate number and particulate mass can be calculated by Equations 3.6 and 3.7 respectively. The 22.7 L/mol term is required because the DMS500 corrects its particulate measurements at 0 °C and 100 kPa; it is these temperatures and pressures that are important, rather than the temperature and pressure in the exhaust pipe.

$$PN(\#) = \int_0^t (10^3 \times PN(\# / cc) \times \frac{22.7}{MW_{exhaust}} \times (\dot{m}_{air} + \dot{m}_{fuel})) dt \quad (\text{Eq. 3.6})$$

$$PM(g) = \int_0^t (10^{-3} \times PM(ug / cc) \times \frac{22.7}{MW_{exhaust}} \times (\dot{m}_{air} + \dot{m}_{fuel})) dt \quad (\text{Eq. 3.7})$$

3.6 SUMMARY

This chapter introduces the experimental setup and apparatus based on the two test rigs used in this thesis. The biodiesel test rig was used to conduct all the biodiesel experiments, which are illustrated in Chapter 4. The rest of the regulated and discrete transient experiments were conducted in the cold cell test rig. The details are given in terms of control systems, cooling systems, diagnostic equipment as well as the post data processing calculations.

CHAPTER 4

INVESTIGATIONS OF TEMPERATURES IMPACT ON DIESEL ENGINE EMISSIONS

The effects of engine temperature on the regular and unregulated engine-out emissions under the New European Driving Cycle (NEDC) were investigated in this chapter. In the first section of this chapter, transient NEDC scenarios were carried out on a modern 3.0 L, V6 turbocharged common rail diesel engine fuelled with winter diesel in the “cold cell” at the University of Birmingham within the varying ambient temperature ranging between +20 °C and -7 °C. The engine with its fuel, coolant, combustion air and lubricating oil were all soaked and maintained at the desired test temperatures during the transient scenarios. Instantaneous engine performances including torque and speed; gaseous emissions such as CO, THC and NO_x; and particulate emissions for its number and mass; were analyzed during each transient scenario under different ambient conditions. The total cumulative gaseous and particulate emissions during the NEDC were examined quantitatively along with the engine parameters for each ambient temperature. In the second part of this chapter, a two-dimensional Gas Chromatography (GC) separation and time-of-flight (TOF) Mass Spectrometry (MS) analyzer was used to investigate semi-volatile organic compounds (SVOC) from cold and warm start NEDC particulate filters. The organic species of alkanes, alkyl-cyclohexanes and PAHs were identified and quantified for discussion.

4.1 LOW AMBIENT TEMPERATURE EFFECTS ON A MODERN TURBOCHARGED DIESEL ENGINE RUNNING IN A DRIVING CYCLE

As has been introduced in the previous chapter 2, diesel engine cold start is a crucial period for normal engine operations. In a severely cold environment, the poor battery performance will result in a lower cranking speed of the starter. High engine friction and oil viscosity will lead to a high demand for starting torque, high blow-by level, as well as the large heat losses from the cylinders. All the above phenomena may deteriorate the engine performances at low temperature environment.

4.1.1 Test Conditions and Procedures

In this section, in order to investigate the cold ambient temperature effects on the modern commercial diesel engine, the New European Driving Cycle (NEDC) is used as a test sequence to evaluate engine transient performances and emissions at the temperature range between -7 and 20 °C. The NEDC sequence consists of 11 seconds of cold start, 4 repeated Urban Driving Cycles (UDC) (also known as ECE) and 1 Extra-urban Driving Cycle (EUDC). A test vehicle (from Jaguar) equipped with the same diesel engine model as in this study with a chassis dynamometer was used to run the NEDC. Engine speed and torque results were recorded as a test sequence to put into the PUMA engine control system in the cold cell in order to complement the real vehicle driving. The engine before each transient scenario was soaked at the desired temperature for at least 8 hours. Sample probes of both AVL i60 and DMS500 were well insulated by thermal insulation materials in order to prevent water condensation and freezing at low ambient temperatures. The signal from the starter was

taken as an analogue input channel into the DMS500 to synchronize the scenario starting time. All the emission sample points were placed upstream of the after-treatment system as shown in Figure 3.7.

The scenarios at normal ambient temperature were repeated for three times and the average results were taken for analysis. Due to the poor repeatability at low ambient temperatures, transient scenarios were repeated five times and the intermediate results were taken for analysis and discussion. The engine control system was set in the N/T mode, which means the dynamometer was used to control the engine speed and the engine was used to control the engine torque.

4.1.2 Transient Engine Performances

Engine performances in terms of speed and torque for the required vehicle speed profile under the NEDC are presented in Figure 4.1. High engine starting speed is observed for the low ambient temperature scenarios. Furthermore, torque fluctuations and unconformities are evident at the beginning of the NEDC. It is interesting that the magnitude of the fluctuations increased when the ambient temperature decreased only within the first few seconds. This is mainly caused by the unstable phenomenon of the engine cold start. Longer cranking period, higher fuel injection quantity, poor lubrication, fuel evaporation and combustion conditions are the critical problems for the engine cold start. As the driving cycle continues, both the engine speed and torque profiles become identical for all temperatures.

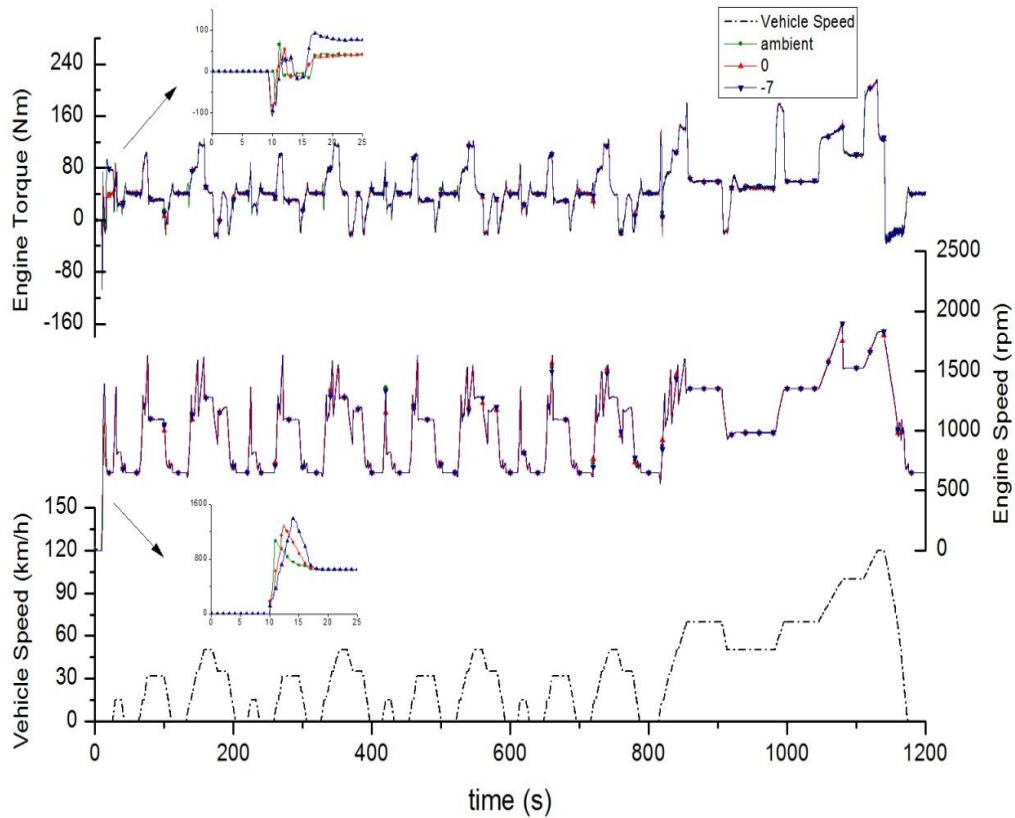


Figure 4.1 Profiles of engine torque, speed, and vehicle speed

Figure 4.2 presents the Air Fuel Ratio (AFR) and Exhaust Gas Recirculation (EGR) during the NEDC. Generally, the engine EGR is calibrated for meeting the NEDC emissions' requirement in the required temperature range. In this study, it is obvious that during the cold start and the first UDC stage the AFR decreases at lower ambient soaking temperatures. As the engine warms up, the AFR becomes higher for the low ambient scenario; meanwhile it becomes lower for the normal ambient NEDC. On the other hand, the EGR valve is closed during the entire -7 °C scenario based on the original engine calibration. For the 0 °C scenario, the EGR is off until the second UDC is completed. During the normal ambient temperature scenario, the EGR valve is open throughout the whole NEDC. The EGR valve of the test rig is located upstream of the turbocharger compressor. This indicates that there is no exhaust energy by-passing through the EGR at the beginning of the 0 °C and -7 °C NEDC scenarios. Moreover, the low ambient temperature will lead to higher air density. Therefore, higher

intake air mass flow is expected in the lower temperature scenario. Nevertheless, in spite of the fact that the intake air mass flow of the cold ambient scenario is higher than that of the normal ambient temperature scenario, the AFR of the cold ambient scenario is still lower than that of the normal ambient temperature scenario due to the dominative high fuel injection quantity. In addition, at the beginning of the EUDC stage, the AFR is reduced with the increasing ambient temperature. This phenomenon can be explained by the higher EGR valve opening position. At the later stage of the EUDC, the AFR is extremely high because of the delayed turbocharger speed reduction which is caused by the turbo-lag.

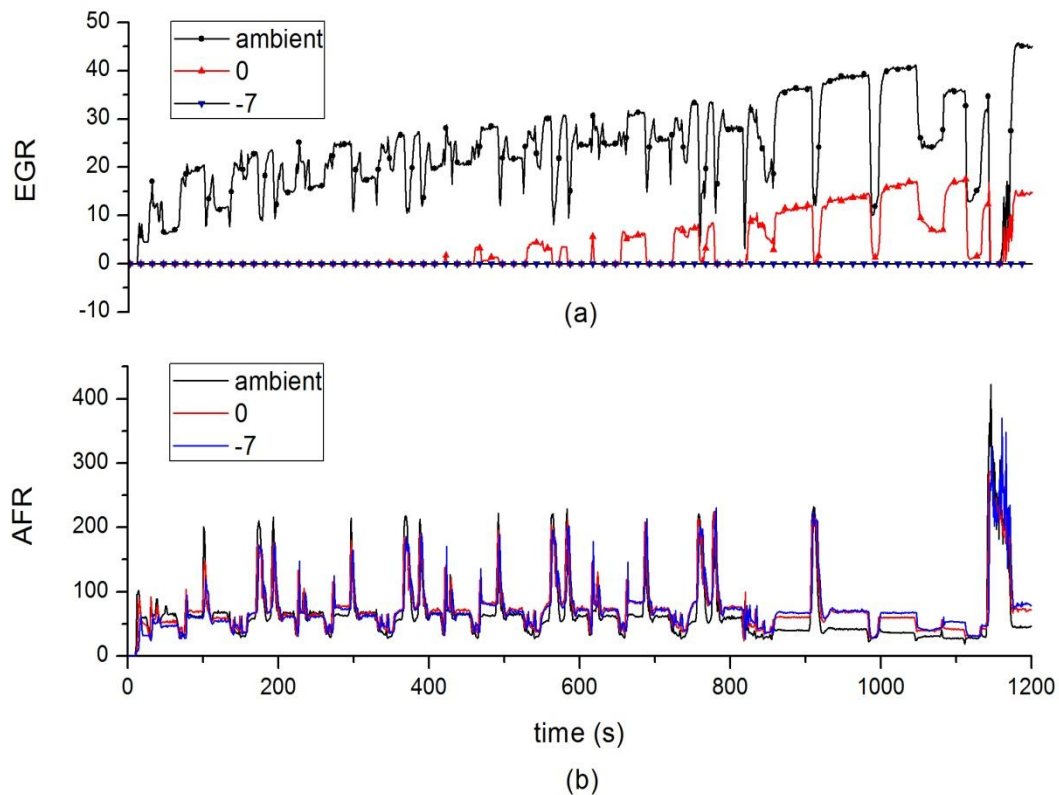


Figure 4.2 a) Air-Fuel Ratio and b) EGR

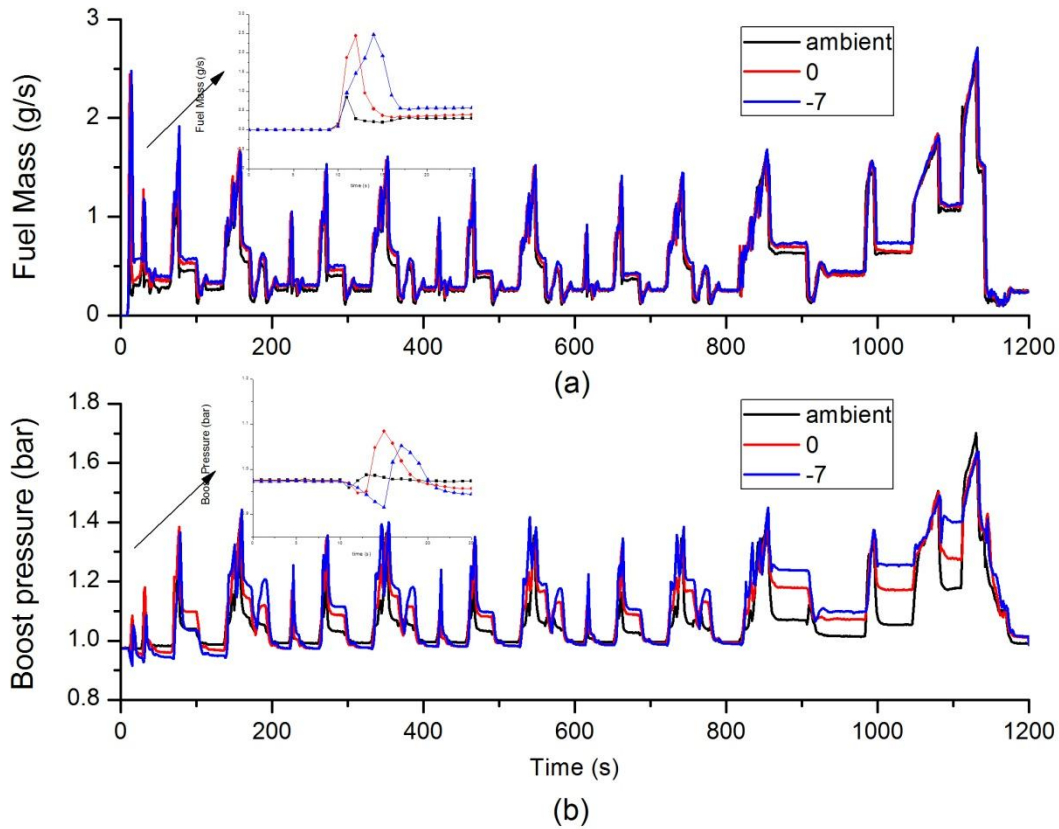


Figure 4.3 a) Boost pressure and b) Injected fuel mass

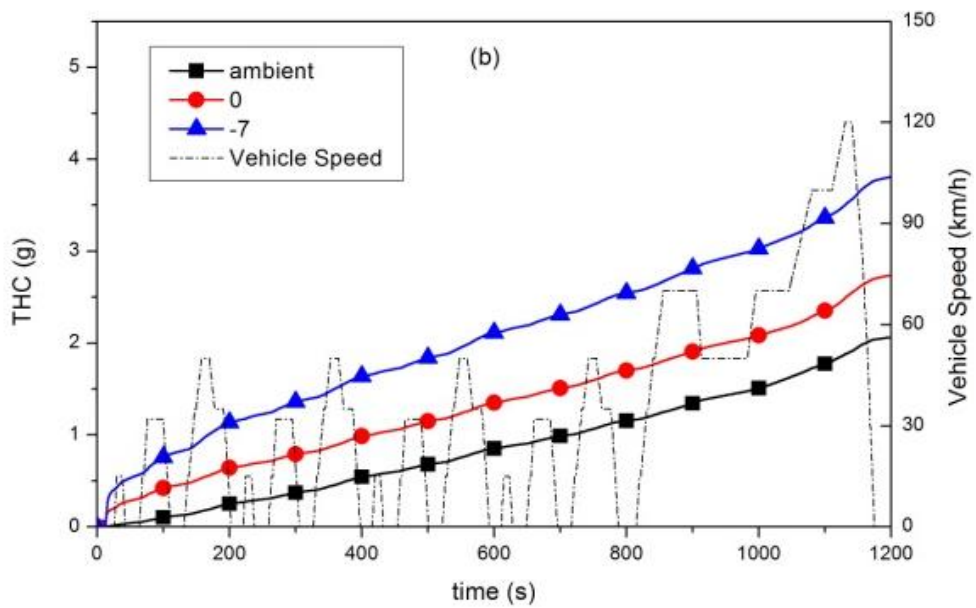
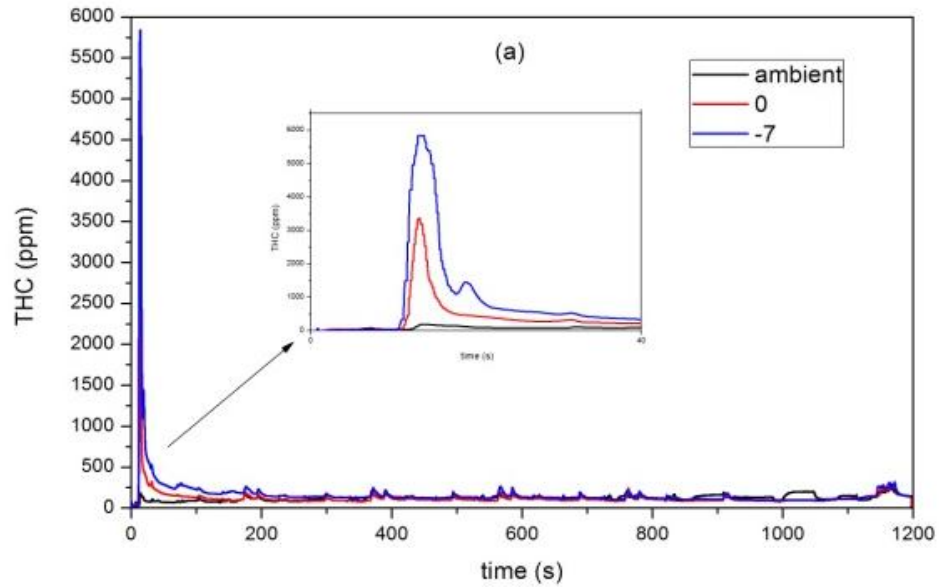
Figures 4.3 (a) and (b) show the fuel injection quantity and the boost pressure for the whole driving cycle respectively. As shown in Figure 4.3 (a), more fuel is injected into the cylinder at low ambient temperature and it is increased when the ambient temperature is decreased. At the beginning of the scenario when the in-cylinder gas temperature is low, more fuel must be injected into the cylinder in order to produce the required engine output. Based on the engine calibration, the engine must overcome the insufficient output under very cold conditions. From Figure 4.3 (b) it is clear that the boost pressure is greatly influenced by the EGR, especially at the EUDC stage and it increases when the ambient temperature decreases. Due to the exhaust energy bypass by the EGR, lower boost pressure is obtained during the normal ambient scenario, which eventually results in a lower AFR.

4.1.3 Transient Gaseous Emissions

Figures 4.4 (a) and (b) illustrate the instantaneous and cumulative THC emissions. The thumbnail in the instantaneous figure gives clear details from 0s to 40s of the entire NEDC transient scenario. The cold ambient scenario emits higher and longer cold transient spikes at the beginning of the NEDC. However, the spike in the normal ambient temperature scenario was almost negligible. The peak THC in the -7 and 0 °C scenario is over 21 and 10 times higher than that of the normal temperature scenario. Furthermore, lower temperature seems to produce a longer cold start recovery period until it reaches relatively stable engine conditions. Also, the -7 °C scenario tends to produce higher THC emissions at most parts of the NEDC compared with the other scenarios. The above features could be attributed to the low AFR at the low ambient temperature, especially during the cold start period. At a low temperature condition the engine may have suffered low combustion efficiency which is caused by the high fuel and oil viscosity, poor fuel evaporation, incomplete combustion and even combustion misfire. The fuel will have higher viscosity and thus higher surface tension at low temperature conditions. As a result, the fuel will undergo slow evaporation, poor atomization or even impingement onto the cylinder wall before combustion. On the other hand, poor performance of the lubricating oil will cause the blow-by problem which deteriorates the engine combustion. The high heat transfer between the cylinder and the environment at the cold ambient temperature scenario could also lead to poor engine combustion. All the above-mentioned factors will finally result in poor fuel-air mixing and incomplete combustion which is favourable for THC emissions.

Figure 4.4 (c) presents the mean specific THC emissions at various transient cycles from cold start to the final EUDC respectively. The first UDC stage in the diagram includes both the engine cold start stage and the first urban driving cycle. The results show that high specific

emissions are produced at the first UDC for both 0 °C and -7 °C, compared with the other driving cycles. The mean specific emissions of the first UDC are nearly 6.5 times higher than those of the EUDC for the -7 °C scenario; 4 times for the 0 °C scenario; and 2 times for the normal temperature scenario.



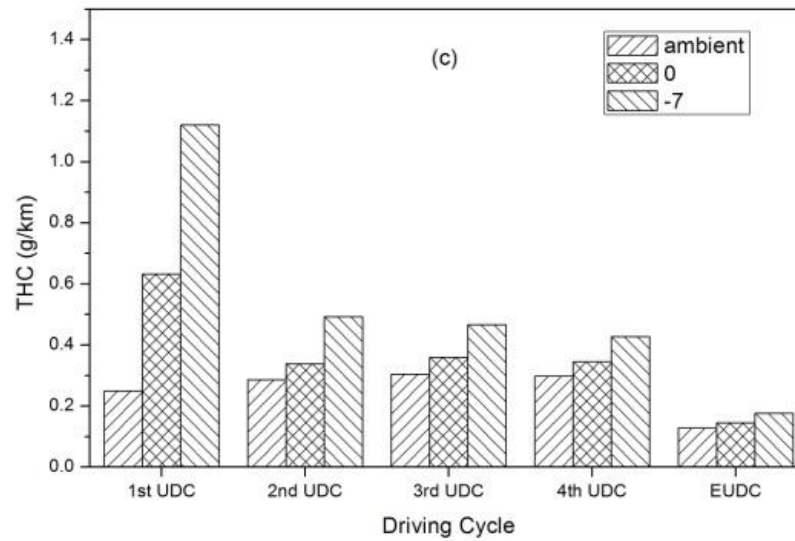
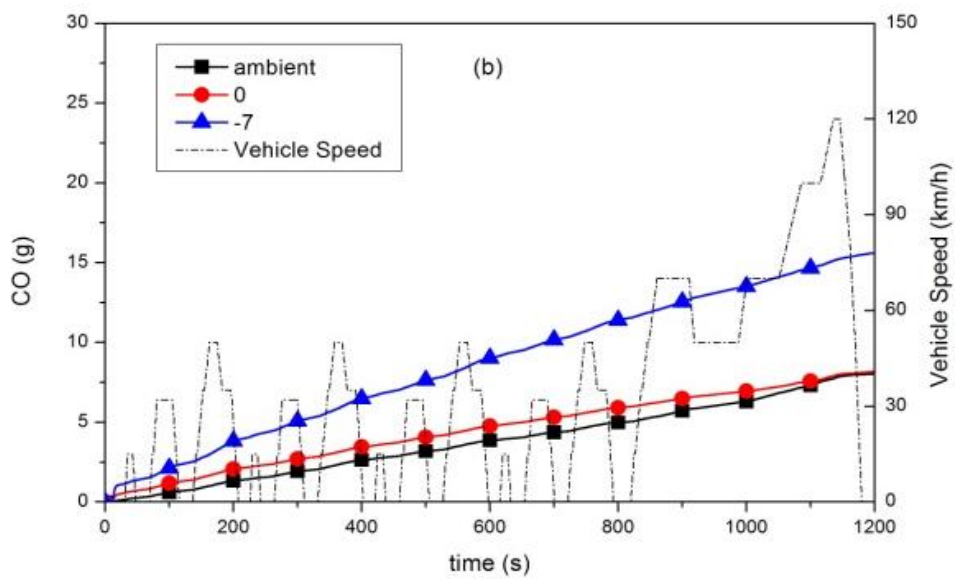
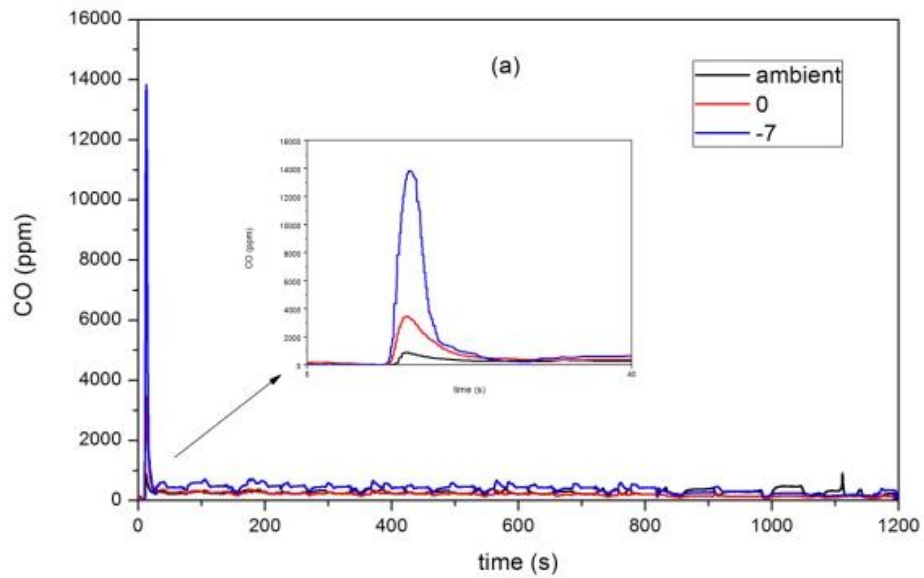


Figure 4.4 Profiles of THC emissions

a) instantaneous, b) cumulative and c) mean mass specific value

Figures 4.5 (a) and (b) show the instantaneous and cumulative CO emissions during the NEDC at different temperatures respectively. The principle of the CO emissions is similar to the THC's emissions as both are generated by the occurrence of the unburned or partially burned fuel. Therefore the trends between the THC and CO are expected to be very close to each other. It is obvious that there are large spikes for all scenarios during engine cold start. The peak of the CO emission of the -7 and 0 °C scenario is approximately 14 and 3 times respectively, higher than that of the normal ambient temperature scenario. Figure 4.5 (c) gives the specific CO emission. There is a slight decrease for the normal ambient specific emissions between the four UDCs. The specific emissions' differential between each temperature is much bigger at the first UDC and becomes very close at the final EUDC stage. This indicates that the effects of the environment temperature on the engine emissions are reduced as the engine warms up due to the smaller coolant temperature differential. The environment temperature in the study was set at the desired temperature (23 °C, 0 °C, -7 °C)

during the whole test process. Figure 4.6 shows the coolant temperature variation during the NEDC.



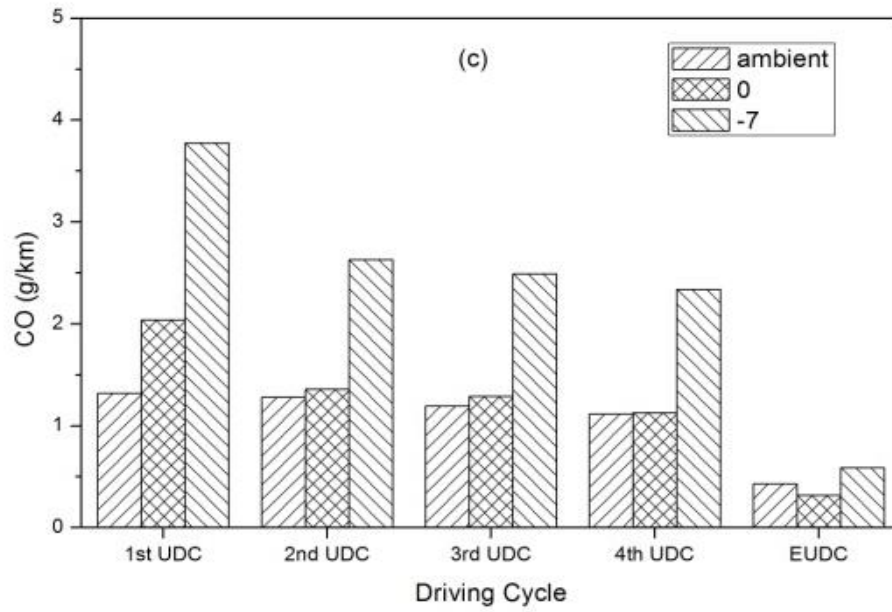


Figure 4.5 Profiles of CO emissions,

a) instantaneous, b) cumulative and c) mean mass specific value

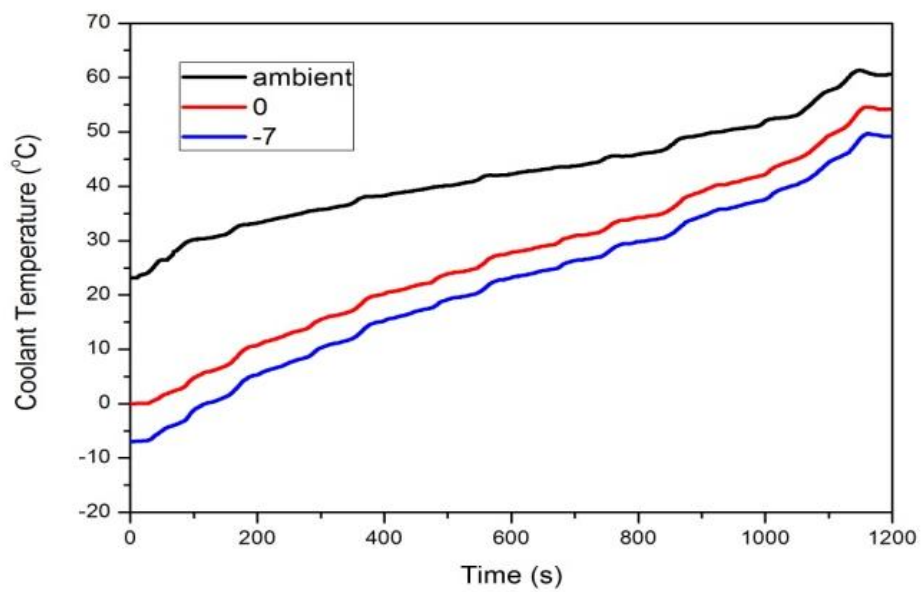
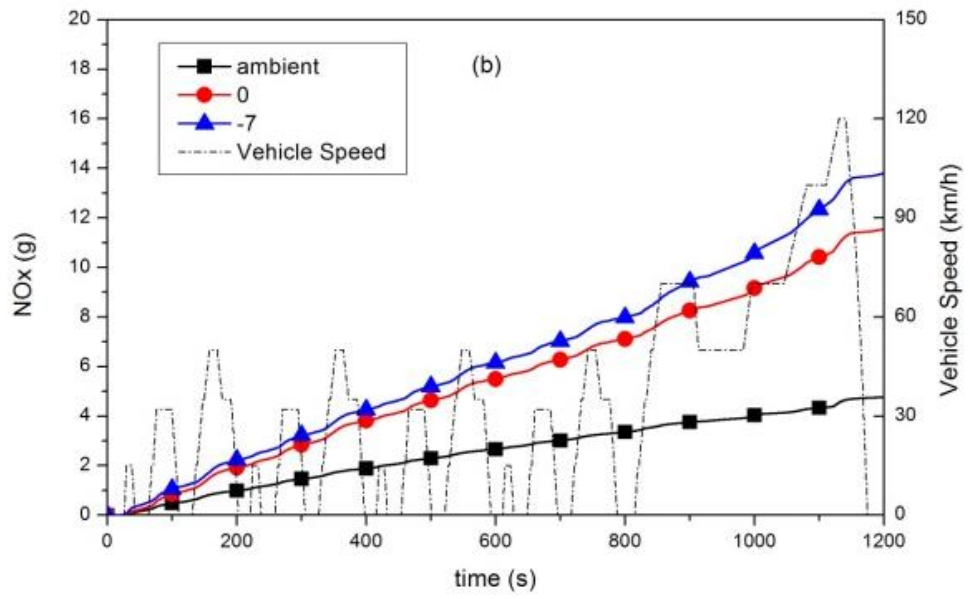
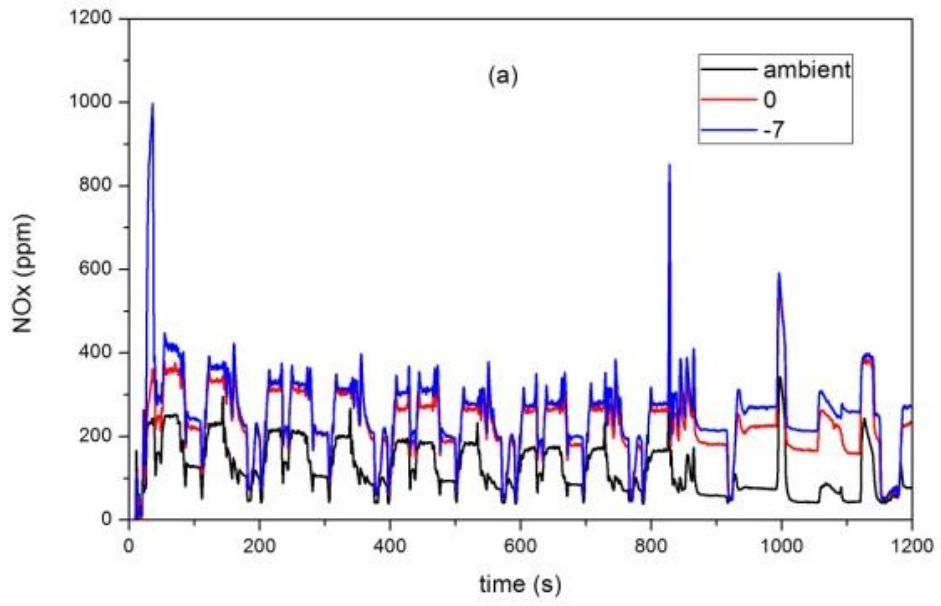


Figure 4.6 Profiles of engine coolant temperature

The instantaneous and cumulative NO_x emissions are presented in Figures 4.7 (a) and (b). As shown in the graph, the NO_x emissions' spikes are clearly displayed at the cold start stage. Moreover, the overall NO_x emissions decrease as the temperature is increasing for the three transient scenarios. Many reasons can be used to explain the above results. Firstly, more fuel is injected into the cylinder chamber at the cold start stage. The excess amount of fuel could increase the combustion temperature and finally raise the NO_x emissions. Furthermore, high glow plug voltage and its long operating duration contribute significantly to the warming up of the cylinder during the cold start period; this may consequently raise the NO_x emissions (Royo et al. 2011). In addition, high intake air mass flow for the low ambient scenario will increase the oxygen availability in the cylinder; this is another reason for the high NO_x emissions. On the other hand, the low overall NO_x emissions of the normal ambient temperature scenario can be explained by the high EGR which is used as a main method to reduce NO_x emissions in modern diesel engines.

Figure 4.7 (c) describes the mean mass specific NO_x emissions during the scenarios. As the engine runs continuously, from the first UDC to the fourth UDC, the specific NO_x emissions slightly decrease for all temperatures. At the EUDC stage, the NO_x emissions of the normal ambient temperature scenario are reduced by nearly five times compared to the first UDC.



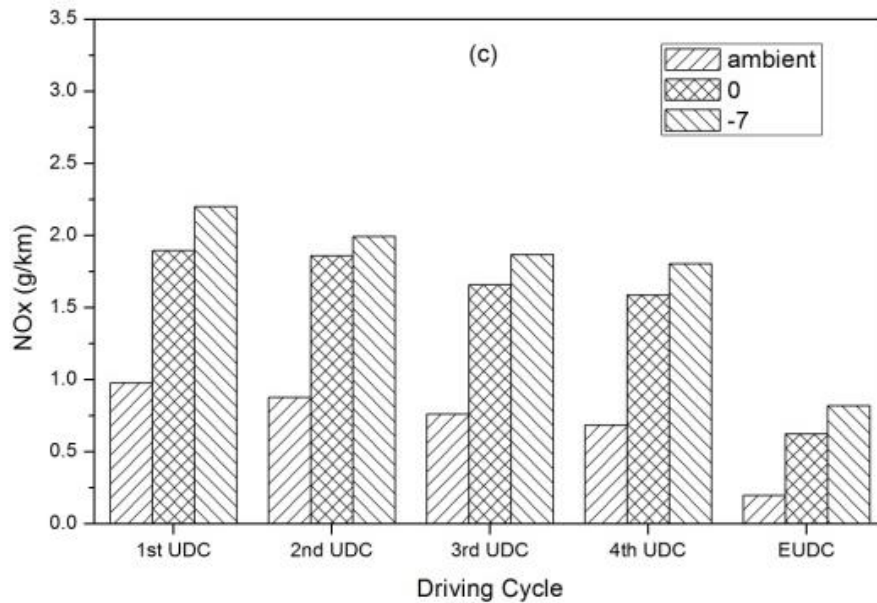


Figure 4.7 Profiles of NOx emissions

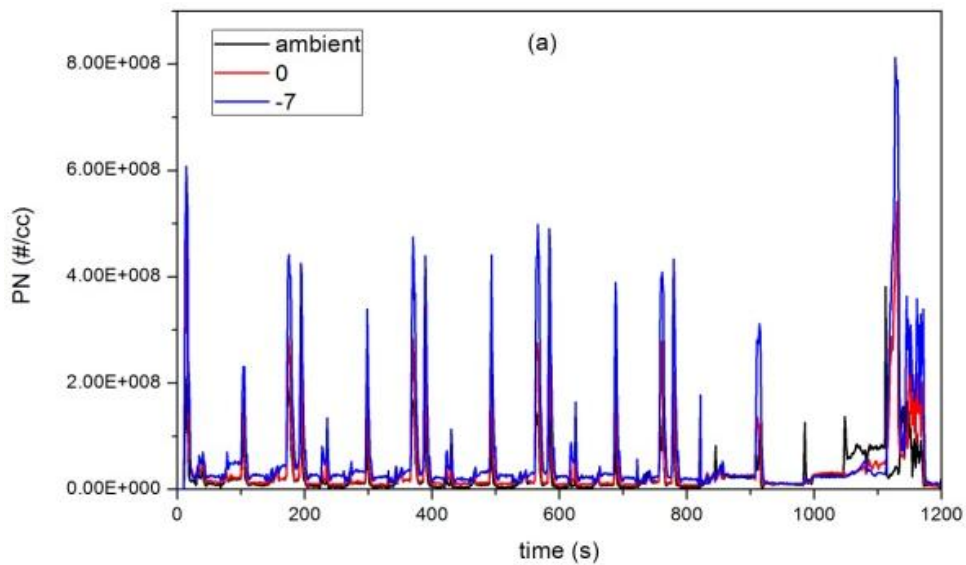
a) instantaneous, b) cumulative and c) mean mass specific value

4.1.4 Transient Particulate Emissions

Figures 4.8 (a) and (b) show the instantaneous particulate number concentration and the cumulative particulates respectively. Figure 4.9 illustrates the first 195 seconds of the total particulate number and the AFR of the ambient transient scenario. The reason causing the PN transient spikes in these graphs could be divided into two different categories. The medium sized spikes which are located at the low AFR regions (acceleration period) are possibly caused by the turbo-lag problem. The turbo-charged diesel engine always suffers insufficient intake air mass flow and low AFR during transients. Under the accelerating condition, the mismatch between the sudden increase of injected fuel and the slowly raised intake air mass flow is dominative due to the delayed turbocharger speed increase. On the other hand, the bigger sized PN spikes (100s, 170s, 190s) are emitted when the vehicle is slowing down, e.g. the engine is operating at extremely high AFR regions. During this period of time, the engine

will undergo very lean burn or partial combustion and eventually emit a large amount of particulates. This could be verified by the THC and nucleation particulate emissions.

In terms of temperature impact, the sizes of the transient spikes in the particulates are bigger at low temperatures because of the high fuel injection quantity and poor fuel atomization. Low temperature scenarios produce a larger gradient of the cumulative particulate number (see Figure 4.8 (b)). Figure 4.8 (c) shows the mean specific emissions of the particulate number. Unlike the previous gaseous emissions, the particulate matter is not highly dependent on the engine warming temperature. From the second UDC to the fourth UDC, at the same testing temperature, the mean specific particulate number remains almost the same.



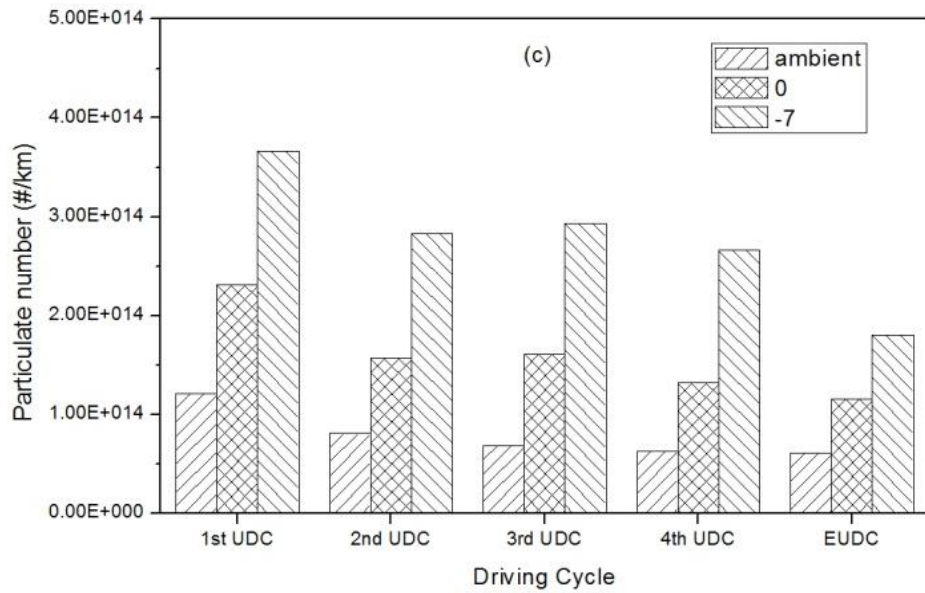
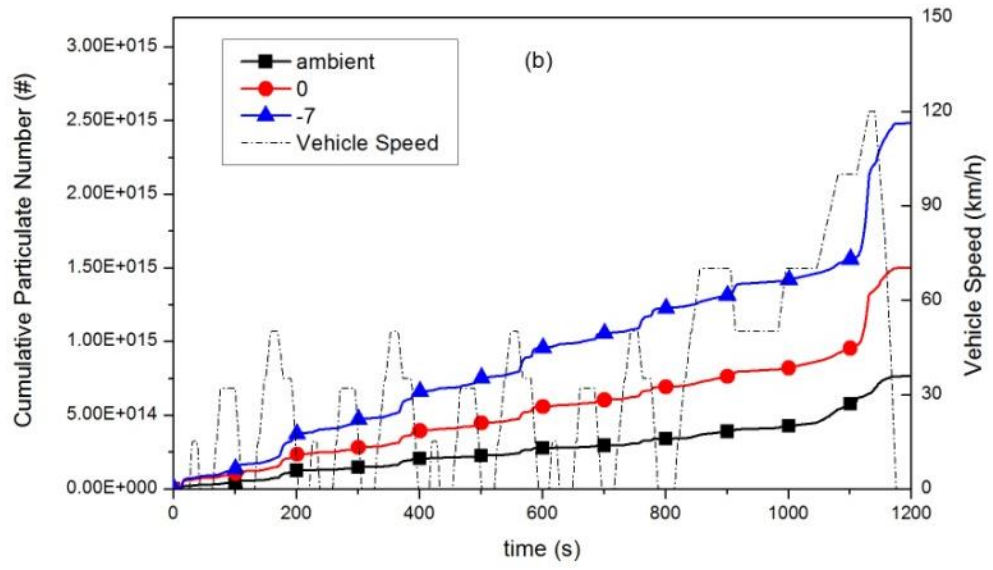


Figure 4.8 Profiles of total particulate number

a) instantaneous, b) cumulative and c) mean mass specific value

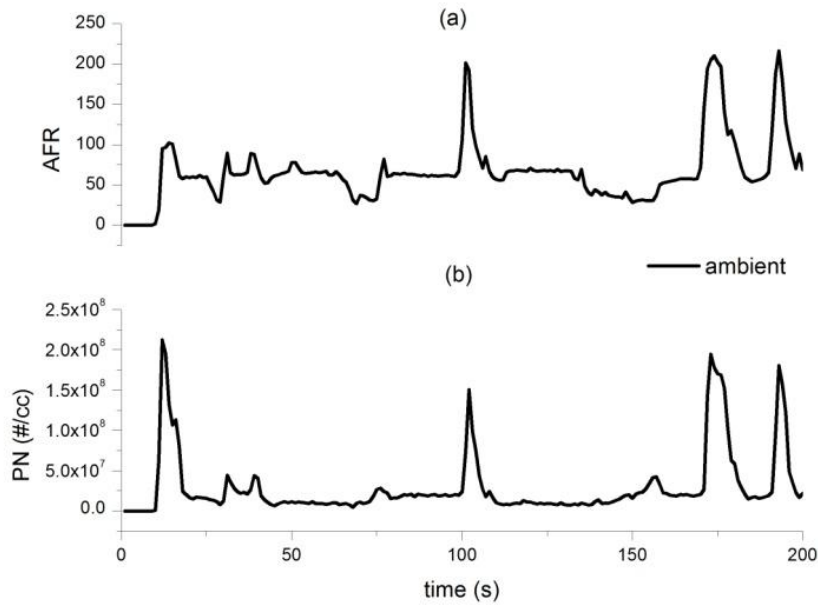
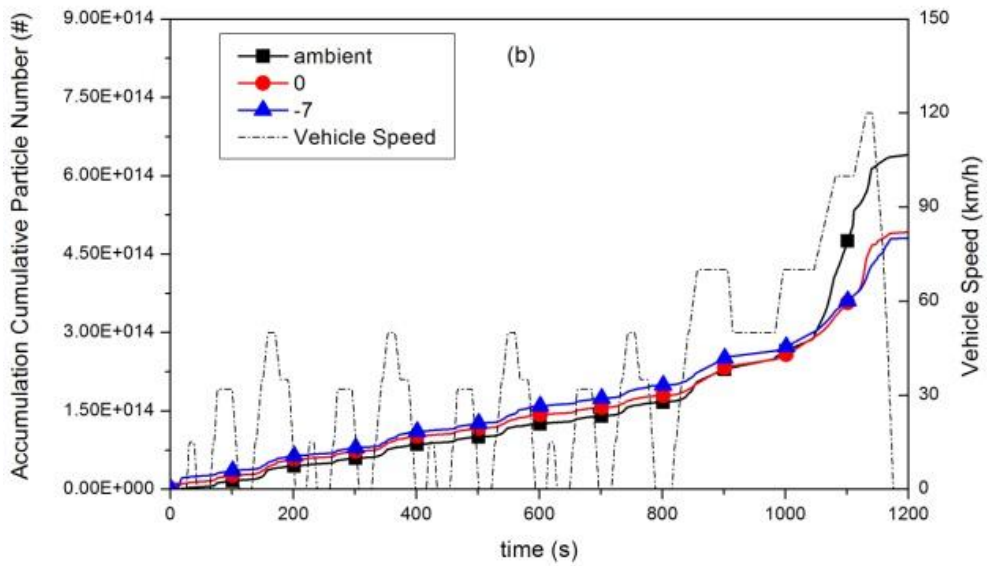
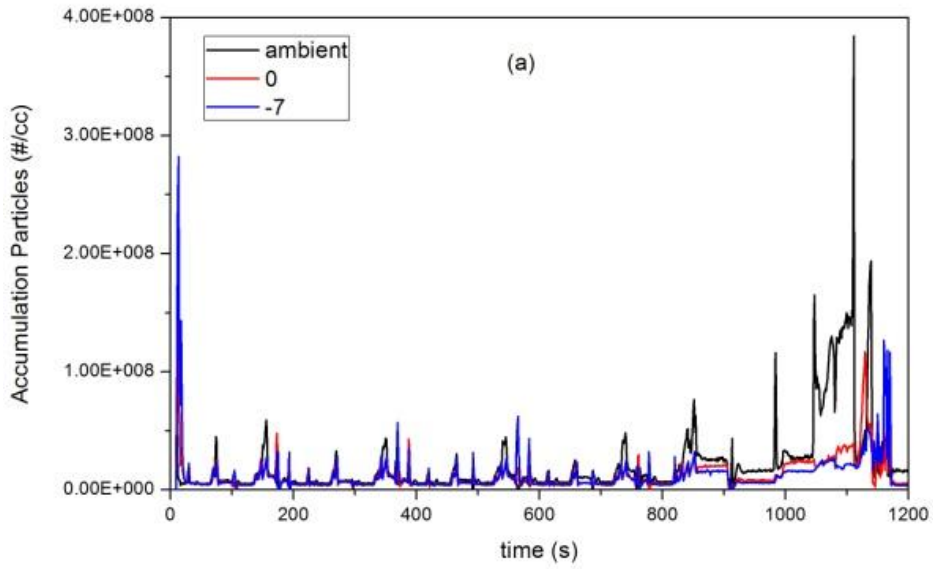


Figure 4.9 a) AFR and b) particulate number in the first 195 seconds

In order to facilitate academic research on the particles' emission, the particles can be normally divided into two different forms: nucleation mode and accumulation mode. In his review paper, Kittelson (1998) described the definition of the particle size range as: nucleation mode from 5 to 50 nm; accumulation mode from 50 to 1000 nm; which is the same definition used in this study. Accumulation mode particulates are formed by many adhered together units which contain agglomerate with some volatiles absorbed on the soot particles (Eastwood 2008). Figure 4.10 indicates the instantaneous, cumulative and mean mass specific accumulation particulates respectively. The cold start and transient spikes appear during the whole NEDC. The size of the transient spike under the very low AFR region is much smaller than that of the nucleation mode particulates (see Figure 4.11 (a)). By contrast, the number of accumulation mode particulates at the low AFR region is bigger than that of the nucleation mode particulates. Under acceleration and low AFR engine conditions, the engine will undergo high in-cylinder temperature. As a consequence, the volatile particulates are easily burned which eventually reduces the nucleation mode particulates and

promotes the accumulation mode particulates. On the other hand, a notable increase of the accumulation particulate could be found for the normal ambient scenario at the EUDC stage. This is attributed to the EGR effect.



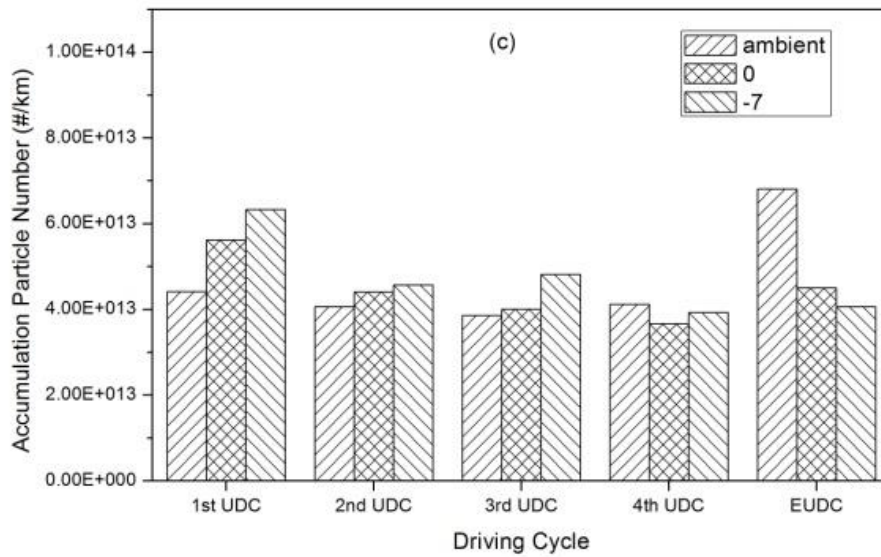
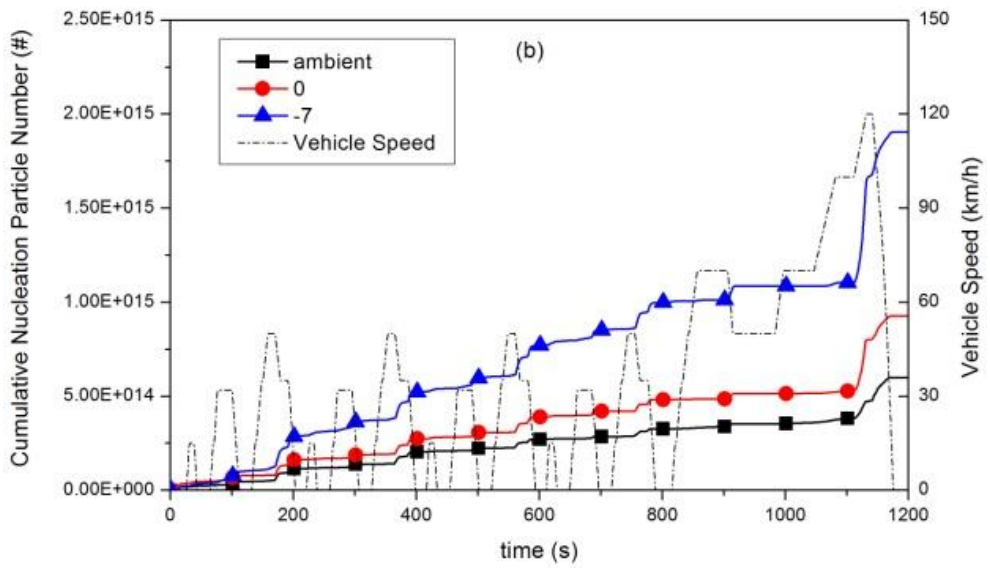
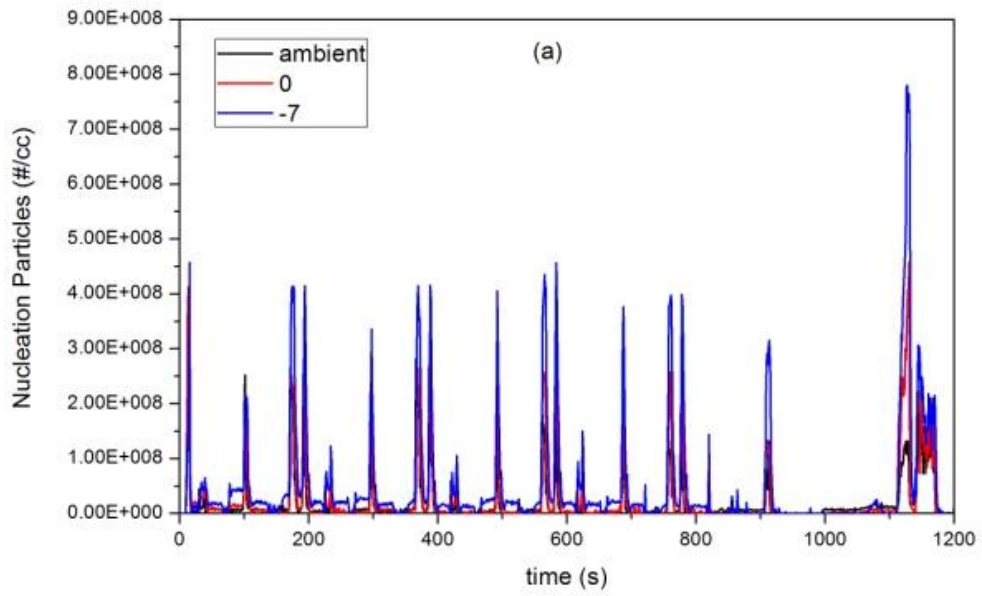


Figure 4.10 Profiles of accumulation particles

a) instantaneous, b) cumulative and c) mean mass specific value

Nucleation mode particulates include particles mainly composed of soluble or volatile organic fraction (SOF/VOF), which are formed mainly from exhaust dilution and cooling processes by the small amount of fuel or evaporated lubricating oil which escapes the oxidation process [21]. Figure 4.11 shows the nucleation mode particulate emission. Big spikes are found for nucleation mode particulates throughout the different scenarios, especially at low temperatures. As is mentioned in above section, the big spikes are located at the extremely high AFR (over-lean) regions that are likely to cause the partial combustion. This phenomenon is more pronounced at low temperature scenarios as the combustion is even worse at cold ambient conditions. The partially burned fuel, partially oxidized products and other combustion by-products will be generated during this period. This eventually leads to excessive emissions of nucleation mode particulates. Moreover, the engine produces a small number of nucleation mode particulates and a large number of accumulation mode particulates at the EUDC stage (from 920s to 1120s). During this period of time, the non-volatile carbonaceous particles increase and absorb the volatile particles to form

accumulation mode particulates and reduce the nucleation mode particulates as a consequence.



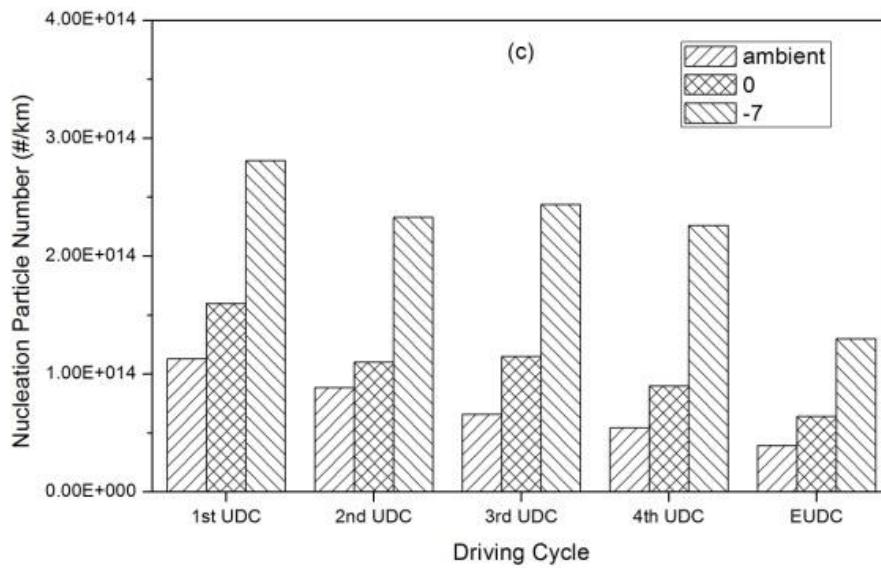


Figure 4.11 Profiles of nucleation particles

a) instantaneous, b) cumulative and c) mean mass specific value

The cumulative and mean specific particulate mass is shown in Figures 4.12 (a) and (b) respectively. At the beginning of the NEDC, the particulate mass is higher at low ambient temperatures. At -7 °C, the mean mass specific particulate emission for the first UDC is nearly 10 times higher than that of the EUDC stage. In contrast, the mass of particulate generated by the normal ambient scenario increased sharply at the later stage of the EUDC; this is caused by the increased accumulation particulate number which accounts for a large amount of the total particulate mass. As the engine warms up, the mean specific particulate mass reduces for the low ambient temperature scenarios but slightly increases for normal ambient temperature scenarios.

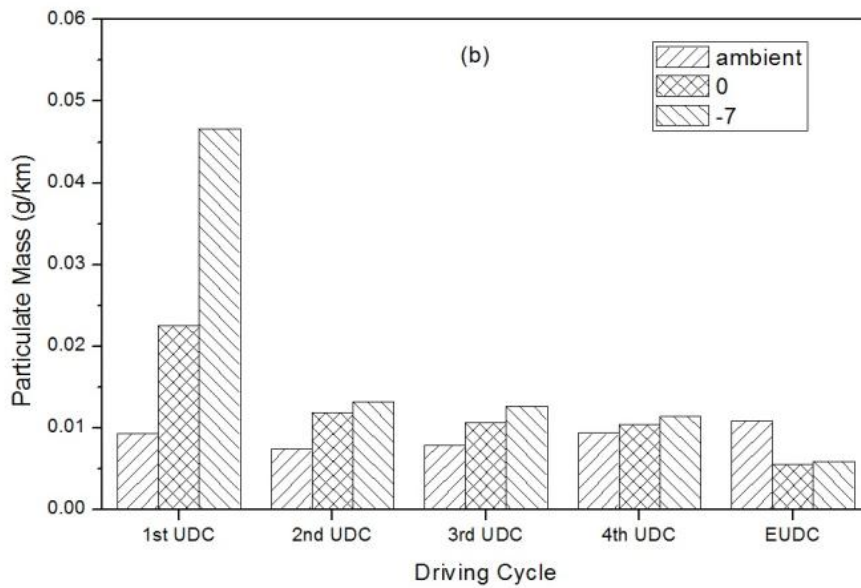
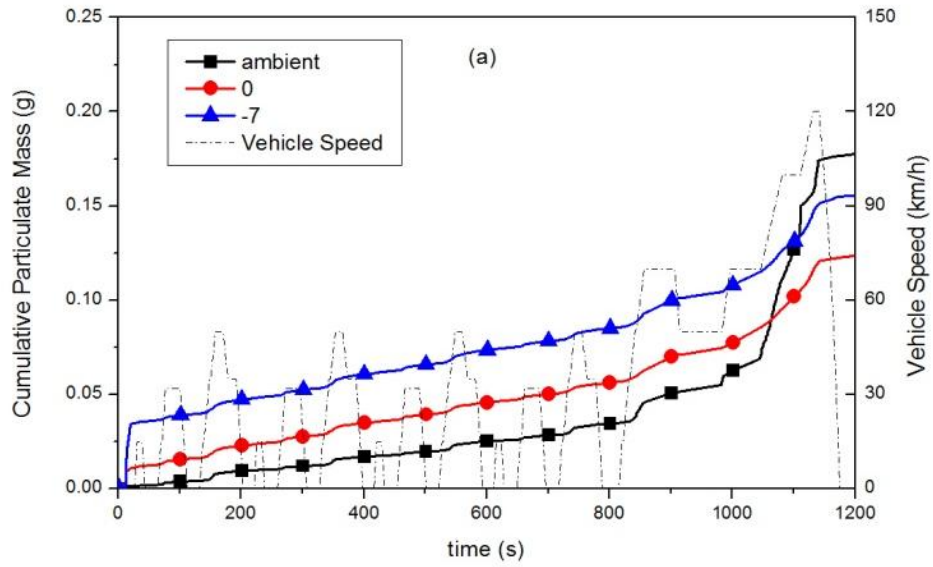


Figure 4.12 Profiles of particulate mass
a) cumulative and b) mean mass specific value

4.2 INVESTIGATIONS OF SVOC COMPOUNDS IN PARTICULATES UNDER COLD AND WARM START NEDC

Semi-volatile organic compounds (SVOC) which are generated by the unburned fuel or lubricating oil has attracted concern from researchers due to its high toxicity and carcinogenicity to human health (Fanick et al. 2015, Kweon et al. 2003). The SVOC particles of cold start (ambient 20 °C) and warm start (85 °C) NEDC with different biodiesel fuels were investigated by using a two-dimensional GC separation and time-of-flight (TOF) MS analyzer in this section. Due to the different operating principle, the two-dimensional GC separation capability is more accurate than the traditional one-dimensional GCMS (Alam et al. 2013). It could significantly reduce the peak co-elution effects and generate high resolving power when analysing particulates with complex components.

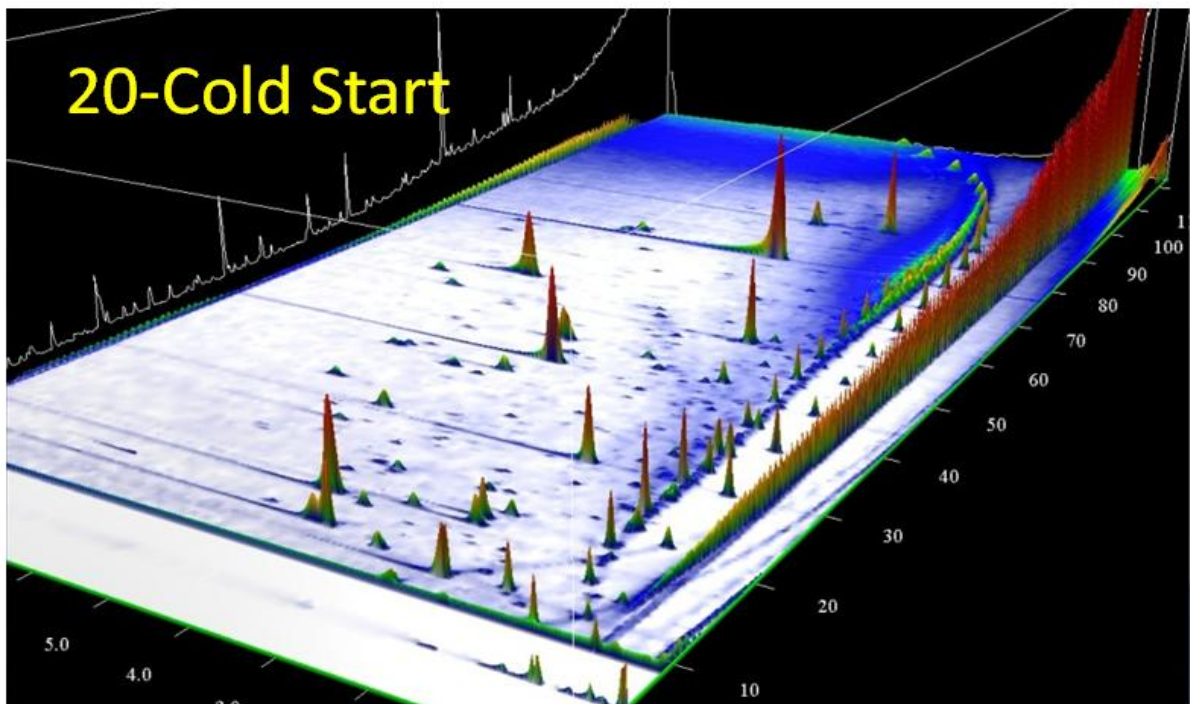
4.2.1 Experimental Procedure

The sampling flowing rate was set to 1.2 g/s for the constant volume sampling (CVS) AVL Smart Sampler to collect the particulate from a glass fibre filter of the NEDC sequence. The Smart Sampler was controlled and operated by the PUMA system. The sampling timing was programmed in the transient test sequence before each of the tests. The Smart Sampler started to collect the particulate 5s before the engine cranked and finished collection after the engine stopped. After the engine tests, filters were kept in a sealed storage before 2D-GC analysis to prevent particle volatilisation. Dichloromethane (DCM) was used as the solvent to extract the particulate from the filter. The inert gas Helium was used as a carrier to deliver the extracted particulates into the 2D-GC equipment. The transient NEDC sequences were set the same as in the previous section. The warm start test sequence was started after the engine coolant and

oil temperature fully warmed to 85 °C. All transient test sequences were repeated three times. Average results were taken for data analysis.

4.2.2 Two-dimensional GC/MS Analysis of Cold and Warm Start Transients

Figures 4.13 and 4.14 show the 3D surface plot and 2D contour plot of the cold and warm started NEDC respectively. As shown in the figures, the volatility retention timing was represented on the x-axis in the unit of minutes, while the polarity retention timing on the y-axis with the unit of seconds. Each of the dark colour dots in the contour plot or peak in the surface plot is an independent chemical. These components could be identified by matching with the mass spectral of a NIST library.



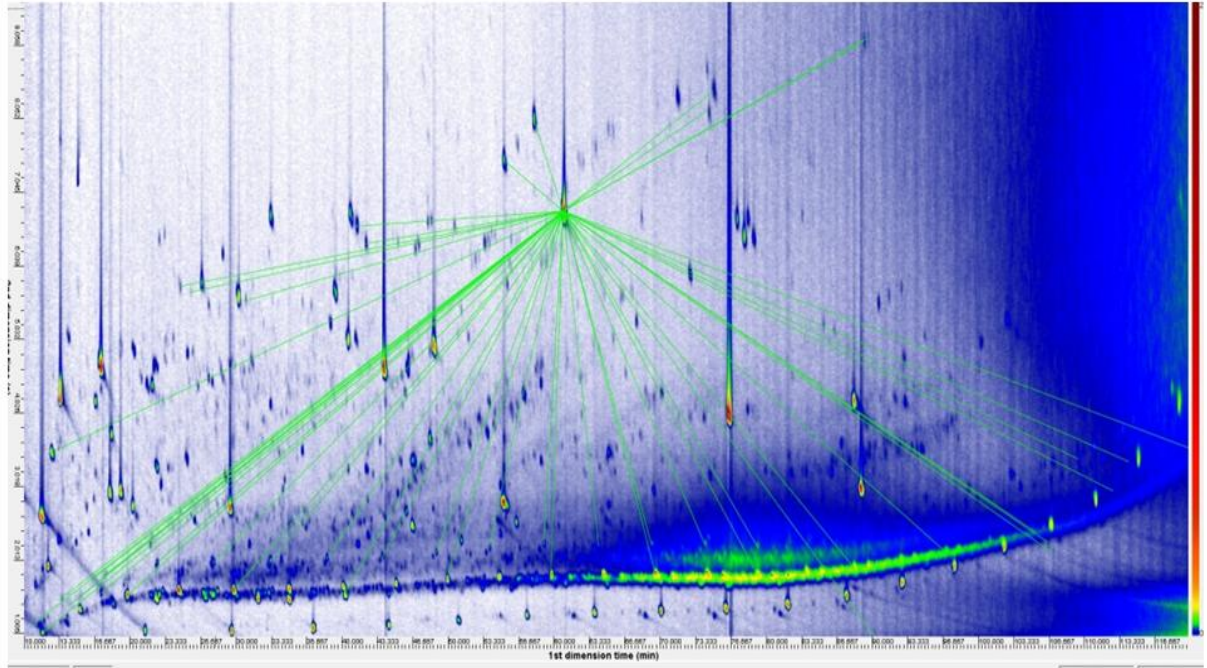
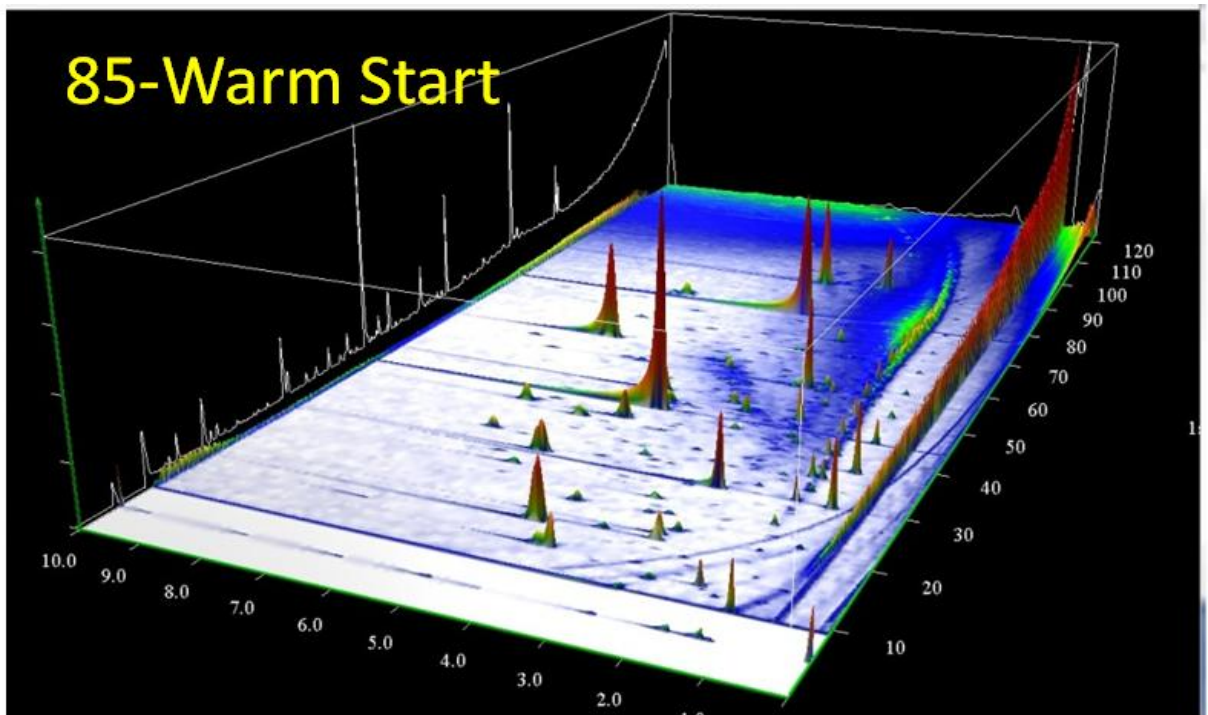


Figure 4.13 3D Surface plot and contour plot of 20 °C cold NEDC sequence



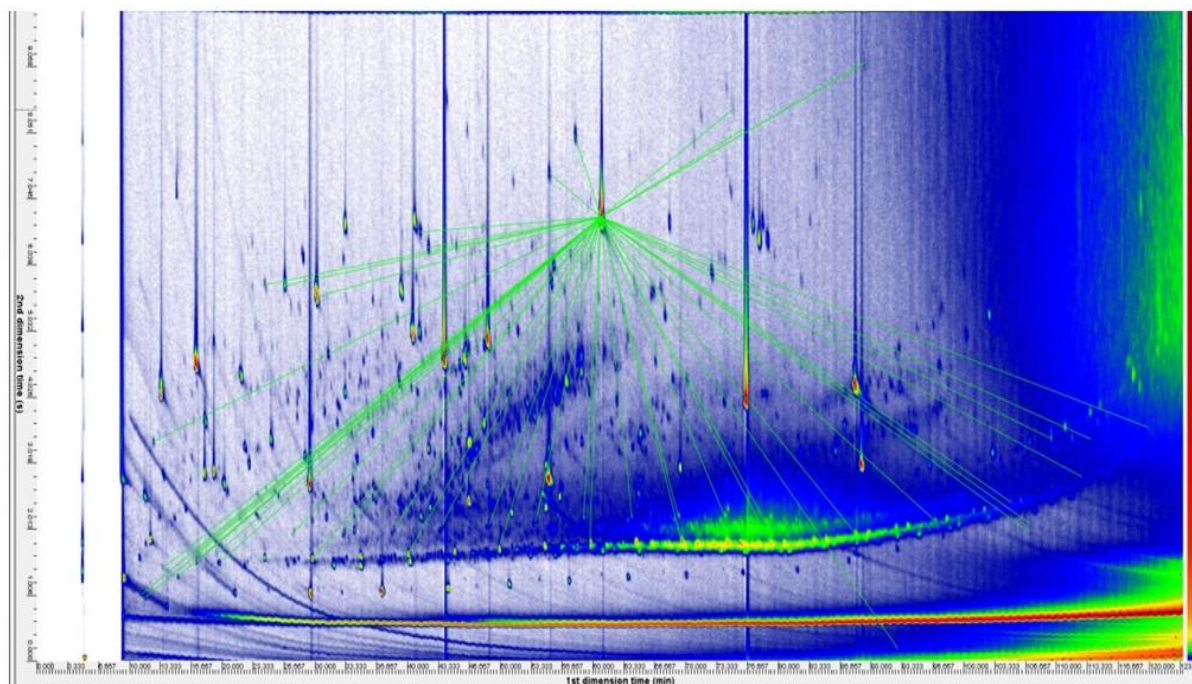


Figure 4.14 3D Surface plot and contour plot of 85 °C warm NEDC sequence

The fuel and engine oil are considered to be the main carbon source to produce the SVOC particulate emissions from the engine. Therefore, the diesel fuel and engine oil that was used in this chapter were analyzed by the 2D-GC device (see Figure 4.15). Unresolved complex mixtures (UCM) were found in each of the plots which were generated by the diesel fuel and engine oil respectively. The carbon number of diesel fuel is generally from C5 to C20; while the engine oil is between C18 and C36. During the engine's combustion process, a tiny fraction of the engine oil's molecules will be pyrolysed or cranked into small molecules, which will always produce a higher carbon number compared with diesel fuel. As a consequence, the SVOC with low and high carbon numbers in the engine emissions' particulate is considered to be caused by the fuel combustion and engine lubricant oil respectively. This is proved with the same conclusions suggested by (Black & High 2015, Eastwood 2008) from their conventional GC analyzer. By a comparison of the 2D-GC results in Figures 4.13 and 4.14, fewer peaks were found for the warm start NEDC in the lighter

molecules region (lower than C18). The engine will inject more fuels under a cold start condition, thus it produces more peaks in the region with low carbon number compounds.

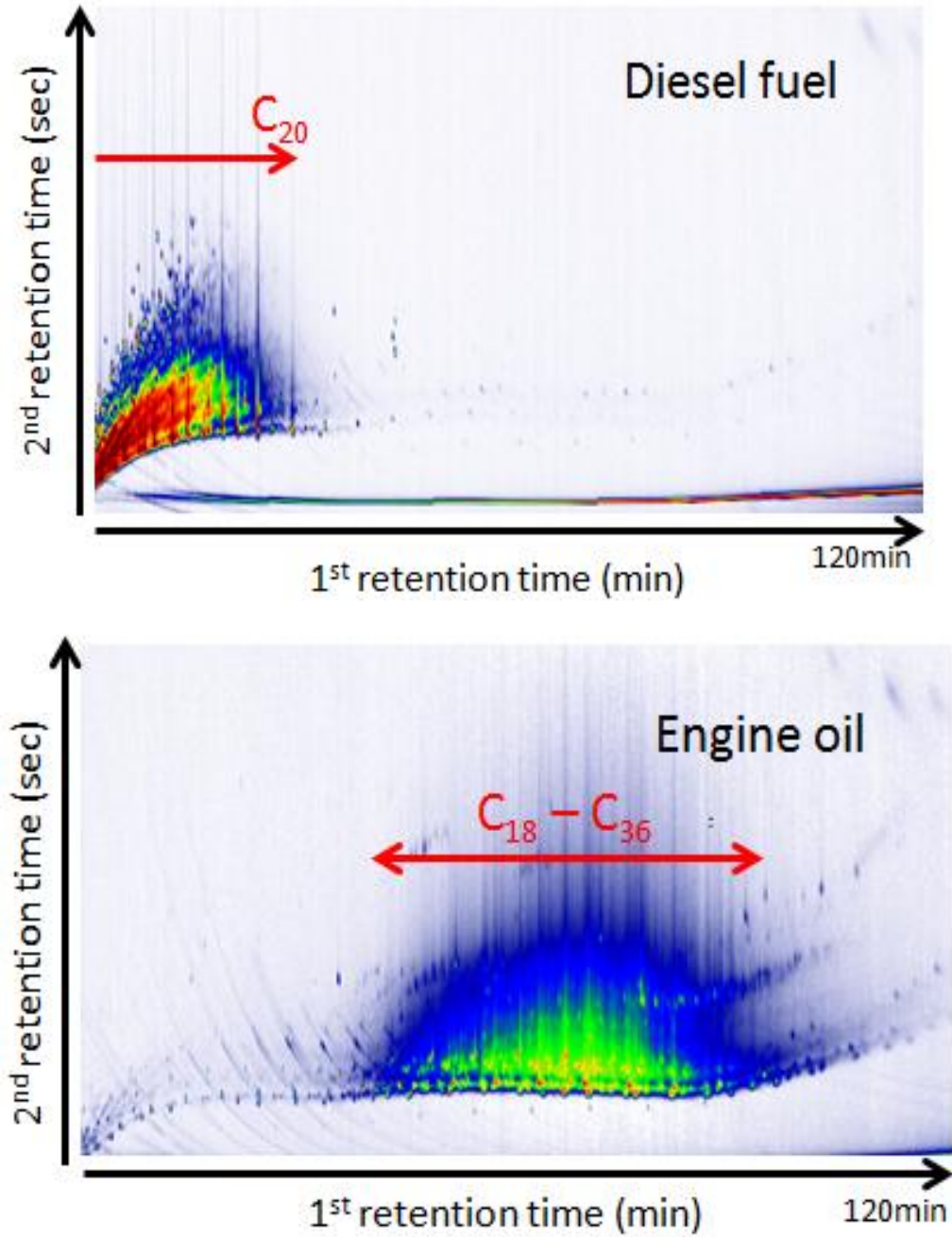


Figure 4.15 2D-GC contour plots of diesel fuel and engine oil

In order to analyze the detected SOVC species data from the 2D-GC/MS, the organic compounds' results were divided into three chemical groups: n-alkanes (Figure 4.16), alkyl-cyclohexanes (Figure 4.17) and polycyclic aromatic hydrocarbons (PAHs) series (Figure 4.18) respectively. Their detailed chemical compositions are given in Table 4.1, 4.2 and 4.3 respectively.

Table 4.1 Alkanes compositions of SVOCs in particulate emissions

Compounds		Cold Start	Warm Start
<i>Alkanes</i>	Carbon Number	ng/m³	ng/m³
dodecane	C12	42.84659	47.16998
tetradecane	C14	220.8442	69.34537
hexadecane	C16	172.4582	84.62135
octadecane	C18	92.67366	76.43393
eicosane	C20	93.71848	182.0507
docosane	C22	133.7098	241.6054
tetracosane	C24	256.2689	797.2061
hexacosane	C26	201.7312	936.4823
octacosane	C28	132.8362	543.8464
triacontane	C30	73.12834	108.8323
dotriacontane	C32	32.76769	85.23383
tetratriacontane	C34	15.39307	20.06773
hexatriacontane	C36	20.50908	21.10355

Table 4.2 Alkyl-cyclohexane compositions of SVOCs in particulate emissions

Compounds		Cold Start	Warm Start
<i>Alkyl-cyclohexane</i>	Carbon Number	ng/m³	ng/m³
cyclohexane, pentyl-	C11	69.47147	69.93984
cyclohexane, hexyl-	C12	42.40525	42.56738
cyclohexane, heptyl-	C13	49.52983	48.60211
cyclohexane, octyl	C14	47.87254	42.01794
cyclohexane, nonyl-	C15	56.63641	48.8453
cyclohexane, decyl	C16	43.99049	35.94719
cyclohexane, undecyl-	C17	36.55066	33.20904
cyclohexane, dodecyl-	C18	31.20046	30.30876
cyclohexane, tridecyl-	C19	25.1207	28.9487
cyclohexane, tetradecyl-	C20	23.51744	28.17409
cyclohexane, n-pentadecyl-	C21	20.15781	26.05743
cyclohexane, hexadecyl-	C22	18.95086	23.79666
cyclohexane, n-heptadecyl-	C23	21.67099	35.59591
cyclohexane, octadecyl-	C24	26.26459	54.69989
cyclohexane, nonadecyl	C25	31.86699	90.41289
cyclohexane, heptacosyl-	C26	19.131	19.09497

Table 4.3 PAH compositions of SVOCs in particulate emissions

Compounds		Cold Start	Warm Start
<i>PAHs</i>	Structure	ng/m ³	ng/m ³
naphthalene		126.315	98.0779
acenaphthylene		60.93278	58.30271
acenaphthene		50.17834	50.24139
fluorene		46.28729	46.08914
phenanthrene		43.08078	41.38745
anthracene		44.33276	44.97226
fluoranthene		42.4683	37.40633
pyrene		46.60254	43.44106
benz[a]anthracene		28.41728	24.81446
chrysene		28.32721	22.48163
benzo[b]fluoranthene		29.73231	29.73231
benzo[k]fluoranthene		30.42586	32.72266
benzo[a]pyrene		36.32548	37.6225
dibenz[a,h]anthracene		38.69434	38.5232
benzo[ghi]perylene		38.37909	61.23001
indeno[1,2,3-cd]pyrene		37.3703	38.40611

The n-alkane series is one of the most common chemical substances that can be detected in diesel fuel and lubricating oil. Particulate alkanes are normally generated from the unburned or partially burned fuel and lubricant oil. During engine combustion (around 800 °C), parts of the fuel may not be able to sufficiently mix with the oxygen and will undergo pyrolysis to form small molecules or SVOCs. Generally, the carbon number for the presence of n-alkanes in the diesel fuel and lubricating oil is less than 35 (Kweon et al. 2003). Figure 4.16 illustrates the concentrations of the n-alkanes series' emissions of the cold and warm start NEDC. Two concentration peaks can be observed for both of the test sequences. The carbon number between C12 and C18 is considered as caused by the diesel fuel. Those alkane species with a length of carbon chain higher than C20 are believed to be caused by the lubricant oil as diesel fuel components are detected lower than that range. The NEDC which starts from the ambient temperature condition produced higher concentrations of lighter n-alkane compounds (fuel fraction region) compared with the warm start sequence; due to its higher amount of fuel injection. The lubricant oil plays a more important role for the n-alkane particles' emission compared with diesel fuel when the engine is running under warm conditions. The second peak concentrations of both transient conditions are located at the alkanes' species with a carbon number between C24 to C26. The peak value in the lubricant oil fraction of a warm start NEDC is approximately four times higher than that of a cold start NEDC. The high engine operating condition will result in low viscosity of the lubricant oil, thus leaving a residual of the lubricant oil in the cylinder which is emitted as particulates (Liu 2014).

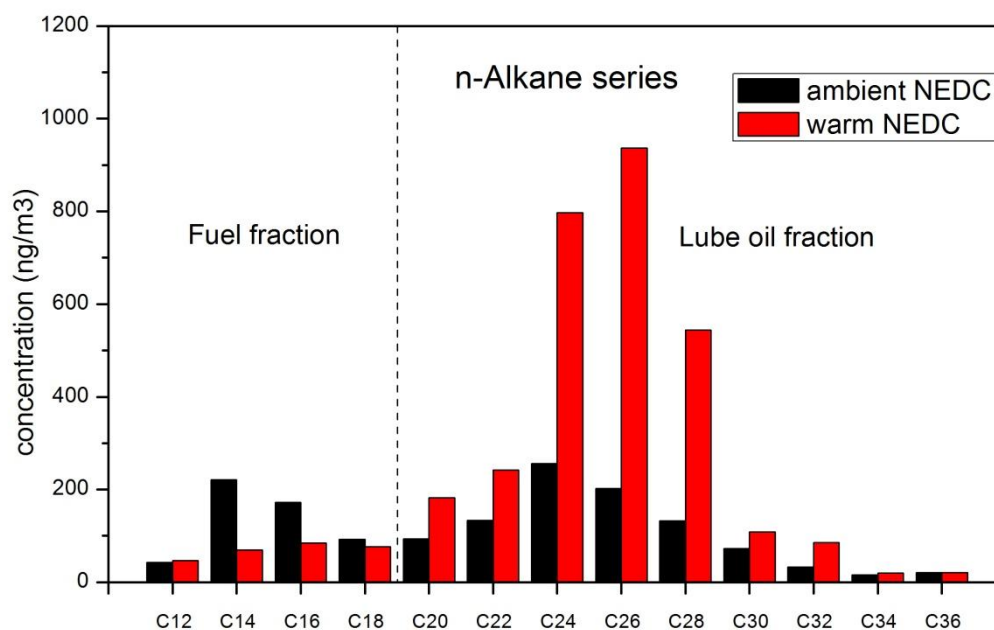


Figure 4.16 Concentrations of n-Alkane series particulates of cold and warm NEDC

The alkyl-cyclohexane series are the chemical compounds consisting of one carbon ring and other hydrocarbon radicals. They commonly appear in diesel fuels and diesel engine particulate emissions. Kweon et al. (2003) found that the alkyl-cyclohexane was around 7 to 14% of the particle-phase organic compounds under their research conditions. Figure 4.17 presents the concentration carbon number distributions of the alkyl-cyclohexane species. The concentration of the ambient start NEDC sequences is slightly higher than that of the warm start in the carbon number region between C11 and C18, which is considered as mainly caused by the fuel. In contrast, different trends were found in the lubricant oil fraction region, with the warm start sequence being much higher than that of ambient cold start. In both test conditions, the fuel consisted of a high fraction of the total identified alkyl-cyclohexane species. Pentyl-cyclohexane (C11) and nonadecyl-cyclohexane (C25) produce the highest concentration value for ambient start and warm start NEDC respectively.

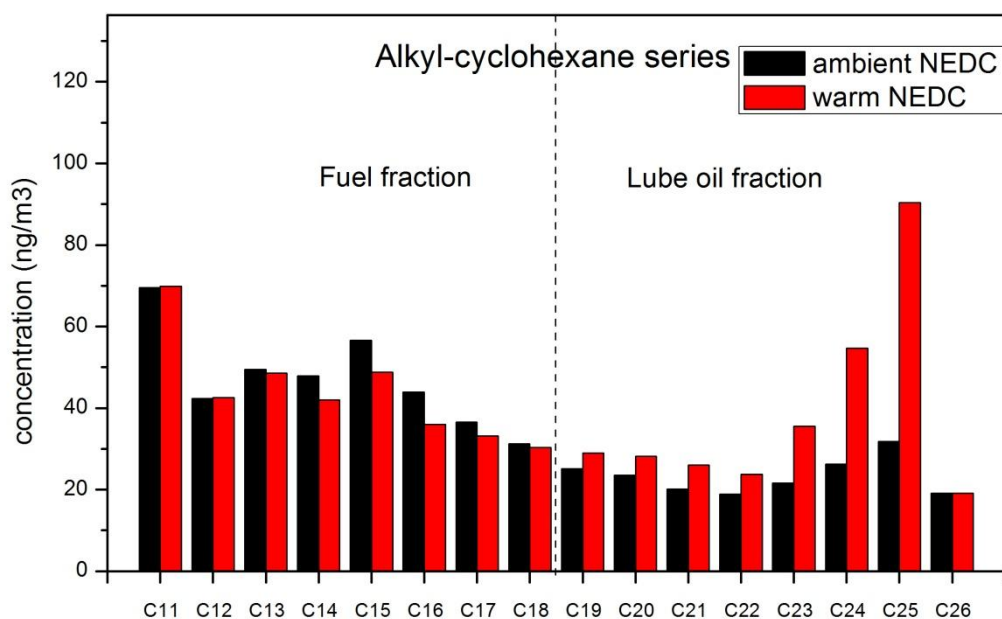


Figure 4.17 Concentrations of Alkyl-cyclohexane series particulates of cold and warm NEDC

PAHs are currently considered as crucial chemical molecules for precursors of soot formations (Heywood 1988). Sixteen of the thirty-two main toxic PAHs that were established by the United States Environmental Protection Agency (EPA) were resolved and quantified by the 2D-GC/MS device from the diesel engine particulate filters in this section (Figure 4.18). All the detected PAHs were displayed as an order of aromatic rings number. The PAH species composed of less aromatic rings produces higher particle emissions. Naphthalene was clearly shown as the highest PAH for both of the test sequences; it was nearly two times higher than the second highest value of acenaphthylene when the engine was running under a cold start NEDC sequence. During engine combustion, after the dehydrogenation and ring-forming processes, the non-aromatic fuel molecules containing 12-22 carbon atoms will result in the formation of benzene with one aromatic ring (Eastwood 2008, Schonborn 2009). The benzene will grow bigger with the process of combustion to form low aromatic ring number PAHs. Therefore, the amount of low ring number PAHs is expected to be higher at

all conditions. Furthermore, most of the PAH species concentrations were lower under a warm NEDC sequence except benzo[ghi]perylene. This may be as a result of the increased fuel injection quantity and incomplete combustion of cold ambient conditions.

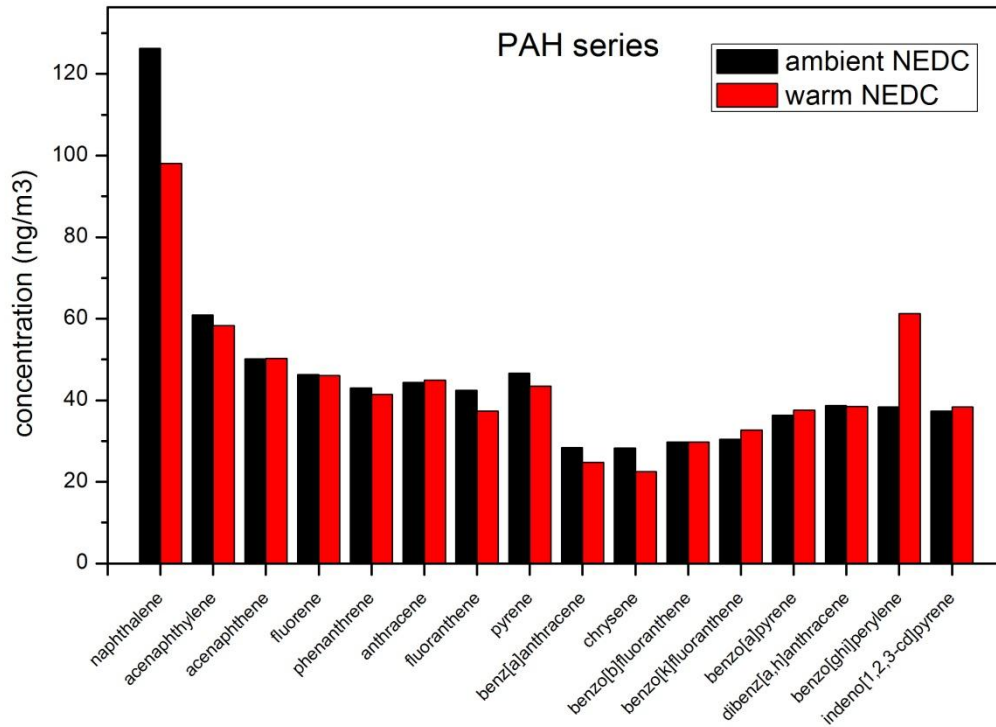


Figure 4.18 Concentrations of PAHs of cold and warm NEDC

4.3 CONCLUSIONS

New European Driving Cycle transient scenarios were carried out on a V6 turbocharged diesel engine at various ambient temperatures between +20 °C and -7 °C. A 2D-GC/MS analyzer was used to investigate SVOCs under cold and warm start NEDCs. The findings can be summarized as follows.

Transient Investigation Parts:

- Gaseous and particulates emissions are increased with decreasing ambient temperature. Cold start is a dominative segment of the NEDC for CO, THC and the total particulate mass emissions. At the EUDC stage, the engine emits low mean mass specific emissions compared with the previous UDCs.
- As the driving cycle runs consecutively, the emissions of the engine are highly dependent on the engine temperature rather than the ambient temperature.
- The EGR valve remained mostly closed throughout the whole -7 °C NEDC scenario. The EGR valve opened more as the temperature increased during the NEDC.
- All of the mean mass specific emission values for different temperature scenarios become closer at the later stage of the NEDC.
- The exhaust particulate mass is higher at the end of the EUDC for normal ambient scenarios due to the increased accumulation mode particulate number. The engine particulate emissions are significantly affected by the EGR level.
- Particulate spikes are observed during transient conditions. The size of the total particulate number spikes is mainly determined by the nucleation mode particulate number. These particulates are generated at both very high and very low AFR conditions. The size of the spikes is bigger at the former condition under the NEDC.

Particulate Chemical Investigation Parts:

- By using a higher resolution of the 2D-GC/MS, it can be proved that both the fuel and engine oil contribute as main carbon sources to produce the SVOC particulate emissions from the engine combustion.

- The fuel injection quantity is a dominating factor in determining the SVOC particles under a cold start condition; it is proportional to the number of chemical compounds in the low carbon length region.
- Two n-alkane species' concentration peaks are observed for both of the cold and warm start sequences. The NEDC start from the ambient temperature cold start condition produces higher concentrations of lighter n-alkane compounds, such as tetradecane and hexadecane, compared to the warm start sequences.
- The lubricant oil indicates it is a more important factor for the n-alkane particles' emission than diesel fuel, when the engine is running under warm conditions.

The concentration of naphthalene is nearly two orders higher than acenaphthylene. As the combustion progresses, the engine tends to produce a high concentration of low carbon number PAHs in the low carbon number region.

CHAPTER 5

EVALUATIONS OF THE IMPACT OF INTAKE AIR HEATING ON DIESEL ENGINE TRANSIENT EMISSIONS IN A SUB-ZERO ENVIRONMENT

As has been discussed in the previous chapter, ambient temperature has significant impact on diesel engine transient emissions. The emissions of the cold start phase account for a substantial amount of the overall regulatory driving cycle emissions. In this chapter, the potential use of intake air heating strategies were evaluated in reducing the driving cycle emissions and engine efficiencies of a CRDI diesel engine at low ambient temperature conditions.

5.1 AIR HEATING APPLICATION ON ENGINE COLD START

A large market share of passenger cars is shifting towards to diesel engines due to their reliability and outstanding engine efficiency (SMMT 2013). Cold start emissions are a crucial issue for diesel engine development; they are related to the engine calibration, fuel injection strategies, fuel characteristics, lubricating oil, environmental temperatures and the after-treatment device's efficiency. Since the cylinder chamber and combustion temperature of the cold start phase is lower than that of normal operating conditions, the engine may suffer insufficient fuel-air mixing and thus high engine emissions. Furthermore, engine downsizing and the reducing compression ratio is another challenge for diesel engines cold start, due to

the limitation of the engine working input (McGhee et al. 2012). This is more pronounced when the engine is operating at low ambient temperature conditions (Han 2001) (MacMillan et al. 2008). The most commonly used auxiliary device to improve cold start behaviour in commercial diesel engines is the glow plug. However, many researchers have reported inhomogeneous heating issues for the implementation of glow plugs during engine combustion (Walter et al. 2009, Manente et al. 2007, Lindl et al. 1999). Intake air mass flow rate, temperature of the environment and re-circulated air were considered as the main factors to affect the combustion charge air temperature. Lindl (1999) concluded that the implementation of an intake air heater or other electrical burner was an effective method to improve the performance of engine cold start, similarly to warm start. It could significantly reduce the gaseous emissions of CO and THC, which are considered to be mainly caused by incomplete combustion.

Since the publication of EURO 3 and 4, low ambient temperature transient testing (-7°C) has been authorized as part of emission standards for gasoline passenger cars (Directive 98/69/EC) (Dardiotis & Martini 2012). Therefore, it is strongly believed that emissions' regulation control at low ambient temperature will also be adopted for diesel vehicles in the near future. Due to the low efficiency of after-treatment systems and engine calibration characteristics, engine cold start is considered as a crucial segment of emissions over a whole driving cycle. Mark and his co-researchers reported that over 50% of cumulative particulates were emitted within the first 200 seconds of the NEDC sequence (Peckham et al. 2011).

In this chapter, evaluations of an air heating system at sub-zero ambient conditions were proposed, under NEDC transient cycles. Engine performances, gaseous emissions, particulates with size and mass, as well as the engine efficiency, were analyzed with the different heating strategies.

5.2 TEST CONDITIONS AND PROCEDURE

The tests were carried out in the cold cell at the University of Birmingham (UoB). The temperature control capability of the transient test bench can be varied down to -20°C . The NEDC was programmed by a PUMA automation control system to evaluate engine transient performances. The detailed description of the cooling systems is given in Chapter 3. The engine was soaked at the desired temperature in the heat insulation cell for at least eight hours prior to the tests to ensure that the coolant, fuel, oil and air temperature were maintained constantly. A ventilation air system was utilized to provide air flow passing around the engine.

In commercial diesel engines, the minimum self-ignition temperature at the end of the compression stroke of the air-fuel mixture is around 410°C when the engine is operated under normal ambient temperature cold start phase (20°C) (Payri et al. 2013). To determine the energy required for heating the intake air system during cold start, three important parameters needs to be considered: the intake air mass flow rate, thermal power dissipated in the air and the temperature of supply air to the heater.

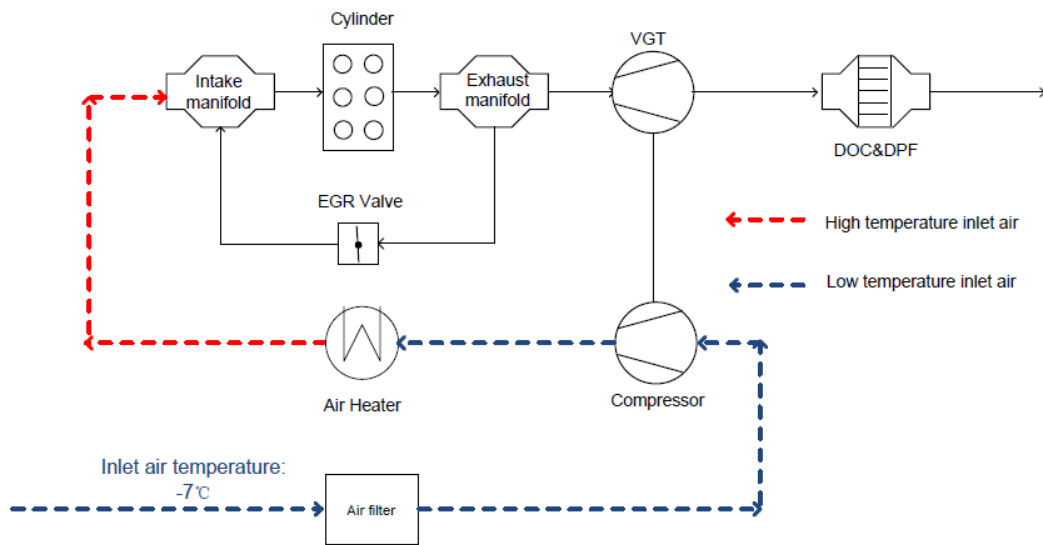


Figure 5.1 Schematic diagram of the air thermal heating system

In the experiment, an intake air heater was installed downstream of the compressor. The electric power for the 3kW air heater was controlled with an external variable voltage source in order to achieve different initial intake air temperatures. The transient sequence was started from the cold start phase; therefore, there was no air flow before the engine was cranked. As a consequence, incremental power ratings of the heater were carried out before each test to obtain the required total electrical energy for the desired intake air temperatures. The total intake air heater operating timing was set to 1 minute including 40 seconds prior to the test and 20 seconds after the engine ignited.

5.2.1 Calculations and Data Processing

Heater Capacity Calculation

The heating capacity was calculated by the following equation before the test to achieve the demanded inlet temperature at the starting phase:

$$Q_h = C_p \times \dot{m}_{air} \times dT \quad (\text{Eq. 5.1})$$

Where C_p is the specific heat capacity of the intake air which is 1KJ/kgK; \dot{m}_{air} is the intake air mass flow rate at the cold start idling speed, which is around 69 kg/h at 650rpm; dT is the temperature differential between the environment and target heating value. The heater efficiency is highly dependent upon the intake air mass flow rate. Based on the research from (Payri et al. 2006), the thermal power from the heater to be dissipated in the air can be assumed at around 75%. With the calculation of the heating capacity, a 3kW heater was chosen combined with a variable voltage source to adjust the intake air temperature.

Engine Efficiency Calculation

The engine brake efficiency η and the engine power output P can be calculated by the following equations (Heywood 1988),

$$\eta(t)(\%) = \frac{3.6 \times P(t)(kW)}{\dot{m}_f (kg/h) \times Q_{HV} (MJ/kg)} \quad (\text{Eq. 5.2})$$

$$P(kW) = 2\pi \times N(\text{rev}/s) \times T(N \cdot m) \times 10^{-3} \quad (\text{Eq. 5.3})$$

Where \dot{m}_f is the mass flow rate of the injected fuel; Q_{HV} is the lower heating value of the diesel fuel used in this study, which is 42.3 MJ/kg; N and T are the engine speed and torque respectively, obtained from the PUMA system.

The overall thermal efficiency η_c was calculated based on the second law by the following equation:

$$\eta_c (\%) = \frac{\int_{t=i}^{t=f} P dt}{\int_{t=i}^{t=f} (Q_h + Q_f) dt} \quad (\text{Eq. 5.4})$$

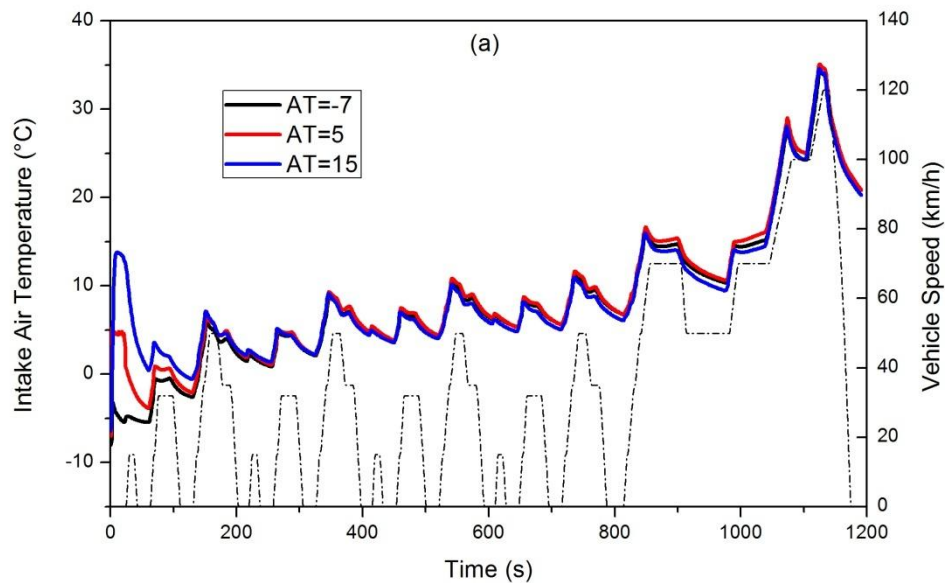
Where P is the engine power output; Q_h is the total heating energy obtained by the whole system; Q_f is the total energy released by the diesel fuel.

5.2.2 Test Procedures

The probe sampling points of the emission analyzers were located upstream of the after-treatment devices. Average results were taken from three repeated experiments for data analysis. After each test, the engine was cranked without fuel injection for several seconds in order to remove the residual fuel mixture which was generated from the previous sequence.

Figure 5.1 shows the temperature profiles of intake air, coolant and oil in the sump over the regulatory driving cycle. It is obvious from Figure 5.1 (a) that the profiles of intake air

temperatures with air heating are kept at the environment temperature ($-7\text{ }^{\circ}\text{C}$) in the first several seconds of the transient sequence. The intake air temperature did not reach the required heating temperatures instantaneously after the engine ignited. The intake air temperature with air heating was increased until the engine was operated at the idling condition; whereas the intake air temperature of $-7\text{ }^{\circ}\text{C}$ was slightly decreased at the beginning of the NEDC. The temperatures were getting closer to each other as the transient sequence was running continuously. Figures 5.1 (b) and (c) present the coolant and oil temperature profiles over the NEDC. It is clearly shown that the coolant and oil sump temperatures were almost identical throughout the whole NEDC transient sequence.



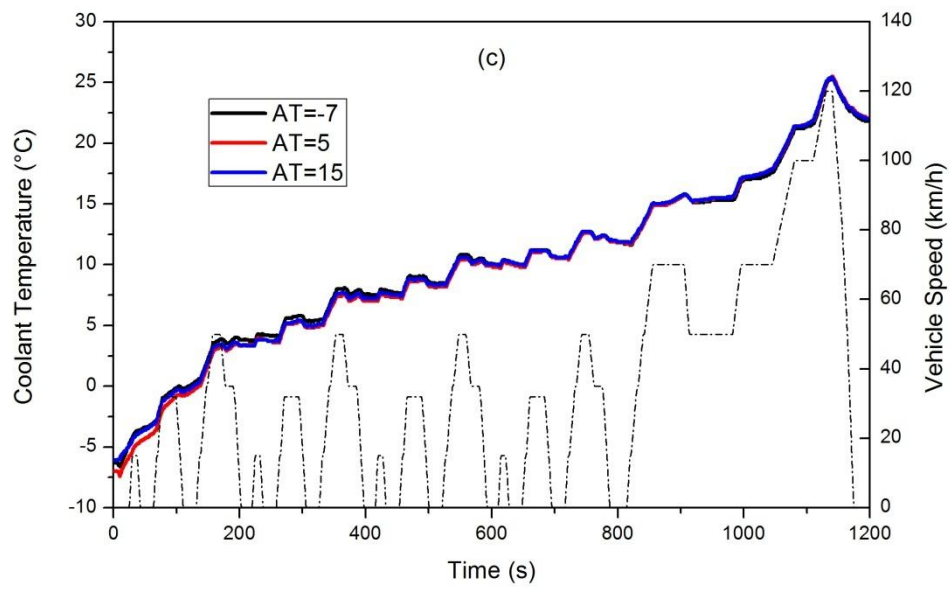
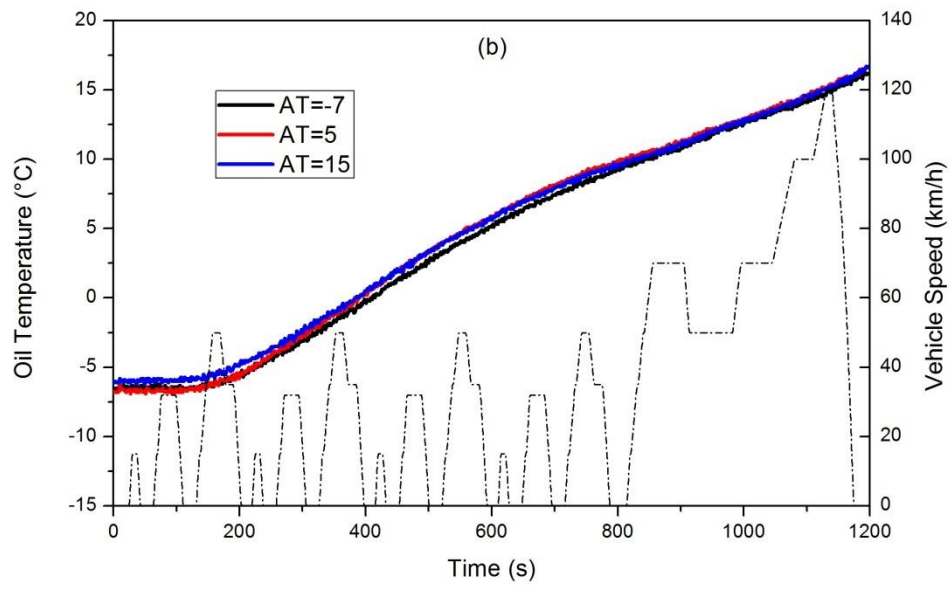


Figure 5.2 Temperature profiles a) intake air, b) engine coolant and c) engine oil

5.3 RESULTS AND DISCUSSION

5.3.1 Engine Performances

The engine speed and torque performances under different air heating strategies at a $-7\text{ }^{\circ}\text{C}$ environment are presented in Figure 5.3. The previous chapter summarized some typical features of engine cold start, which are high components' friction, poor fuel atomization, high heat transfer or heat loss and lubricating oil deterioration. In order to overcome the above issues, the engine ECU calibration at low ambient environment tends to inject more quantity of fuel to achieve the initial engine combustion. As a result, more fuel is accumulated inside the cylinder after several revolutions of the crankshaft. As the in-cylinder pressure and temperature increased, the fuel burned abruptly and that led to the rapid rise in engine speed to reach a peak value.

It can be observed from Figure 5.3 that the intake air temperature profile has significant impact on the engine performance. In terms of engine speed, the intake air heater reduced the cold start cranking period and increased the peak engine cranking speed. On the other hand, torque fluctuations and unconformities were observed during the first several seconds of the NEDC. This is due to higher frictional and pumping forces and incomplete combustion of fuel at very cold ambient temperatures. The peak speed value of the engine at $-7\text{ }^{\circ}\text{C}$ environment temperature of the transient sequence with $5\text{ }^{\circ}\text{C}$ and $15\text{ }^{\circ}\text{C}$ air heating strategy is about 17% and 22% higher than that of the sequence without a pre-heating stage. The higher intake air temperature improved the cold fuel evaporation, fuel-air mixing and combustion. Moreover, it will also reduce the frictional forces, produce better performance of the lubricating oil and eventually result in high initial starting peak speed and short crank period.

However, during the later stages of the driving cycle, both the engine speed and torque profiles became identical for all the intake air temperature sequences.

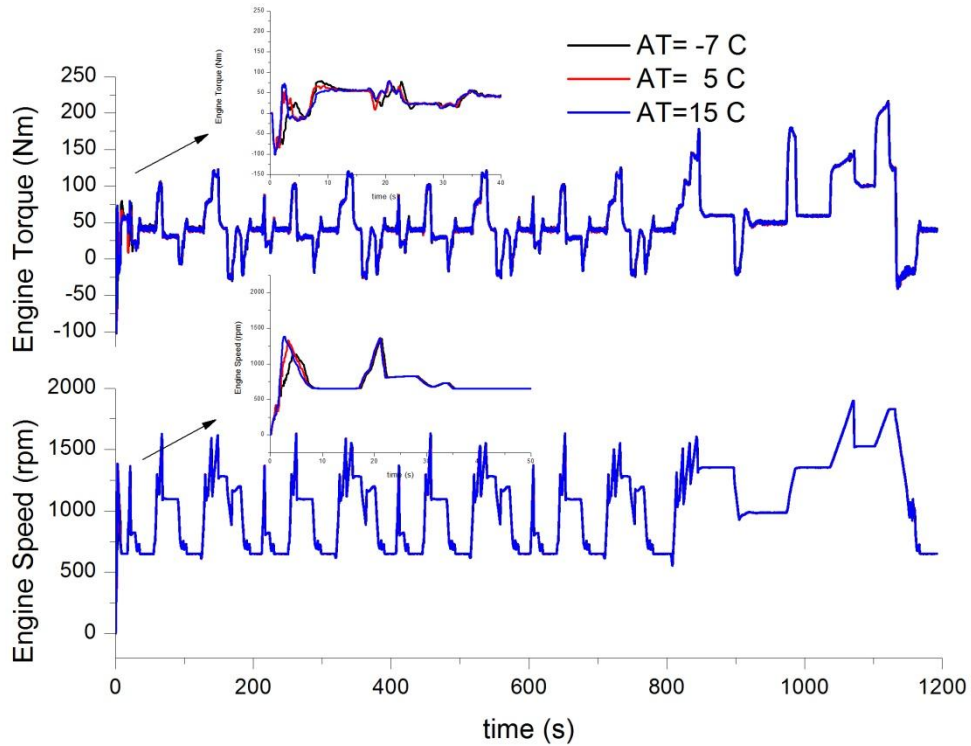
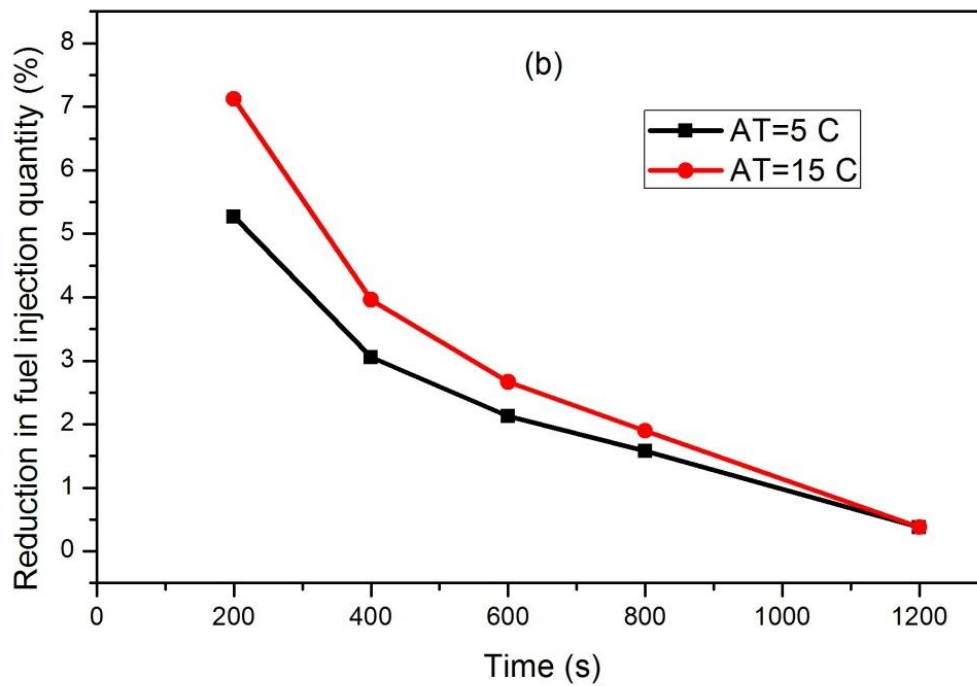
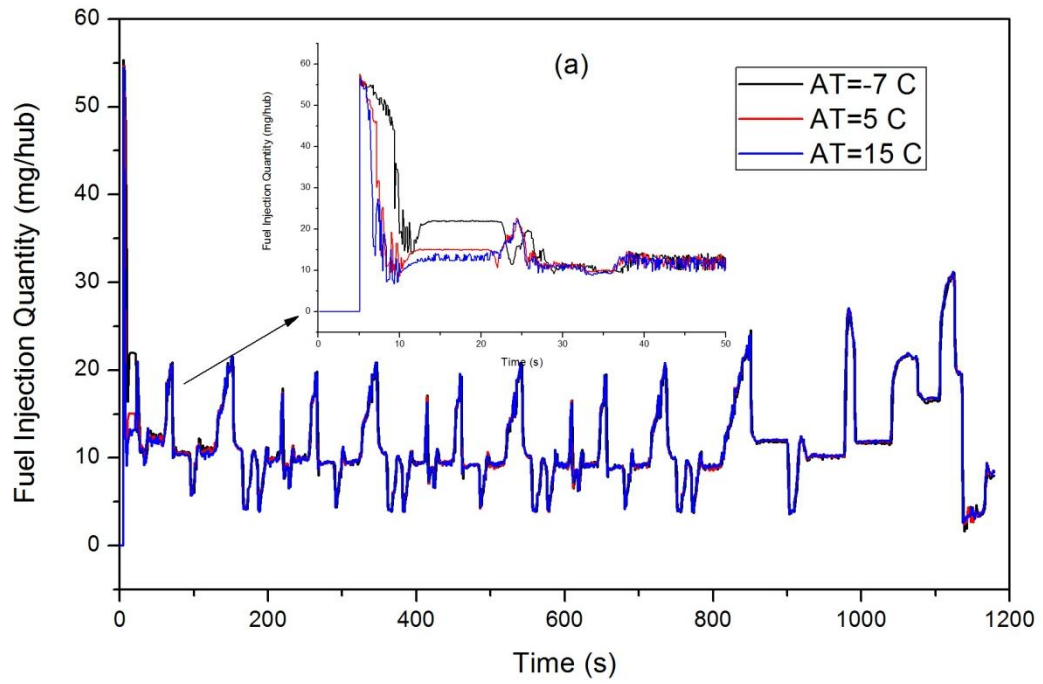


Figure 5.3 Engine speed and torque profiles at different intake air temperatures

Figure 5.4 (a) illustrates the instantaneous fuel injection quantity over the NEDC. It is clearly shown that the fuel injection quantity decreases as the heating temperature increases at the beginning of the transient sequence. The detailed fuel injection quantity percentage reduction profiles between the preheated intake air of 5, 15 °C and -7 °C sequences are presented in Figure 5.4 (b). Higher intake air temperature significantly improved the engine combustion performance when the engine is operating at the early stage of the NEDC. The fuel injection quantity percentage reduction becomes smaller as the driving cycle continues. At the end of the NEDC, the quantity of the fuel injection of the preheated and reference sequence become closer to each other.



**Figure 5.4 Profiles of fuel injection quantity a) instantaneous
(b) percentage of reduction using heating strategies**

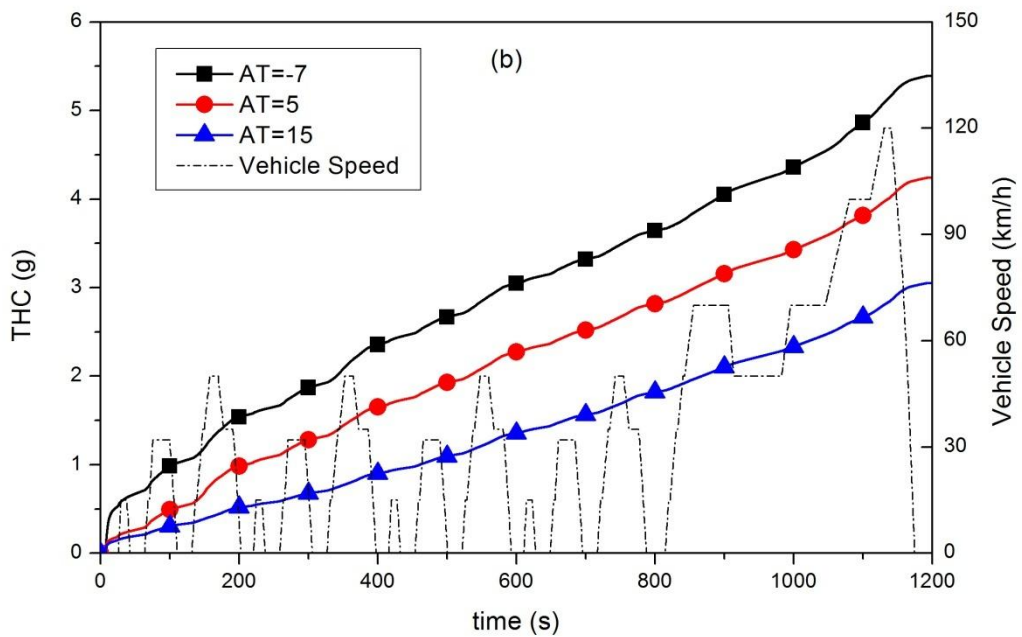
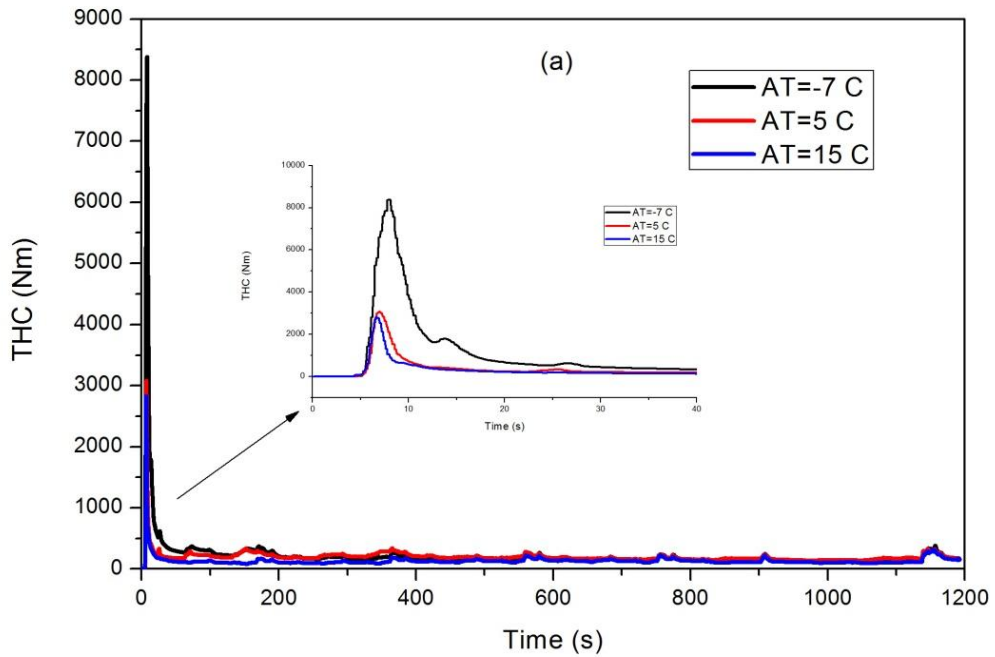
5.3.2 *Gaseous Emissions*

Hydrocarbon Emissions

The instantaneous and cumulative THC emissions under various thermal heating strategies over the NEDC are presented in Figure 5.5. It is clearly shown that the engine operating at a sub-zero condition without pre-heating produces larger transient spikes at the beginning of the cycle. This could be attributed to the higher fuel injection quantity at the low ambient temperatures, especially during the cold start period. Furthermore, the fuel could have higher viscosity and thus higher surface tension at low temperature conditions. As a result, the fuel would undergo slow evaporation, poor atomization or even impingement into the cylinder wall before combustion. On the other hand, poor performances of lubricating oil could cause the blow-by problem which deteriorates the engine combustion. The high heat transfer between the cylinder and the environment at the cold ambient temperature will enhance the flame quenching and thus increase the THC emissions. Another important factor for the increasing THC could be attributed to the over-lean fuel-air mixture, where the fuel can be oxidized by the relatively slow thermal-oxidation reaction. All the above-mentioned factors will finally result in poor fuel-air mixing and incomplete combustion that favours THC emissions.

Figure 5.5 (b) demonstrates the cumulative THC emissions over the whole NEDC cycle. It is obvious that the engine's cold start phase and the first UDC stage account for a large amount of the total cumulative THC. The pre-heated intake air significantly improved the initial combustion chemical reactions and resulted in ignition delay reduction. Therefore, the intake air heating strategy substantially reduced the cumulative THC, especially during the cold start phase. The intake air temperatures of 5 and 15 °C reduced the first phase of the NEDC cold

start phase emissions by approximately 40% and 65%, compared with the NEDC test conducted at $-7\text{ }^{\circ}\text{C}$.



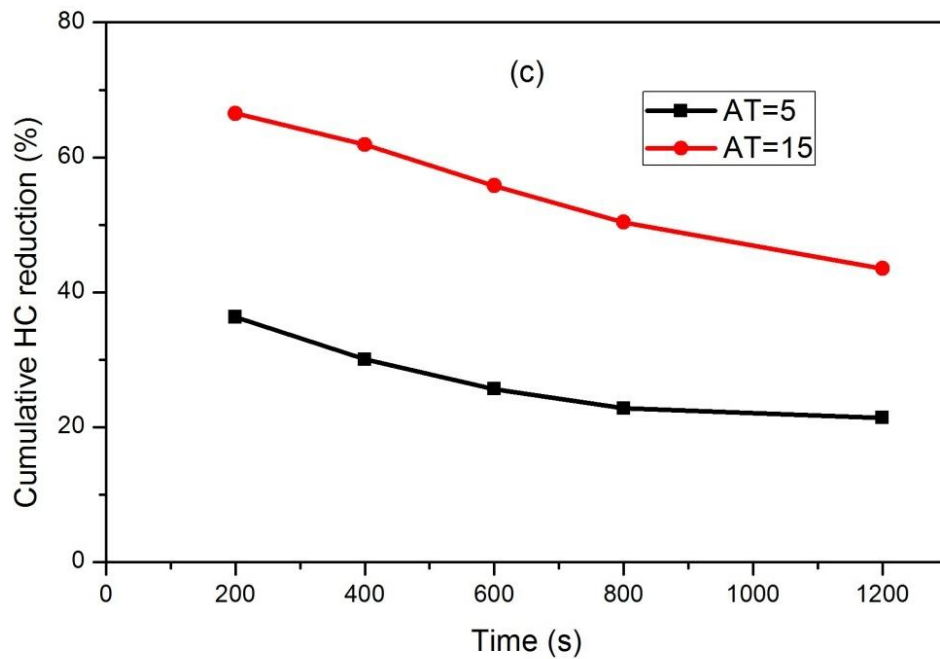


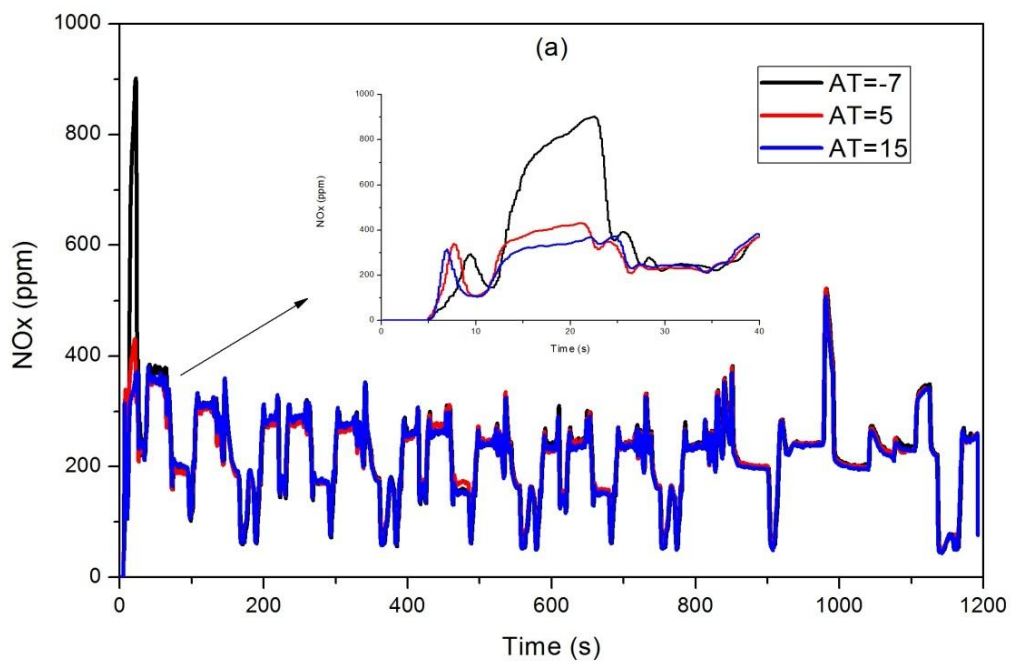
Figure 5.5 Total hydrocarbon emissions at different intake air temperatures
a) instantaneous, b) cumulative and c) percentage reduction

Nitrogen Oxides Emissions

Figure 5.6 presents the nitrogen oxides (NO_x) emissions over the NEDC sequence in the environment temperature of -7 °C. The instantaneous NO_x emissions of the sequence with a pre-heating stage were lower than those of the benchmark scenario. The transient emissions spike reduced with the increasing heating temperature. The engine calibration would be changed depending upon the shifting environment temperature matrix. In this study, the EGR valve was kept closed for the all test sequences conducted in the -7 °C ambient temperature conditions. Therefore, the increased combustion temperature at the cold start segment of the NEDC is considered to be caused by the increasing fuel injection quantity for the test sequence without heating aids; which eventually resulted in a notable NO_x emissions penalty. Furthermore, low intake air temperature scenarios boost the intake air mass flow, which will

increase the oxygen availability for combustion and thus increase the NO_x emissions. With the progress of the legislative cycle, the instantaneous NO_x emissions of different heating strategies become identical for all the sequences. However, the cumulative emissions for the low intake air temperature were higher than those of the preheated intake air (Figure 5.5 (b)).

Figure 5.6 (c) shows the percentage reduction in NO_x emissions over the NEDC sequence. The cumulative NO_x emissions in the first 200 seconds of the NEDC sequence with intake air heating at 5 and 15 °C decreased by approximately 8.5% and 9.5% respectively, compared with the transient scenario without a pre-heating stage; whereas the overall NO_x for the whole NEDC reduced by 3.75 and 5% respectively when the air-heating was utilized. The percentage reduction in the cumulative NO_x emissions between the air heating and -7 °C scenarios reduced as the transient sequence ran continuously. This indicated that the thermal heated intake air strategy was more effective at the cold start segment and the early stage of the transient sequence.



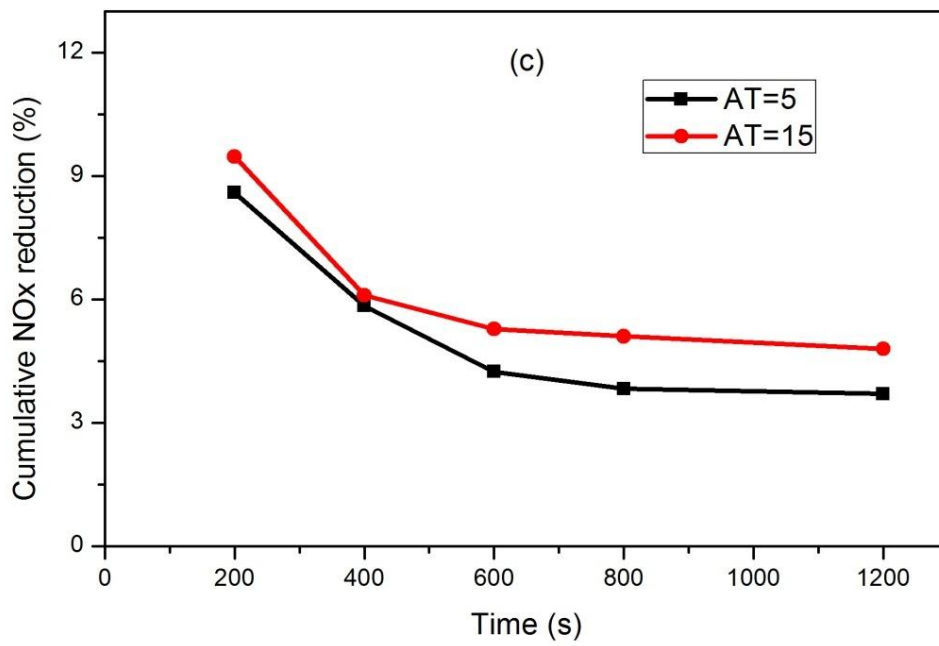
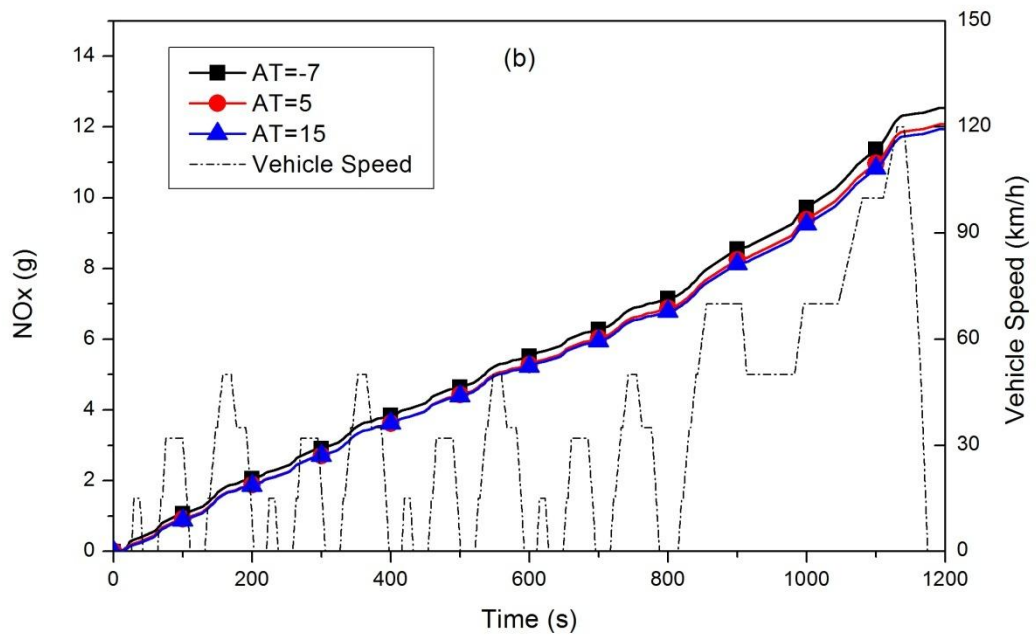


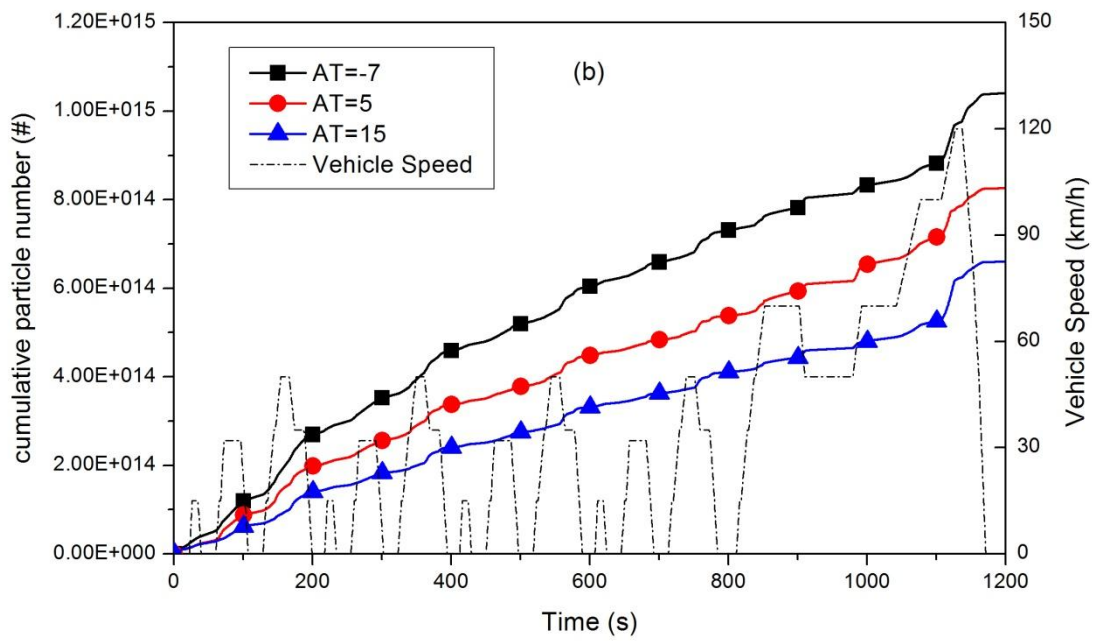
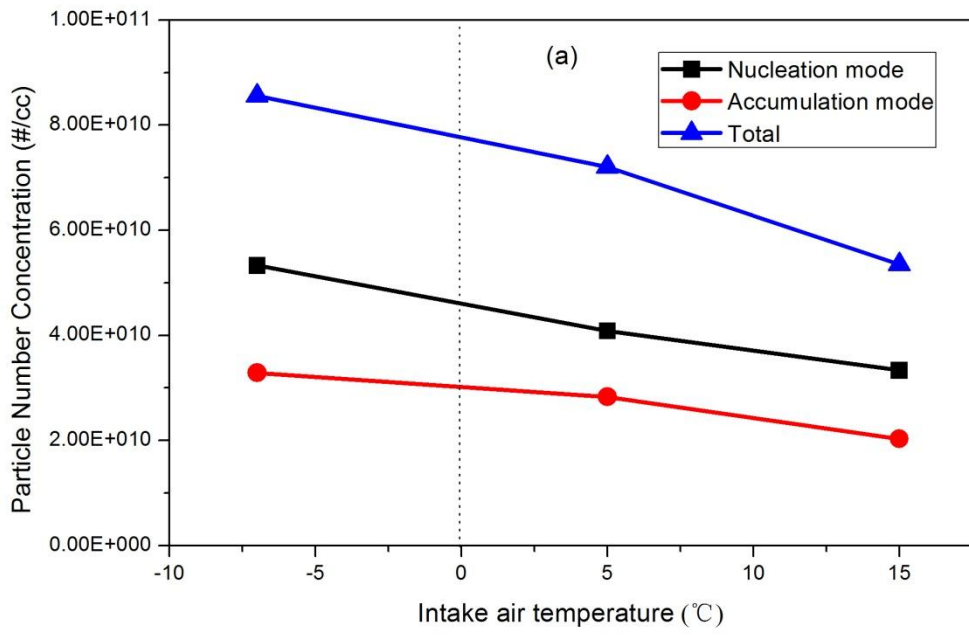
Figure 5.6 Nitrogen oxides emissions at different intake air temperatures,
 a) instantaneous b) cumulative c) percentage reduction

5.3.3 *Particulate Emissions*

Particle Number

The particulates for engine research mainly consist of nucleation mode and accumulation mode particles. In the previous chapter the nucleation mode particles were defined in the range between 5 and 50 nm; while accumulation mode particles are between 50 and 1000 nm. Figure 5.7 (a) represents the nucleation mode, accumulation mode and total particulate emissions over the NEDC sequences conducted with various intake air temperatures at -7 °C ambient condition. It is obvious that all kinds of the particulates decreased with the increasing intake air temperature. High intake air temperature improved the in-cylinder temperature and engine combustion at a low temperature environment; this is a benefit for particulate emissions. Moreover, the increased fuel injection quantity and poor fuel atomization in a cold environment are also favourable for soot formation and lead to excessive particle emissions.

The characteristics of the cumulative particulate number over the NEDC using different heating strategies are presented in Figure 5.7 (b). The transient sequence with heated intake air supply produced low particulate emissions throughout the whole scenario due to the low fuel injection quantity and better fuel-air mixing. Figure 5.7 (c) illustrates the average particle number concentration for the first UDC and the whole NEDC sequence at the three intake air temperature conditions. The particles emitted from the first UDC accounted for around 25% of the total particles in the -7 °C environment without heating; whereas it was around 20% for the sequence with an air heating supply. Therefore, the air heating strategy reduces the cold start phase impact on the overall particulate emissions over the NEDC.



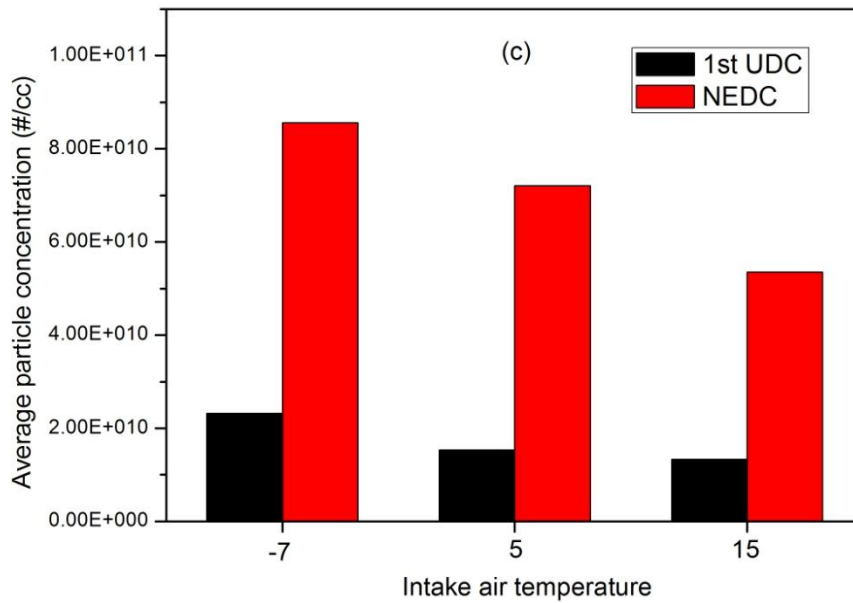


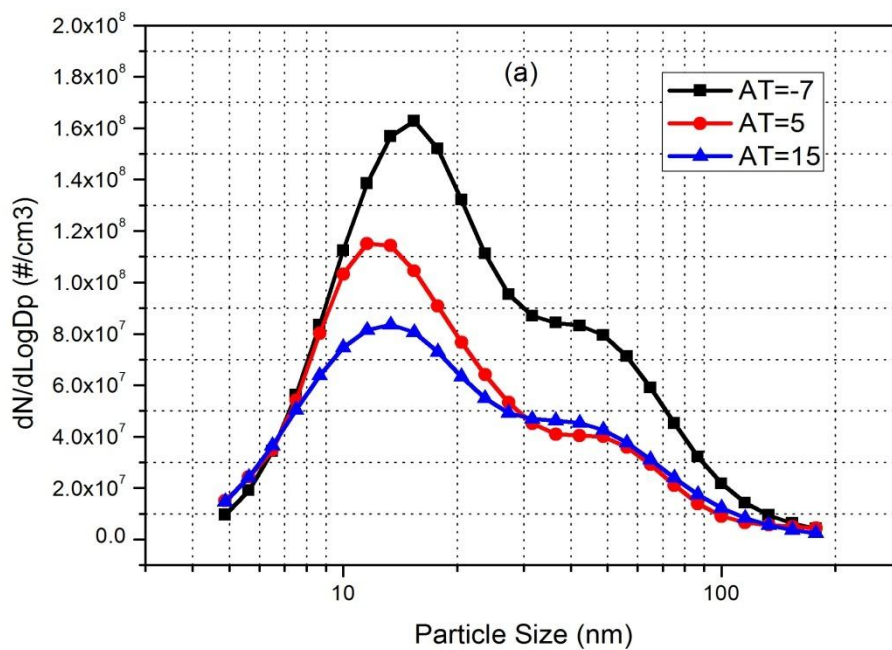
**Figure 5.7 Particulate emissions at different intake air temperatures,
a) breakup b) cumulative c) total**

Particle Size Spectral Density

The average size spectral density (SSD) with particle number and size over the whole NEDC under various heating strategies is described in Figure 5.8 (a). It is obvious that the particulates generated from a cold environment without a heating stage produce a higher amount of particle numbers in the size range between 10 and 100 nm. The peak value point of the particle number for all sequences was shifted towards the small particle diameter as the air heating temperature increased. Furthermore, the nucleation mode particles' number decreased when the air heating temperature increased. Soot formation from engines is significantly impacted upon by the localized temperature distribution, fuel evaporation, atomization and oxidation in the fuel-rich regions. With the utilization of the intake air heater, the fuel injected into the cylinder chamber will undergo better oxidation with the charging air

and thus reduce the fuel pyrolysis and particle nuclei. This eventually decreases the nucleation and acceleration mode particles in size and concentration simultaneously.

Figure 5.8 (b) indicates the percentage of particle size range distribution over the NEDC under different heating strategies. It is clearly shown that the particles with a diameter between 10 and 23nm account for around 42% to 45% of the total particles for all transient sequences. While the particles whose diameter is between 23 and 100nm, account for around 35% of the total particulates. The percentage contribution of smaller size particles (diameter less than 10 nm) was increased as the intake air temperatures increased. In addition, higher intake air temperatures reduced the particles in both diameter and number compared with the particles emitted in a -7 °C environment.



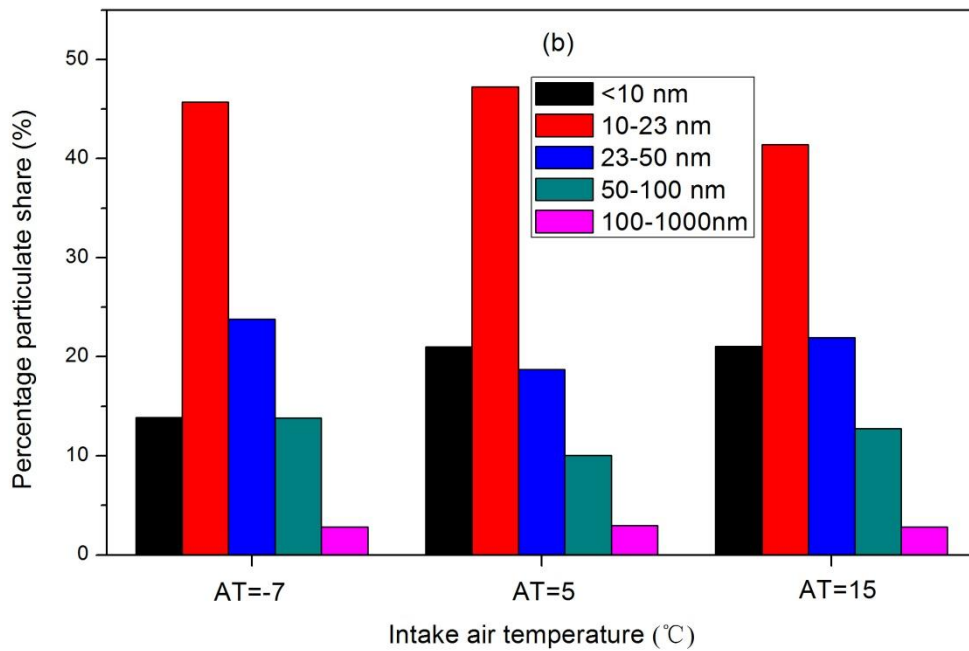


Figure 5.8 Particle size spectral density

a) size distribution b) percentage share

Particle Surface Area

Particle surface area (PSA) is a crucial factor of particulate research to indicate the capability of volatile hydrocarbon fractions and PAHs' adsorption (Dhar et al. 2013). The particle number and surface area are important parameters indicative of potential health problems, especially for the respiratory system of human beings (Kasper & Burtscher 2005). Assuming that the measured particulate is in a spherical shape, the particle surface area can be calculated by the following formula (Eq. 5.5):

$$dS = dN \cdot 4\pi \cdot r_p^2 \quad (\text{Eq. 5.5})$$

Where dN is the particulate number concentration in a unit area and r_p is the mean radius of particulates.

Figure 5.9 shows the surface area of accumulation and nucleation total particulates during the first UDC stage at different intake air temperatures. It is observed that the surface area of the accumulation mode particles account for a large amount of the total particles for all the temperature conditions.

The total surface area of the particles was reduced with the increasing intake air temperatures due to the improved combustion. The surface area of the nucleation particles was reduced by about 60% and 40% for intake air temperatures of 5 °C and 15 °C respectively. The surface area of the accumulation particles was reduced by nearly 50% when the intake temperatures increased from -7 to 5 °C. The reduction proportion was almost kept constant when the intake air temperature increased further. As discussed in the previous section, the particle number concentration was decreased as the intake air temperature increased. Therefore, the mean radius per unit volume was increased when the engine intake air heated from 5 to 15 °C.

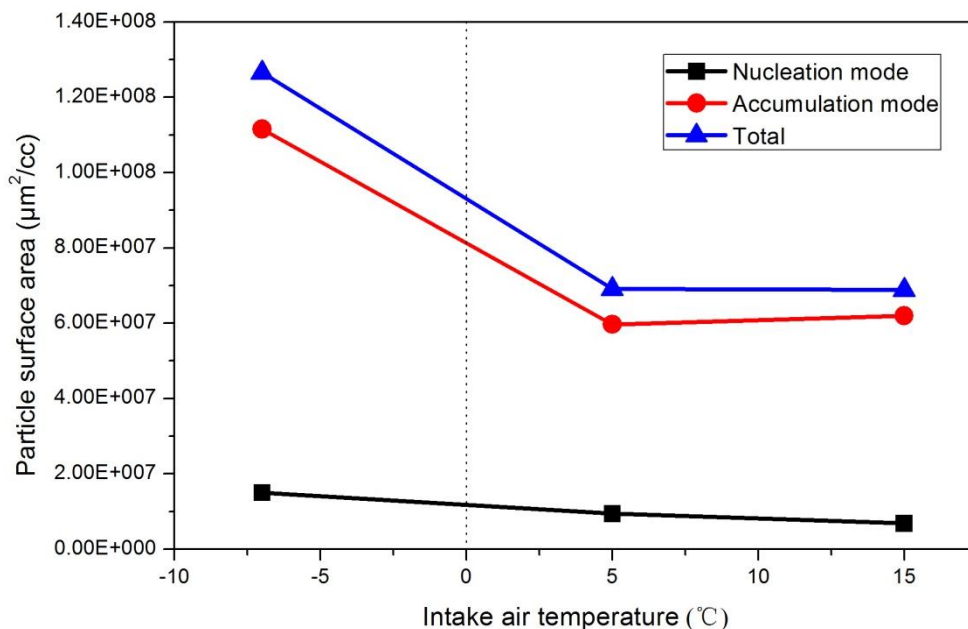


Figure 5.9 Particle surface area at different intake air temperatures

Particulate Mass

The particulate mass (PM) over the NEDC with different intake air temperatures are described in Figure 5.10.

As can be seen from the figure, the particulate mass profile increased significantly at the beginning of the NEDC cycle for all the transient sequences. The particulate mass of the test sequence without a pre-heating stage grew faster than the sequence with air heating as the transient sequence ran continuously. The cumulative particulate mass of the first UDC stage at $-7\text{ }^{\circ}\text{C}$ was about 20% of the entire NEDC; whereas the percentage was around 12-14% for the sequence with the intake air heating. With intake air heating the engine will undergo less fuel injection quantity, better fuel evaporation/atomization and thus better combustion and less soot precursor. All the above mentioned features are the crucial factors for the particle mass reduction when the engine is operated with air heating. Also, it is observed from the figure that the particulate mass increased sharply at the later stage of the EUDC for all the transient sequences. This is believed to be caused by the increasing accumulation mode particles which account for a large amount of the total particulate mass.

Moreover, the engine produces a small number of nucleation mode particulates and a high number of accumulation mode particulates at the EUDC stage. During this period of time, the non-volatile carbonaceous particles increase and absorb the volatile particles to form accumulation mode particulates and reduce the nucleation mode particulates as a consequence. Under acceleration and low AFR engine conditions, more fuel is injected and thus a high in-cylinder temperature is achieved. As a consequence, non-volatile carbonaceous particulates were burned which eventually reduced the accumulation mode particulates and promoted the volatiles to form the nucleation mode particulates.

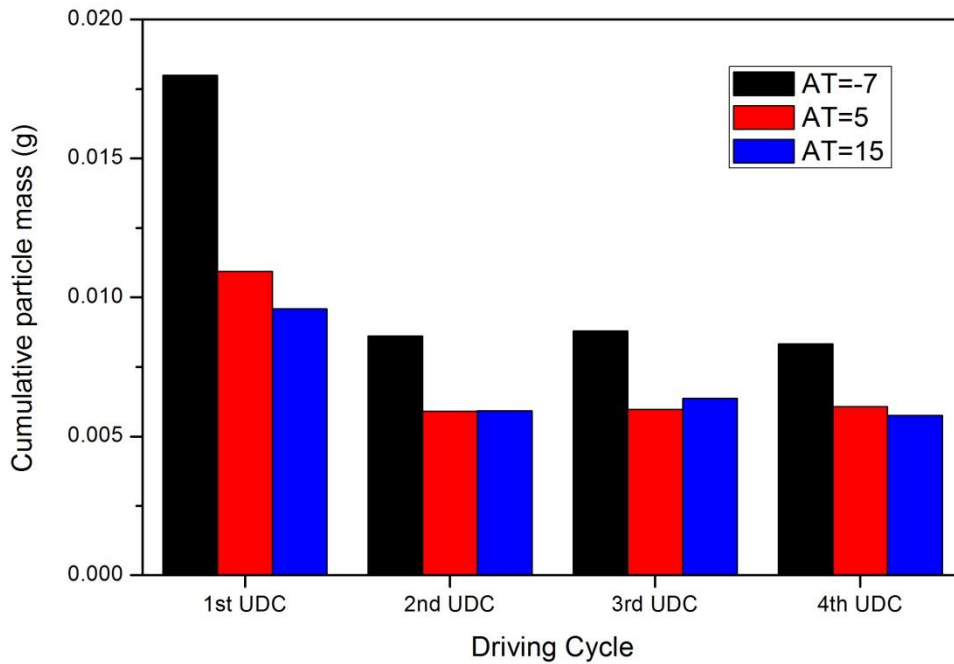


Figure 5.10 Particulate mass characteristics with different intake air temperatures

Engine Efficiency

The instantaneous engine efficiency calculated by Equation 5.2 is given in Figure 5.11. The test sequence with higher heating temperatures produced higher engine efficiency in the first 40 seconds of the transient NEDC. The engine efficiencies tended to become identical after the air thermal heating system was deactivated. Figure 5.12 shows the cumulative gaseous and particulate emissions versus engine efficiency over the first UDC of the NEDC sequence. The intake air heating strategy of 5 and 15 °C applied in this research improve the engine efficiency by approximately 0.85 and 1.46% respectively. On the other hand, the cumulative THC and PN for the first UDC decreased significantly by up to 71% and 48% respectively; whereas the NOx emissions decreased by around 15% for the sequence with 5 and 15 °C air heating.

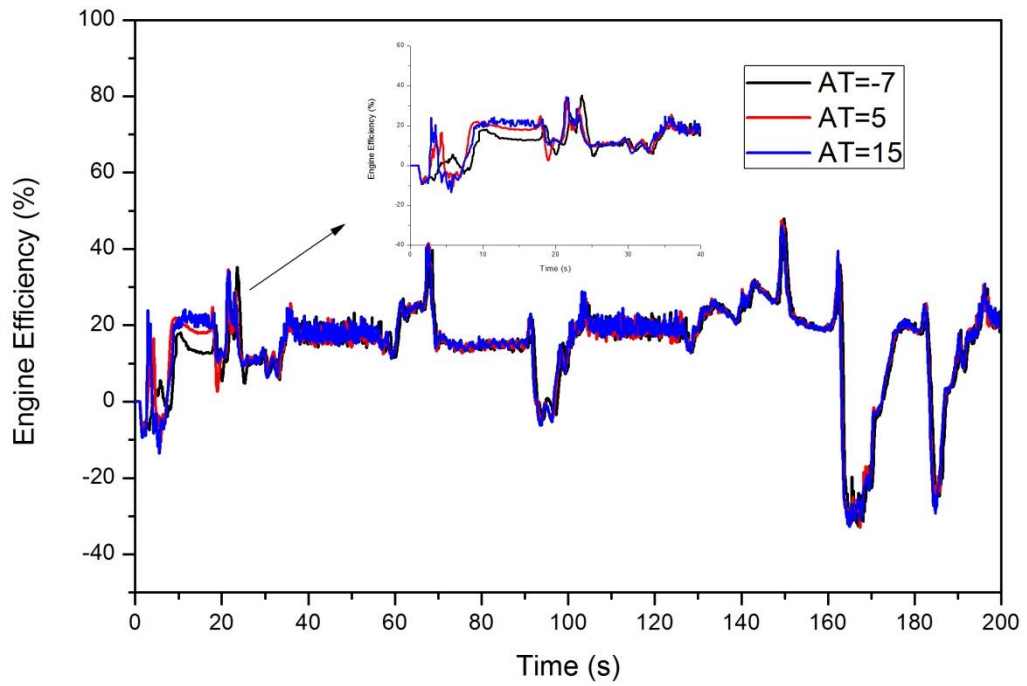


Figure 5.11 Engine efficiency characteristics at different intake air temperatures

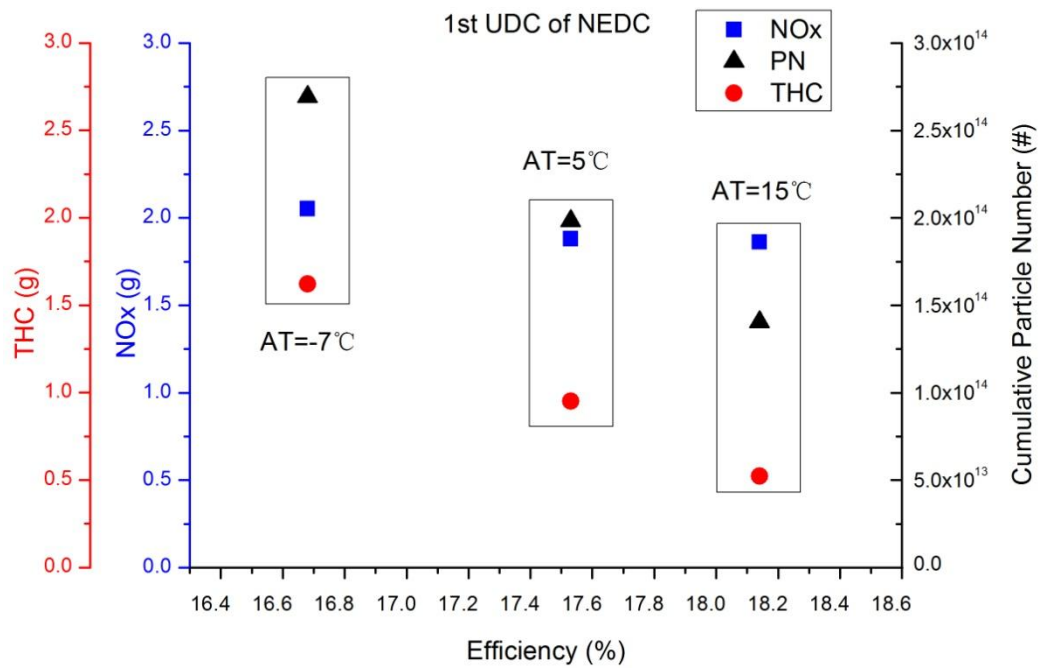


Figure 5.12 Overall engine efficiencies and emission characteristics at different intake air temperatures

5.4 CONCLUSIONS

This chapter investigates the effect of intake air temperatures on transient cycle emissions from a CRDI diesel engine at cold ambient temperatures. A 3kW heater was installed upstream of the intake manifold with a variable voltage source to vary the intake air temperature. NEDC sequences were conducted to evaluate the transient performance of the engine. Some findings can be summarized as follows.

- Intake air heating at cold ambient temperature conditions improved the evaporation of the fuel and thereby reduced the engine cranking period. Torque fluctuations were observed at the beginning of the transient sequence.
- The intake air heating has significant impact on the engine performance and emissions during the first stage of the NEDC. However, almost all of the engine parameters and emissions tend to become identical at the later stage of the transient sequence.
- The intake air heating reduced the cold start THC spike significantly. The cumulative emissions of the first UDC for the 5 and 15 °C heating strategy were reduced by approximately 40 and 65% respectively, compared to the sequence without heating.
- The heated intake air improved the NO_x emissions by up to 10% over the first UDC stage due to the reduced fuel injection quantity. However, the higher degree of intake air heating temperature has a very tiny influence on the NO_x emissions' reduction.
- Relatively higher intake air temperatures reduced the diameter and number of the particles. The particulates with the diameter range between 10 and 23 nm accounted for around 45% of all the intake air temperature sequences.

- The particle number for the first UDC occupied around 25% of the overall NEDC sequence in the $-7\text{ }^{\circ}\text{C}$ intake air temperature environment. This value was reduced to about 20% when the engine was operated with the heated air supply. The particulate mass was higher (around 20% of NEDC) during the initial stages of the NEDC due to the higher number of accumulation particulates at $-7\text{ }^{\circ}\text{C}$ and was reduced to 12-14% by using intake air heating.
- The engine efficiency during the first UDC was increased by approximately 0.85 and 1.46% with the intake air heating temperature at 5 and 15 $^{\circ}\text{C}$ compared with the $-7\text{ }^{\circ}\text{C}$ sequence.

In summary, implementation of an intake air heating strategy in a CRDI diesel engine improved the cold start performance and fuel economy of the engine, as well as reducing the gaseous and particulate emissions significantly during the NEDC test at low ambient temperatures.

CHAPTER 6

STEADY AND TRANSIENT ANALYSES RUNNING WITH BIODIESEL BLENDS

This chapter investigates the effects of different biodiesel blends on the engine combustion and emissions under various steady-state and transient conditions using fast response diagnostic equipment. The experimental work was conducted by using mineral diesel (B0) and three different blending ratio rapeseed methyl esters (RME) (B30, B60, B100 by volume) without any modifications of the engine's parameters. The purpose of this chapter is to investigate the characteristics of the engine-out emission performances, especially for the particulate matter when the engine is running under acceleration and load changing transient conditions. The combustion and particulate distribution was analyzed under the corresponding steady-state conditions. Three mode shifting transition scenarios were applied in order to evaluate the turbo-lag effects on the engine emissions. The influence of acceleration duration on transient is evaluated in the second part of this chapter. The particle number, gaseous emissions and their cumulative emissions were calculated and discussed under various transient conditions.

6.1 INTRODUCTION

The emission characteristics of an engine during transient conditions have attracted attention from researchers in recent years because of stricter exhaust emissions' legislation and the

high frequency of occurrence of transients in daily driving. Many researchers agree that engine performance during transient conditions is worse than the steady-state performance due to sudden changes in the engine's parameters (Nuszkowski et al. 2008, Kang & Farrell 2005). This issue is more pronounced in turbocharged diesel engines mainly because of the lag response of the turbocharger speed adjustment (Terdich et al. 2011). The particulate matter, as well as the other kinds of gaseous emissions, is significantly affected by the insufficient intake air mass under transient conditions. Biodiesel, as one of the most widely used alternative fuels at present, contains oxygen atoms in its molecular structure. It is expected that the surplus oxygen from biodiesel could improve combustion especially in the region of non-homogeneous air-fuel mixture.

6.2 TEST CONDITIONS AND PROCEDURE

Three discrete engine transient sequences were carried out between four steady state engine modes as listed in Table 6.1. The test modes were selected from the engine calibration map (provided by Jaguar Cars Ltd), which were the most representative conditions during conventional driving cycles. The data recording time of all the transient tests was 45 seconds, including purge (10 seconds), transient and eventually stabilized stages. All the transient tests were conducted during a 12 seconds changing period or “recovery period”(Rakopoulos 2009), with two tests in which load and speed were changed simultaneously and one test with only load changing. The mode of 1-3 represented the engine accelerating from low load, low speed conditions to medium load, medium speed engine operating conditions. The mode of 2-4 represented the acceleration from a higher initial engine operating condition compared to the mode 1-3. The cumulative emissions of PM, NO and THC were calculated in a 15 seconds transient period; this being longer than the 12 seconds of the recovery period. The main

purpose of this schedule is to give a reasonable time interval in order to obtain an accurate calculation of the cumulative emissions during the transient changing period. For the aim of evaluating the effects of the turbo-lag issue on the engine emissions, three different transition time intervals (5s, 8s and 12s) are applied under the same engine speed constant, torque increased, transient condition (mode 2-3).

The steady-state results for those initial conditions were obtained 1 minute before the transition was being triggered. The final condition steady-state results were gained 2 minutes after the transition finished. To analyze the combustion characteristics under steady-state conditions, 100 cycles were taken to calculate the average in-cylinder pressure using AVL Indicom software. The Rate of Heat Release (RoHR) was gained through Equation 3.2, which was explained in the previous chapter. Twenty seconds of the steady-state condition were taken for the particulate matter distribution analyses. To ensure the repeatability and reliability of the results, the engine was completely warmed up for 20 minutes before each test. Moreover, the test cell temperature was maintained at $25 \pm 1^\circ\text{C}$ by a ventilating system. The fuel supply system filters were changed and lines were purged before each fuel change.

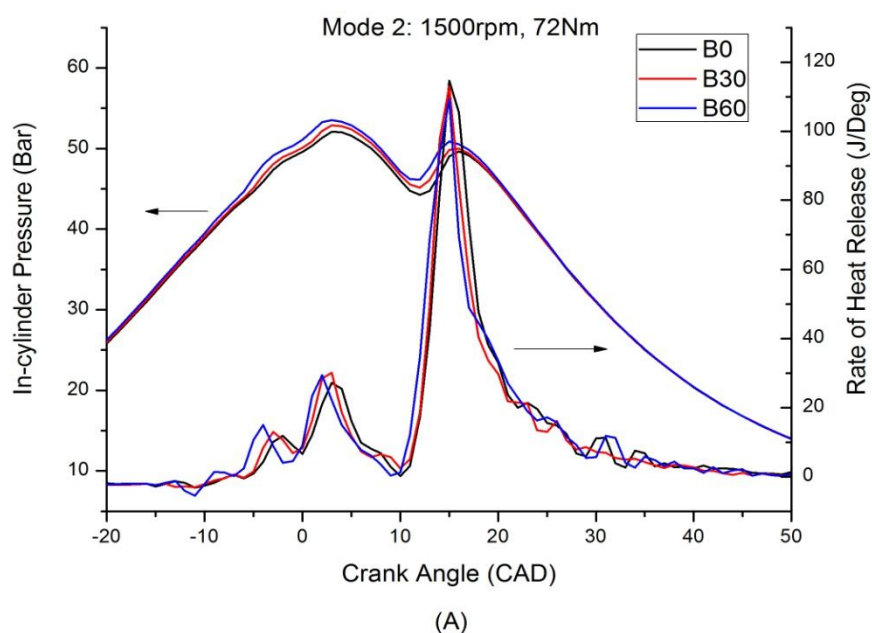
Table 6.1 Engine test conditions

Test mode	Initial Condition	Final Condition
1-3	750 RPM, 36 Nm	1500 RPM, 143 Nm
2-3	1500 RPM, 72 Nm	1500 RPM, 143 Nm
2-4	1500 RPM, 72 Nm	2000 RPM, 167 Nm

6.3 COMBUSTION AND EMISSIONS UNDER STEADY STATE CONDITION

6.3.1 Biodiesel Impact on Combustion Performances

The in-cylinder pressure and RoHR under steady state conditions were analyzed in order to understand the combustion behaviours between each operating condition. Figures 6.1 (A) and (B) present the biodiesel blending ratio impact on the in-cylinder pressure and RoHR at two steady state conditions: 1500rpm 72Nm (mode 2) and 143Nm (mode 3) respectively. It is obvious that three RoHR spikes could be found at mode 2 which is caused by two pilots and one main fuel injection. In contrast, an additional post injection was activated when the engine is operating at a higher engine condition (mode 3). Furthermore, two pressure humps are observed for the in-cylinder pressure profiles with a bigger size at the beginning and followed by a smaller size of hump. The peak in-cylinder pressure was located close to the TDC (Top Dead Centre) and was several crank angles after the second pilot injection.



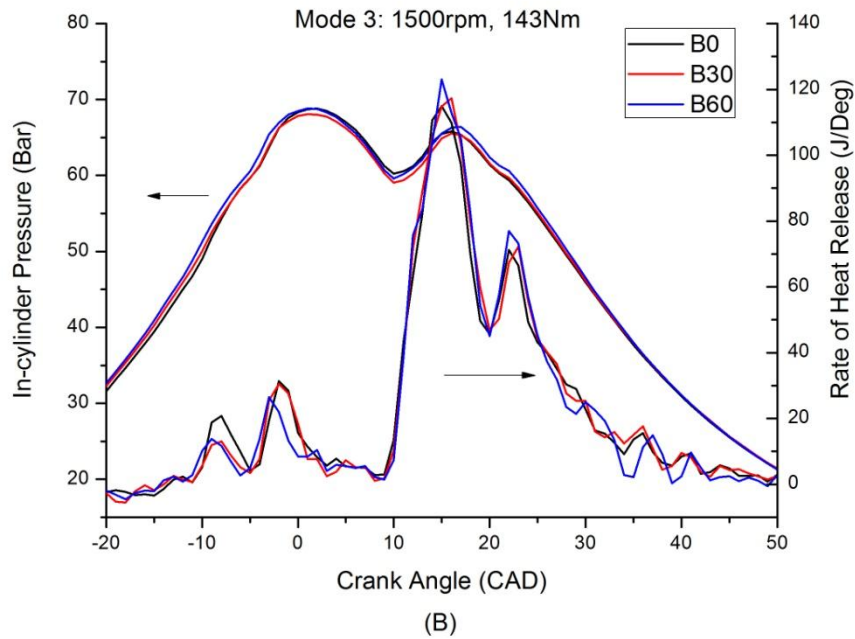


**Figure 6.1 Combustion profiles of diesel and biodiesel blends at
(A) 1500RPM, 72Nm; (B) 1500RPM, 143Nm**

In terms of biodiesel impact on the engine combustion, the SOC (Start of Combustion) was postponed when the engine was running with low biodiesel percentage fuel under both engine conditions. The reason for this postponement is expected to be the high CN (Cetane Number) characteristic of biodiesel which reduces the ignition delay period during combustion. However, a lower first RoHR peak is generated when the engine is fuelled with biodiesel blends under engine mode 3. In contrast, the second peak value becomes higher with a higher percentage of biodiesel blends. The first peak of RoHR is significantly influenced by the fuel spray atomization. The biodiesel used in this research is RME, which has higher viscosity and surface tension properties compared to normal diesel. Due to the low Calorific Value (CV) of biodiesel, more fuel is expected to be injected for combustion. As a result, the peak in-cylinder pressure of biodiesel blends is higher compared to mineral diesel fuel.

6.3.2 Emission Profiles under Steady State Conditions

Figures 6.2 and 6.3 present the particle number concentrations and distributions of various biodiesel blends. It is clearly shown that biodiesel generates fewer particulate emissions than diesel fuel. The total particle number from pure biodiesel was reduced by at least 50% compared to normal diesel at all engine conditions. This phenomenon is believed to contribute to the presence of oxygen in biodiesel fuels. The content of nearly 11% oxygen by molecular weight in neat biodiesel could largely improve the combustion efficiency of the fuel in the cylinder chamber; this leads to more complete combustion and lower particle numbers. Furthermore, the zero percentage content of aromatics in biodiesel fuels could also lead to a particulate reduction; this is caused by the decreased soot precursors' (PAHs) production (Tziourtzioumis et al. 2009).

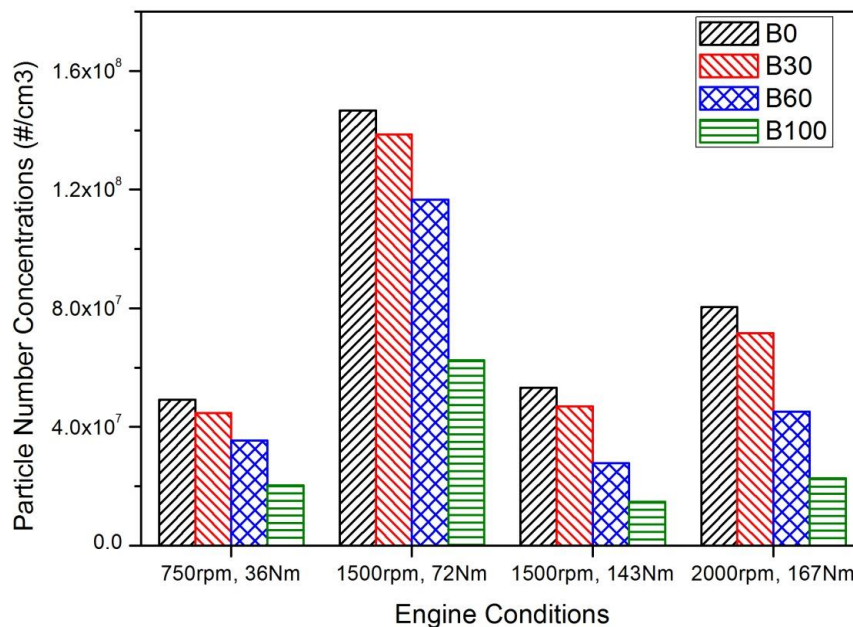
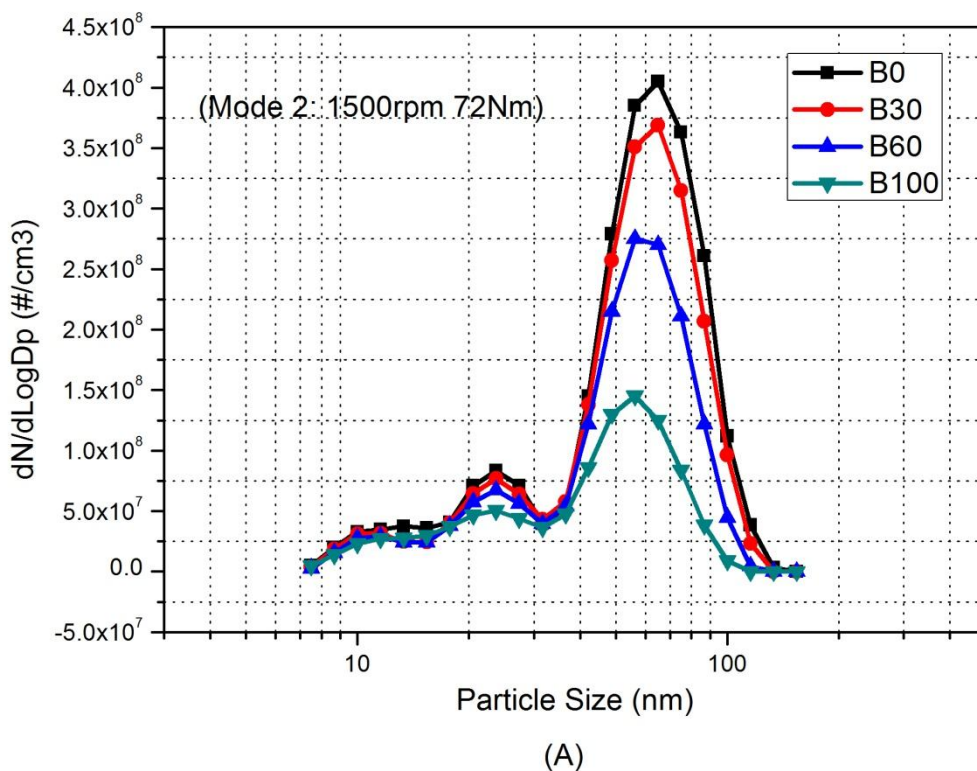


Figure 6.2 Particle number concentrations of diesel and biodiesel blends under steady state

The particulate matter distributions of mode 2 and mode 3 are displayed in Figure 6.3. In this chapter, the accumulation particle is classified between 50 nm and 1000 nm; while the others are measured as a nucleation mode particle. As is shown in the figure, the mean diameter of both the accumulation mode and nucleation mode particles is decreased as the biodiesel blending ratio increases. The increased fraction of the intake fresh air mass flow, as well as the oxygen contents in the biodiesel fuels, provided sufficient oxygen atoms to oxidize the soot particles in the heterogeneous mixture regions. As a consequence, the number of large sized particles reduced to form smaller sized particles. With the continuous combustion process, further oxidization occurs for the volatile or soluble organic compounds and reduces the emission of nucleation mode particles; due to the availability of sufficient remaining oxygen under these conditions.



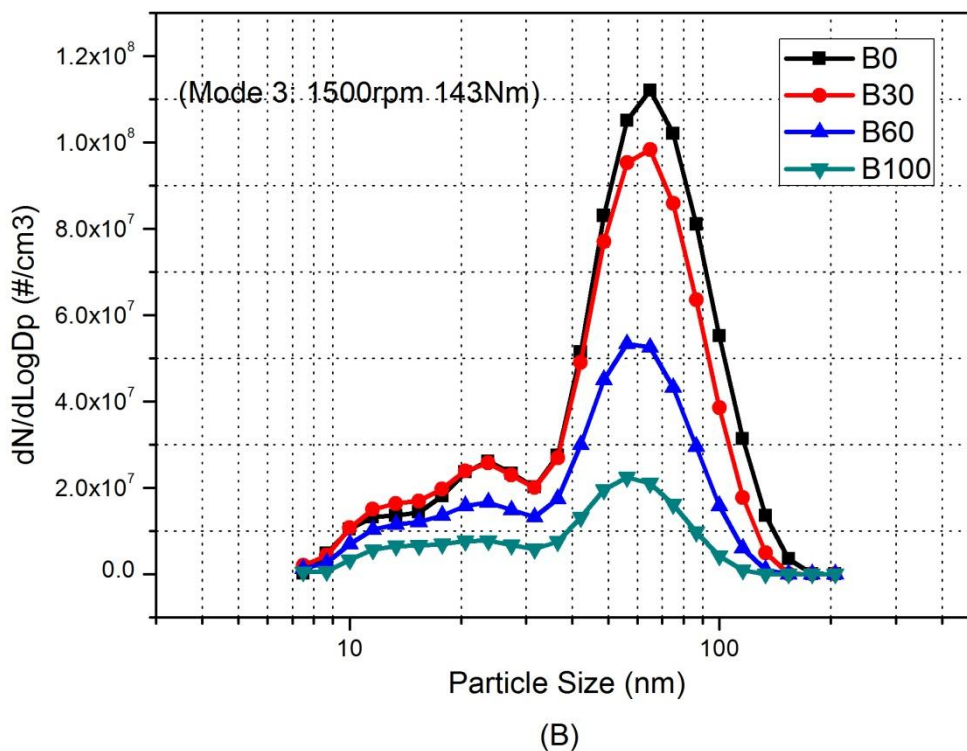


Figure 6.3 Particulate size distributions of steady state conditions

(A) 1500RPM, 72Nm; (B) 1500RPM, 143Nm

The gaseous emission profiles of various fuel blends in concentration are displayed in Figures 4.4 and 4.5 respectively. The NO emissions increases dramatically at a high engine speed or torque conditions because of the high injection quantity; thus it promotes the peak combustion temperature. Moreover, it is obvious that biodiesel blends emitted higher NO under all engine conditions. This should be attributed to the improved combustion condition inside the cylinder due to the oxygen content of biodiesel, which increased the local flame temperature and was more prone to NO formation. Also, the chemical composition of the biodiesel combustion product has lower radiative emission characteristics compared with diesel (Bannister et al. 2010); thus less heat is lost to the cylinder walls, which by itself caused a higher local temperature leading to higher NO formation. In addition, the EGR rate is an important factor in the NO emission level. Due to the lower energy densities of biodiesel blends, the EGR rate for biodiesel is lower than for mineral diesel. The lower EGR

of biodiesel blends could enhance the fresh air mass amount in the inlet manifold and increase the combustion temperature. Consequently, high NO emissions are emitted by the engine. The decreased NO emission at mode 4 (2000 rpm, 167 Nm) compared with mode 3 (1500 rpm 143 Nm) can be explained combine with particulate matter emissions in Figure 6.2.

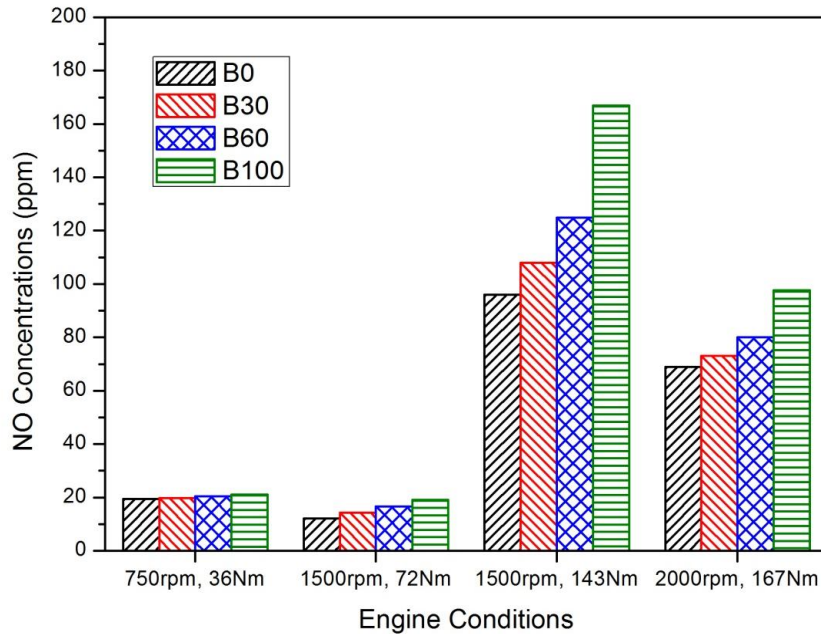


Figure 6.4 NO emissions of diesel and biodiesel blends under steady state

The total hydrocarbon (THC) emissions are presented in Figure 6.5. They are decreased as the biodiesel blending ratio increases. In terms of engine effects, the EGR rate running with biodiesel fuel is set to be lower than with diesel under the same engine operating condition. The reduced EGR gas recycling will boost the intake air mass flow and increase the available oxygen atoms for combustion. Furthermore, the increased fuel injection pressure of biodiesel could improve the fuel spray and provide better atomization and better fuel-air mixture. In terms of fuel impact, the neat biodiesel contents of nearly 11% oxygen will dramatically improve the combustion quantity at local fuel-rich regions. As is mentioned in the previous chapter, the THC is primarily caused by the incomplete combustion. The oxygen content of biodiesel can lead to complete combustion and a subsequent decrease in the THCs.

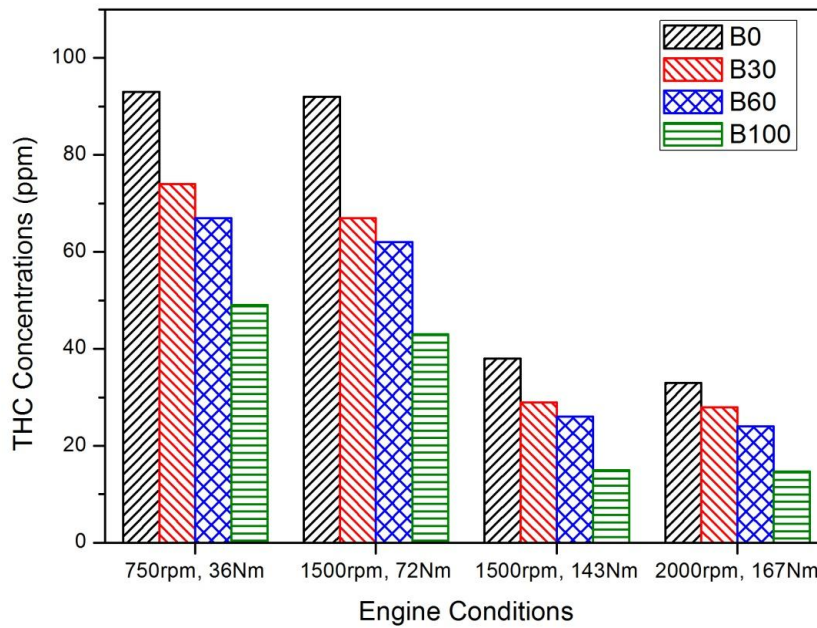


Figure 6.5 Total hydrocarbon emissions of diesel and biodiesel blends under steady state

6.4 MODE SHIFTING TRANSIENT CONDITIONS

6.4.1 Low Initial Engine Condition Transients

The transient test mode 1-3 was used for investigating the acceleration process of the diesel engine from a low load and low speed condition to a medium load medium speed engine operating condition. Figure 6.6 shows the variation trend of the total particle numbers over a 45 seconds transition period (including 12 seconds recovery period) for the four different fuels tested. As shown in Figure 6.6, the total particulate emissions decreased with the biodiesel blend ratio increasing throughout the entire transient test period.

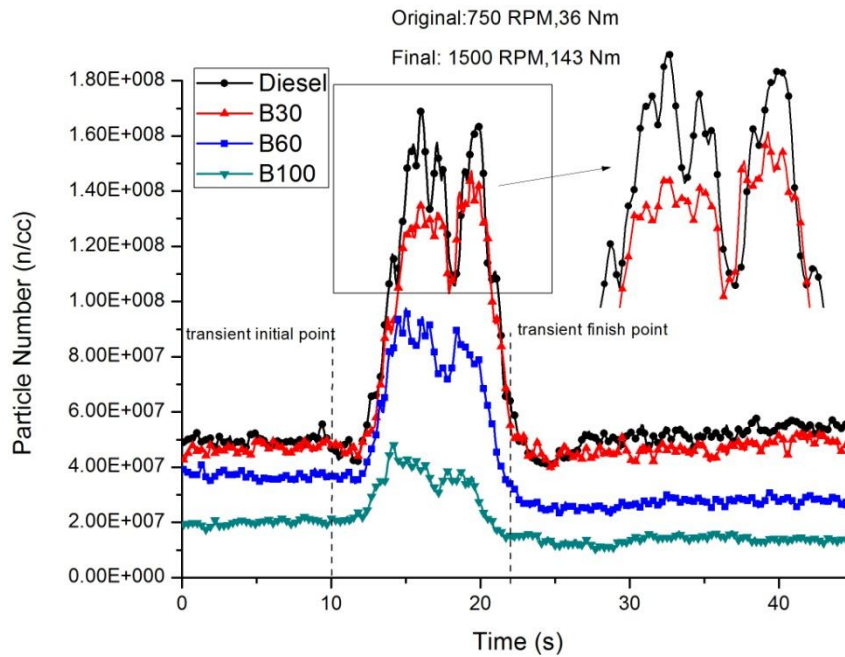


Figure 6.6 Particle numbers for mode 1-3

The figure also shows large spikes of PN during the 12 seconds accelerating phase for each of the fuels. This is believed to be due to the mismatch between the instantaneous increased fuel injection mass and the corresponding desired intake air. The insufficient air intake mass flow is mainly caused by the slow change of turbocharger speed, which is attributed to its moment of inertia and the low exhaust energy of the engine (Glewen et al. 2011). The latter feature is caused by the bypass flow of the EGR valve which is located upstream of the turbocharger in the exhaust manifold, see Figure 3.6.

The intake air mass, injected fuel mass and air-fuel ratio variations are given in Figure 6.7 for the mineral diesel fuel. It is obvious that there is a discrepancy between the intake air flow and fuel injection quantity match during the accelerating process. The air-fuel ratio during the recovery period is always less than the normal operated conditions. Over-rich combustion in the acceleration process results in incomplete combustion; thereby creating soot formation and a high number of PN. It should be mentioned that the turbo-lag problem was an off-

design feature of turbocharged diesel engines. It did not have an effect on the evaluation of the various blended fuels.

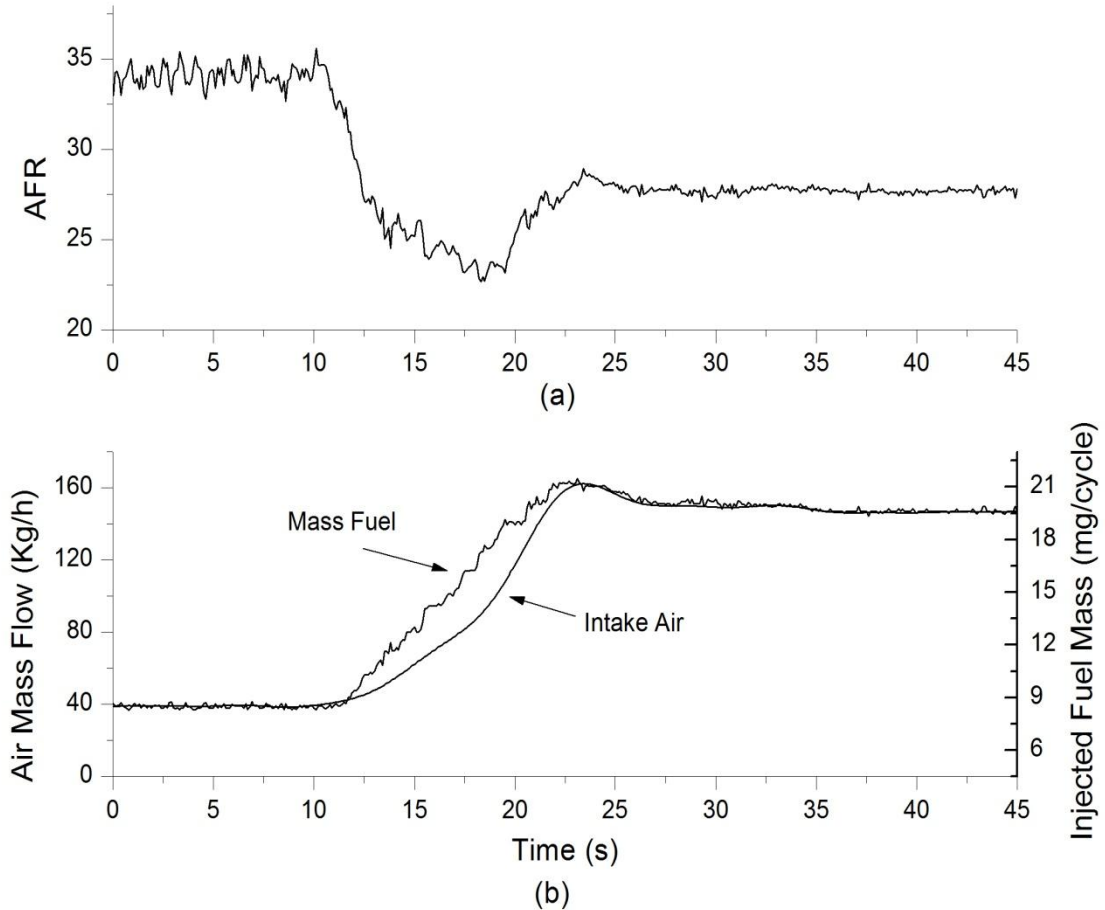


Figure 6.7 (a) Diesel AFR and (b) Intake air with fuel injection for mode 1-3

The PN spike size was different for each fuel tested. The maximum particle number of mineral diesel during mode 1-3 recovery period was about 3.6 times higher than its initial steady-state value. This number became smaller as the biodiesel blend ratio increased. For B30, B60 and neat biodiesel, the ratios between the peak values and the corresponding original level were approximately 3, 2.6 and 2.3 respectively; which is lower than that of mineral diesel. During the engine accelerating process, more fuel was injected into the cylinder in order to achieve the desired engine torque and speed. As a result, the instant air-fuel ratio inside the cylinder dropped during the acceleration. Biodiesel fuels contain oxygen

which could dramatically improve the combustion at the local fuel-rich region; this is considered as the most favoured condition for the formation of soot particles. Wang et al. also concluded that biodiesel's oxygen content has a dominative performance in local rich regions (Wang et al. 2010).

Moreover, the transient EGR performance is another critical factor to impact on the transition particulate matter emission. Figure 6.8 illustrates the EGR rate profiles under transient mode 1-3. It is clear that biodiesel produces a lower EGR rate throughout the whole process of transience, compared to diesel. As is mentioned above, the lower EGR rate will increase the exhaust energy and reduce the impact of the turbo-lag issue. Therefore, biodiesel blends achieve lower particulate peak emissions compared to diesel. Due to the lower heating value of biodiesel blends, the engine has to injected more fuels to achieve the demanded power output. The engine ECU will subsequently calculate the total mass of fuel injection and calibrate to improve the inlet air mass flow rate and eventually reduce the EGR rate.

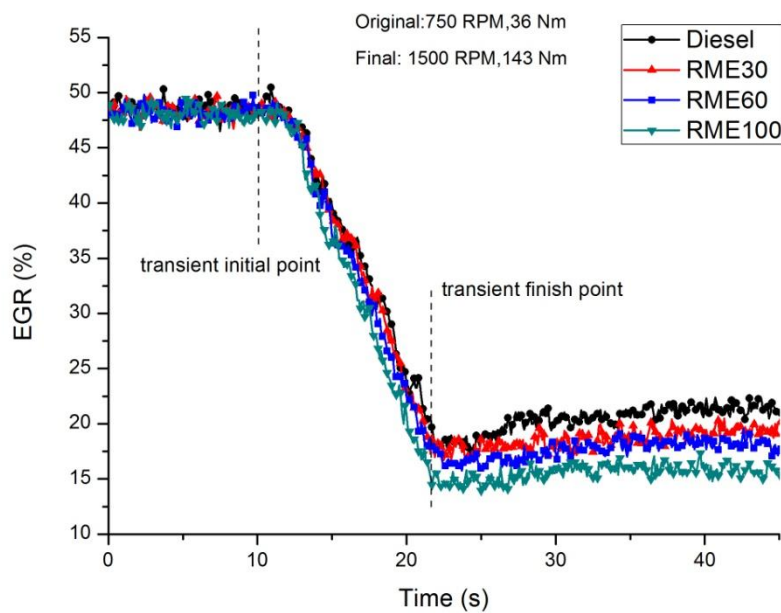


Figure 6.8 EGR profiles for mode 1-3

On the other hand, the oxygen content of biodiesel also has a significant influence on the length of the PN recovery period, because biodiesel requires less air to burn at a stoichiometric condition than diesel and it reaches the final stabilized burning condition earlier (Glewen 2011). It can be seen in Figure 6.6 that the transient PN periods between the initial starting and the final stabilizing point of biodiesel blends were shorter than those of diesel. The transient period length decreased as the biodiesel blend ratio increased.

The instantaneous NO emissions for mode 1-3 are shown in Figure 6.9. For diesel and B100, the NO emissions increased by approximately 130 ppm and 70 ppm respectively. Moreover, biodiesel emitted higher NO during the overall transient test mode 1-3. The reason has been explained in the above section. The instantaneous NO emissions were not increased instantly as the acceleration phase started. Compared with the particle number emission in Figure 6.6, the particulate matter emission is increased at the beginning of the transients, during this period of time the injected fuel is partially undergo pyrolysis to form soot which reduce the peak in-cylinder temperature and reduce the NO_x formation. In addition, in Figure 6.9 small drops could be found in the NO emissions of mineral, B30 and B60, but no drops for B100. Before the engine reached the final quasi-steady condition, small humps of the NO emissions were found. They can be attributed to the corresponding instantaneous fuel mass injection (see Figure 6.10). Due to the lower calorific value of biodiesel fuels, more fuel is needed for injection in order to achieve the requirement of torque and speed change. At the end of the 12 seconds of the speed up phase, the fuel is still injected even if the engine has already reached the demanded output; due to the engine PID control strategy. The increased mass of fuel results in increased heat release, thus increasing the temperature within the engine cylinder leading to the local humps in the NO emissions' trend.

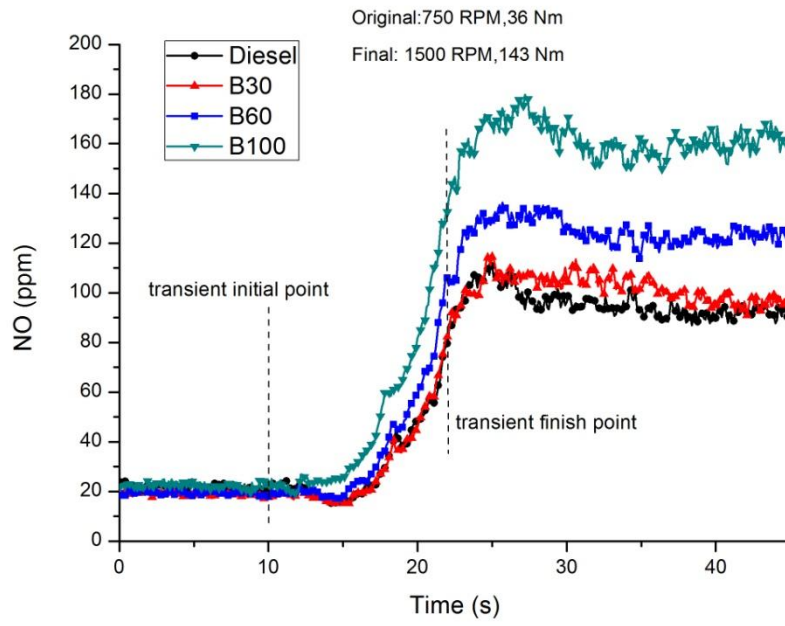


Figure 6.9 NO emissions for mode 1-3

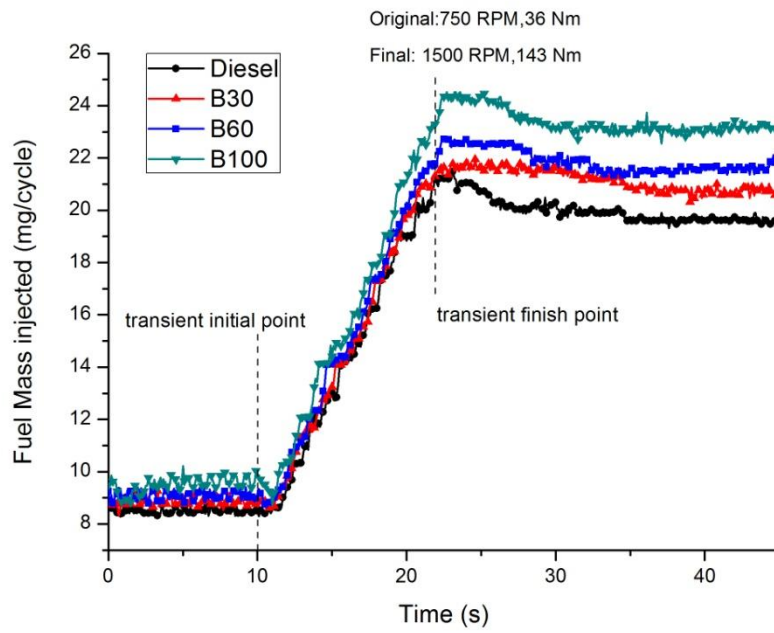


Figure 6.10 Fuel mass injected for mode 1-3

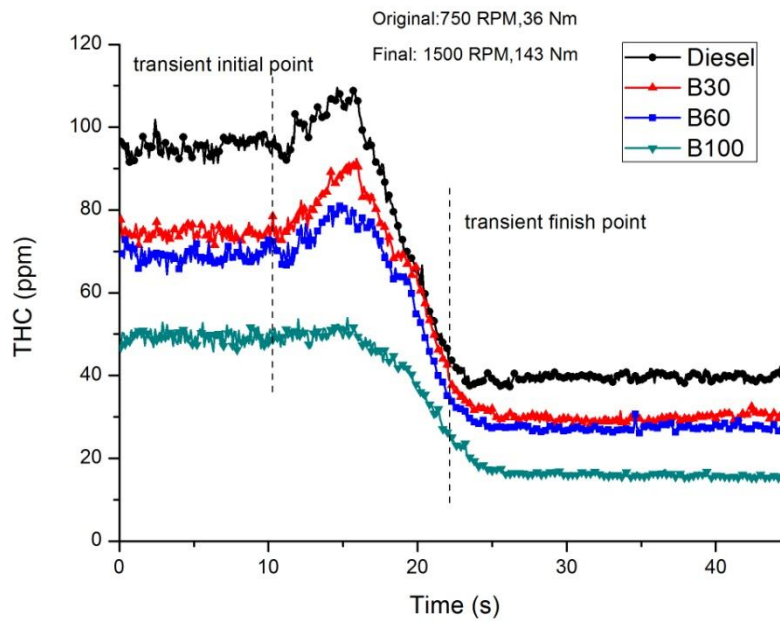


Figure 6.11 THC emissions for mode 1-3

The THC emissions for mode 1-3 are shown in Figure 6.11. Due to the reduced EGR rate, the increased fuel rail pressure and the increased in-cylinder pressure and temperature, the THC emissions were decreased after the acceleration process for all the tested fuels. Furthermore, it was observed that biodiesel blends emitted lower THCs under both the steady-state and transients conditions. This indicates that the oxygen content of biodiesel led to complete combustion in all conditions. On the other hand, the low air-fuel ratio at the initial transient period resulted in small humps for B0, B30 and B60 as shown in Figure 6.11. However, smaller humps were found for neat biodiesel which are most likely due to the absence of aromatic (Evangelos G. Giakoumis et al. 2012) and oxygen content as well as the slight decrease in the injected fuel mass at the beginning of the acceleration, as can be seen in Figure 6.10.

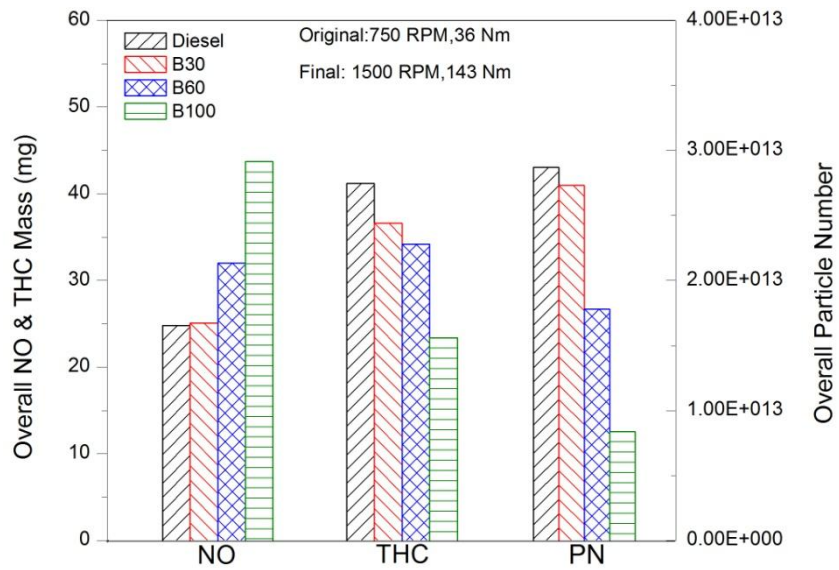


Figure 6.12 Cumulative emissions for mode 1-3

Cumulative emissions of NO, THC and PN during the entire 15 seconds time interval are given in Figure 6.11. The NO emissions increased and THC emissions decreased as the biodiesel blending ratio increased. The NO and total particle number of mineral diesel and B30 are almost the same. Neat biodiesel emitted nearly 76% more NO and 43% less THC than diesel. On the other hand, the neat biodiesel had dramatically lower overall particulates. Compared to diesel, the PN was reduced by nearly 70% when the engine was fuelled with pure biodiesel.

6.4.2 Torque Increase Transients

Test mode 2-3 was used to investigate a transient load increase at constant engine speed. The engine speed was maintained at 1500 rpm by the dynamometer and the torque was increased by varying the accelerator pedal from 72 Nm to 143 Nm during a 12 seconds time interval.

Figure 6.13 gives the number of particle emissions for mode 2-3. The engine particle emissions increased as the biodiesel blend ratio decreased in all of the transient processes. The ratio between the peak and the initial steady-state PN value of mineral diesel was about 2.3. Similar to mode 1-3, this ratio became smaller when the biodiesel blending ratio increased. However, the PN spikes during the recovery period in mode 2-3 were much lower compared with test mode 1-3. For B100, the PN spike almost disappeared because in the mode 2-3 transient process, the engine speed remained unchanged (1500rpm, higher than mode 1-3) and the torque increase level was also lower than that of the 1-3 mode. Thus, during the test of mode 2-3, the intake air mass flow was higher than mode 1-3 and the gradient of the injected fuel mass was lower, as shown in Figures 6.10 and 6.14. This resulted in increased air-fuel ratios for mode 2-3 which improved the combustion conditions and reduced the particle emission spikes during the transient process. Furthermore, the recovery period of the biodiesel particle emissions seemed to be shorter than the diesel fuel. As discussed earlier, the reason is probably due to the oxygen content of biodiesel.

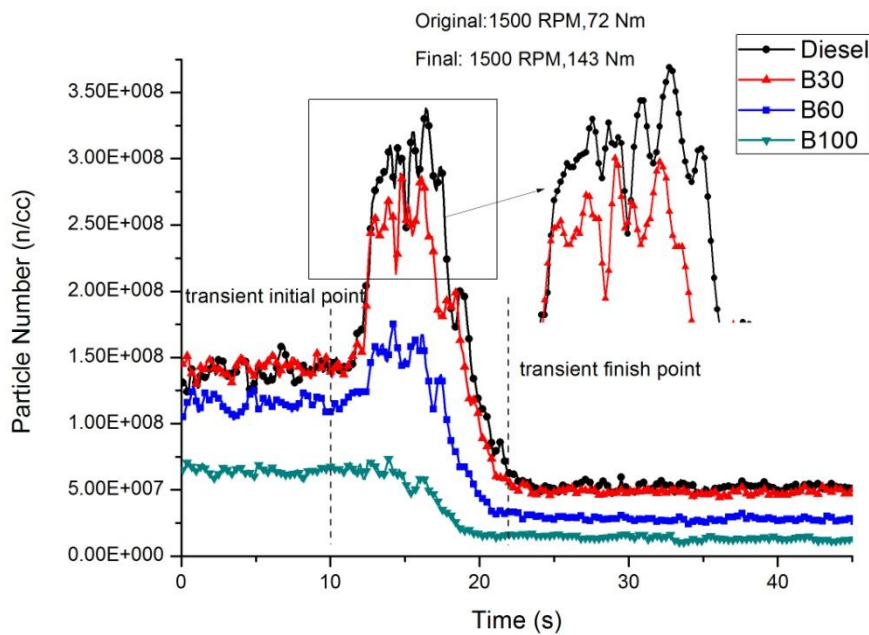


Figure 6.13 Particle numbers for mode 2-3

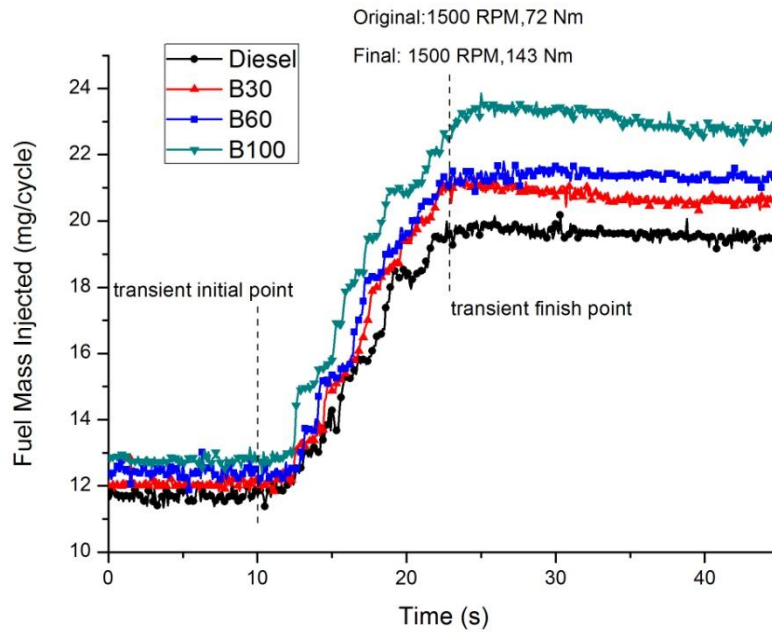


Figure 6.14 Fuel mass injected for mode 2-3

The NO emissions of mode 2-3 are displayed in Figure 6.15 and show similar trends as for mode 1-3. With the blending ratio of biodiesel increasing, the NO emissions' level, its time-gradient and final stabilized value, all increased. The NO concentration of B0 and B100 increased approximately by 80 ppm and 140 ppm respectively during the transient period. However, unlike mode 1-3, the humps close to the final steady-state conditions almost disappeared under these load varying test conditions. The corresponding PID tuning, low demand of fuel injection quantity and high instantaneous AFR at the end of the transient step during transient mode 2-3, can be attributed to the disappearance of the transient humps compared with those which are present in mode 1-3, Figure 6.14.

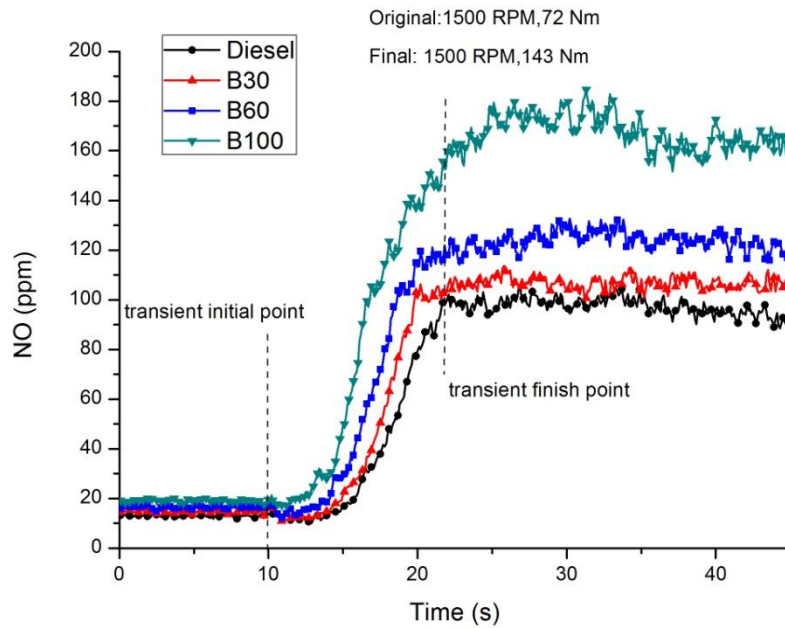


Figure 6.15 NO emissions for mode 2-3

On the other hand, the instantaneous fuel injection quantity has also affected the THC emissions. An obvious difference compared with mode 1-3 was the size of the local spikes at the beginning of the transient step for mode 2-3, which were smaller, shown in Figure 6.16. The peak values of diesel, B30 and B60 in mode 1-3 were around 12 ppm to 15 ppm higher than the initial steady-state operating point. However, the values were reduced to about 6 ppm for mode 2-3. The main reason could be attributed to the injected fuel mass. The smaller instantaneous fuel injection rate led to reduced transient THC emissions.

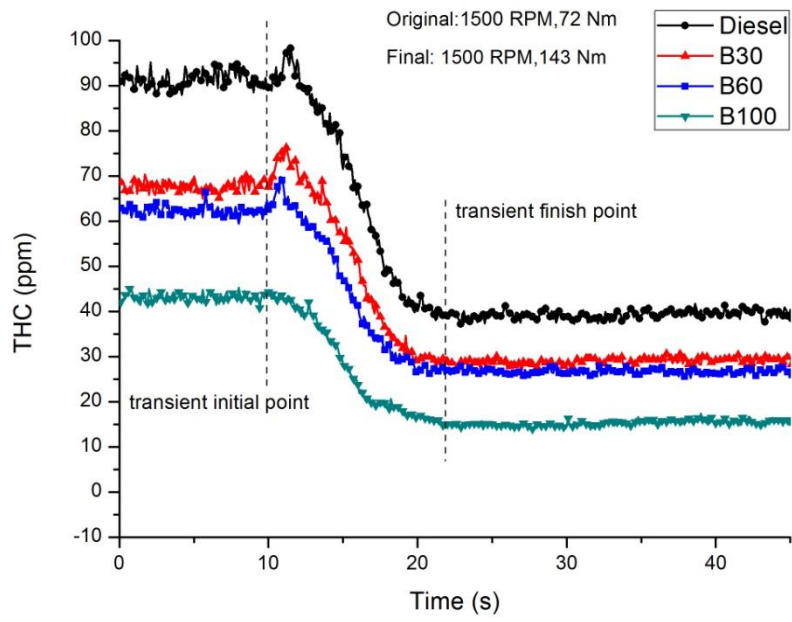


Figure 6.16 THC emissions for mode 2-3

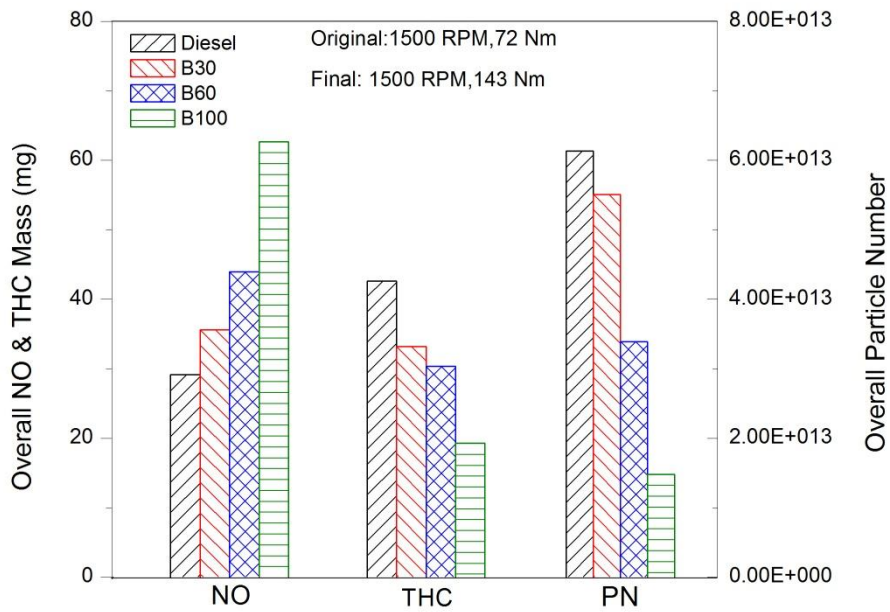


Figure 6.17 Cumulative emissions for mode 2-3

The three overall types of emissions in mode 2-3 are similar in trend to mode 1-3, as shown in Figure 6.17. The NO emissions of B100 were more than double the amount recorded for diesel fuel. On the other hand, the THC emissions of B100 were reduced by nearly half compared to those of diesel. For particle matter emissions, the difference of PN between the mineral fuel and B30 was small. However, similarly to mode 1-3, B100 in mode 2-3 emitted extremely low particulate emissions; nearly 75% less than mineral diesel.

6.4.3 Higher Initial Engine Speed and Torque Transients

Sequence mode 2-4 was an investigation into the acceleration process from relatively higher initial and final engine conditions (1500 rpm, 72 Nm to 2000 rpm, 167 Nm) compared to mode 1-3. Due to the difference in various engine parameters for the two engine operating modes, different transient emissions' characteristics were observed in mode 2-4; although both modes were representing acceleration conditions.

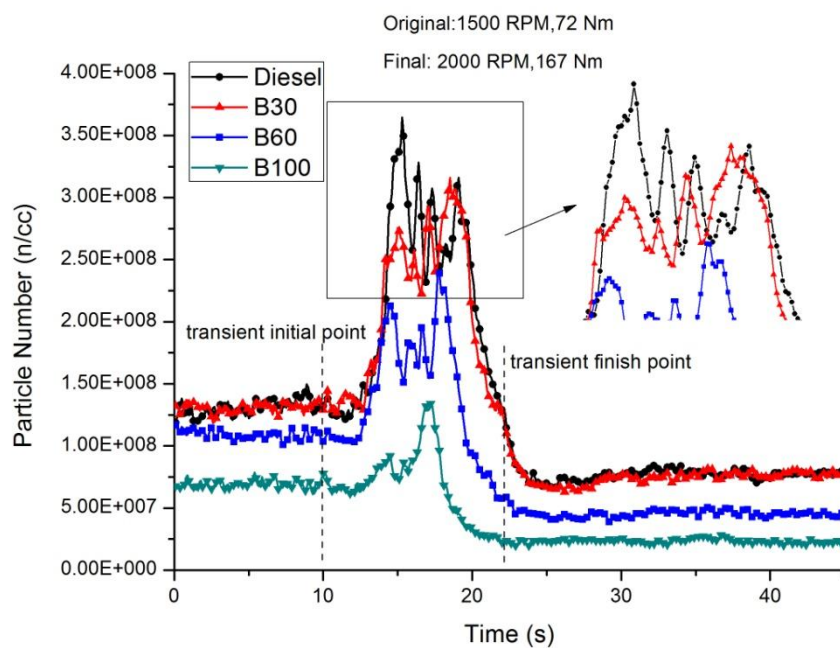


Figure 6.18 Particle numbers for mode 2-4

It can be seen from Figure 6.18 that the spikes in PN are still apparent in this transient process. The duration of the transient step decreased with the increasing biodiesel blending ratio. This trend was similar to mode 1-3 and 2-3 as previously explained. Moreover, the ratio of transient peak values to the starting steady-state values for diesel and B100 were about 2.6 and 1.8 respectively; which were lower than for mode 1-3. The initial engine operating condition for mode 2-4 was higher than for mode 1-3; hence the initial speed of the turbocharger for mode 2-4 was higher. Moreover, the exhaust energy in mode 2-4 was larger than in mode 1-3, not only because of the lower EGR rate but also because of the higher exhaust air mass flow rate. Therefore, for the sequence mode 2-4, the higher intake air mass flow results in smaller effects from the turbo-lag issue during the transition and thus lower PN spikes, compared with mode 1-3. The gaseous emissions are given in Figures 6.19 and 6.20. Both the NO and THC emissions for the entire transient process seemed more stable with smaller fluctuations, compared to the previous two transient conditions; again this was because of the better combustion conditions.

The cumulative emissions of mode 2-4 are shown in Figure 6.21. Similarly to mode 1-3, the NO and the total number of particulate emissions of both B30 and mineral diesel were almost the same. The overall NO and THC emissions of neat biodiesel decreased and increased by about 50% and 66% respectively, compared to running with neat diesel. Neat biodiesel emitted about 68% less particle numbers than diesel fuel.

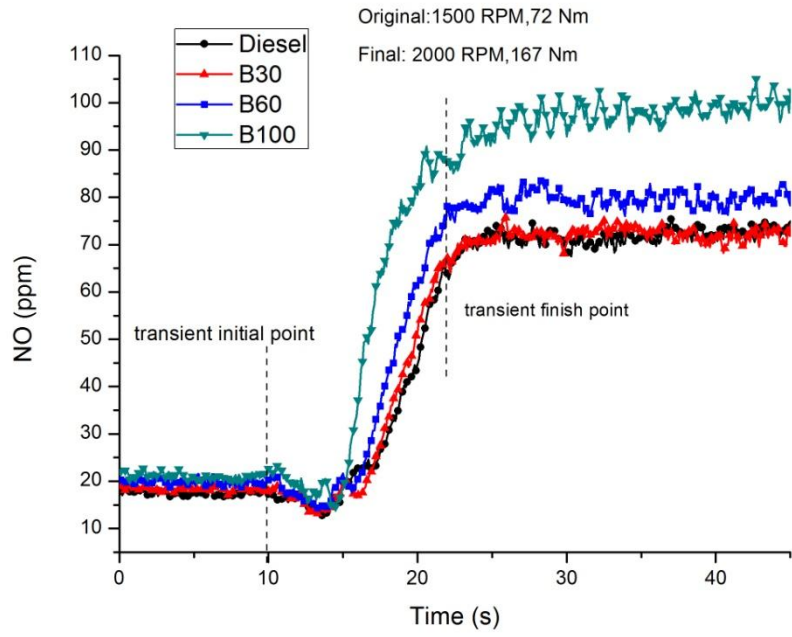


Figure 6.19 NO emissions for mode 2-4

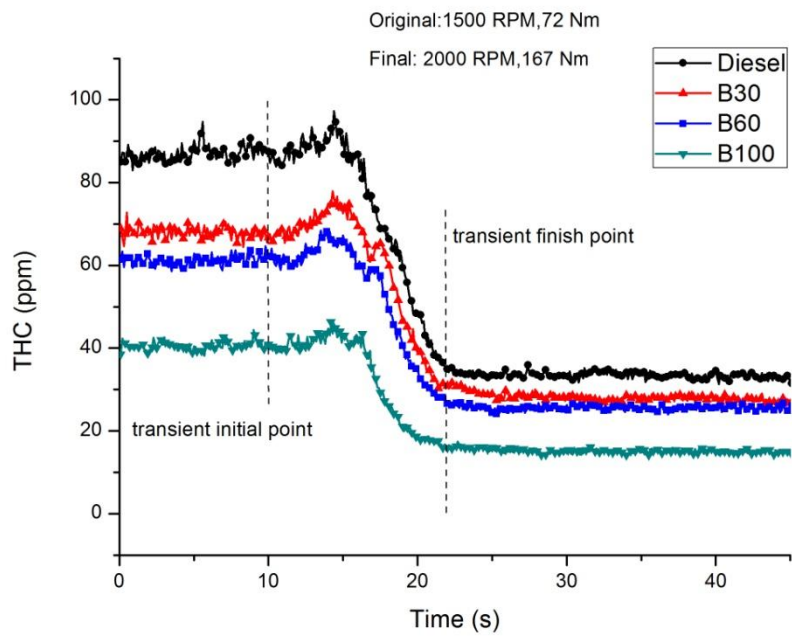


Figure 6.20 THC emissions for mode 2-4

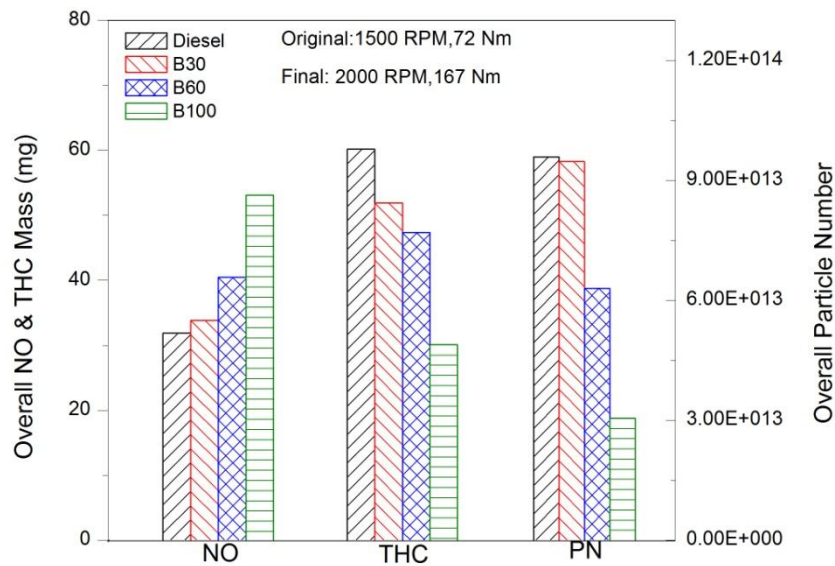


Figure 6.21 Cumulative emissions for mode 2-4

6.5 ACCELERATION DURATION EFFECT ON TRANSIENT EMISSIONS

In order to investigate the turbo-lag effects on the engine transient behaviours, 5s, 8s and 12s transition time durations were applied in this section under the same load increase transient condition, e.g. mode 2-3. The biodiesel blends were not included in this section as they will produce the same trend in terms of acceleration timing changes.

Figure 6.22 illustrates the profiles of total particle number emissions of the three transient scenarios. It is obvious that the peak value of the particulate emissions is decreasing with the increasing time duration. Moreover, the PN of the 5s scenario increased sharply at the beginning of the transition compared with the more stable instantaneous particulate emissions of the 12s scenario. This indicates that the turbo-lag issue is more dominative under aggressive transient conditions.

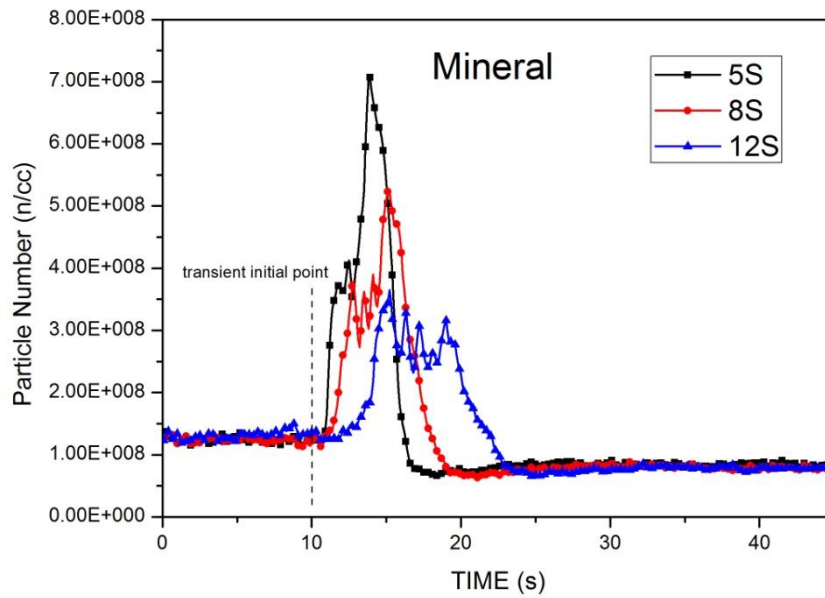


Figure 6.22 Particle number of various acceleration timing transients

Figures 6.23 and 6.24 show the injected fuel mass and the intake air mass flow during the entire transient period. The intake air mass flow rates of the three scenarios are almost identical during the first several seconds after the transition begins. This is believed to be due to both the EGR performance (see Figure 6.25) and the turbocharger inertia. By contrast, in terms of fuel injection profiles, the trends of the short transition time scenarios increased instantly after the derivation points of the transience. As a consequence, the instantaneous AFR is reduced for the shortened transition timing scenario and delivers higher particle number spikes.

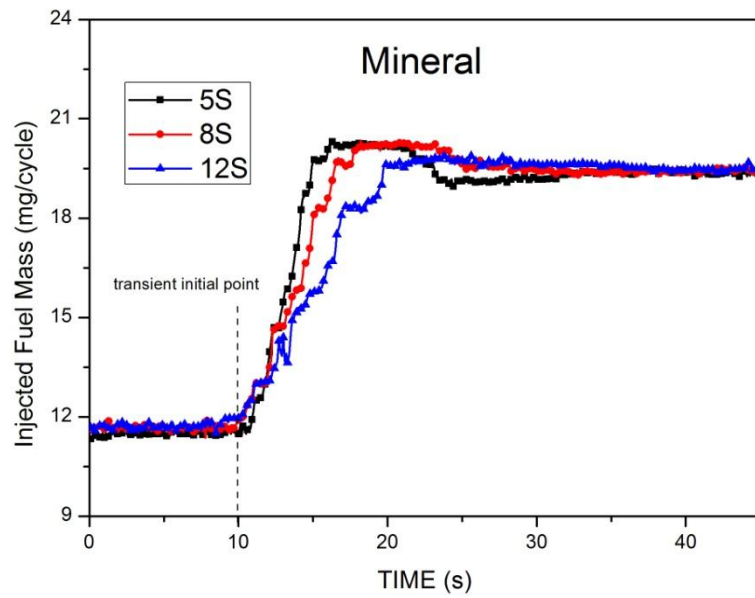


Figure 6.23 Mass of fuel injection of various acceleration timing transients

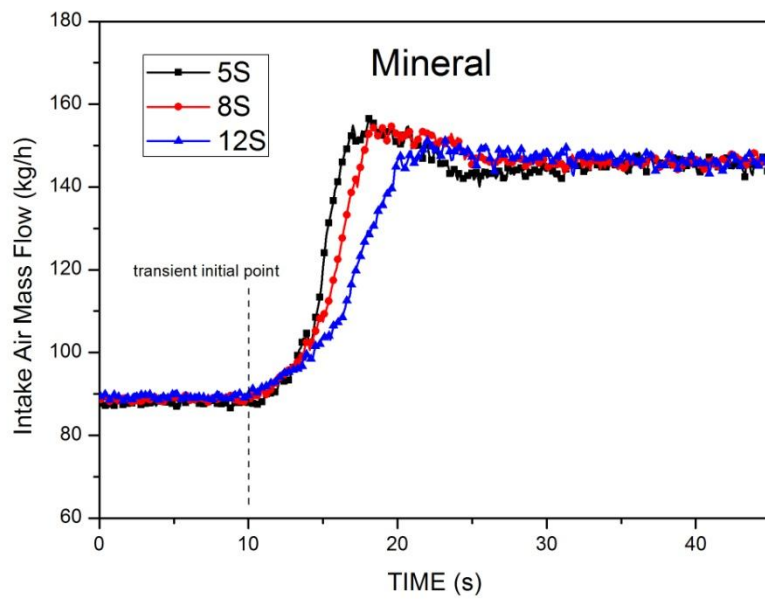


Figure 6.24 Intake air mass flow of various acceleration timing transients

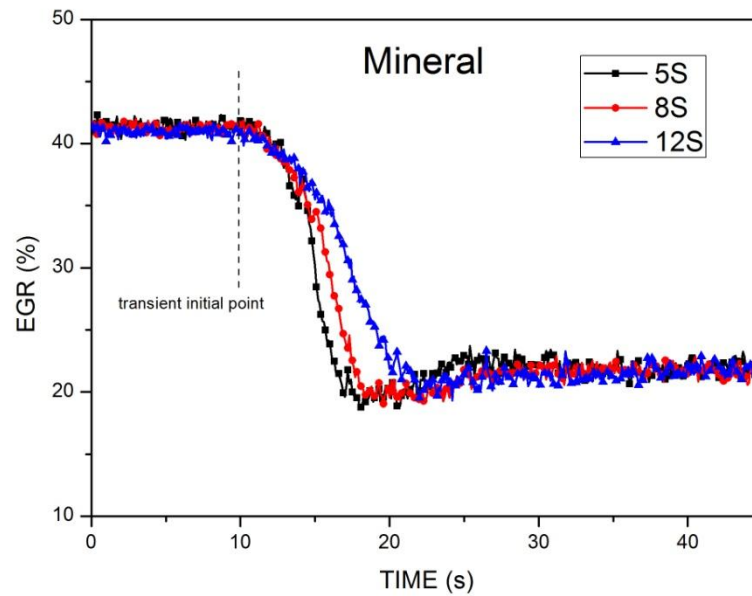


Figure 6.25 EGR of various acceleration timing transients

The gaseous emissions of NO and THC are displayed in Figures 6.26 and 6.27. It is clearly shown that the engine produces small drops of instantaneous NO after the transition begins. Due to the transient lags of EGR and the high particulate emissions, the combustion temperature is lower than ideal transient conditions (e.g. no dynamic lags). Therefore, lower NO emissions are expected at the beginning of the acceleration phase. Similar explanations could be used for the THC humps in Figure 6.27. A shorter acceleration period produces higher THC transient spikes due to its more severe turbo-lag effects; thus it worsens the deteriorated combustion conditions. However, the spikes of the THC emissions are not as big as those produced by the particulate emissions.

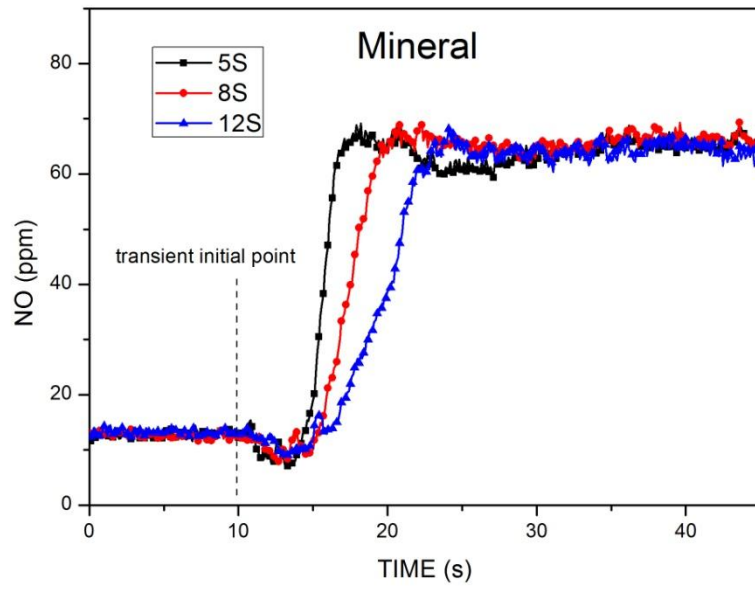


Figure 6.26 NO emissions of various acceleration timing transients

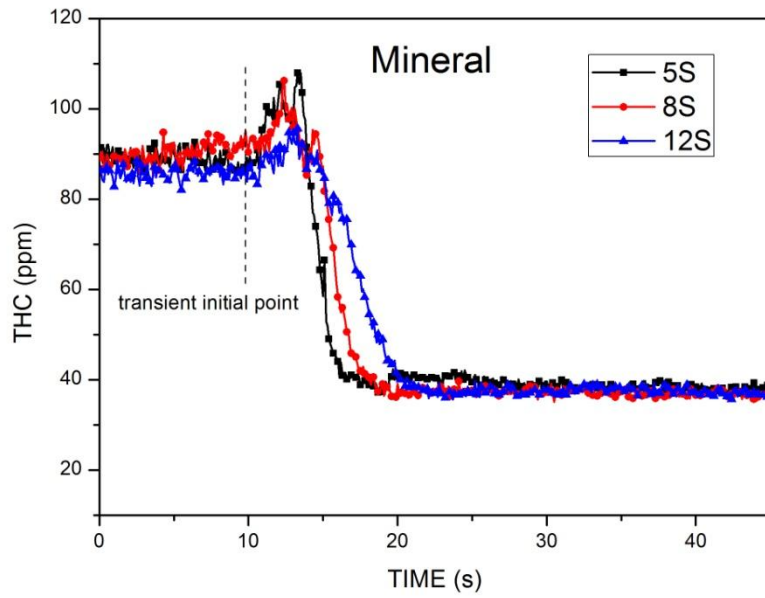


Figure 6.27 THC emissions of various acceleration timing transients

6.6 CONCLUSIONS

The effects of four different biodiesel blends on the engine-out emissions under steady-state as well as the acceleration and load changing transient operations have been studied in this chapter. The turbo-lag issue effects on the engine have been evaluated by varying the transition timing. Fast response diagnostic equipment was used to measure the emissions of particulate matter (in number), nitrogen monoxide and total hydrocarbons. The conclusions drawn from the results are:

- The advanced SOC and lower first RoHR peak was generated when the engine was running with biodiesel blends. In contrast, the second peak value of RoHR became higher with a higher percentage of biodiesel blends.
- As the biodiesel blending ratio increased, PN and THC decreased; whereas NO increased for all examined conditions.
- Spikes in transient particulate matter emissions were observed in all the transient sequences. The ratio between the maximum PN and its initial value (i.e. the size of spikes) decreased with the increasing biodiesel blending ratio.
- Due to the turbocharger lag issue, AFR was greatly influenced during the entire transient recovery period. The instantaneous AFR affected both particulate and gaseous emissions. The spikes (or humps) of transient particulates were bigger than those of NO and THC.

- The oxygen content is an important factor to determine the duration of the particulate emissions' recovery period. The duration decreased with the increasing biodiesel blending ratio for all the engine transient scenarios.
- For engine accelerating transients, the engine with higher initial/final engine load and speed operating conditions emitted lower PN and gaseous emission spikes, compared to the low speed and load engine transient operation.
- For the three selected transient tests in a period of 15 seconds, the cumulative PN and THC emissions of biodiesel were lower by up to 75% and 50% respectively; while the NO emissions were almost doubled compared to diesel.
- The instantaneous PN peak value was notably influenced by the length of the acceleration timing period. The shorter transition timing resulted in a higher emissions' peak value. The transient spike of PN is more obvious than that of the gaseous emissions.

CHAPTER 7

NOVEL OPTIMIZED INCREMENTAL VARIATIONS OF EGR UNDER TORQUE INCREASED TRANSITION

In this chapter, time variable EGR reduction during transition operation was developed and investigated as a novel strategy to improve performance and emissions in a commercial turbo-charged diesel engine. The EGR% was reduced by 20, 50, 75 and 100% during different time intervals of 1, 2, 3, 5 and 8 seconds under specially designed transient operations. With the novel EGR changing strategies during transition, the exhaust power is significantly promoted to compensate the transient turbo-lag issue. The particulate matter, NO_x, as well as THC emissions, are analyzed and evaluated by fast response diagnostic instruments.

7.1 EGR IMPACTS ON ENGINE TRANSIENTS

Diesel engines have high thermal efficiency which makes them attractive, but their NO_x and particulate matter emissions are their drawback. Transience is considered as the most commonly used operating condition during daily transportation and has attracted researchers' attention in recent years. The more stringent emissions legislation under the regular transient driving cycles (such as NEDC and FTP-75) also enforces automotive manufacturers put more efforts on reducing the engine transition emissions. As has been introduced in the literature chapter, many researchers have observed dramatic emission spikes under the acceleration

transient operating condition, especially for particulate matter emissions (Armas et al. 2006, Tian et al. 2013, Tan et al. 2013, Giakoumis & Lioutas 2010). It is commonly agreed that the main cause of transient emission spikes is due to the instantly reduced AFR with the corresponding over-rich combustion. During the early stage of acceleration transient cycles, the intake air mass flow cannot match the rapid increased injected fuel at the onset of the transience. This phenomenon is caused by the delay time of the turbocharger responding to the transience and is called the turbo-lag issue which is considered to be a crucial factor affecting transient performances and emissions of turbo-charged diesel engines. The delayed intake air flow or boost pressure increase is mainly caused by the rotor inertia of the turbocharger-compressor system and air pressure wave travel time (Galindo et al. 2004).

As has been introduced in section 2.5, EGR is currently widely used as the most effective method to reduce NO_x emissions of automobile engines. It reduces the peak combustion temperature by recycling a portion of the exhaust gas back into the intake manifold. Many researchers investigated the EGR impact on NO_x-particulate matter emissions. Liu et al. (2013) investigated the sensitivity of the EGR rate's effects on the soot emissions. They showed that the soot emissions were very sensitive to the EGR rate when the EGR rate region was between 15% and 35%. Maiboom et al. (2008) delayed combustion by varying the EGR rate and the boost pressure in their studies in order to simultaneously reduce NO_x and particulate matter emissions under certain operating conditions. Generally, engine operating conditions are determined by their calibration map which is based on steady-state operation (Armas et al. 2009). Thus, it is most likely that engines are not operating at their optimum condition during transience and are producing more emissions than necessary. In modern commercial diesel engines, the EGR valve is located upstream of the turbocharger in the exhaust manifold. Therefore, part of the exhaust energy that is used to power the turbocharger-compressor system is by-passed by the EGR valve during transient acceleration.

As a consequence, the transient response time of the intake air mass flow is significantly influenced by the EGR variation.

In terms of transition control, two critical parameters can be used to control the intake air mass flow rate, namely the EGR rate and the variable geometry turbocharger (VGT) setting. However, primary experiments to simultaneously control these two parameters during transience did not lead to the desired results due to their different lag times. Controlling the EGR rate by itself produced sufficient boost pressure rise under transience and for this reason it was selected as the control parameter for this investigation. Different incremental variations of EGR at the onset of the transience are investigated as a novel control strategy, to reduce emissions under torque increased transience with a constant engine speed of 1000 rpm. The exhaust power is significantly promoted to compensate the transient turbo-lag issue. The NO_x, particulates, as well as THC emissions, are analyzed and optimized by implementation of the novel EGR control strategy.

7.2 TEST CONDITIONS AND PROCEDURE

The schematic diagram of the test cell is shown in Figure 3.8. The test facility was specifically designed for the purpose of transient and cold operations. The experiments were conducted by a six-cylinder direct injection 3.0 L Jaguar diesel engine. The specific details were given in the previous chapter 3. The transient speed and torque loading was controlled by a PUMA control system. The engine parameters were measured and controlled by INCA V5.3 software. All the selected transient ECU data were recorded by the PUMA control system. The speed and torque were controlled by the dynamometer and engine respectively.

The gaseous emissions were detected by an AMA i60 exhaust measurement system from AVL Ltd. It integrated various traditional emission analyzers together. A chemiluminescence detector (CLD) was used to measure the NO and NO_x; a flame ionization detector (FID) for the THC (C₃) and an infrared detector (IRD) for the CO respectively. All instantaneous gaseous emissions were measured by the same sample probe with a data acquisition frequency of 10 Hz. All gaseous emissions' data were recorded by the PUMA control system. A differential mobility spectrometer (DMS500) from Cambustion Ltd was implemented to measure the particulate matter. Sampling points of both the gaseous and particle analyzers were located upstream of the after-treatment system. The DMS500 emission signal was used as an analogue input channel into the PUMA for synchronizing the control system with the spectrometer.

In this chapter, 14 discrete transient scenarios were tested including one reference transient and 13 optimized transients with different incremental EGR control strategies. The transient test sequences for both the benchmark and the optimized scenarios were conducted by increasing the engine torque from 50 to 167 Nm within a 10 seconds ramping period while maintaining the engine speed at 1000 rpm. The engine was kept at a relatively low speed, which was believed to be a dominant condition for the turbo-lag issue to prevail. In order to ensure the repeatability of the transient tests, the engine was warmed up for 20 minutes as the pre-conditioning stabilization period for each of the sequences. All instantaneous results showed in this study were acquired in a 25 seconds sampling time which included 5 seconds initial, 10 seconds transitions and 10 seconds post engine conditions. The gaseous analyzers, particulate spectrometer, as well as the INCA and PUMA systems, were synchronized at the signal derivation points of transience.

For the benchmark scenario, all ECU parameters were applied without any modification based on the original engine calibration map. For the optimized transient scenarios, the transient speed and torque profiles were the same as the benchmark scenario. However, the instantaneous EGR rate was restructured into 13 different scenarios with various magnitude changes and time intervals, as in Table 7.1.

Table 7.1 Optimized two steps incremental transient EGR test sequences

Magnitude	Time Interval Steps			
100%, 0%	1s, 9s	2s, 8s	5s, 5s	8s, 2s
75%, 25%	1s, 9s	2s, 8s	3s, 7s	/
50%, 50%	1s, 9s	2s, 8s	3s, 7s	
25%, 25%	1s, 9s	2s, 8s	3s, 7s	

As is shown in the table, all optimized transient sequences consisted of two stages. A portion of the total required EGR% change was applied in the first stage (XX%) and the rest (YY%) in the second stage; ZZ and FF represent the tow time periods in which the total transient time was divided. A combination of XX%, YY% with ZZ FF means XX% of EGR reduction was applied in ZZ seconds and YY% reduction was applied in FF seconds. The total required EGR reduction value was obtained from the reference transient sequence. Each EGR scenario was implemented by changing the engine EGR map before each test.

7.3 EFFECTS OF NOVEL TRANSIENT EGR STRATEGIES' EFFECTS ON ENGINE PERFORMANCES

7.3.1 Transient EGR Modification

Instantaneous variations of both reference and optimized EGR rates under the same controlled transient operating condition of constant engine speed at 1000 rpm and torque increase from 50 to 167 Nm are presented in Figure 7.1. The EGR rate was the only parameter changed by the engine ECU based on different maps proposed for this experimental investigation. Ideally, the engine EGR rate setting in the calibration map should combine with the integrated effects of delay times and gas dynamic behaviour of passages. However, due to the research and development costs associated with the product development cycle, the engine calibration is mainly focused on the steady state. In this chapter, the actual EGR is calculated by an ECU supplied by Bosch which has its own calculation routine and may not represent the exact value. However, the values provide the trends for further analysis of the boost pressure and intake air mass flow variations. Actual EGR rates for all optimized calibration scenarios were lower than those of the reference calibration sequence over the entire 10 seconds of the transient recovery period.

A notable feature of diesel engine transience at low engine speed is the turbo-lag phenomena. The steady state calibrated reference map leads to the AFR lower than the stoichiometric value under transient acceleration condition due to the effects of turbo-lag. This is one of the main reasons for the apparent particulate matter spike observed in transient operations. The optimized EGR curves were designed to increase the instantaneous air fuel ratio (AFR) during transient operation. Due to the limitations of the engine control, a slight undershoot of

the EGR rate is produced for the full reduction (100%) cases shown in Figure 7.1 (D). The variations of EGR rates directly affect other engine parameters which are discussed in the following section.

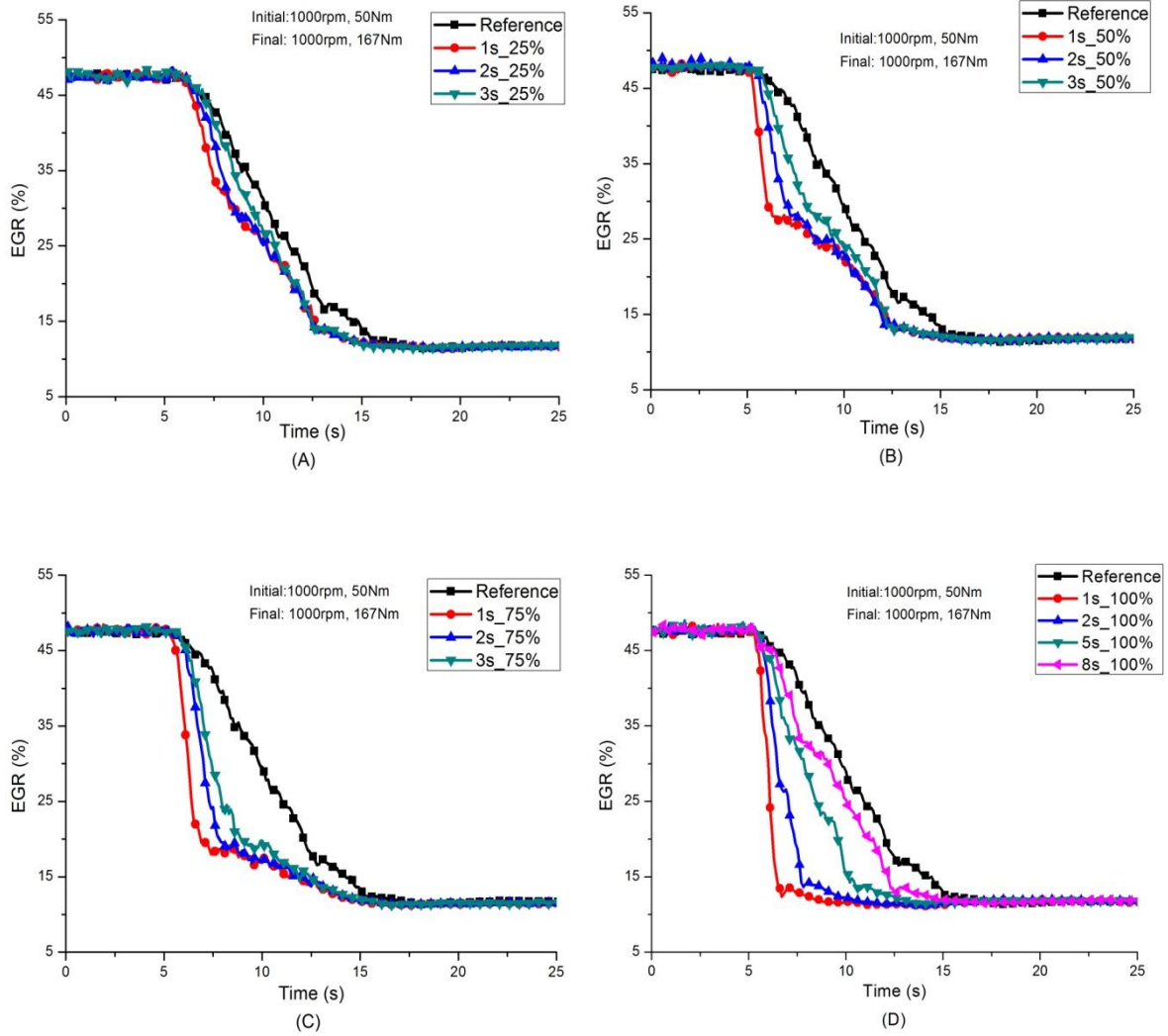


Figure 7.1 Instantaneous EGR profiles A) 25% EGR reduction, B) 50% EGR reduction, C) 75% EGR reduction and D) 100% EGR reduction

7.3.2 Effects of the Varying EGR on Engine Parameters

The intake air mass flow was significantly influenced by the EGR variation due to the exhaust energy bypass of the EGR valve. In the experimental setup, the INCA air flow sensor was located upstream of the turbocharger compressor in the intake manifold. Therefore, the measurements indicated the total fresh air inlet flow during the transition. The actual intake air flow rate was affected by the combined interaction of the EGR valve position and the VGT blade angle. This complex interaction of two dynamic systems combined with the gas dynamics response resulted in variations of intake air flow. This dynamic interaction has to be considered in future calibration maps for transient operations. However, it was experimentally observed that the simultaneous control of VGT with EGR resulted in undesirable flow rate fluctuations during the short transient operations. Also, since emission control was the main focus of this investigation, emphasis was given to EGR variations. For these reasons the VGT control was not included in this study. Furthermore, the control of the EGR valve positions by itself provided a sufficient reduction of the EGR flow rate during transient operation to obtain the desired AFRs.

The intake air mass flow of both reference and modified optimized sequences are displayed in Figure 7.2. Inlet air flow overshoot (hump) was observed for the reference and the 25% reduction sequences at the transition end. During the torque increasing phase of the transition, the turbocharger system was activated to provide the demanded engine output. A corresponding proportional-integral-derivative (PID) control strategy was then triggered which eventually led to the air flow hump. The same phenomenon has been reported by previous researchers (Armas et al. 2006, Rakopoulos 2009)

The instantaneous intake air was significantly affected by the varying EGR valve position. Reducing the EGR rate resulted in less by-passed energy through the EGR valve and improved the transient exhaust energy. The increased exhaust gas energy was utilized to drive the turbocharger-compressor system and eventually promoted the intake air mass flow. This phenomenon was more obvious for those calibration sequences with a high fraction of EGR rate reductions. In addition, unlike the reference calibration sequence, the hump was reduced with an increased fraction of the EGR reduction in the optimized sequences.

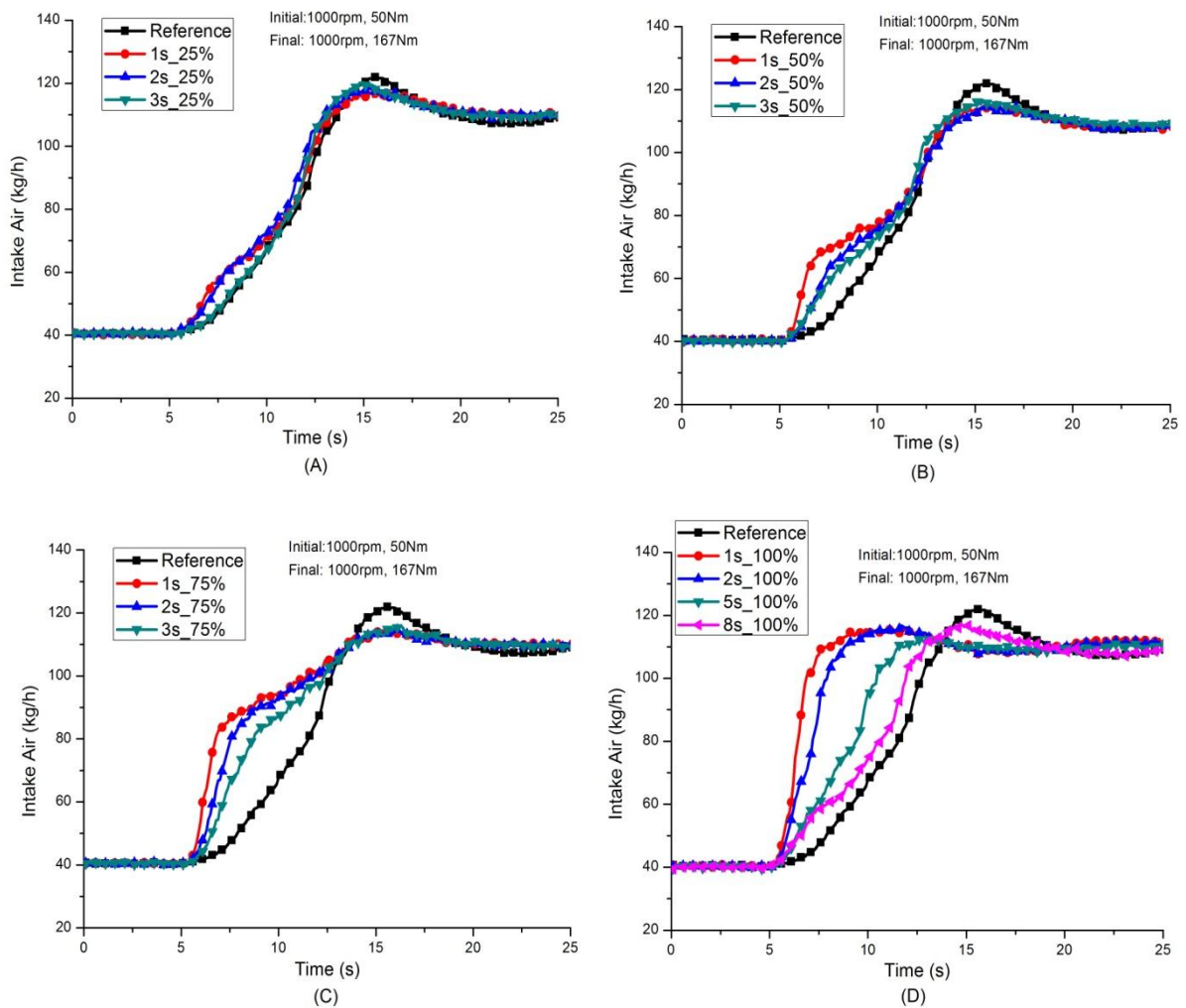


Figure 7.2 Intake air mass flow profiles A) 25% EGR reduction, B) 50% EGR reduction, C) 75% EGR reduction and D) 100% EGR reduction

The fuel injection quantity for each of the transient sequences is displayed in Figure 7.3. During the transition phase, the amount of fuel injected by the reference sequence was higher than that of the optimized sequences. For all transient optimization sequences, transients with shorter EGR reduction timing always resulted in less fuel injection quantity. The trend was more pronounced for the sequences with more than 50% reduction of the total EGR. The promoted intake air mass flow from the instantly reduced EGR rate improved the engine combustion during the acceleration transition cycles. Therefore, less fuel was required by the engine control unit (ECU) to fulfil the demanded engine output.

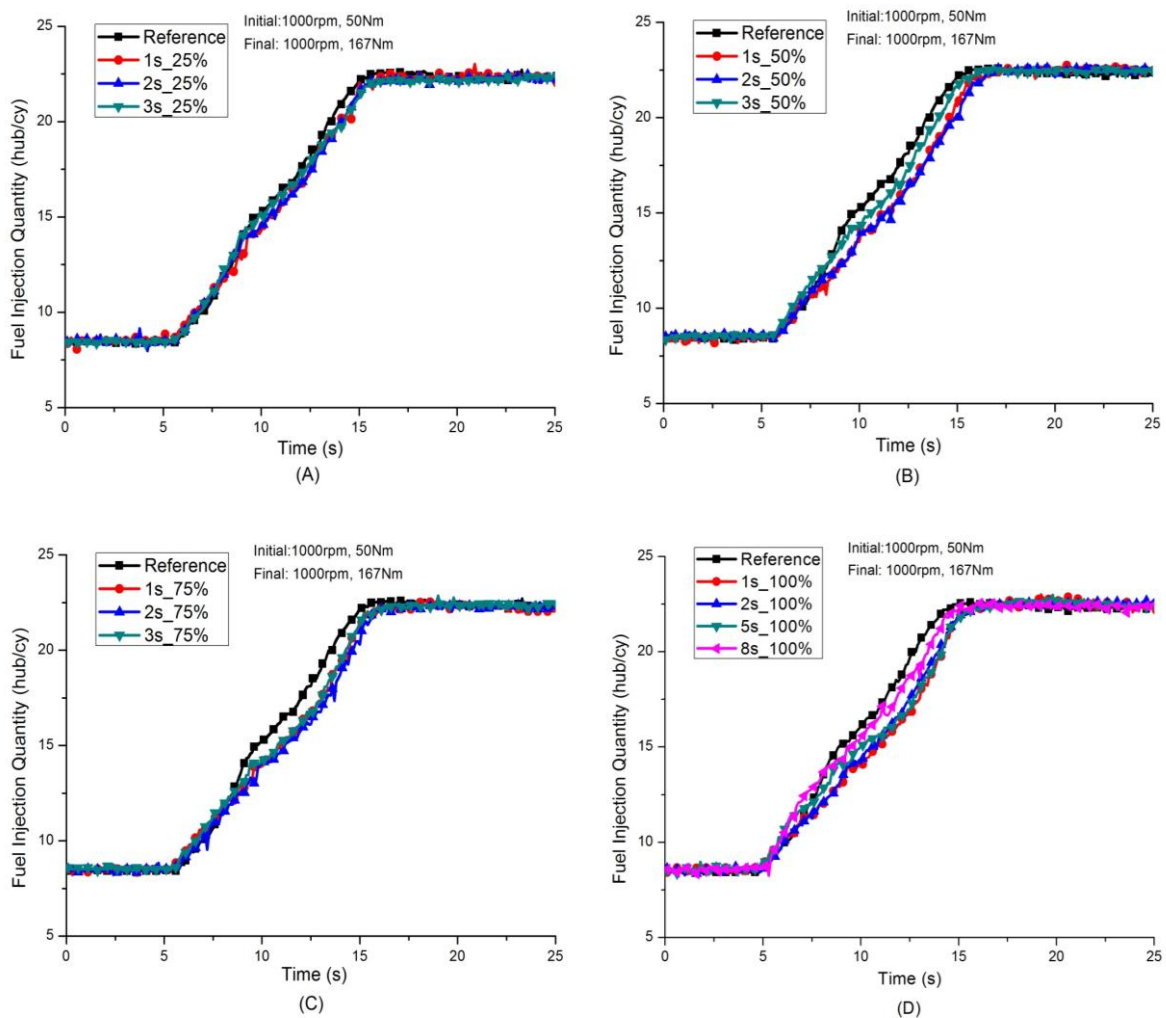


Figure 7.3 Fuel injection quantity profiles A) 25% EGR reduction, B) 50% EGR reduction, C) 75% EGR reduction and D) 100% EGR reduction

Figure 7.4 presents the instantaneous air fuel ratio (AFR) during the 30 second transient periods. The reference sequence produced a lower instantaneous AFR ratio from the start of the transition compared to the previous quasi-steady condition and this was followed by an increasing trend at the end of the transition. The reference sequence was based on steady state calibration. Therefore, the AFR was suddenly reduced for the transient period because of the mismatch between the slowly increasing turbocharger boost pressure and the instantly increased fuel injection mass. As the transition phase approached the final steady state condition, the overshoot of the intake air mass flow increased the AFR value and produced the second peak.

In terms of the optimized sequences, two small transition AFR humps could be found for the sequences with 25% and 50% EGR reductions (Figure 7.4, A and B). They occurred at the positions where the intake air was boosted during the transition. Moreover, the AFR was significantly improved by the optimized EGR variations, especially for the sequence with a high EGR reduction value and short transition timing. The optimized calibration sequence with 100% reduced value and 1 second reduction timing improved the instantaneous AFR by more than doubling its value (Figure 7.4 D). Also, there was no second hump observed for the 100% reduction of the EGR sequences; since for these cases, there were no intake mass flow humps towards the end of the transition.

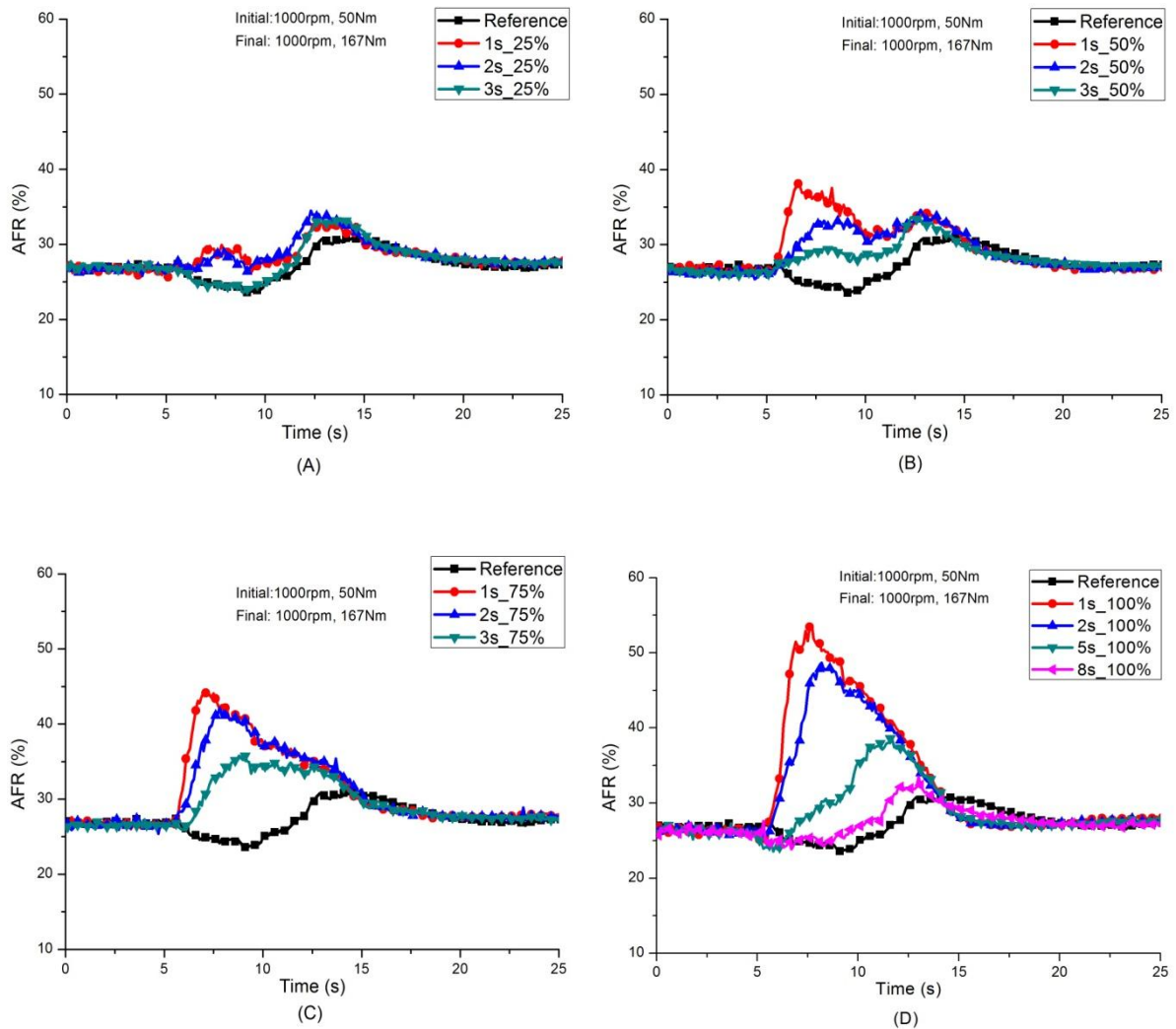


Figure 7.4 Air-fuel ratio profiles A) 25% EGR reduction, B) 50% EGR reduction, C) 75% EGR reduction and D) 100% EGR reduction

7.3.3 Gaseous Emissions

The instantaneous THC emissions for different calibration sequences over the transition period are presented in Figure 7.5. Almost all of the optimized sequences eliminated the THC emissions' spikes except the calibration sequence with 25% EGR reduction and 3 second EGR transient timing. In general, incomplete combustion is considered to be the main reason for THC emissions' presence in the exhaust gas. Under acceleration conditions, the mechanical delay of the turbocharger-compressor system and EGR valve (Figure 7.1) led to a

delayed response of the intake air mass flow rate. The mismatch between the intake air mass flow and the fuel injection quantity deteriorated the combustion inside the cylinder. Therefore, high THC emissions for the case of the reference calibration sequence were emitted during the transition. For the optimized sequences, EGR rates during the transition were always lower than for the reference sequence. As a consequence, the combustion temperature as well as the oxygen content was higher than that of the reference based transient and eventually improved the combustion quality during transition.

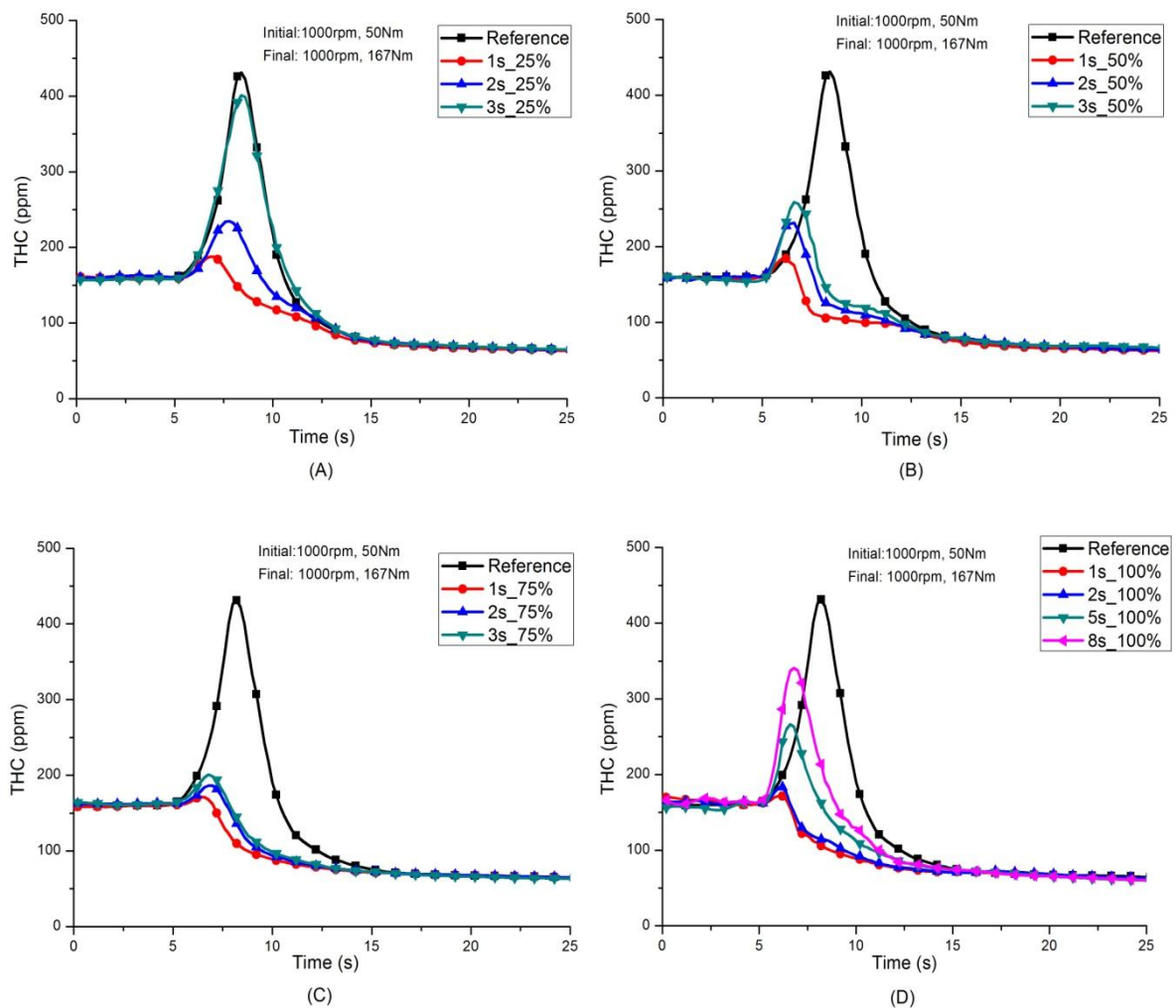


Figure 7.5 Total hydrocarbon (THC) emissions profiles A) 25% EGR reduction, B) 50% EGR reduction, C) 75% EGR reduction and D) 100% EGR reduction

The use of EGR is one of the crucial techniques to reduce the NO_x emissions in modern diesel engines. The optimized sequences utilized in this study were used to reduce the instantaneous EGR under the load changed transient conditions in order to achieve the reduction of emission spikes of both particulate matter and THC. Due to the EGR reduction influence on the engine emissions, some NO_x emissions were generated in this investigation which is a drawback. The oxygen content and peak temperature of combustion are the key factors causing the NO_x production. Furthermore, the trade-off between the NO_x and particulate matter could be improved by some certain combustion strategies which have been proposed by many researchers (Zhang et al. 2011, Aoyagi et al. 2008). However, most previous research was focused on the steady state condition. Under a transient condition, the air intake mass flow was varying continuously which directly impacted on the combustion temperature during the transient period and finally affected the NO_x and particulate matter trade-off.

Figure 7.6 illustrates the profile of the NO_x emissions under various transient EGR strategies. The NO_x emissions for the reference and small EGR reduction fraction calibration sequences were kept constant for about 4 to 6 seconds after the torque increase. By contrast, the NO_x increased sharply at the beginning of the transient period for those sequences with EGR reduction above 75% as a result of the EGR valve closing. The NO_x emissions trends became smoother after 20 seconds of the start of the transient period for the 25%, 50% and 75% EGR reduction sequences, compared with the reference transient period.

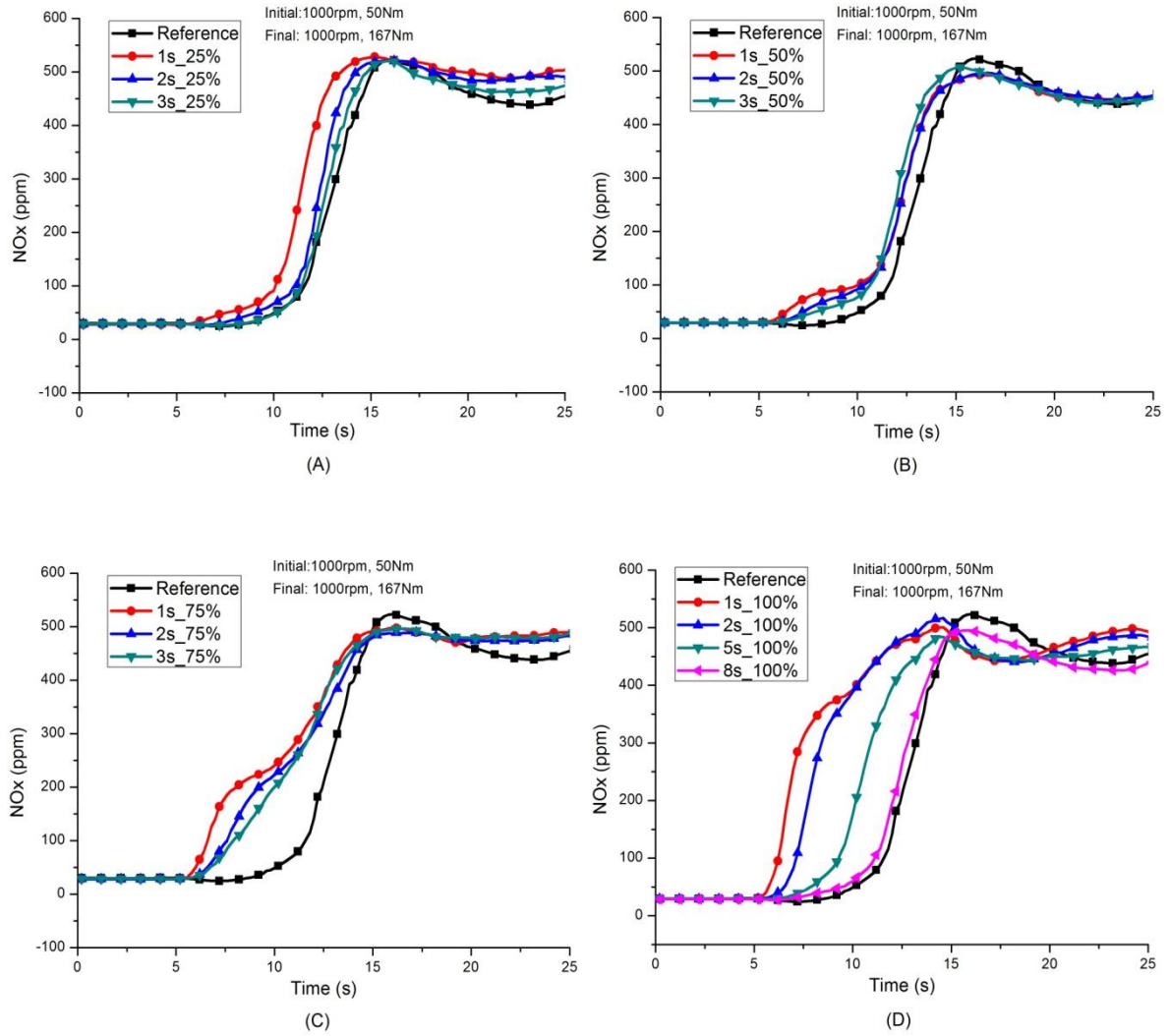


Figure 7.6 NOx emissions profiles A) 25% EGR reduction, B) 50% EGR reduction, C) 75% EGR reduction and D) 100% EGR reduction

7.3.4 Particulate Matter Emissions

The comparison of the total particulate number (PN) concentrations between the reference and optimized sequences for different transient strategies are shown in Figure 7.7. For the optimized sequences, the EGR rates under a transient condition were designed to be below the values of the reference. Therefore, the total PN value was improved for all the optimized sequences.

As has been suggested by many researchers, the PN spike of the reference based sequence is obvious during the acceleration transition sequence due to the turbo-lag issue. As a consequence, the reference sequence produced the highest and longest PN spike during the transition compared with the other sequences. Moreover, the emission spike duration was decreased significantly with the higher EGR reduction rate for sequences with a high percentage of EGR reduction (Figure 7.7, A and B).

With the high fraction of EGR reduction rate during the transience, the intake air flow rate, the turbocharger boost pressure, as well as the turbulence of the inlet air, improved significantly. The increased air inlet turbulence inside the cylinder provided better fuel atomization and fuel-air mixture in the fuel rich diffusion flame region. Moreover, the lower amount of exhaust gas reintroduced back into the cylinder provided more fresh air for combustion; thus more oxygen was available during the combustion phase. This caused the already formed soot particles to be oxidized and eventually reduced the particulate emissions. Furthermore, the EGR valve was implemented to reintroduce the last cycle exhaust gas back for combustion, which contained a higher fraction of particulate matter compared to fresh air. All the above mentioned factors resulted in improved engine combustion.

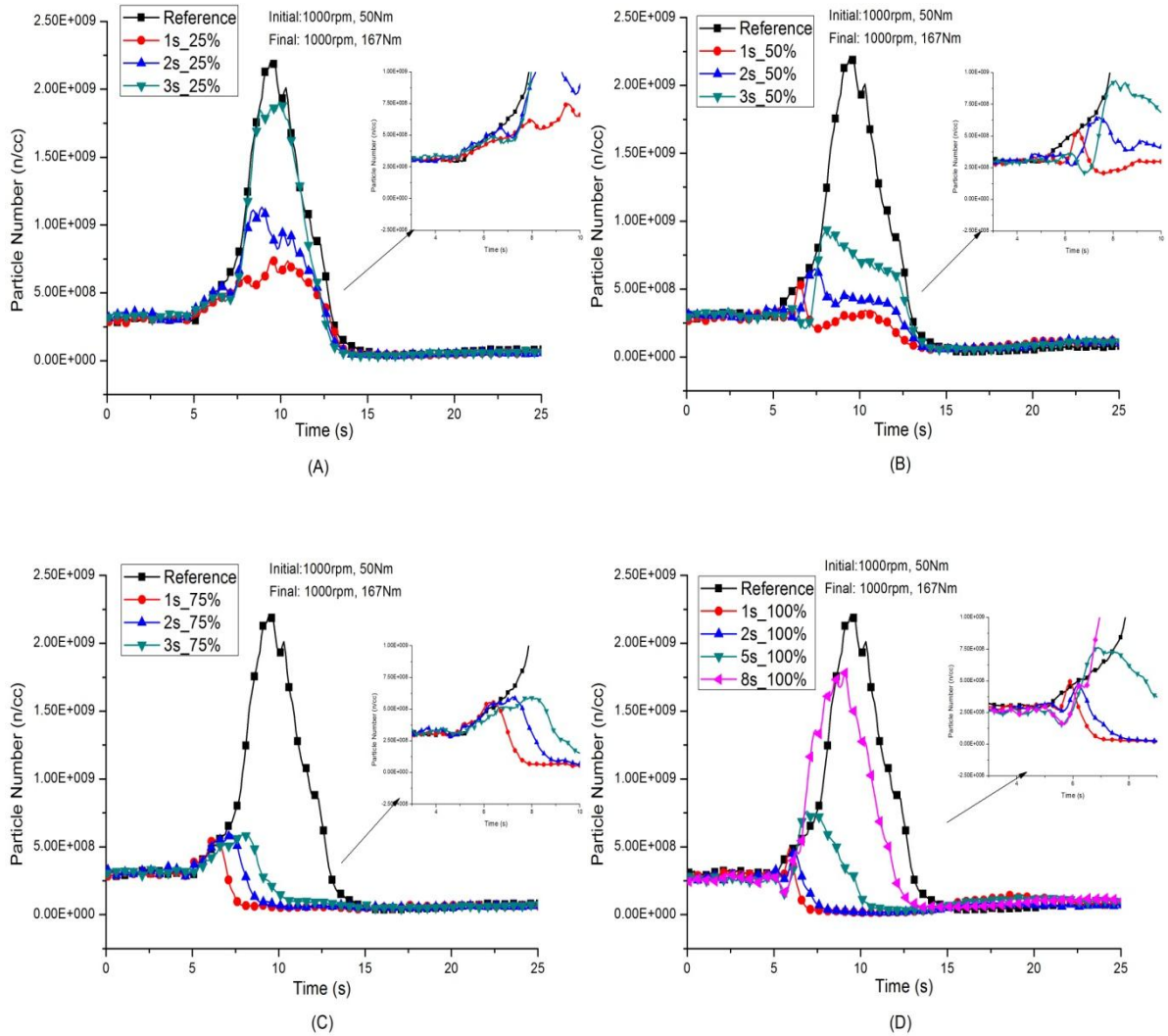


Figure 7.7 Total particle number profiles A) 25% EGR reduction, B) 50% EGR reduction, C) 75% EGR reduction and D) 100% EGR reduction

Two hump (bimodal) distributions were found for the optimized sequences with the 25% and 50% of EGR reduction strategy. As the EGR reduction percentage increased, the transition peak point shifted forward and its magnitude was reduced (Figure 7.7, C and D). In addition, the concentration of the particulate matter was significantly reduced for those sequences with high EGR reduction values and rates. Transient PN levels for fully reduced EGR transient sequences were even lower than the level for the post engine stabilization conditions.

As can be seen from Figure 7.7, certain transient sequences produced short periods of post emission fluctuations after the torque transition was finished. Therefore, a 15 second total time interval after the beginning of transition was taken into account for calculating the cumulative emissions. Figure 7.8 shows the cumulative emissions' trade-off between NOx and PN. With the implemented incremental EGR strategies, the cumulative PN value during the transition was reduced by as much as 83%. When more than 5 seconds of 100% EGR reduction strategies was implemented, the PN emissions' increase became more sensitive to the EGR transition timing. In contrast, NOx emissions for cases with less than 5 seconds EGR transition timing were the most sensitive. In addition, it was observed that 75% EGR reduction sequences were not sensitive to the PN emissions when varying the EGR reduction rate. In contrast, when the 50% EGR transient strategies were implemented, the NOx emissions were always stabilized at a relatively low level; while PN emissions were relatively sensitive to the varying EGR transition timing.

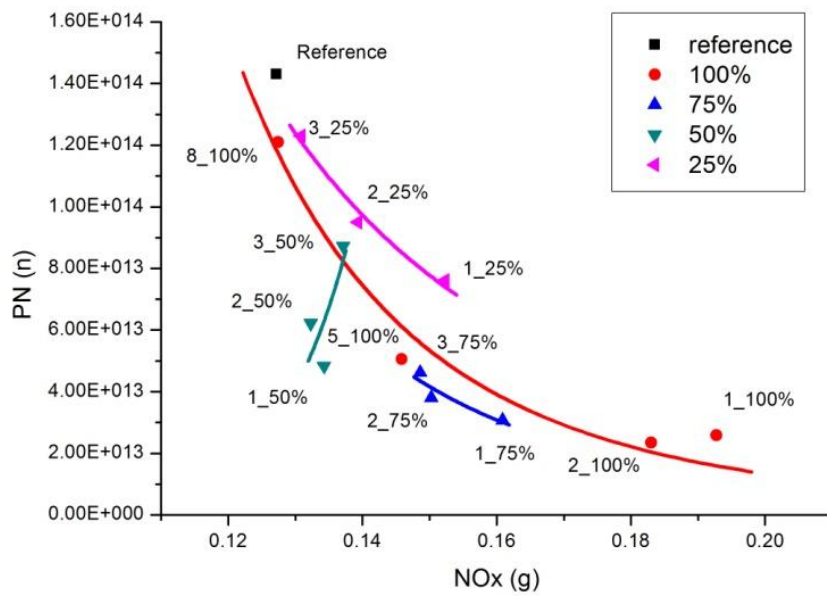


Figure 7.8 Cumulative results for the particulate, NOx trade-off

Although a 100% EGR reduction in a short period was the most effective method to reduce the particulate emissions, it also produced the highest NO_x emissions. In modern commercial diesel engines, SCR is one of the most commonly used technologies to reduce the NO_x emissions. However, it is difficult to control urea in the SCR in order to form NH₃ at a low engine condition due to its low evaporation and decomposition properties (Johnson 2012). In this study, the engine was operated in a relatively low condition range. Therefore, attention must be given to restrict the NO_x emissions level when this novel EGR control strategy is applied. Figure 7.9 shows the cumulative emissions relative differences between the optimized and reference sequences. With the utilization of the 100% EGR reduction strategy, the cumulative PN was reduced by up to 83%. Nevertheless, a 50% increase of NO_x emissions was observed under this EGR control mode. The 25% EGR reduction sequence produced the lowest level of PN reduction compared with the other strategies as the intake air mass flow was not improved a lot under this transient control strategy. The cumulative PN of 50% EGR reduction with 1 and 2 seconds reduction timing decreased by 66.2% and 56.5% respectively; meanwhile the NO_x emissions increase was kept within a tolerance of 6%. These two transient EGR control modes are considered as the most suitable strategies under the current research transient conditions.

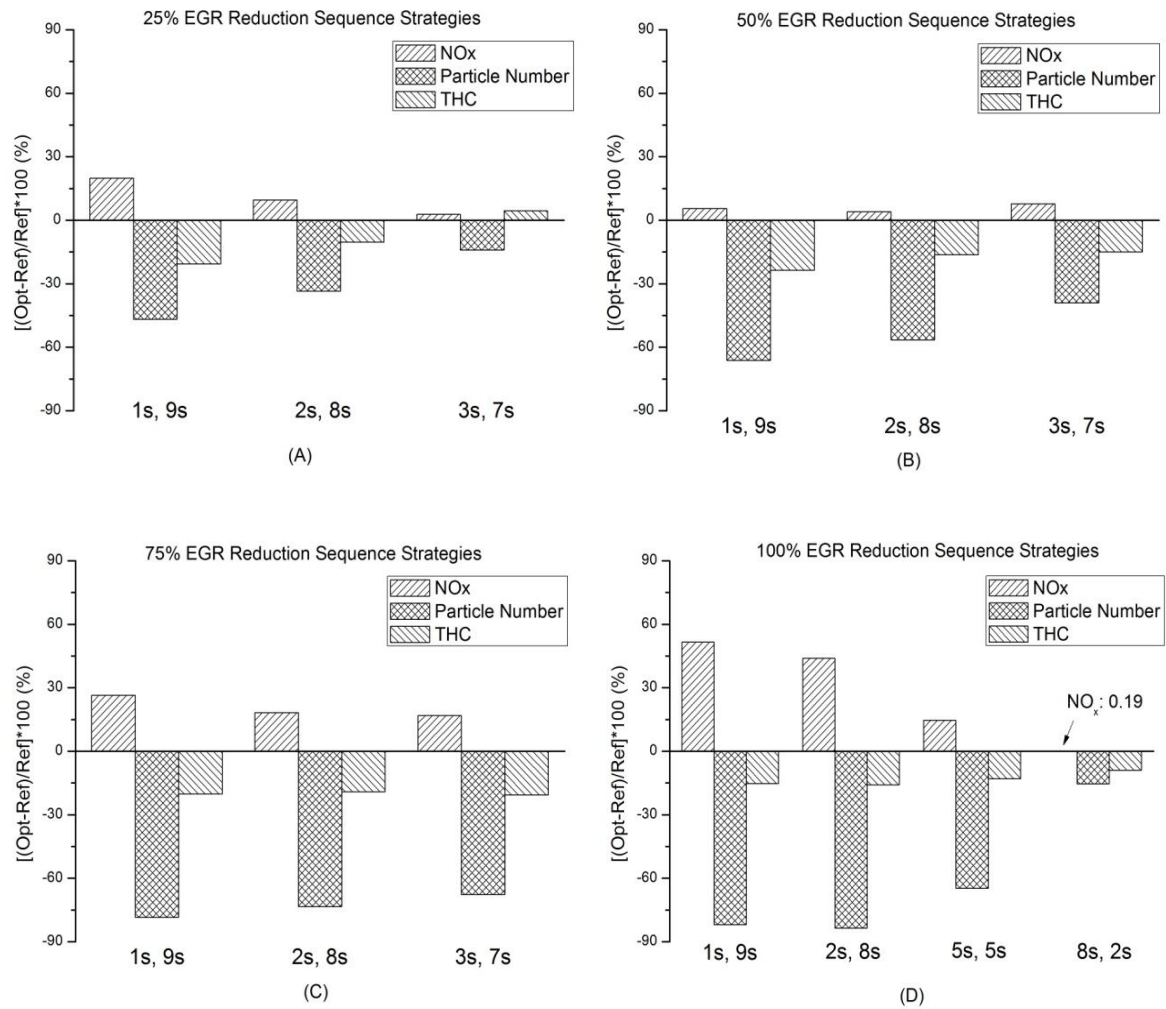


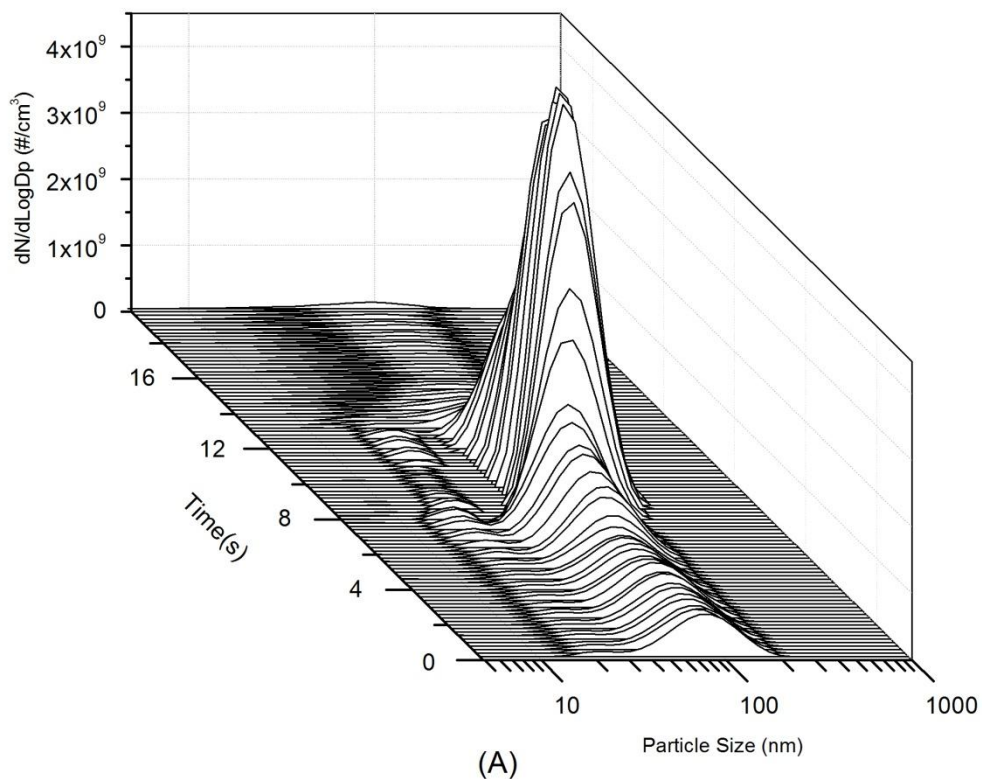
Figure 7.9 Cumulative emission variations between optimized and reference sequences

Three test sequences were selected for the particle size distribution analysis in this section; they are the most representative scenarios in this study. Figures 7.10 A to C demonstrate the particle size-number distribution for the reference, optimized sequences of 50% and 100% reduction with 1 second EGR transition timing respectively.

As is seen from the diagram, the engine emitted more nucleation mode particles during the 10 second transition periods when it was running under the reference condition. The AFR under the load-changed only transient period was extremely low due to the turbo-lag issue. Poor atomization as well as the deteriorated air-fuel mixture and high local equivalence ratio led to more fuel rich combustion regions and less oxidation process inside the engine cylinder.

These factors have been proposed by many researchers as the most favoured situations for the nucleation mode particles production.

Moreover, it is obvious that the concentration of accumulation particles was dramatically reduced during the transition when the optimized EGR strategies were applied to the engine. The accumulative mode particulates were mainly formed by soot agglomerates conglomerating with the liquid state hydrocarbons. The accumulation mode particles were classified between 50 to 1000 nm by the particulate size. The decreased number of accumulative particulates could have contributed to the elevated air supply and improved the engine combustion. On the other hand, larger sizes of accumulation particles were produced for all sequences once the engine load was increased, which was believed due to the increased fuel injection quantity.



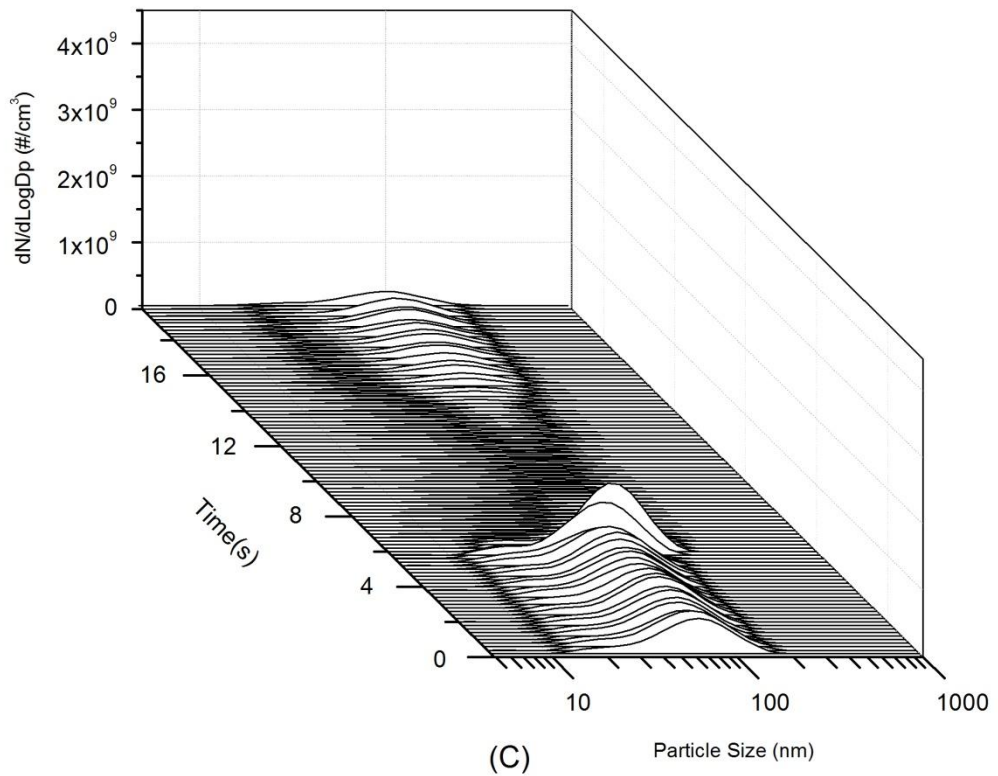
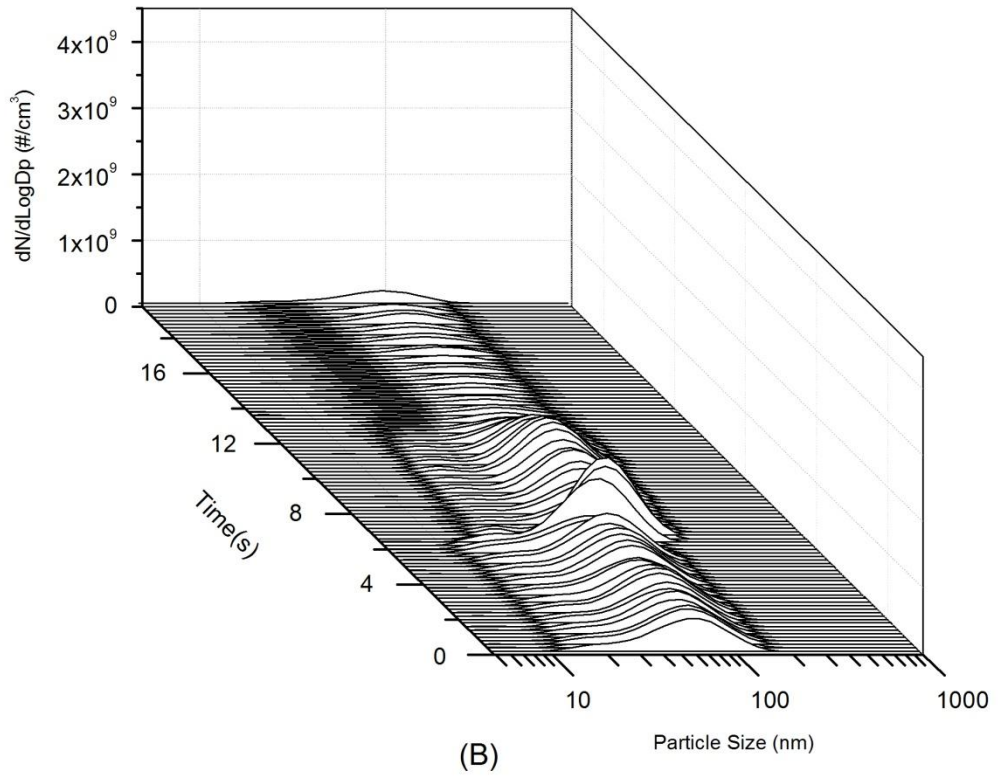


**Figure 7.10 Dynamic particle distribution behaviours of reference and optimized sequences,
 A) reference, B) 50% EGR reduction and C) 100% EGR reduction**

7.4 CONCLUSIONS

Time variable EGR reduction during transition operation has been used as a novel strategy to improve performance and emissions in a commercial turbo-charged diesel engine. The EGR amount was reduced by 20, 50, 75 and 100% during specific time intervals of 1, 2, 3, 5, and 8 seconds under transient operations. The transient conditions applied for the tests were at an engine speed of 1000 rpm, while the load increased from 72 to 167 Nm. The starting condition was intentionally selected as a relatively low operating condition to reveal the turbo-lag effect more profoundly in transient operation modes. The major findings are presented below.

- The reference scenario used the steady state calibration sequence that produced significant particulate and THC spikes during the transient periods which originated from the turbo-lag issue.
- The time variable EGR reduction strategy effectively improved intake air mass flow rates during transient periods which contributed to two facts: 1) more fuel gas was driving the turbocharger and 2) reduction of EGR provided more fresh air to be charged in the cylinders.
- This novel strategy resulted in reduced fuel injection quantity compared to the reference scenario due to the higher AFR and consequently improved combustion.
- The strategy improved the THC and particulate emissions substantially. The THC and particulate matter emissions were reduced by up to 23.6% and 83.5% for the cases of 50 and 100% EGR reduction in the 1 second time interval respectively.
- The nucleation mode was reduced by application of the strategy because of the improved AFR and greater availability of oxygen in the cylinders. A drawback for this strategy was that the reduction of EGR resulted in a NO_x increase for all different strategies tested.

- The case with 50% EGR reduction in the 2 second time interval provided the best result considering both the performance and emissions' trade-off.

To further improve the time-varying EGR reduction strategy, the simultaneous increase of speed and torque during transition has to be considered in future works. Also, the dynamic behaviour of turbo-lag has to be investigated and implemented into the ECU maps.

CHAPTER 8

CONCLUSIONS AND FUTURE WORK

The investigations of this thesis were focused on the regulated/discrete transient and cold start performance and emission characteristics of a modern turbocharged diesel engine. The research work is carried out based on the approaches of understanding and improving the engine transition behaviours. Firstly, the experimental work was focused on the ambient temperature impacts on the engine performances and emissions. Further evaluations regarding the potential use of intake air heating are introduced to increase engine efficiency and emissions. In addition, the elimination of transient emission spikes was achieved by using alternative biodiesel fuels, as well as novel incremental EGR strategies. This chapter aims to summarize the most significant findings drawn from the previous chapters and give the suggestions for further research.

8.1 RESEARCH CONCLUSIONS

The following sections are divided into four parts which are dedicated to remark the important findings from this thesis research.

8.1.1 Temperature Impacts on Engine Transient Emissions

With the deteriorated combustion environment, the gaseous and particulates' emissions are increased with the decreasing ambient temperature. The cumulative results show that cold start is a dominative segment of a NEDC sequence for the gaseous (mainly CO and THC) and particulate emissions. However, as the transient sequence runs consecutively, the emissions of the engine are highly dependent on the engine temperature rather than the ambient temperature. As a consequence, all of the mean mass specific emissions for different temperature scenarios become closer at the later stage of the NEDC. The increased accumulation mode particulates contribute to the increase of particulate mass at the end of the EUDC stage; whereas the nucleation mode particulates cause transient particulate number spikes during the whole of the transient scenarios. These particulates are generated at both very high and very low AFR conditions. The size of the spikes is bigger at the former condition under the NEDC, due to the over-lean combustion mixtures.

It can be concluded from the 2D-GC/MS experiments that the SVOC particulate emissions from the diesel engine originated from both diesel fuel and engine oil. The diesel fuel has a dominating contribution to the number of particulate species under cold start NEDC transient conditions; whereas the lubricating oil plays an important role for the n-alkane particles' emission where the carbon number is between C24 and C28. For the PAH emissions, the concentration of naphthalene is nearly two orders higher than acenaphthylene. As the combustion progresses, the engine tends to produce a high concentration of low carbon number PAHs in the low carbon number region.

8.1.2 Evaluations of Intake Air Heating Influences in a Sub-zero Environment

By using the intake air heating system, the engine performance and emissions are significantly improved during the first stage of the NEDC. The cumulative THC emissions of the first UDC can be reduced by more than 60% when using the higher degree of the heating strategy. However, the NO_x emissions are not significantly influenced by the temperature of the intake air heating when the heating temperature is over 5 °C. As the test sequence runs continuously, the emission trends become identical for all heating strategies at the later stage of the NEDC. The intake air heating can reduce the particulate matter emissions in both size and number. The PN for the first UDC occupied around 25% of the overall NEDC sequence in a -7 °C intake air temperature environment. This value was reduced to about 20% when the engine was operated with the heated air supply. The engine efficiency can be improved by up to 1.46% when using the higher temperature heating strategy.

8.1.3 Steady and Transient Performances of Biodiesel Blends

The transient PN emission spikes were observed in all the transient sequences due to the turbocharger lag issue. The AFR was greatly influenced during the entire transient recovery period. For engine accelerating transients, the engine with higher initial/final engine load and speed operating conditions emitted lower PN and gaseous spikes compared with low speed and load engine transient operation. The particulate matter spikes can be significantly eliminated by using blended biodiesel fuels. The oxygen content is an important factor to determine the duration of the particulate emissions' recovery period. The duration decreased with the biodiesel blending ratio increasing for all the engine transient scenarios. The 15

seconds cumulative PN and THC emissions can be reduced by up to 75% and 50% respectively, when running with biodiesel fuels; while the NO emissions are almost doubled compared with those of diesel. The transient PN peak value is notably influenced by the length of the acceleration timing. The shorter transition timing resulted in a higher emission peak value.

8.1.4 Incremental Variations of EGR under Torque Increase Transition

Using the incremental transient EGR strategy can effectively improve the instantaneous intake air mass flow rate under acceleration transient conditions, due to the transient turbocharger performance improvements and the increased amount of inlet fresh air flow. Furthermore, the fuel injection quantity is reduced for the sequence using the novel EGR strategy. This is contributed to the higher AFR and the improved combustion conditions. By using the aggressive incremental EGR strategy, the particulate matter emissions can be significantly reduced by up to 83.5%. By considering the NO_x emissions' trade-off, the case with 50% EGR reduction in the 2 seconds time interval provided the best solution for which the particulate number is reduced by 56.5% and the NO_x emission increase was kept within a tolerance of 6%.

8.2 *FUTURE WORK*

Based on the experimental study conducted in this thesis, there are several recommendations for further research and investigations:

- To improve the engine energy balance and increase the engine performance during the cold start phase, a thermal energy storage device with Phase-change Material (PCM) are recommended to be used. They are able to store and release the exhaust heating energy to achieve the same function as an intake air heating system.
- More experimental work should be undertaken to investigate the intake air heating strategies. A statistical model should be established based on the data in order to control the emissions' level with the minimum thermal heating energy consumption.
- Extend the particulate chemical composition research in a low temperature environment to biodiesel fuels. Biodiesel fuels have been investigated in this thesis which is of benefit for particulate matter emissions. However, their poor cold flow properties may lead to many issues at a low ambient environment. Additional calibration work will need to be conducted in terms of fuel injection systems and other engine parameters.
- The particulate matter can be analyzed via Micro-oriform Uniform Deposition Impactor (MOUDI) techniques in order to detect the particulate compositions with a selective size distribution. Furthermore, it should be of benefit for particulate formation research if further investigations can locate the sample probe at different places along the exhaust manifold.

- The concept of the incremental EGR transient strategy can be further implemented into various ranges of engine transient conditions. The simultaneous increase of speed and torque during transition needs to be considered in future works.
- Furthermore, the transient EGR can be incremented and coupled with a VGT, as both of them can contribute to the intake air path characteristics. It is also worth creating a statistical model for the purpose of optimization of the transient EGR strategy and the engine performance with more experimental data.

Appendix A

Table A 1 Engine measurement variables

Abbreviation	Description	Unit
Epm_nEng	Engine speed	rpm
Oil_tSwmp	Oil temperature	℃
APP_rRaw	Acceleration pedal sensor	%
FuelT_t	Fuel temperature	℃
Air_tCACDs	Charged air temperature downstream	℃
EGRVlv_rActB1	EGR actuator position bank 1	%
EGRVlv_rActB2	EGR actuator position bank 1	%
AFS_dmB1	Value of air mass bank1	kg/h
AFS_dmB2	Value of air mass bank1	kg/h
InjSys_qTot	Total fuel injection quantity	mg/stk
AirCtl_rEGREst_r32	EGR rate	%
GlvPlg_u	Glow plug voltage	mV
TrbCh_rActB1	Turbocharger bank 1	%
TrbCh_rActB2	Turbocharger bank 2	%
APP_r	Pedal value	%
ThrVlv_rAct	Actuator Position	%
Air_pCACDs	Charged air cooler downstream pressure	hPa
Rail_pSetPoint	Fuel pressure desired	Mpa
InjCrv_phiPil1Des	Pilot injection timing 1	℃CRK
InjCrv_phiPil2Des	Pilot injection timing 2	℃CRK
InjCrv_phiMI1Des	Main injection timing	℃CRK
InjCrv_phiPol1Des	Post injection timing 1	℃CRK
InjCrv_phiPol2Des	Post injection timing 2	℃CRK

Appendix B

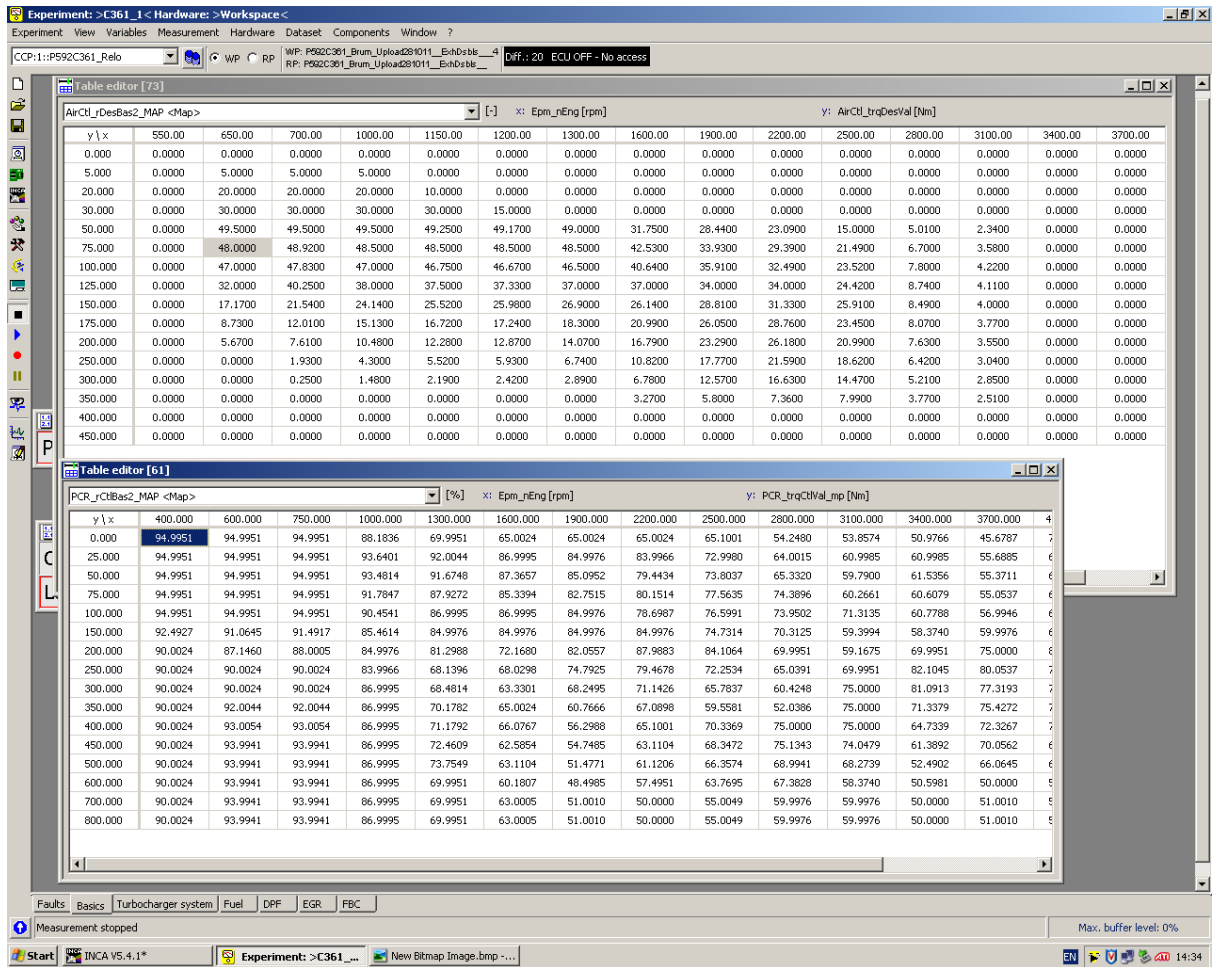


Figure A 1 Engine EGR calibration map

References

- Abbass, M.K., Andrews, G E and Williams, P.T. (1990) The Composition of the Organic Fraction of Particulate Emissions of a Diesel Engine Operated on Vegetable Oil. **SAE Technical Paper**, 901563.
- Abdullah, N. (2011) **Effects of Split Injection and Exhaust Gas Recirculation Strategies on Combustion and Emissions Characteristics in a Modern V6 Diesel Engine**. PhD thesis. University of Birmingham.
- Agarwal, A.K., Gupta, T. and Shukla, K. et al. (2015) Particulate Emissions from Biodiesel Fuelled CI Engines. **Energy Conversion and Management**, 94, pp.311–330.
- Agarwala, D., Sinhab, S. and Agarwal, A. (2006) Experimental Investigation of Control of NO_x Emissions in Biodiesel-fueled Compression Ignition Engine. **Renew Energ**, 36, pp.2356–2369.
- Alam, M.S., West, C. and Scarlett, A. et al. (2013) Application of 2D-GCMS Reveals Many Industrial Chemicals in Airborne Particulate Matter. **Atmospheric Environment**, 65, pp.101–111.
- Altıparmak D, Deskin A and Koca A, et al. (2007) Alternative Fuel Properties of Tall Oil Fatty Acid Methyl Ester-diesel Fuel Blends. **Bioresource Technol**, 98.
- Al-Zaini, E.O., Olsen, J. and Nguten, T. et al. (2011) Transesterification of Waste Cooking Oil in Presence of Crushed Seashell as a Support for Solid Heterogeneous Catalyst. **SAE International Journal of Fuels and Lubricants**, 4(2), pp.139–157.
- Andrews, Gordon E, Abdelhalim, S.M. and Li, H. (1999) The Influence of Lubricating Oil Age on Oil Quality and Emissions from IDI Passenger Car Diesels. **SAE Technical Paper**, 1999-01-1135.
- Aoyagi, Y., Shimada, K. and Osada, H. (2008) Diesel Emissions Improvement by RME in a High Boost and EGR Single Cylinder Engine. **SAE Technical Paper**, 2008-01-1376.
- Armas, O, Hernandez, J. and Cardenas, M. (2006) Reduction of Diesel Smoke Opacity from Vegetable Oil Methyl Esters during Transient Operation. **Fuel**, 85(17-18), pp.2427–2438..
- Armas, Octavio, Garc ía-Contreras, R. and Ramos, Á. (2012) Pollutant Emissions from Engine Starting with Ethanol and Butanol Diesel Blends. **Fuel Processing Technology**, 100, pp.63–72..
- Armas, Octavio, Gómez, A. and Cárdenas, M.D. (2009) Biodiesel Emissions from a Baseline Engine Operated with Different Injection Systems and Exhaust Gas Recirculation (EGR) Strategies during Transient Sequences. **Energy & Fuels**, 23(12), pp.6168–6180.

- Armas, Octavio, Gómez, A. and Ramos, Á. (2013) Comparative Study of Pollutant Emissions from Engine Starting with Animal Fat Biodiesel and GTL Fuels. **Fuel**, 113, pp.560–570.
- Armas, O., Yehliu, K. and Boehman, A. (2010) Effect of Alternative Fuels on Exhaust Emissions during Diesel Engine Operation with Matched Combustion Phasing. **Fuel**, 89, pp.438–456.
- Arumugam, R. et al., Xu, H.M. and Liu, D. (2015) Key Factors Affecting the Cold Start of Diesel Engines. **International Journal of Green Energy**.
Doi:10.1080/15435075.2014.938748
- Aydin H, B.H. (2010) Performance and Emission Analysis of Cottonseed Oil Methyl Ester in a Diesel Engine. **Renew Energ**, 35(5), pp.88–92.
- Bannister, C.D., Hawley, J. and Ali, H. et al. (2010) The Impact of Biodiesel Blend Ratio on Vehicle Performance and Emissions. **Proceedings of the Institution of Mechanical Engineers, Part D: Journal of Automobile Engineering**, 224(3), pp.405–421.
- Ban-Weiss, G., Chen, J. and Buchholz, B. et al. (2007) A Numerical Investigation into the Anomalous Slight NO_x Increase when Burning Biodiesel; A new (old) theory. **Fuel Processing Technology**, 88, pp.659–667.
- Bielaczyc, P. (2001) Investigation of Exhaust Emissions from DI Diesel Engine During Cold and Warm Start. **SAE Technical Paper**. 2001-01-1260.
- Black, F. and High, L. (2015) Methodology for Determining Particulate and Gaseous Diesel Hydrocarbon Emissions. **SAE Technical Paper**, 790422.
- Brown, N., Gupta, V. and Rocca, A. et al., (2007) Investigations of Fuel Injection Strategy for Cold Starting Direct-injection Diesel Engines. **Proceedings of the Institution of Mechanical Engineers, Part D: Journal of Automobile Engineering**, 221(11), pp.1415–1424.
- Cambustion.com, DMS Dilution System. Available at:
<http://www.cambustion.com/sites/default/files/instruments/DMS500/DMS500engine.pdf>
[Accessed March 21, 2015].
- Cambustion.com (FID), FAST FID. Available at:
<http://www.cambustion.com/products/hfr500/fast-fid-principles> [Accessed March 14, 2015].
- Caresana, F. (2011) Impact of Biodiesel Bulk Modulus on Injection Pressure and Injection Timing. The effect of residual pressure. **Fuel**, 90(2), pp.477–485.
- Chartier, C. Aronsson, U. and Andersson, O. et al. (2009) Effect of Injection Strategy on Cold Start Performance in an Optical Light-Duty DI Diesel Engine. **SAE Technical Paper**, 2009-24-0045.

- Cheng, A.S., Upatnieks, A. and Mueller, C.J., (2006) Investigation of the Impact of Biodiesel Fuelling on NO_x Emissions using an Optical Direct Injection Diesel Engine. **International Journal of Engine Research**, 7, pp.297–318.
- Chuepeng, S et al. Xu, H.M. and Tsolakis, A. et al. (2008) Particulate Emissions From a Common Rail Fuel Injection Diesel Engine with RME-based Biodiesel Blended Fuelling using Thermo-gravimetric Analysis. **SAE Technical Papers**, (724).
- Chuepeng, S., Xu, H.M. and Tsolakis, A. et al. (2011) Particulate Matter size Distribution in the Exhaust Gas of a Modern Diesel Engine Fuelled with a Biodiesel Blend. **Biomass and Bioenergy**, 35(10), pp.4280–4289.
- CLD, Cambustion. co., FAST CLD. Available at: <http://www.cambustion.com/products/cld500/cld-principles>.
- Dardiotis, C. and Martini, G. (2012) **Revision of Low Temperature Emission Standards for Petrol Vehicles**
- Delphi, (2015) **Worldwide emissions standards**. Available at: <http://delphi.com/docs/default-source/catalogs/delphi-worldwide-emissions-standards-pc-ldv-15-16.pdf?sfvrsn=2> [Accessed February 3, 2015].
- Demirbas, A., 2008. **Biodiesel: A Realistic Fuel Alternative for Diesel Engine**, London: Springer-Verlag.
- Dhar, A., Agarwal, A.K. and Srivastava, D.K. et al. (2013) Effect of Fuel Injection Pressure on Diesel Particulate Size and Number Distribution in a CRDI Single Cylinder Research Engine. **Fuel**, 107, pp.84–89.
- DIESELNET, **Emission Standards**. Available at: <http://www.dieselnet.com/standards/eu/ld.php> [Accessed February 4, 2015].
- Eastwood, P. (2008) **Particulate emissions from vehicles**, Wiley.
- EPA, **ATSDR**. Available at: <http://www.atsdr.cdc.gov/> [Accessed April 8, 2015].
- EUROPA, **Renewable energy in fuel consumption of transport in EU**. Available at: <http://ec.europa.eu/eurostat/tgm/graph.do?tab=graph&plugin=1&pcode=tsdcc340&language=en&toolbox=data> [Accessed May 4, 2015].
- Fanick, E.R., Kroll, S. and Simescu, S., (2015) Sampling System Investigation for the Determination of Semi- Volatile Organic Compounds (SVOC) Emissions From Engine Exhaust Experimental Set-Up. **SAE Technical Paper**, 2015-01-10.
- Fenimore, C.P. (1971) Formation of Nitric Oxide in Premixed Hydrocarbon Flames. **Thirteenth symposium (International) on Combustion**, 13(1), pp.373–380.
- Florio, S., Pellegrini, L. and Alfe, M. et al. (2011) Chemical and Spectroscopic Characterization of SOF and Soot From a Euro-4 diesel Engine Fuelled by Model Fuels. **JSAE**, 2011-01-2098.

- Galindo, J., Lujan, J. and Serrano J. et al. (2004) Design of an Exhaust Manifold to Improve Transient Performance of a High-speed Turbocharged Diesel Engine. **Experimental Thermal and Fluid Science**, 28(8), pp.863–875.
- Giakoumis, E.G. and Lioutas, S.C. (2010) Diesel-engined Vehicle Nitric Oxide and Soot Emissions during the European Light-duty Driving Cycle using a Transient Mapping Approach. **Transportation Research Part D: Transport and Environment**, 15(3), pp.134–143.
- Giakoumis, Evangelos G., Rakopoulos, C. and Dimaratos, A. et al. (2012) Exhaust Emissions of Diesel Engines Operating under Transient Conditions with Biodiesel Fuel Blends. **Progress in Energy and Combustion Science**, 38(5), pp.691–715.
- Glewen, W., Meyer, C. and Foster, D. et al. (2011) Sources and Tradeoffs for Transient NO and UHC Emissions with Low Temperature Diesel Combustion. **SAE Technical Paper**, 2011-01-1356.
- Hagena, J.R., Filipi, Z.S. and Assanis, D.N. (2006) Transient Diesel Emissions : Analysis of Engine Operation During a Tip-In. **SAE Technical Paper**, 2006-01-1151.
- Han, Y., Liu, Z. and Zhao J. et al. (2008) EGR Response in a Turbo-charged and After-cooled DI Diesel Engine and its Effects on Smoke Opacity. **SAE Technical Paper** 2008-01-1677.
- Han, Z. (2001) Diesel Engine Cold Start Combustion Instability and Control Strategy. **SAE Technical Paper**, 2001-01-12.
- Hara, H., Itoh, Y. and Henein, N.A. (1999) Effect of Cetane Number with and without Additive on Cold Startability and White Smoke Emissions in a Diesel Engine. **SAE Technical Paper**, 1999-01-1476.
- Herzog, T., Pershing, J. and Baumert, K. (2005) Greenhouse Gas Data and International Climate Policy. **Navigating the Numbers**, 1-56973-59.
- Heywood, J.B. (1988) **Internal combustion engines fundamentals**, McGraw-Hill.
- Hoekman, S.K. and Robbins, C. (2012) Review of the Effects of Biodiesel on NOx Emissions. **Fuel Processing Technology**, 96, pp.237–249.
- Jaroonjitsathian, S., Sae-ong, P. and Siangsanorh, S. (2011) A Study of the Effect of Biodiesel Blended Fuel on Diesel Combustion. **SAE Technical Paper**, 2011-01-1952.
- Jessica, L. (2010) Investigation of NOx Predictions from Biodiesel fueled HCCI Engine Simulations Using a Reduced Kinetic Mechanism. **SAE Technical Papers**, 2010-01-05.
- John, D. et al., (2011) Experiences in Cold Start Optimization of a Multi-Purpose Vehicle Equipped with 2.2L Common Rail Diesel Engine. **SAE Technical Paper**, 2011-01-0124.

- Johnson, T. V., (2012) Vehicular Emissions Control Highlights of the Annual Society of Automotive Engineers (SAE) International Congress. **Platinum Metals Review**, 56, pp.75–82.
- Jothithirumal, B. and Jamesgunasekaran, E. (2012) Combined Impact of Biodiesel and Exhaust Gas Recirculation on NO_x Emissions in Di Diesel Engines. **Procedia Engineering**, 38, pp.1457–1466.
- Kampman, B. (2013) **Options to Increase EU Biofuels Volumes Beyond the Current Blending Limits**, Available at: https://ec.europa.eu/energy/sites/ener/files/documents/2013_11_bringing_biofuels_on_the_market.pdf.
- Kang, H. and Farrell, P. V, (2005) Experimental Investigation of Transient Emissions (HC and NO_x) in a High Speed Direct Injection (HSDI) Diesel Engine. **SAE Technical Paper**, 2005-01-3883.
- Kaplan C. and Arslan R, S.A., (2006) Performance Characteristics of Sunflower Methyl Esters as Biodiesel. **Energ Source Part A**, 28(8), pp.751–755.
- Karabektas, M. (2009) The Effects of Turbocharger on the Performance and Exhaust Emissions of a Diesel Engine Fuelled with Biodiesel. **Renew Energ**, 34, pp.89–93.
- Karavalakis G, Stournas S, B.E. and Evangelos, B. (2009) Effects of Diesel/biodiesel Blends on Regulated and Unregulated Pollutants from a Passenger Vehicle Operated over the European and the Athens Driving Cycles. **Atmos Environ**, 43, pp.1745–1752.
- Kasper, A. and Burtscher, H. (2005) Particle Emissions from SI-Engines During Steady State and Transient Operating Conditions. **SAE Technical Paper**, 2005-01-3136.
- Kawano D, Ishii H and Goto Y. et al. (2006) Application of Biodiesel Fuel to Modern Diesel Engine. **SAE Technical Paper**, 2006-01-0233.
- Kawano, D., Ishii, H. and Goto, Y. (2008) Effect of Biodiesel Blending on Emission Characteristics of Modern Diesel Engine. **SAE Technical Paper**, 2008-01-2384.
- Kim, C.H. Paratore, M. and Gonze, E. et al. (2012) Electrically Heated Catalysts for Cold-Start Emissions in Diesel Aftertreatment. **SAE Technical Papers**, 2012-01-10.
- Kittelson, D.B. (1999) **Review of Diesel Particulate Matter Sampling Methods**.
- Kittelson, D. (1998) Engines and Nanoparticles: A review. **Journal of Aerosol Science**, 29(5-6), pp.575–588.
- Knothe, G.; Van Gerpen, J. and Krahl, J. (2005) **The Biodiesel Handbook**, AOCS Press: Campaign, IL,.
- Kobayashi, M., Aoyagi, Y. and Adachi, T. et al. (2011) Effective BSFC and NO_x Reduction on Super Clean Diesel of Heavy Duty Diesel Engine by High Boosting and High EGR Rate. **SAE Technical Paper**, 2011-01-0369.

- Kousoulidou, M., Fontaras, G. and Ntziachristos, L. et al. (2010) Biodiesel Blend Effects on Common-rail Diesel Combustion and Emissions. **Fuel**, 89(11), pp.3442–3449.
- Kousoulidou, M., Fontaras, G. and Ntziachristos, L. et al. (2009) Evaluation of Biodiesel Blends on the Performance and Emissions of a Common-Rail Light-Duty Engine and Vehicle. **SAE Technical Paper**, 2009-01-0692.
- Kweon, C. Okada, S. and Foster, D. et al. (2003) Effect of Engine Operating Conditions on Particle-Phase Organic Compounds in Engine Exhaust of a Heavy-Duty Direct-Injection (D . I .) Diesel Engine. **SAE Technical Paper**, 2003-01-03.
- Lapuerta, M., Armas, O and Rodriguezfernandez, J. (2008) Effect of Biodiesel Fuels on Diesel Engine Emissions. **Progress in Energy and Combustion Science**, 34(2), pp.198–223.
- Last, B. (2008) **Influence of Modern Diesel Cold Start Systems on the Cold Start , Warm-up and Emissions of Diesel Engines**, Ludwigshurg.
- Lea-langton, A., Li, H. and Andrews, G. (2008) Comparison of Particulate PAH Emissions for Diesel , Biodiesel and Cooking Oil using a Heavy Duty DI Diesel Engine. **SAE Technical Paper**, 2008-01-1811.
- Lea-langton, A., Li, H. and Andrews, G. (2009) Investigation of Aldehyde and VOC Emissions during Cold Start and Hot Engine Operations using 100 % Biofuels for a DI Engine. **SAE Technical Paper** 2009-01-1515.
- Lee, C. and Choi, N. (2002) Effect of Air Injection on the Characheristics of Transient Response in a Turbocharged Diesel Engine. **Int. J. Therm. Sci**, 41, pp.63–71.
- Lindl, B. and Schmitz, H., (1999) Cold Start Equipment for Diesel Direct Injection Engines. **SAE Technical Paper**, 1999-01-1244.
- Liu, D. (2014) **Combustion and Emissions of an Automotive Diesel Engine Using Biodeisel Fuels under Steady and Start Conditions**. PhD thesis. University of Birmingham.
- Liu, D., Xu, H. and Tian, J. et al. (2013) Cold and Warm Start Characteristics using HVO and RME Blends in a V6 Diesel Engine. **SAE International Journal of Fuels and Lubricants**, 6(2), pp.478–485. Available at: <http://papers.sae.org/2013-01-1306>.
- Liu, D., Ghafourian, A. and Xu, H. et al. (2013) Phenomenology of EGR in a Light Duty Diesel Engine Fuelled with Hydrogenated Vegetable Oil (HVO), Used Vegetable Oil Methyl Ester (UVOME) and Their Blends. **SAE Technical Paper**, 2013-01-16.
- Liu, D., Ghafourian, A., and Xu, H., (2013) Phenomenology of EGR in a Light Duty Diesel Engine Fuelled with Hydrogenated Vegetable Oil (HVO), Used Vegetable Oil Methyl Ester (UVOME) and Their Blends. **SAE Technical Paper**. 2013-01-1688

- MacMillan, D., La rocca, A. and Shayler, P. (2008) The Effect of Reducing Compression Ratio on the Work Output and Heat Release Characteristics of a Diesel Engine under Cold Start Conditions. **SAE Technical Paper**, 2008-01-13.
- Maiboom, A., Tauzia, X. and Héret, J.-F., (2008) Experimental Study of Various Effects of Exhaust Gas Recirculation (EGR) on Combustion and Emissions of an Automotive Direct Injection Diesel Engine. **Energy**, 33(1), pp.22–34.
- Manente, V., Tunestål, P. and Johansson, B. (2007) A Study of a Glow Plug Ignition Engine by Chemiluminescence Images. **SAE Technical Paper**, 2007-01-1884.
- Mark S. peckham, A.F. and Bruce Campbell, Phil Price, M.D., (2011) Study of Particle Number Emissions from a Turbocharged Gasoline Direct Injection Engine Including Data from a Fast Response Particle Size Spectrometer. **SAE Technical Paper**, 2011-01-1224.
- Martin, G. and Berkau, E. (1971) **An Investigation of the Conversion of Various Fuel Nitrogen Compounds to NO in Oil Combustion.** In San Francisco: In: Paper presented at 70th AIChE National Meeting.
- McCormick, R., Alvarez, J. and Graboski, M. (2012) **Effects of Biodiesel Blends on Vehicle Emissions**, Available at: <http://www.nrel.gov/docs/fy07osti/40554.pdf> .
- McGhee, M. Shayler, P. and LaRocca, A. et al. (2012) The Influence of Injection Strategy and Glow Plug Temperature on Cycle by Cycle Stability Under Cold Idling Conditions for a Low Compression Ratio, HPCR Diesel Engine. **SAE International Journal of Engines**, 5(3), pp.923–937.
- Mohammadi, P. Nikbakht, A. and Tabatabaei, M. et al. (2012) Experimental Investigation of Performance and Emission Characteristics of DI Diesel Engine Fueled with Polymer Waste Dissolved in Biodiesel-blended Diesel Fuel. **Energy**, 46(1), pp.596–605.
- Monyem A and Van Gerpen JH, C.M., (2001) The Effect of Timing and Oxidation on Emissions from Biodiesel-fueled Engines. **Trans ASAE**, 44(1), pp.35–42.
- Moon, G., Lee, Y. and Choi, K. et al. (2009) Experimental Study on Characteristics of Diesel Particulate Emissions with Diesel , GTL and Blended Fuels. **SAE Technical Paper**, 2009-24-0098.
- Nanba, Syuichi. Iijima, A., Shoji, H. and Yoshida, K. (2013) A Study on Influence of Forced Over Cooling on Diesel Engine Performance. **JSAE**, 2011-32-06(3).
- Nuszkowski, J., Thompson, G. and Tincher, R. et al., (2008) Heat Release and Emission Characteristics of B20 Biodiesel Fuels During Steady State and Transient Operation. **SAE Technical Paper**, 2008-01-1377.
- Nuszkowski, J., Flaim, K. and Thompson, G. (2011) The Effects of Cetane Improvers and Biodiesel on Diesel Particulate Matter Size. **SAE Technical Paper**, 2011-01-0330.

- Osuka, I., Nishimura, M. and Tanaka, Y. et al. (1994) Benefits of New Fuel Injection System Technology on Cold Startability of Diesel Engines - Improvement of Cold Startability and White Smoke Reduction by Means of Multi Injection with Common Rail Fuel System (ECD-U2). **SAE Technical Paper** (412) 1994-03-01.
- Ozgunay H, C ,olak S, Zengin G, Sari O, Sarikahya H, Y.L. (2007) Performance and Emission Study of Biodiesel from Leather Industry Pre-fleshings. **Waste Manage**, 27(1), pp.897–901.
- Pace, L. and Presti, M. (2011) An Alternative Way to Reduce Fuel Consumption During Cold Start: The Electrically Heated Catalyst. **SAE Technical Papers**, 2011-24-01.
- Pastor, J. V, Garcia, J. and Pastor J. et al. (2009) Experimental Facility and Methodology for Systematic Studies of Cold Startability in Direct Injection Diesel Engines. **Measurement Science and Technology**, 20(9), p.095109.
- Payri, F., Broatch, A. and Serrano, J. et al. (2013) Study of the Potential of Intake Air Heating in Automotive DI Diesel Engines. **SAE Technical Paper** , 2006-01-1233
- Prime, J. and Khan, S. (2014) **Energy Consumption in the UK 2014**. Available at: https://www.gov.uk/government/uploads/system/uploads/attachment_data/file/337454/e_cuk_chapter_2_transport_factsheet.pdf [Accessed February 4, 2015].
- Raihan, K.A. and Takimoto, F. (2001) Time-Resolved Behavior of Unburned Hydrocarbon Components in Diesel Exhaust under Transient Operations. **SAE Technical Papers**, 2001-01-12.
- Rakopoulos, C.D., Dimaratos, A. and Evangelos, G. et al. (2010) Investigating the Emissions during Acceleration of a Turbocharged Diesel Engine Operating with Bio-diesel or n-butanol Diesel Fuel Blends. **Energy**, 35(12), pp.5173–5184.
- Rakopoulos, D.C., Giakoumis, E.G., 2009. **Diesel Engine Transient Operation**, London: Springer.
- Reifarth, S. and Ångström, H. (2010) Transient EGR in a High-Speed DI Diesel Engine for a set of different EGR-routings. **SAE Technical Paper**, 2010-01-1271.
- Rounce, P., Tsolakis, A. and York, A.P.E. (2012) Speciation of Particulate Matter and Hydrocarbon Emissions from Biodiesel Combustion and its Reduction by Aftertreatment. **Fuel**, 96, pp.90–99.
- Royo, R. Albertos, A. and Carcel, J. et al. (2011) Thermographic Study of the Preheating Plugs in Diesel Engines. **Applied Thermal Engineering**, 37, pp.412–419. Available at: <http://linkinghub.elsevier.com/retrieve/pii/S1359431111006879>.
- Rubino, L., Phillips, P. and Twigg, M. (2005) Measurements of Ultrafine Particle Number Emissions from a Light-Duty Diesel Engine Using SMPS , DMS , ELPI and EEPS Measurements of Ultrafine Particle Number Emissions from a Light-Duty Diesel Engine Using SMPS , DMS , ELPI. **SAE Technical Paper**, 2005-24-015.

- Sahoo, P., Das, L. and Babu, M. et al. (2009) Comparative Evaluation of Performance and Emission Characteristics of Jatropha, Karanja and Polanga Based Biodiesel as Fuel in a Tractor Engine. **Fuel**, 88, pp.1698–1707.
- Saravanan, S., Nagarajan, G. and Anand, S. et al. (2012) Correlation for Thermal NO_x Formation in Compression Ignition (CI) Engine Fuelled with Diesel and Biodiesel. **Energy**, 42(1), pp.401–410.
- Savvidis, D., Triandafyllis, J. and Grammatikis, V. (2007) Influence of Various Blends Cottonseed Methyl ester Biodiesel on Steady State Emissions Using an Old Technology Ford Escort on a Chassis Dynamometer. **SAE Technical Paper**, 2007-01-4062.
- Schonborn, A. (2009) **Influence of the Molecular Structure of Biofuels on Combustion in a Compression Ignition Engine**. PhD thesis. University of College London.
- Shahir, V.K., Jawahar, C.P. and Suresh, P.R. (2015) Comparative Study of Diesel and Biodiesel on CI Engine with Emphasis to Emissions—A Review. **Renewable and Sustainable Energy Reviews**, 45, pp.686–697.
- SMMT, 2013. **Car CO₂ report 2013**.
- Starck, L. Perrin, H. and Walter, B. et al. (2011) Evaluation of Diesel Engine Cold-Start Performance : Definition of a Grading System To Assess the Impact of Fuel. **Energy & Fuel**, pp.4906–4914.
- Stone, R., 1999. **Introduction to Internal Combustion Engines** 3rd ed., PALGRAVE MACMILLAN.
- Storey, J., Lewis . S. and West, B. et al. (2005) **Hydrocarbon Species in the Exhaust of Diesel Engines Equipped with Advanced Emissions Control Devices**. Final Report CRC Project. Available at: <http://www.crcao.com/reports/recentstudies2005/AVFL-10b-2%20Final%20Report%20January%2031%202005.pdf> [access date: 02/03/2015]
- Sun, J., Caton, J. a. and Jacobs, T.J. (2010) Oxides of Nitrogen Emissions from Biodiesel-fuelled Diesel Engines. **Progress in Energy and Combustion Science**, 36(6), pp.677–695. Available at: <http://linkinghub.elsevier.com/retrieve/pii/S0360128510000237>.
- Sun, L., Liu, Y. and Zhou, L. et al. (2013) Experimental Investigation of Cycle-by-Cycle Variations in a Natural Gas/Diesel Dual Fuel Engine with EGR. **SAE Technical Paper**, 2013-01-0853
- Szybist JP, Boehman A. and Taylor JD, M.R. (2005) Evaluation of Formulation Strategies to Eliminate the Biodiesel NO_x Effect. **Fuel Process Technol**, 86.
- Tan, C. Xu, H.M. and Shuai, S. et al. (2013) Investigation on Transient Emissions of a Turbocharged Diesel Engine Fuelled by HVO Blends. **SAE International Journal of Engines**, 6(2), pp.1046–1058.
- Tan, P., Hu, Z. and Lou D. et al. (2012) Exhaust Emissions from a Light-duty Diesel Engine with Jatropha Biodiesel Fuel. **Energy**, 39(1), pp.356–362.

- Tan, Piqiang et al., 2013. Particle-Bound PAHs Emission from a Heavy Duty Diesel Engine with Biodiesel Fuel. , pp.3–8. Available at: <http://papers.sae.org/2013-01-2573>.
- Tan, P. Zhao, J. and Hu, Z. et al. (2013) Effects of Fuel Properties on Exhaust Emissions from Diesel Engines. **Journal of Fuel Chemistry and Technology**, 41(3), pp.347–355.
- Terdich, N., Martinez, R. and Howet, D. et al. (2011) Off-Road Diesel Engine Transient Response Improvement by Electrically Assisted Turbocharging. **SAE Technical Papers**, 2011-24-0127.
- Tesfa, B., Mishra, R. and Gu, F. (2010) Emission Behavior of a CI Engine Running by Biodiesel under Transient Conditions. **SAE Technical Paper**, 2010-01-1280.
- Tian, J. Xu, H.M. and Ghafourian, A. et al. (2013) Transient Emissions Characteristics of a Turbocharged Engine Fuelled by Biodiesel Blends. *SAE International Journal of Fuels and Lubricants*, 6(2), pp.457–465. Available at: <http://papers.sae.org/2013-01-1302>.
- Turns, S.R., 1996. **An Introduction to Combustion: Concepts and Applications**, New York: McGraw-Hill.
- Tziourtzioumis, D., Demetriades, L. and Zogou, O. et al. (2009) Experimental Investigation of the Effect of a B70 Biodiesel Blend on a Common-rail Passenger Car Diesel Engine. **Part D: Automobile Engineering**, 223, pp.685–701.
- Ueki, S. and Minra, A. (1999) Effect of Difference of High Pressure Fuel Injection Systems on Exhaust Emissions from HDDI Diesel Engine. **JSAE Review**, 20(4), pp.555–557.
- Valentino, G. Corcione, F. and Iannuzzi, S. et al. (2011) Effects of Premixed Low Temperature Combustion of Fuel Blends with High Resistance to Auto-ignition on Performances and Emissions in a High Speed Diesel Engine. **SAE Technical Paper**, 2011-24-0049.
- Varatharajan, K. and Cheralathan, M. (2012) Influence of Fuel Properties and Composition on NOx Emissions from Biodiesel Powered Diesel Engines: A Review. **Renewable and Sustainable Energy Reviews**, 16(6), pp.3702–3710..
- Walter, B., Perrin, H. and Dumas, J. et al. (2009) Cold Operation with Optical and Numerical Investigations on a Low Compression Ratio Diesel Engine. **SAE Technical Paper** , 2009-01-2714.
- Wang, X.G., Zheng, B. and Huang, Z.H. (2010) Performance and Emissions of a Turbocharged, High-pressure Common rail Diesel Engine Operating on Biodiesel/diesel Blends. **Part D: Journal of Automobile Engineering**, 225, pp.127–139.
- Will, F. and Boretti, A. (2011) A New Method to Warm Up Lubricating Oil to Improve the Fuel Efficiency During Cold Start. **SAE International Journal of Engines**, 4(1), pp.175–187..
- Williams, P.T., Andrews, G.E. and Bartle, K.D. (1987) The Role of Lubricating Oil in Diesel Particulate and Particulate PAH Emissions. **SAE Technical Paper**, 872084.

- Wu, F., Wang, J. Chen, W. et al. (2009) A Study on Emission Performance of a Diesel Engine Fueled with Five Typical Methyl Ester Biodiesels. **Atmospheric Environment**, 43(7), pp.1481–1485..
- Xue, J. (2013) Combustion Characteristics, Engine Performances and Emissions of Waste Edible Oil Biodiesel in Diesel Engine. **Renewable and Sustainable Energy Reviews**, 23, pp.350–365.
- Xue, J., Grift, T.E. and Hansen, A.C. (2011) Effect of Biodiesel on Engine Performances and Emissions. **Renewable and Sustainable Energy Reviews**, 15(2), pp.1098–1116.
- Yehliu, K., Boehman, A.L. and Armas, O. (2009) Emissions from Different Alternative Diesel Fuels Operating with Single and Split Fuel Injection. **Fuel**, 89(2), pp.423–437.
- Yokomura, H. Kouketsu, S. and Kotooka, S. et al. (2004) Transient EGR Control for a Turbocharged Heavy Duty Diesel Engine. **SAE Technical Paper**, 2004-01-0120.
- Young, L.-H., Liou, Y. and Cheng, M. et al. (2011) Effects of Biodiesel, Engine Load and Diesel Particulate Filter on Nonvolatile Particle Number Size Distributions in Heavy-duty Diesel Engine Exhaust. **Journal of hazardous materials**, 199-200, pp.282–9..
- Yucesu, H. and Ilkilic, C. (2006) Effect of Cotton Seed Oil Methyl Ester on the Performance and Exhaust Emission of a Diesel Engine. **Energ Source Part A**, 28(4), pp.389–398.
- Zahedh, A., Henein, N. and Brtzik, W. (1990) Diesel Cold Starting: Actual Cycle Analysis under Border Line Conditions. **SAE Technical Paper**, 900441.
- Zhang, F., Xu, H.M. and Zhang, J. et al. (2011) Investigation into Light Duty Dieseline Fuelled Partially-Premixed Compression Ignition Engine. **SAE International Journal of Engines**, pp.2124–2134..
- Zhong, S.G., Naeim, A. and Henein, W. (2007) Lower Temperature Limits for Cold Starting of Diesel Engine with a Common Rail Fuel Injection System. **SAE Technical Paper**, 2007-01-0934.